Geochemical Variability in Fossil Soils and Implications for Past Biogeochemical Cycling, Climates, and Atmospheres

by

Rebecca M. Dzombak

A dissertation submitted in partial fulfillment
of the requirements for the degree of
Doctor of Philosophy
(Earth and Environmental Sciences)
in the University of Michigan
2021

Doctoral Committee:

Professor Nathan D. Sheldon, Chair
Professor Rose M. Cory
Professor Gregory J. Dick
Assistant Professor Jena E. Johnson
Professor Donald R. Zak

Rebecca M. Dzombak

rdzombak@umich.edu

ORCID iD: 0000-0003-3810-2451

Dedication

I dedicate this dissertation to my grandparents, whose encouragement and support helped me reach this point and become the person I am today.

Acknowledgements

Although there is only one author on the title page, there are countless people behind the scenes of my work without whom reaching this point would have been far less enjoyable. First and foremost, I'd like to thank my advisor, Nathan, with whom I have now worked for nearly seven years. I signed up for his Environmental Geology course as a communications student looking to get a science credit; I left as a geology major, never knowing that in a few years, he would end up being my Ph.D. mentor. I always appreciated our collegial discussions and the freedom I had to explore whatever scientific questions caught my eye. I also thank the members of my dissertation committee for their helpful feedback and thoughtful discussions on my work. Their expertise has certainly improved my work over the years, and I enjoyed our discussions. Thanks to my various funding sources over the years: Geological Society of American, American Philosophical Society, Rackham Graduate School, and of course the Department of Earth and Environmental Sciences. A big thanks to Anne, Paula, and everyone else who makes the front office run!

Katy Rico, my labmate and mentor, is one of the main reasons I could see myself going to grad school and carrying out my own research. As an undergraduate in the lab, new to geochemistry, she took the time to hang out in lab and explain things, never shying away from a frank discussion about research or some unknown thing. She set a wonderful example of an engaged, balanced scientist and graduate student that I have been lucky to follow. Along with older graduate students (many of whom I had as GSIs myself, like Ian Winkelstern, Jenny Bowen, and Alex Tye), she made me feel welcome and capable. Then there is Bekah Stein, my

dear friend and labmate. I wouldn't have made it through without Kirk Townsend, a great Camp Davis co-GSI and friend, and Billy Medwedeff, who always has a project to distract us from work. Thanks to the rest of my amazing, supportive cohort; our time in that first-year office really set the stage for a fun and supportive five years. Thanks to Madelyn, Marlon, Phoebe, and Bian for being great co-GSMs. Thanks to Katie Seguin, Sonya Vogel, and Bianca Gallina for being an absolute joy to work with in lab and in the field; I can't wait to see where you go in the world. There are so many others in the department with whom I have interacted over the years; if I missed you, thank you, too.

A huge thank you to my best and oldest friends, Camille and Brittany, for always being there for me. Thanks to the other Dr. R. Dzombak—my cousin Rachel, who has been a wonderful guide and sounding board throughout graduate school. I look forward to years of accidental citations. I have also been lucky to get support from my partner's entire extended family, especially Nik's parents, Lori and Svein. They have welcomed me into their family, sent good cheeses and chocolates, and reminded both of us to look up and see the outside world every once in a while. My brothers, Chris and Jesse, along with their wonderful partners Thu and Anna, have been there for game nights and campfires when I needed to de-stress, and provided decades of love and support before grad school. Above all, my parents always encouraged me to learn, set great examples as lifelong learners and teachers, and ensured I never felt something was beyond my reach. Their unwavering love, support, and guidance have given me the confidence and ability to pursue my dreams. For that and for so much else, I will be ever grateful. Last but not least is Nikolas, who inspires me every day and pushes me to be my best self. I'm so glad we ended up in that first-year office together.

I conducted fieldwork in areas of Wyoming and Utah on lands traditionally occupied by the Cheyenne, Shoshone, Shoshone-Bannock, Apsalooké (Crow), Ute, and Pueblos peoples. The University of Michigan is on lands traditionally stewarded by the Anishinaabe.

Table of Contents

List of Figures

List of Appendices

Abstract

The co-evolution of the terrestrial biogeochemical cycle, the atmosphere, and the marine biosphere remain relatively poorly understood, with outstanding questions surrounding terrestrial-marine links, climate, and tectonics. In particular, the terrestrial sediment source (i.e., soils) remains understudied relative to the marine sediment sink, with the source essentially defined by the record in the sediment sink rather than being considered equally important. Both the sediment source and sink need to be well-constrained in order to understand global biogeochemical changes. Additionally, interpretations of trends in paleosol (fossil soil) geochemistry are only loosely constrained by large-scale modern soil chemical variability, limiting our ability to assess potential changes in biogeochemical cycling through time.

This dissertation focused on two primary goals: improving quantitative constraints on terrestrial biogeochemical cycling and weathering over geologic time, and improving our ability to accurately interpret those records by understanding both modern context and what the paleosol record actually represents. To address these goals, I analyzed the geochemical composition of soils and paleosols (fossil soils) over the past three billion years. Because soils form in the 'critical zone'—the intersection of the biosphere, geosphere, and atmosphere at Earth's surface—they record surficial conditions more directly than other geologic records, providing valuable insight into past climates, atmospheres, and ecosystems. After providing generalized, quantitative constraints on geochemical and weathering variability in modern soils (Chapter II), I used the paleosol record to test for state changes in soil P (Chapter III) and weathering intensity (Chapter IV) on land during key biogeochemical transitions. I also explored a variety of processes that could bias the distribution of paleosols through space and time (e.g., preservation, sampling), which needs to be better constrained in order to interpret paleosols accurately.

In modern soils, I found weaker than expected relationships between soil P and Fe geochemistry and key environmental factors (climate, vegetation, parent material), but weathering intensity, the presence of vegetation, and P concentrations were related. The weak relationships could be due to the continental rather than localized scale of analysis. While the

latter might have provided predictive relationships between soil chemistry and soil-forming factors, a highly-localized scale is often not considered in deep-time biogeochemical modeling. In paleosols, I found that both the P composition and weathering intensity have been stable through time. Discrete, state changes in P composition or weathering intensity—as have been hypothesized based upon marine records—were not recorded. A discrete change was present in the concentration of Ca in paleosols, which increased in the Phanerozoic, perhaps reflecting a shift in pedogenic processes as vascular, rooting plants evolved. Roots and vascularity allowed plants to colonize more arid environments and facilitated the formation of pedogenic carbonate—an important C sink. Therefore, while the advent of land plants may not have led to a global state change in either terrestrial P retention or weathering intensity, plants facilitated the growth of the soil C sink. Because weathering intensity is consistent through time, other factors (e.g., land area, erosion rates) would have been dominant controls on marine nutrient supply through time, with shorter-term perturbations in weathering intensity occurring before returning to the stable baseline. Finally, the distribution of paleosols through time is uneven, with more paleosols being more common (a) towards the present and (b) during peaks in zircon ages, suggesting a formation and/or preservation bias related to the supercontinent cycle.

Chapter 1
Introduction

1.1 Biogeochemical transitions in Earth's history

Over the past three billion years, Earth has undergone several periods of transition involving interconnected systems in the biosphere, geosphere, and atmosphere. These global, encompassing processes are referred to as *biogeochemical* because of how closely-associated the biosphere and geosphere are. Major biogeochemical transitions have defined the course of our planet's history, setting the stage for complex life currently unknown elsewhere in the universe. Discovering how this unique planet and the life it hosts evolved is a critical step in informing our search for life beyond the Blue Marble and remains a topic of fascination for geologists. While our understanding of Earth's biogeochemical history has been improved dramatically over the past few decades as analytical approaches and data have evolved, major uncertainties around some of the most important events in Earth's history remain. Each of these events has sparked an entire field of research, but here I briefly introduce them as motivation for my dissertation research, which focuses on constraining changes in terrestrial biogeochemistry over geologic time in an effort to help answer some of these questions.

1.1.1 Links between the continents and oceans

Continental sediment source, marine sediment sink

Global biogeochemical cycles today are driven in part by the flow of sediments from the continents to the ocean (e.g., Filippelli, 2002). The same was likely true in the past, with entire subdisciplines focused on describing and quantifying that flow. Sediments are generated on landmasses as orogenies occur and as bedrock is broken down by physical and chemical weathering processes. After spending some amount of time on the continent—determined by proximity to the coast, erosion rates, residence time in basins and soils, and fluvial transport—some fraction of sediments eventually enter fluvial systems and are transported to deltas and deposited to the oceans, where some yet smaller fraction settles to the seafloor and is preserved.

(Windblown sediments can also be deposited in oceans.) The landmass is referred to as the sediment source and the oceans as the sink.

Biogeochemical changes can be considered in the context of source-to-sink fluxes of nutrients or other elements that are relevant for biology or marine chemistry. For example, dramatic increases in primary productivity have been observed in lakes and coastal areas where nutrient-rich runoff from agricultural areas is present (Baker et al., 2014). In cases like these, we consider both the sediment source (the fields) and the sink (the lake) to explain an observed biogeochemical change in the lake. In biogeochemical models for much of Earth's history, the same general process is applied, only on much larger scales and with greater uncertainty surrounding the mechanisms behind the records. The rock record leaves us with only patches of the sink and snippets of the source to decode as evidence for ancient biogeochemical transformations.

The sink—represented in the geologic record as marine shales—is typically well-preserved, with shale records present for much of Earth's history and at relatively high temporal resolution (e.g., Reinhard et al., 2017; Wei Wei and Algeo, 2020; Lipp et al., 2021). Because of that data density, shales are a well-studied rock type over the past ca. 3 billion years (Ga), and many of our conceptual underpinnings for biogeochemical transitions are based upon shales. Terrestrial sediments that could be used to infer changes in biogeochemical cycles, on the other hand, tend to be less common in the geologic record. With that imbalance, although both the source and sink are equally important for understanding global biogeochemical changes, the sink has received more attention. Understanding the composition of terrestrial sediments, the processes that determine how sediments move on continents, and how those factors have changed over the past 3 Ga (since the probable onset of subaerially-emerged continents) is a critical step in defining how sediment sources and sinks have evolved and how they may have controlled some of the most dramatic biogeochemical changes in Earth's history.

Continental weathering and sediment mobilization

Weathering is a necessary process for transforming bedrock into mobile sediments that can move between ecosystems on land and eventually be deposited in the oceans. The rate and intensity of weathering are controlled by many factors, including climate, tectonic uplift, and biological processes (Jenny, 1941). The degree of weathering intensity in any given location on a

continent will change over time in response to fluctuations in these (and other) factors. Generally speaking, weathering intensity is greater in warmer and wetter climates and with greater biotic influence (Jenny, 1941). The relationship between tectonic activity and continental weathering is complex, but generally, as mountains uplift, erosion rates increase locally and more fresh bedrock is made available for weathering (e.g., Montgomery and Brandon, 2002). This effectively increases the volume of sediments on the continents. The feedback cycle between tectonic uplift and climate—whether uplift causes cooling, or vice versa—is debated (e.g., Molnar and England, 1990; Raymo and Ruddiman, 1992; Willenbring and von Blanckenburg, 2010).

As subaerially-exposed bedrock is chemically and physically weathered, it begins to form soil (pedogenesis), changing in terms of sediment size distribution and evolving mineralogically (i.e., increasing clays, organic matter; gain or loss of certain elements). At early weathering stages (immature soils), there is relatively little differentiation throughout the vertical profile; the soil lacks *horizons*. As weathering and pedogenesis progress, the soil begins to have differentiable chemical, mineral, and physical properties throughout the profile—horizons form (Jenny, 1995). Soils continue to weather essentially as long as they are exposed at the surface. All the while, their geochemical composition evolves to reflect the climate, atmosphere, and biosphere in which the soils are forming. Soils sit at the surface until they are buried or eroded.

If the soils are eroded, their sediments are then transported by fluvial systems and wind off the continents and to the oceans. Sr and Nd isotopes in rivers have commonly been used to estimate continental weathering intensity and estimate sediment fluxes (e.g., Brass, 1975; Martin and Macdougall, 1995), but that method was found to be controlled primarily by watershed lithology (Blum et al., 1998). Erosional fluxes to rivers are also important to consider for estimating nutrient transport (e.g., Filippelli 2007), and biogeochemical models commonly use modern sediment fluxes to estimate past behavior. Once in the oceans, nutrients (e.g., C, P, Fe, Ca, Mg) contribute to their chemical composition and productivity, with P assumed to be limiting in marine ecosystems on geologic timescales (Tyrell, 1999). This source-to-sink flow of sediments has been posited as a primary driver for biogeochemical changes to continents, oceans, and the atmosphere throughout the past 3 billion years. Quantifying the sediment source rather than relying on the sink to estimate it is essential, and these fossilized soils are a key record for the sediment source.

1.1.2 Precambrian transitions (3.2 Ga–0.543 Ga)

Onset of plate tectonics and emergence of continents

The behavior of the mantle and tectonics has changed over time, and geologists are still working to describe the nature and timing of this evolution (Figure 1.1e; Korenaga 2018, and refs. therein). An exhaustive review of the hypotheses behind mantle and crustal evolution is beyond the scope of this thesis, but I will highlight some key themes. The onset of "modern" plate tectonics, with features like a differentiated lithosphere and asthenosphere, coherent plate boundaries, and the Wilson ("supercontinent") cycle has been modeled, has been modeled as occurring as early as the Hadean to as late as the Neoproterozoic (Korenaga 2013, and refs. therein). The timing of the onset of plate tectonics is relevant for questions around global biogeochemical transitions because that mantle evolution is required for the formation of continental crust. Once continental crust was formed, there is also a question of when those crustal masses were subaerially exposed—that is, weatherable continents. Continental emergence has been estimated over a similarly wide range to mantle evolution, with the earliest estimates around 3–3.5 Ga and the latest estimates in the Neoproterozoic (see Table C4). Global sea level also plays a role in determining the area of exposed land. Once continents were consistently subaerially emerged, the continent-ocean sediment flow could begin.

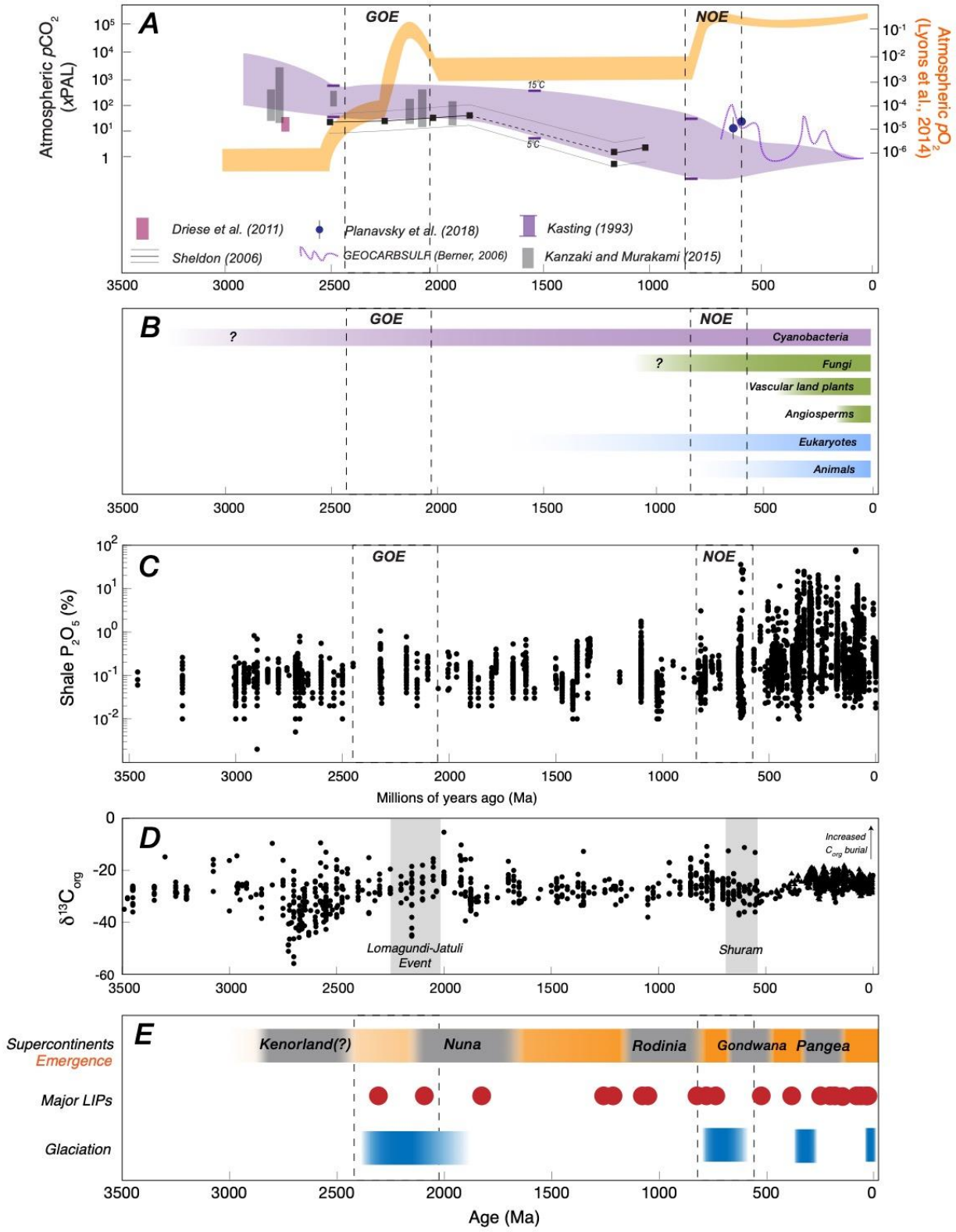

Figure 1.1. Major geologic, biologic, and atmospheric Earth history.

(A) Changes in the composition of the atmosphere through time. Atmospheric oxygen is shown in the orange bar, with estimates for the Great and Neoproterozoic Oxygenation Events (GOE, NOE) denoted by dashed lines. Multiple estimates for atmospheric CO_2 are shown; legend in figure. (B) Key biological innovations through time (see Wellman and Strother, 2015). (C) P_2O_5 in shales (Reinhard et al., 2017). (D) The evolution of organic C isotopes through time, with major carbon isotope excursions (CIEs) marked by gray bars (Krissansen-Toten et al., 2015; Nordt et al., 2016). (E) Major tectonic and climatic contexts through time. Supercontinents are marked by gray bars (Voice et al., 2011; Domeier et al., 2018; Pastor-Galán et al., 2019), with general continental emergence in orange (Korenaga 2013, 2018). The occurrence of major Large Igneous Provinces (LIPs) through time are shown in red (Ernst et al., 2021). Global periods of glaciation are shown with blue bars.

Cyanobacterial evolution and the Great Oxygenation Event

Cyanobacteria (the earliest photosynthesizing microorganisms) evolved some time prior to 3 Ga and expanded dramatically during the Paleoproterozoic (Sánchez-Baracaldo and Cardona, 2020, and refs. therein). This expansion coincided with an increase in atmospheric oxygen (pO_2) from ca. 2.4–2.2 Ga (Figure 1.1a; the Great Oxygenation Event, or GOE; Farquhar et al., 2000; Holland, 2002; Canfield, 2005; Holland, 2006), although locally-limited oxygen "oases" as well as short-term "whiffs" of oxygen have been interpreted as occurring prior to the state change (Anbar et al., 2007; Crowe et al., 2013; Olson et al., 2013; Planavsky et al., 2014a; Ossa Ossa et al., 2019). The loss of easily-oxidized S minerals (e.g., pyrite) serves as an additional line of evidence for oxygenation (Lyons et al., 2014, and refs. therein). The deep oceans, however, remained dominantly anoxic (very low oxygen levels) until probably the Neoproterozoic (Lyons et al., 2014, and refs. therein), although the regional nature of many shale geochemical records complicates the extrapolation of single-basin records to entire oceans (see section 1.2.1). Mantle redox evolution (e.g., Kasting, 1993), atmospheric hydrogen escape (Catling et al., 2001), gradual biogeochemical evolution following photosynthesis (Alcott et al., 2019), and tectonics/volcanism (e.g., Kump and Barley, 2007; Campbell and Allen, 2008) have been hypothesized to trigger the GOE. Although the chemical composition of the ocean evolved during this period, changes in continental weathering intensity or the flux of sediments from continents to oceans are not thought to have driven this biogeochemical change, so while it is undoubtedly important, the GOE is not widely discussed throughout this dissertation.

Neoproterozoic Oxygenation Event

A second major increase in atmospheric oxygen occurred between ca. 800–600 million years ago (Ma), termed the Neoproterozoic Oxygenation Event (NOE; Canfield, 2005; Berner, 2006; Lyons et al., 2014). Its progress constrained primarily by changes in marine shale chemistry reflective of an increase in oxic conditions on continents, and in the oceans and atmospheres (e.g., S, Mo, V, U, Cr; Sahoo et al., 2012; Lyons et al., 2014; Planavsky et al., 2015; Cole et al., 2016; Colwyn et al., 2019). However, the timing of oxygenation events is difficult to establish on a global scale because changes in oxidation (redox) state can be limited to individual basins, reflecting local conditions rather than that of a full ocean (e.g., Sperling et al., 2013; Raiswell et al., 2018; Rico et al. 2019a). An additional complication is that assumptions of seafloor sediment geochemistry reflecting water column conditions may not be accurate (e.g., Rico et al., 2019b) and that some of the theoretical assumptions about the mineral carrier phase and redox element speciation are not reproduced in actual samples (Tessin et al., 2019). Despite these hurdles, on a global scale, the NOE has been generally well-established, with its driving mechanisms remaining in question (Och and Shields-Zhou, 2012, and refs. therein).

The mechanisms of the NOE are in question partially because major changes in the geosphere, biosphere, and climate all coincided. Supercontinent breakup and assembly, the diversification of eukaryotes and the evolution of metazoans, and a global ice age all occurred around the same time as the increase in atmospheric oxygen (Och and Shields-Zhou, 2012). Tectonics could have contributed via uplift, increased weathering and erosion, delivering nutrients to spike primary productivity and contribute to increased C burial (as evidenced by higher $\delta^{13}C_{org}$ values in shales), along with increased volcanic activity (Lenton and Watson, 2004; Campbell and Squire, 2010; Mills et al., 2011; Horton et al., 2015; Lee et al., 2016; Zaffos et al. 2017). Paleogeography—the distribution of continental land area—could have moderated tectonic activity, with large areas of low-latitude continents increasing the average weathering intensity experienced on continents (e.g., Donnadieu et al., 2004) and contributing to the onset of low-latitude glaciation (Schrag et al., 2002). An expansion of the terrestrial biosphere and consequent weathering fluxes has been hypothesized (Knauth and Kennedy, 2009), although the terrestrial biosphere is now thought to have been active prior to the NOE (e.g., Beaty and Planavsky, 2021). Increased sediment mobilization (and therefore P mobilization) from glaciation, and consequent increases in marine primary productivity, have been proposed (Lenton and Watson, 2004; Mills et al., 2011; Keller et al., 2019).

Eukaryotic diversification and complex animal life

Coincident with the NOE were two important biological events: a dramatic and rapid diversification of eukaryotes (Knoll et al., 2006) and the appearance of the earliest confidently-described multicellular animal life (metazoans; see Planavsky et al., 2015, and refs. therein; Reinhard et al., 2020, and refs. therein; Figure 1.1b). The cause of the sudden eukaryotic expansion and diversification, including the rise in oxygen, remains debated (Sperling et al., 2013; Planavsky et al., 2014b; Reinhard et al., 2016, and refs. therein). The evolution of metazoans during this period has also been tied to the oxygenation of the oceans, but changes in the redox state and chemical composition of the oceans (along with element/nutrient seafloor burial) are generally considered to have played an important, if yet unclear, role (e.g., Fike et al., 2006; Scott et al., 2008; Sahoo et al., 2012; Lyons et al., 2014; Reinhard et al., 2017; Laakso et al., 2020). In particular, the dissolved P concentration in oceans is thought to have increased along with increased organic C burial, based on C:P ratios in shales (e.g., Lenton and Watson, 2004; Planavsky et al., 2010; Reinhard et al., 2017), whether from increased continental erosion during global glaciations (e.g., Mills et al., 2011), changes in marine nutrient use efficiency (e.g., Kipp and Stuëken, 2017; Reinhard et al., 2017), changes in deep-ocean water chemistry like transient/localized euxinia (e.g., Poulton and Canfield, 2011), or a combination of each of those factors. The increase in P generally increases in step with proposed changes in oxygen (e.g., Reinhard et al., 2020), solidifying the link between marine nutrients and oxygenation but without clarifying the underlying mechanisms or connections to the biosphere. In this dissertation, I test hypothesized changes in terrestrial P (Chapter III).

1.1.3 Phanerozoic (0.543 Ga – present)

Prior to the Phanerozoic, the terrestrial biosphere was limited to microbial and algal mats and possibly fungi (Wellman and Strother, 2015, and refs. therein). In the early Paleozoic, primarily the Silurian and Devonian, terrestrial plants with vascular systems evolved and diversified, along with terrestrial arthropods and symbiotic (mycorrhizal) fungi (see Kenrick et al., 2012). Those evolutionary events are thought to have intensified terrestrial weathering, impacted the carbon cycle, and increased atmospheric oxygen (e.g., Berner, 1992, 1998; Algeo and Scheckler, 1998; Driese et al., 2000; Lenton and Watson, 2004; Lu et al., 2018), as well as

altered the distribution and availability of terrestrial ecosystems (e.g., Retallack, 2001; Davies and Gibling, 2010; Morris et al., 2015; Wallace et al., 2017; Pawlik et al., 2020). Workers have hypothesized that the terrestrial P cycle in particular would have been affected by the evolution of rooting, vascular land plants and associated mycorrhizae, which evolved in part to aid in P acquisition (e.g., Landeweert et al., 2001). The Paleozoic ice age approximately coincided with a rise in oxygen and has been hypothesized as a driver of weathering intensity (Montañez and Poulsen, 2013; Krause et al., 2018; Richey et al., 2020).

The advent of land plants is thought to have dramatically changed the C cycle by increasing terrestrial silicate weathering, increasing CO_2 drawdown (and C_{org} burial through increased erosion rates; Figure 1.1d), and growing the terrestrial C sink in soils (e.g., Berner, 1992, 1998, 2004). While I do not directly address the C cycle in this dissertation, I test hypotheses around changes in terrestrial weathering that have implications for the C cycle.

1.2 Quantifying biogeochemistry in deep-time

1.2.1 Shales

Shales are widely-studied records due to their relatively global and consistent distribution through time (Figure 1.1c), providing relatively high-density data for periods of interest such as the GOE, NOE, and evolution of complex life (Figure 1.1c). The chemical composition of shales offers insight into elemental burial on the seafloor, ocean chemistry, and indirect views into terrestrial sediments and processes. Both major (C, P, S) and trace (e.g., Cr, Mo, U, V) elements in shales have been used over the past 3 Ga, and although elemental proxies in shales are continually being refined, they have provided the outlines for many biogeochemical transitions such as those described above (e.g., Sahoo et al., 2012; Crowe et al., 2013; Lyons et al., 2014; Reinhard et al., 2017). Additionally, C, O, Sr, and other isotopes in shales have been used to reconstruct the isotopic composition of seawater over time, with wide-ranging implications for both the biosphere and geosphere (e.g., Allègre and Dominique, 1984; Reinhard et al., 2017; Wei Wei and Algeo, 2020). Shales offer excellent insight into ocean and seafloor conditions, but they tend to integrate over large areas (e.g., entire ocean basins, multiple terrestrial watersheds) and times. This integration perhaps raises some difficulty in connecting relatively small-scale terrestrial changes to global processes (i.e., if a basin on land undergoes some dramatic climate

shift, would it be reflected in shales?). Therefore, shales (the sediment sink) should not be relied upon entirely to discern changes in terrestrial sediment sources (see section 1.2.3).

1.2.2 Terrigenous sedimentary rocks

Sedimentary rocks from the continents, generally speaking, represent the sediment source. Geochemical analyses of bulk sedimentary records for elucidating global biogeochemical changes are uncommon; more typical uses involve analyzing mineral and sediment-size distributions through time and space to constrain regional changes in provenance/tectonics, hydrology, and landscape evolution (e.g., Kraus and Aslan, 1988; Davies et al., 2011). However, some global, long-term distributions of different lithologies (e.g., Husson and Peters, 2018; Loydell et al., 2021) through time have been used to test for changes in landscape structure and evolution due to tectonics (relevant for the carbon cycle) and the biosphere (e.g., land plants stabilizing the land, increasing clay minerals).

An additional source of terrestrial sedimentary records are glaciers, which mobilize large volumes of sediment through scraping and proglacial fluvial networks and have been posted as drivers of biogeochemical change (e.g., Mills et al., 2011; Gaschnig et al., 2014; Keller et al., 2019). (Whether glaciers increase or decrease weathering rates remains debated; e.g., Stumpf et al., 2012; Dubnick et al., 2017; Martin et al., 2020.) Analyses of the geochemistry glacially-derived sediments (e.g., tillites, diamictites; Gaschnig et al., 2014, 2016) can lend insight into composition of terrestrial sediments more broadly, as sources like fluvial sediments and soils could be re-integrated. In that sense, glacially-derived sediments are similar to shales (integrating broader regions). Collecting global datasets circumvents this issue of relatively local integration (for many lithologies) and allows insight into fundamental global controls (Ronov 1980; Keller et al., 2019; Husson and Peters 2018).

1.2.3 Paleosols

What are paleosols and what do they represent?

Paleosols are fossilized soils, formed in the paleo-‘critical zone’ where the biosphere, atmosphere, and geosphere meet (Brantley et al., 2007). Therefore, soil chemical compositions reflect variables like climate, atmospheric composition, and biological activity. In this way, paleosols capture processes on land far more directly than relying on marine records. Paleosols

are also critical records because, as direct products of terrestrial weathering (along with glacially-derived sediments and fluvial sedimentary rocks), they represent the global source of sediments. While marine records are used to reconstruct continental processes and conditions (e.g., continental weathering), they primarily reflect the ocean as a sediment sink, integrating large spatial and temporal scales and preserving only a fraction of the sediments that are originally delivered from the continents. As mentioned above, although the continental half of weathering and sediment supply is a critical component of the global biogeochemical pump, biogeochemical models often include assumptions on the timing, magnitude, and composition of terrestrial weathering and sediment fluxes, with parameters typically defined with very little quantitative basis. For example, sediment fluxes have been assumed to equate to the composition of continental crust (e.g., Hao et al., 2020, in part due to a need to simplify models), or to change through time as conditions on land change (e.g., Lenton et al., 2018). Weathering intensity and consequent erosional fluxes have also been assumed to change corresponding to pCO_2, although the nature of that relationship is complex and remains a hotly-studied field (e.g., Berner, 1998; Molnar and England, 1990; Raymo and Ruddiman, 1992; Dixon et al., 2009; Willenbring and von Blanckenburg, 2010). These assumptions limit the accuracy of model results, so quantifying the terrestrial half of global biogeochemistry—the sediment source for oceans—is necessary.

Soil formation through geologic time

The five factors of soil formation (pedogenesis) are climate, biosphere, relief, parent material, and time (Jenny, 1941), each of which varies greatly over space and time in the geologic record. Climate, biosphere, and time largely control weathering, with relief controlling erosion (and, indirectly, weathering), and parent material controlling the soil's starting composition and which elements are available to be mobilized. During many of the biogeochemical transitions described above, these soil forming factors were in flux, representing their rapidly-changing environment. This is both the strength and weakness of paleosols: disentangling the effects of one factor from another (e.g., climate vs. time, relief vs. climate) can be difficult. Different combinations of factors can produce a similar value for, say, a paleo-precipitation proxy. For example, a soil that undergoes less-intense weathering for a prolonged period may end up looking geochemically similar to a soil that undergoes rapid, intense weathering. Additionally, simply knowing a geochemical concentration or proxy value is in and

of itself not particularly useful: a broader context, whether landscape, ecosystem, or climatic, is required to interpret that value meaningfully and to analyze any potential trends for significance.

Pedogenesis likely evolved over geologic time as each of these factors changed (Figure 1.2). As the first continents emerged under a high pCO_2/low pO_2 atmosphere, with less relief than is possible today, and likely with a limited terrestrial biosphere, weathering would have been dominated by abiotic CO_2-acid weathering driven by time (Sheldon, 2006). After the GOE, oxidative weathering along with an expanded terrestrial biosphere would have changed the balance of pedogenic factors, as would a ramping-up of tectonic activity. Then, during the Phanerozoic as rooting vascular plants and their fungal symbionts evolved, pedogenesis would have responded to that increase in biotic influence.

Because of these changes and the complex, interconnected nature of pedogenic processes, placing paleosols in broad tectonic and climatic contexts is important for accurately interpreting their geochemistry. However, our understanding of the evolution of pedogenesis as well as potential biases in the paleosol record is relatively limited due to the lack of a comprehensive paleosol database.

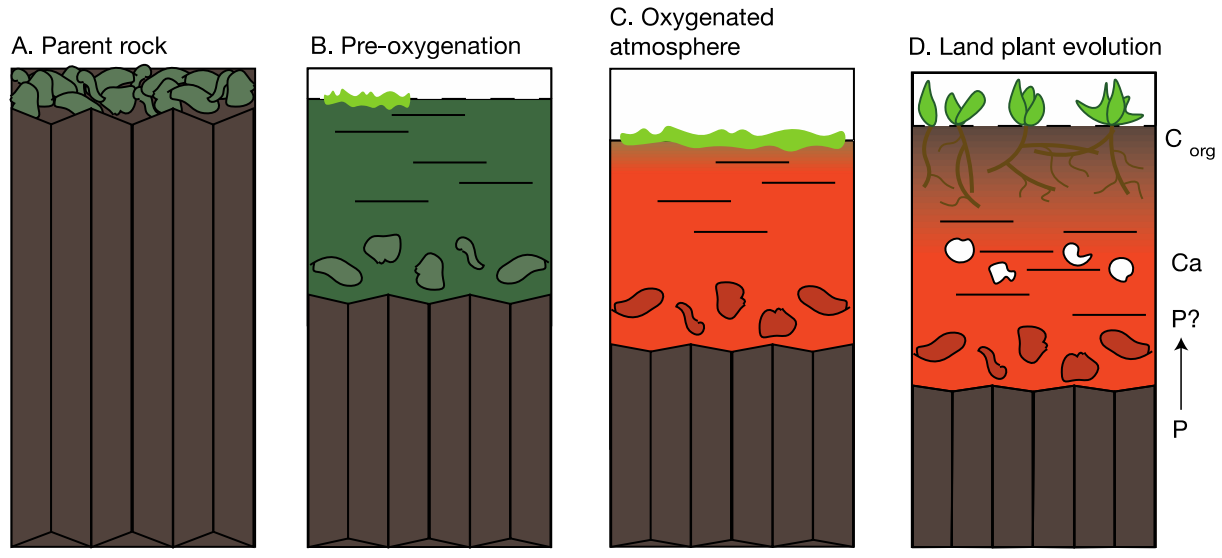

Figure 1.2. Pedogenesis through time.

(A) An unweathered column of parent rock, with non-pedogenic surface alteration. (B) Weathered bedrock in a high CO_2 atmosphere, with weathering driven by carbonic acid and limited organic acid weathering. (C) Under higher O_2, oxidative weathering processes dominate in soils. The influence of biotically-mediated weathering likely increases. (D) Once land plants

evolve, weathering is hypothesized to be more intense, with deeper and more rapid pedogenesis and greater element mobility in soils. Plants may also have increased the volume of sediments and soils retained in the profile (rather than lost to erosion). Organic carbon and carbonate are sequestered in soils.

History of use of paleosols for biogeochemical reconstructions

Paleosols were first widely used to constrain the oxygenation of the atmosphere using Fe composition (e.g., Zbinden et al, 1988; Holland et la., 1989; Rye and Holland, 1998; Yang et al., 2002) and to reconstruct changes in pCO_2 and the global C cycle using C isotope systematics (e.g., Cerling 1984, 1992; Ekart et al., 1999; Nordt et al., 2002; Figure 1.1a). Work then expanded to include more bulk geochemical approaches, with proxies for weathering intensity and, later, paleoclimates being developed during the 1990s and 2000s, and improved upon today (Nesbitt and Young, 1982; Maynard, 1992; Sheldon et al., 2002; Gallagher and Sheldon, 2013; Montañez, 2013; Babechuk et al., 2014; Driese et al., 2015; Stinchcomb et al., 2016; Lukens et al., 2019; Chapter V). Despite the growth of paleosol-based proxies and applications of both bulk and isotope geochemistry, comprehensive databases for the former do not yet exist, a clear discrepancy between marine and terrestrial records. Some attempts at compiling terrestrial weathering and geochemical changes have been made (e.g., Colwyn et al., 2019; Beaty and Planavsky et al., 2021), but nothing approaching the scale available for the marine (e.g., Reinhard et al., 2017; Lipp et al., 2021).

Despite how frequently continental weathering has been posited as a driver for atmospheric and marine biogeochemical changes, it remains poorly quantified. Several recent efforts have been made to quantify terrestrial weathering both directly (Beaty and Planavsky, 2021) and indirectly (Lipp et al., 2021); critically, both found that contrary to common assumptions made in biogeochemical modeling, continental weathering intensity is stable on long timescales. However, their results are limited in dataset size (Beaty and Planavsky, 2021) and directness (Lipp et al., 2021, which uses shale geochemistry rather than terrestrial sediments). I address this data gap in this dissertation (Chapters III, IV).

On a smaller scale, an additional hurdle in using paleosol-based geochemical proxies is establishing the significance of potential trends through time. Common practice for paleosol studies is to sample a relatively limited number of profiles over either space or time—occasionally even reporting on a single paleosol profile—rather than attempting to sample

broadly and at higher resolution. For work whose aim is to extrapolate paleosol geochemical interpretations of climates to basinwide or even global scales (as is commonly done), a source of uncertainty in the form of inherent geochemical variability is introduced. Without defining noise (i.e., the background level of geochemical variability across both space and time), a meaningful signal (e.g., an increase in temperature associated with ice-sheet retreat) cannot be confidently defined. Yet, few studies have attempted to constrain geochemical variability on basinwide scales (Tabor et al., 2008; Hyland and Sheldon, 2016). I address this knowledge gap in Chapter V.

1.3 In this dissertation

In this dissertation, I modified a large dataset of modern soil geochemistry (top 5 cm, A, B, and C horizons; $n_{top,A,C}$= 4857, n_B=247) and compile a new large dataset of paleosols ($n_{profiles}$=261, $n_{samples}$=2849) with bulk geochemical data. Together, I use these datasets to improve constraints on terrestrial biogeochemistry and our ability to interpret paleosol geochemistry in a robust way. In Chapter II, I quantify variability in modern soil geochemistry on continental scales, providing a baseline for interpreting paleosol geochemistry. I also constrain potential trends between soil geochemistry and soil forming variables of interest in the geologic record (e.g., precipitation, weathering intensity), and I test potential controls on biologically-relevant elements (P, Fe) in soils. In Chapter III, I test the hypothesis that P composition of soils underwent state changes through geologic time. In Chapter IV, I test the hypothesis that terrestrial weathering intensity underwent state changes through geologic time. I identify potential sources of bias in the distribution of paleosols through time which could affect the quality of geochemical interpretations. Finally, I use an Eocene paleosol transect as a case study in the practical application of weathering-based proxies and provide a quantitative approach to constraining intra-paleosol geochemical variability.

The work in this thesis draws widely from published literature and datasets that have not before, for the most part, been compiled. This reflects a basic gap in the field of paleosol geochemistry that other sedimentary geology-focused fields have begun to fill. This dissertation will hopefully serve as a springboard for others to improve upon and collaborate widely to build a more comprehensive soil and paleosol geochemistry database.

References

1. Alcott, L. J., Mills, B. J. W. & Poulton. Stepwise Earth oxygenation is an inherent property of global biogeochemical cycling. *Science* **1337**, 1333–1337 (2019).

2. Algeo, T. J. & Scheckler, S. E. Terrestrial-marine teleconnections in the Devonian: links between the evolution of land plants, weathering processes, and marine anoxic events. *Philos. Trans. R. Soc. London B* **353**, 113–130 (1998).

3. Allègre, C. J. & Rousseau, D. The growth of the continent through geological time studied by Nd isotope analysis of shales. *Earth Planet. Sci. Lett.* **67**, 19–34 (1984).
4. Anbar, A. D. *et al.* A whiff of oxygen before the great oxidation event? *Science* **317**, 1903–1906 (2007).

5. Babechuk, M. G., Widdowson, M. & Kamber, B. S. Quantifying chemical weathering intensity and trace element release from two contrasting basalt profiles, Deccan Traps, India. *Chem. Geol.* **363**, 56–75 (2014).

6. Baker, D. B. *et al.* Phosphorus loading to Lake Erie from the Maumee, Sandusky and Cuyahoga rivers: The importance of bioavailability. *J. Great Lakes Res.* **40**, 502–517 (2014).

7. Beaty, B. J. & Planavsky, N. J. A 3 b.y. record of a biotic influence on terrestrial weathering. *Geology* **49**, 407–411 (2021).

8. Berner, R. A. The carbon cycle and CO_2 over Phanerozoic time: The role of land plants. *Philos. Trans. R. Soc. B Biol. Sci.* **353**, 75–82 (1998).

9. Berner, R. A. Weathering, plants , and the long-term carbon cycle. *Geochemica Cosmochim.* **56**, 3225–3231 (1992).

10. Berner, R.A. The Phanerozoic Carbon Cycle: CO_2 and O_2. Oxford University Press, Oxford, UK (2004).

11. Berner, R. A. GEOCARBSULF: A combined model for Phanerozoic atmospheric O2 and CO2. *Geochim. Cosmochim. Acta* **70**, 5653–5664 (2006).

12. Blum, J. D., Gazis, C. A., Jacobson, A. D. & Chamberlain, C. P. Carbonate versus silicate weathering in the Raikhot watershed within the High Himalayan Crystalline Series. *Geology* **26**, 411–414 (1998).

13. Brantley, S. L., Goldhaber, M. B. & Vala Ragnarsdottir, K. Crossing disciplines and scales to understand the critical zone. *Elements* **3**, 307–314 (2007).

14. Brass, G. W. The effect of weathering on the distribution of strontium isotopes in weathering profiles. *Geochim. Cosmochim. Acta* **39**, 1647–1653 (1975).

15. Campbell, I. H. & Squire, R. J. The mountains that triggered the Late Neoproterozoic increase in oxygen: The Second Great Oxidation Event. *Geochim. Cosmochim. Acta* **74**, 4187–4206 (2010).

16. Campbell, I. H. & Allen, C. M. Formation of supercontinents linked to increases in atmospheric oxygen. *Nat. Geosci.* **1**, 554–558 (2008).

17. Canfield, D. E. The early history of atmospheric oxygen: Homage to Robert M. Garrels. *Annu. Rev. Earth Planet. Sci.* **33**, 1–36 (2005).

18. Catling, D. C., Zahnle, K. J. & McKay, C. P. Biogenic methane, hydrogen escape, and the irreversible oxidation of early earth. *Science* **293**, 839–843 (2001).

19. Cerling, T. E. The stable isotopic composition of modern soil carbonate and its relation to climate. *Earth Planet. Sci. Lett.* **71**, 229-240. (1984).

20. Cerling, T. E. Use of carbon isotopes in paleosols as an indicator of the pCO_2 of the paleoatmosphere. *Global Biogeochem. Cycles* **6**, 307–314 (1992).

21. Cole, D. B. *et al.* A shale-hosted Cr isotope record of low atmospheric oxygen during the Proterozoic. *Geology* **44**, 555–558 (2016).

22. Colwyn, D. A. *et al.* A paleosol record of the evolution of Cr redox cycling and evidence for an increase in atmospheric oxygen during the Neoproterozoic. *Geobiology* **17**, 579–593 (2019).

23. Crowe, S. A. *et al.* Atmospheric oxygenation three billion years ago. *Nature* **501**, 535–538 (2013).

24. Davies, N. S. & Gibling, M. R. Cambrian to Devonian evolution of alluvial systems: The sedimentological impact of the earliest land plants. *Earth Sci. Rev.* **98**, 171–200 (2010).

25. Davies, N. S., Gibling, M. R. & Rygel, M. C. Alluvial facies evolution during the Palaeozoic greening of the continents: Case studies, conceptual models and modern analogues. *Sedimentology* **58**, 220–258 (2011).

26. Dixon, J. L., Heimsath, A. M. & Amundson, R. The critical role of climate and saprolite. *Earth Surf. Process. Landforms* **34**, 1507–1521 (2009).

27. Domeier, M., Magni, V., Hounslow, M. W. & Torsvik, T. H. Episodic zircon age spectra mimic fluctuations in subduction. *Sci. Rep.* **8**, 17471 (2018).

28. Donnadieu, Y., Godderis, Y., Ramstein, G., Nedelec, A. & Meert, J. A 'snowball Earth' climate triggered by continental break-up through changes in runoff. *Nature* **541**, 303–306 (2004).

29. Driese, S. G., Mora, C. I. & Elick, J. M. The Paleosol Record of Increasing Plant Diversity and Depth of Rooting and Changes in Atmospheric pCO_2 in the Siluro-Devonian. *Paleontol. Soc. Pap.* **6**, 47–62 (2000).

30. Driese, S. G. & Nordt, L. C. New weathering index improves paleorainfall estimates from Vertisols. *Geology* **38**, 4407–410 (2015).

31. Dubnick, A. *et al.* Trickle or treat: The dynamics of nutrient export from polar glaciers. *Hydrol. Process.* **31**, 1776–1789 (2017).

32. Ekart, D. D., Cerling, T. E., Montañez, I. P. & Tabor, N. J. A 400 million year carbon isotope record of pedogenic carbonate: Implications for paleoatmospheric carbon dioxide. *American Journal of Science* **299**, 805–827 (1999).

33. Ernst, R. *et al.* Part I. The temporal record of large igneous provinces (LIPs). in *Large Igneous Provinces: A Driver of Global Environmental and Biotic Changes* (eds. Ernst, R. E., Dickson, A. J. & Bekker, A.) American Geophysical Union and John Wiley & Sons, Inc., Washington, D.C. 2021.

34. Farquhar, J., Bao, H. & Thiemens, M. Atmospheric Influence of Earth's Earliest Sulfur Cycle. *Science* **289**, 756–758 (2000).

35. Fike, D. A., Grotzinger, J. P., Pratt, L. M. & Summons, R. E. Oxidation of the Ediacaran ocean. *Nature* **444**, 744–747 (2006).

36. Filippelli, G. M. The Global Phosphorus Cycle. *Rev. Mineral. Geochemistry* **48**, 391–425 (2002).

37. Gallagher, T. M. & Sheldon, N. D. A new paleothermometer for forest paleosols and its implications for Cenozoic climate. *Geology* **41**, 647–650 (2013).

38. Gaschnig, R. M., Rudnick, R. L., Mcdonough, W. F. & Kaufman, A. J. Onset of oxidative weathering of continents recorded in the geochemistry of ancient glacial diamictites. *Earth Planet. Sci. Lett.* **408**, 87–99 (2014).

39. Gaschnig, R. M. *et al.* Compositional evolution of the upper continental crust through time, as constrained by ancient glacial diamictites. *Geochim. Cosmochim. Acta* **186**, 316–343 (2016).

40. Hao, J., Knoll, A. H., Huang, F., Hazen, R. M. & Daniel, I. Cycling phosphorus on the Archean Earth: Part I. Continental weathering and riverine transport of phosphorus.

Geochim. Cosmochim. Acta **273**, 70–84 (2020).

41. Holland, H. D. The oxygenation of the atmosphere and oceans. *Philos. Trans. R. Soc. B Biol. Sci.* **361**, 903–915 (2006).

42. Holland, H. D. Volcanic gases, black smokers, and the great oxidation event. *Geochim. Cosmochim. Acta* **66**, 3811–3826 (2002).

43. Holland, H. D., Feakes, C. R. & Zbinden, E. A. The Flin Flon Palaeosol and the Composition of the Atmosphere 1.8 BYBP. *American Journal of Science* **289**, 362–389 (1989).

44. Horton, F. Did phosphorus derived from the weathering of large igneous provinces fertilize the Neoproterozoic ocean? *Geochemistry, Geophys. Geosystems* **16**, 1723–1738 (2015).

45. Husson, J. M. & Peters, S. E. Nature of the sedimentary rock record and its implications for Earth system evolution. *Emerg. Top. Life Sci.* **2**, 125–136 (2018).

46. Hyland, E. G. & Sheldon, N. D. Examining the spatial consistency of palaeosol proxies: Implications for palaeoclimatic and palaeoenvironmental reconstructions in terrestrial sedimentary basins. *Sedimentology* **63**, 959–971 (2016).

47. Jenny, H.J. Factors in soil formation. McGraw-Hill, New York, United States. 1941.

48. Jenny, H. & Amundson, R. Factors of Soil Formation: A System of Quantitative Pedology. 1994.

49. Kasting, J. F. Earth's Early Atmosphere. *Science* **259**, 920–926 (1993).

50. Keller, C. B. *et al.* Neoproterozoic glacial origin of the Great Unconformity. *Proc. Natl. Acad. Sci.* **116**, 1136–1145 (2019).

51. Kenrick, P., Wellman, C. H., Schneider, H. & Edgecombe, G. D. A timeline for terrestrialization: consequences for the carbon cycle in the Palaeozoic. *Philos. Trans. R. Soc. London B* **367**, 519–536 (2012).

52. Kipp, M. A. & Stüeken, E. E. Biomass recycling and Earth's early phosphorus cycle. *Sci. Adv.* **3**, 1–7 (2017).

53. Knauth, L. P. & Kennedy, M. J. The late Precambrian greening of the Earth. *Nature* **460**, 728–732 (2009).

54. Knoll, A. H., Javaux, E. J., Hewitt, D. & Cohen, P. Eukaryotic organisms in Proterozoic oceans. *Philos. Trans. R. Soc. B Biol. Sci.* **361**, 1023–1038 (2006).

55. Korenaga, J. Initiation and evolution of plate tectonics on earth: Theories and observations. *Annu. Rev. Earth Planet. Sci.* **41**, 117–151 (2013).

56. Korenaga, J. Crustal evolution and mantle dynamics through Earth history. *Philos. Trans. R. Soc. A Math. Phys. Eng. Sci.* **376**, 2132 (2018).

57. Kraus, M. J. & Aslan, A. Eocene hydromorphic paleosols: Significance for interpreting ancient floodplain processes. *J. Sediment. Petrol.* **63**, 453–463 (1988).

58. Krause, A. J. *et al.* Stepwise oxygenation of the Paleozoic atmosphere. *Nat. Commun.* **9**, 1–10 (2018).

59. Krissansen-Totton, J., Buick, R. & Catling, D. C. A statistical analysis of the carbon isotopic record from the Archean to Phanerozoic and implications for the rise of oxygen. *Am. J. Sci.* **315**, 275–316 (2015).

60. Kump, L. R. & Barley, M. E. Increased subaerial volcanism and the rise of atmospheric oxygen 2. 5 billion years ago. *Nature* **448**, 1033–1036 (2007).

61. Laakso, T. A., Sperling, E. A., Johnston, D. T. & Knoll, A. H. Ediacaran reorganization of the marine phosphorus cycle. *Proc. Natl. Acad. Sci.* **117**, 11961–11967 (2020).

62. Landeweert, R. *et al.* Linking plants to rocks: Ectomycorrhizal fungi mobilize nutrients from minerals. *Trends Ecol. Evol.* **16**, 248–254 (2001).

63. Lee, C. A. *et al.* Two-step rise of atmospheric oxygen linked to the growth of continents. *Nat. Geosci.* **9**, 417–424 (2016).

64. Lenton, T. M., Daines, S. J. & Mills, B. J. W. Earth-Science Reviews Invited review COPSE reloaded: An improved model of biogeochemical cycling over Phanerozoic time. *Earth-Science Rev.* **178**, 1–28 (2018).

65. Lenton, T. M. & Watson, A. J. Biotic enhancement of weathering, atmospheric oxygen and carbon dioxide in the Neoproterozoic. *Geophys. Res. Lett.* **31**, L05202 (2004).

66. Lipp, A. G. *et al.* The composition and weathering of the continents over geologic time. *Geochemical Perspect. Lett.* **17**, 21–26 (2021).

67. Lu, W. *et al.* Late inception of a resiliently oxygenated upper ocean. *Science* **5372**, 1–8 (2018).

68. Lukens, W. E., Nordt, L. C., Stinchcomb, G. E., Driese, S. G. & Tubbs, J. D. Reconstructing pH of Paleosols Using Geochemical Proxies. *J. Geol.* **126**, 427–449 (2018).

69. Lyons, T. W., Reinhard, C. T. & Planavsky, N. J. The rise of oxygen in Earth's early ocean and atmosphere. *Nature* **506**, 307–315 (2014).

70. Martin, E. E. & Macdougall, J. D. Sr and Nd isotopes at the Permian/Triassic boundary: A record of climate change. *Chem. Geol.* **125**, 73–99 (1995).

71. Martin, J. B., Pain, A. J., Martin, E. E., Rahman, S. & Ackerman, P. Comparisons of nutrients exported from Greenlandic glacial and deglaciated watersheds. *Geobiology* **34**, e2020GB006661 (2020).

72. Maynard, J. B. Chemistry of modern soils as a guide to interpreting Precambrian paleosols. *J. Geol.* **100**, 279–289 (1992).

73. Mehra, A., Keller, B.C., Zhang, T. *et al*. Curation and analysis of global sedimentary geochemical data to inform earth history. *GSA Today* **31**, 4-9 (2021).

74. Mills, B. J. W., Watson, A. J., Goldblatt, C., Boyle, R. & Lenton, T. M. Timing of Neoproterozoic glaciations linked to transport-limited global weathering. *Nat. Geosci.* **4**, 861–864 (2011).

75. Molnar, P. & England, M. H. Late Cenozoic uplift of mountain ranges and climate: chicken or egg? *Nature* **346**, 29–34 (1990).

76. Montañez, I. P. Modern soil system constraints on reconstructing deep-time atmospheric CO2. *Geochim. Cosmochim. Acta* **101**, 57–75 (2013).

77. Montañez, I. P. & Poulsen, C. J. The late Paleozoic ice age: An evolving paradigm. *Annu. Rev. Earth Planet. Sci.* **41**, 629–656 (2013).

78. Montgomery, D. R. & Brandon, M. T. Topographic controls on erosion rates in tectonically active mountain ranges. *Earth Planet. Sci. Lett.* **201**, 481–489 (2002).

79. Morris, J. L. *et al.* Investigating Devonian trees as geo-engineers of past climates: Linking palaeosols to palaeobotany and experimental geobiology. *Palaeontology* **58**, 787–801 (2015).

80. Nesbitt, H. W. & Young, G. M. Early Proterozoic climates and plate motions inferred from major element chemistry of lutites. *Nature* **299**, 715–717 (1982).

81. Nordt, L., Atchley, S. & Dworkin, S. I. Paleosol barometer indicates extreme fluctuations in atmospheric CO_2 across the Cretaceous-Tertiary boundary. *Geology* **30**, 703–706 (2002).

82. Nordt, L., Tubbs, J. & Dworkin, S. Stable carbon isotope record of terrestrial organic materials for the last 450 Ma yr. *Earth-Science Rev.* **159**, 103–117 (2016).

83. Och, L. M. & Shields-Zhou, G. A. The Neoproterozoic oxygenation event: Environmental perturbations and biogeochemical cycling. *Earth-Science Rev.* **110**, 26–57 (2012).

84. Olson, S. L., Kump, L. R. & Kasting, P. J. Quantifying the areal extent and dissolved oxygen concentrations of Archean oxygen oases. *Chem. Geol.* **362**, 35–43 (2013).

85. Ossa, F. *et al.* Limited oxygen production in the Mesoarchean ocean. *Proc. Natl. Acad. Sci.* **116**, 6647–6652 (2019).

86. Pastor-Galán, D., Nance, R. D., Murphy, J. B. & Spencer, C. J. Supercontinents: Myths, mysteries, and milestones. *Geol. Soc. Spec. Publ.* **470**, 39–64 (2019).

87. Pawlik, Ł. *et al.* Impact of trees and forests on the Devonian landscape and weathering processes with implications to the global Earth's system properties–A critical review. *Earth-Science Rev.* **205**, (2020).

88. Planavsky, N. J. *et al.* Evidence for oxygenic photosynthesis half a billion years before the Great Oxidation Event. *Nat. Geosci.* **7**, 283–286 (2014).

89. Planavsky, N. J. *et al.* Low mid-Proterozoic atmospheric oxygen levels and the delayed rise of animals. *Science* **346**, 635–638 (2014).

90. Planavsky, N. J. *et al.* The evolution of the marine phosphate reservoir. *Nature* **467**, 1088–1090 (2010).

91. Planavsky, N. J. *et al.* Late Proterozoic transitions in climate, oxygen, tectonics, and the rise of complex life. in *Earth-Life Transitions: Paleobiology in the Context of Earth System Evolution* (eds. Polly, P. D., Head, J. J. & Fox, D. L.) **21**, 1–36 (The Paleontological Society, 2015).

92. Poulton, S. W. & Canfield, D. E. Ferruginous conditions: A dominant feature of the ocean through Earth's history. *Elements* **7**, 107–112 (2011).

93. Raiswell, R. *et al.* The iron paleoredox proxies: A guide to the pitfalls, problems and proper practice. *Am. J. Sci.* **318**, 491–526 (2018).

94. Raymo, M. E. & Ruddiman, W. F. Tectonic forcing of late Cenozoic climate. *Nature* **359**, 117–122 (1992).

95. Reinhard, C. T. *et al.* The impact of marine nutrient abundance on early eukaryotic ecosystems. *Geobiology* **18**, 139–151 (2020).

96. Reinhard, C. T., Planavsky, N. J., Olson, S. L., Lyons, T. W. & Erwin, D. H. Earth's oxygen cycle and the evolution of animal life. *Proc. Natl. Acad. Sci.* **113**, 8933–8938

(2016).

97. Reinhard, C. T. *et al.* Evolution of the global phosphorus cycle. *Nature* **541**, 386-389 (2017).

98. Retallack, G.J. Soils of the past: An introduction to paleopedology. Oxford, United Kingdom. 2001.

99. Richey, J. D. *et al.* Influence of temporally varying weatherability on CO2-climate coupling and ecosystem change in the late Paleozoic. *Clim. Past* **16**, 1759–1775 (2020).

100. Rico, K. I., Sheldon, N. D., Gallagher, T. M. & Chappaz, A. Redox Chemistry and Molybdenum Burial in a Mesoproterozoic Lake. *Geophys. Res. Lett.* **46**, 5871–5878 (2019).

101. Rico, K. I. & Sheldon, N. D. Nutrient and iron cycling in a modern analogue for the redoxcline of a Proterozoic ocean shelf. *Chem. Geol.* **511**, 42–50 (2019).

102. Ronov, A. B., Khain, V. E., Balukhovsky, A. N. & Seslavinsky, K. B. Quantitative analysis of Phanerozoic sedimentation. *Sediment. Geol.* **25**, 311–325 (1980).

103. Rye, R. & Holland, H. D. Paleosols and the evolution of atmosopheric oxygen: a critical review. *Am J Sci* **298**, 621–672 (1998).

104. Sahoo, S. K. *et al.* Ocean oxygenation in the wake of the Marinoan glaciation. *Nature* **489**, 546–549 (2012).

105. Sánchez-Baracaldo, P. & Cardona, T. On the origin of oxygenic photosynthesis and Cyanobacteria. *New Phytol.* **225**, 1440–1446 (2020).

106. Schrag, D. P., Berner, R. A., Hoffman, P. F. & Halverson, G. P. On the initiation of a snowball Earth. *Geochemistry, Geophys. Geosystems* **3**, 1–21 (2002).

107. Scott, C. *et al.* Tracing the stepwise oxygenation of the Proterozoic ocean. **452**, 27–31 (2008).

108. Sheldon, N. D. Precambrian paleosols and atmospheric CO_2 levels. *Precambrian Res.* **147**, 148–155 (2006).

109. Sheldon, N. D., Retallack, G. J. & Tanaka, S. Geochemical Climofunctions from North American Soils and Application to Paleosols across the Eocene-Oligocene Boundary in Oregon. *J. Geol.* **110**, 687–696 (2002).

110. Sperling, E. A., Halverson, G. P., Knoll, A. H., Macdonald, F. A. & Johnston, D. T. A basin redox transect at the dawn of animal life. *Earth Planet. Sci. Lett.* **371**–**372**, 143–

155 (2013).

111. Stinchcomb, G. E. *et al.* A data-driven spline model designed to predict paleoclimate using paleosol geochemistry. *American Journal of Science* **316**, 746-777 (2016).

112. Stumpf, A. R. *et al.* Glacier meltwater stream chemistry in Wright and Taylor Valleys, Antarctica: Significant roles of drift, dust and biological processes in chemical weathering in a polar climate. *Chem. Geol.* **322**–**323**, 79–90 (2012).

113. Tabor, N. J., Montañez, I. P., Scotese, C. R., Poulsen, C. J. & Mack, G. H. Paleosol archives of environmental and climatic history in paleotropical western Pangea during the latest Pennsylvanian through Early Permian. *Geol. Soc. Am. Spec. Pap.* **2441**, 291–303 (2008).

114. Tessin, A., Chappaz, A., Hendy, I. & Sheldon, N. Molybdenum speciation as a paleo-redox proxy: A case study from Late Cretaceous Western Interior Seaway black shales. *Geology* **47**, 59–62 (2019).

115. Tyrrell T. The relative influences of nitrogen and phosphorus on oceanic primary production. *Nature* **400**, 525–531 (1999).

116. Voice, P. J., Kowalewski, M. & Eriksson, K. A. Quantifying the Timing and Rate of Crustal Evolution: Global Compilation of Radiometrically Dated Detrital Zircon Grains. *J. Geol.* **119**, 109–126 (2011).

117. Wallace, M. W. *et al.* Oxygenation history of the Neoproterozoic to early Phanerozoic and the rise of land plants. *Earth Planet. Sci. Lett.* **466**, 12–19 (2017).

118. Wei, W. & Algeo, T. J. Secular variation in the elemental composition of marine shales since 840 Ma: Tectonic and seawater influences. *Geochim. Cosmochim. Acta* (2020).

119. Wellman, C. H. & Strother, P. K. The terrestrial biota prior to the origin of land plants (embryophytes): A review of the evidence. *Palaeontology* **58**, 601–627 (2015).

120. Willenbring, J. K. & Von Blanckenburg, F. Long-term stability of global erosion rates and weathering during late-Cenozoic cooling. *Nature* **465**, 211–214 (2010).

121. Yang, W., Holland, H. D. & Rye, R. Evidence for low or no oxygen in the late Archean atmosphere from the 2.76 Ga Mt. Roe #2 paleosol, Western Australia: Part 3. *Geochim. Cosmochim. Acta* **66**, 3707–3718 (2002).

122. Zaffos, A., Finnegan, S. & Peters, S. E. Plate tectonic regulation of global marine animal diversity. *Proc. Natl. Acad. Sci. U. S. A.* **114**, 5653–5658 (2017).

123. Zbinden, E. A., Holland, H. D., Feakes, C. R. & Dobos, S. K. The sturgeon falls paleosol and the composition of the atmosphere 1.1 Ga BP. *Precambrian Res.* **42**, 141–163 (1988).

Chapter 2
Weathering Intensity and Presence of Vegetation Are Key Controls on Soil Phosphorus Concentrations: Implications for Past and Future Terrestrial Ecosystems[1]

2.i Abstract

Phosphorus (P) is an essential limiting nutrient in marine and terrestrial ecosystems. Understanding natural and anthropogenic influence on P concentration in soils is critical for predicting how its distribution in soils may shift as climate changes. While it is known that P is sourced from bedrock weathering, relationships between weathering, P, and other soil-forming factors have not been quantified at continental scales, limiting our ability to predict large-scale changes in P concentrations. Additionally, while we know that Fe oxide-associated P is an important P phase in terrestrial environments, the range in and controls on soil Fe concentrations and species (*e.g.*, Fe in oxides, labile Fe) are poorly constrained. Here, we explore the relationships between soil P and Fe concentrations, soil order, climate, and vegetation in over 5000 soils, and Fe speciation in ca. 400 soils. Weathering intensity has a nuanced control on P concentrations in soils, with the range in P concentrations peaking at intermediate weathering intensities (CIA~60). The presence of vegetation (but not plant functional type) affected soils' ability to accumulate P. Contrary to expectations, P was not more strongly associated with Fe in oxides than other Fe phases. These results are useful both for predicting changes in potential P fluxes from soils to rivers under climate change and for reconstructing changes in terrestrial nutrient limitations in Earth's past. In particular, soils' tendency to accumulate more P with the presence of vegetation suggests that biogeochemical models invoking the evolution and spread of land plants as a driver for increased P fluxes in the geological record may need to be revisited.

[1] *This chapter is published as Dzombak and Sheldon (2020) in Soil Systems 4(4), 73.*

2.1 Introduction

Phosphorus (P) is an essential, often limiting nutrient in ecosystems across the globe [1,2]. P has been studied in plants, soils, rivers, lakes, and oceans – both modern and ancient – and is at the center of critical questions about Earth's past and future. Today, concerns around P in terrestrial settings focus on soil fertility and crop yields, as well as on agricultural runoff and its effect on eutrophication [3-5]. Climate, vegetation, and weathering and erosion rates are inextricably linked, so in order to improve quantitative constraints on potential P fluxes from soils, each of these factors must be considered. The redox-sensitive metal iron (Fe) is often associated with both P and organic matter/carbon (C) in soils (*e.g.*, [6-9]). The P-Fe oxide pathway is critical for terrestrial P transport; however, it is currently less well-understood than other aspects of terrestrial P cycling, such as P-C associations. Additionally, while much research linking P, weathering, and soil age has been done, such work has typically done on relatively small scales (*e.g.*, chronosequences in Hawai'i) relative to the global scale of the questions that we ask here. Therefore, constraining climate, vegetation, and weathering controls on soil P and Fe is critical for predicting changes to fluxes of P from soils to rivers and beyond, and to improving our understanding of how regional soil fertility may evolve in response to a changing climate.

Prior to the evolution and expansion of land plants, changes in the flux of P from continents to oceans are thought to have been a primary control on marine productivity, and consequently, on the concentration of oxygen in the atmosphere [10,11]. It remains debated whether land plants' colonization of continents would have increased [12] or decreased [13] that P flux. The better we understand the modern distribution of and controls on P in soils, the better we can model global biogeochemical changes in Earth's past.

P, Fe, and weathering and erosion

P is released from bedrock via the weathering of P-bearing minerals (primarily apatites, which are Ca minerals relatively resistant to weathering; [4]). Weathering depends on all soil-forming factors (climate, biology, topography, time, parent material), but is primarily controlled by climate (*e.g.*, precipitation, temperature, seasonality) and time (surface age, length of exposure; [14]). Organic matter also serves as an important pool of P in soils ([4,5]), and vegetation, fungi, and microbial life play an important role in both P and Fe liberation and mobilization through symbiotic (mycorrhizal) relationships [15,16]. The presence of plants, then,

changes how both P and Fe are distributed in soils - but the links between landscape-scale soil chemistry, plant functional type, climate, and weathering intensity have not been quantified.

P can be depleted from a soil profile within thousands to tens of thousands of years [4, 17, 18, 19, 20]. In terrestrial vegetation (biomass), P's residence time is ~13 years, and residence in soil is ~600 years without P replenishment by dust [4]. Soil P can be also replenished through dust deposition (*e.g.*, [17, 21, 22]). The natural progression of a soil, with a slow accumulation of Fe and Al oxides and a loss of mobile cations and nutrients, means that P is typically very low in old and/or intensely weathered soils [19]. Other soil properties, such as clay content, are also linked to weathering and vegetation, and could affect the concentrations of both P and Fe. Clay minerals and clay grain-size fractions can sorb considerable amounts of P and Fe, and clay content typically increases with weathering time and/or intensity [23,24]. Weathering intensity is expected to decrease with latitude due to colder temperatures, drier precipitation regimes, and less vegetation and shallower rooting depths [23,24]. Additionally, because the potential volume of erodible material generally increases as weathering intensity increases (though varies with factors like slope and uplift rate; *e.g.*, [25-29], weathering is linked to P fluxes not only through direct apatite dissolution, but also through erosion rates (*e.g.*, [30,31]). Understanding how weathering intensity is related to soil P (and Fe) concentrations is important for predicting how their erosional fluxes and transport may change in response to climate change (*e.g.*, [30,31]).

After weathering, dust deposition is an important secondary source of P, particularly for old soils whose P has been depleted through weathering, erosion, and biological use. For example, chronosequence studies in Hawaii have shown that for older soils, dust replenishment of P is critical to maintaining fertility once bedrock sources have been depleted [17,32,33]. Dust is also a critical source of P in the Amazon basin, which receives significant dust fluxes from Africa [18,34-36], compensating for P loss in deeply weathered tropical soils. Dust-sourced P is less significant for areas that receive little dust deposition, for younger soils that still have a regular input of P from bedrock weathering, or for shorter timescales than either for significant dust accumulation or timescales of soils losing their bedrock-sourced P (*i.e.*, anthropogenic timescales). Arvin et al. [21] found that dust deposition is an important P source in montane soils, despite their relatively "fresh" bedrock. The balance between weathering rate and dust accumulation is also relevant for determining how important the latter is in soil P [22]. Dust is also commonly a source of Fe oxides, increasing soil fertility [35,37,38].

P and Fe kinetics in soils

P and Fe are chemically associated in soils in part because of P's affinity to sorb to Fe (oxyhydr)oxides (*e.g.*, [4,9,39,40,41,42]). Orthophosphate, the common ion form of free P in soils, is reactive towards those oxides and becomes immobile (not readily bioavailable) when they associate into neoformed minerals or are sorbed onto existing mineral surfaces. Fe-bound P may be a critical mode of P transport among terrestrial ecosystems and from terrestrial/aquatic to marine environments, as oxyhydroxide-bound P is one of the major bioavailable/exchangeable forms of P in fluvial systems [5].

While we know that Fe oxide-adsorption of P is kinetically favorable in soils and other environments where P is being exchanged (*e.g.*, [43-45]), our understanding of first-order controls on Fe concentration and speciation (*i.e.*, Fe^{3+} in oxides versus labile Fe^{2+}) in soils could be improved. Examining a full suite of extractable Fe (rather than only dithionite-citrate and/or ammonium oxalate) allows a more nuanced picture of Fe phases in soils, which can ultimately be linked to variable P mobility in different soil redox conditions [43, 46, 47]. It is possible that regional climate factors (precipitation, temperature) exert control on Fe speciation (*i.e.*, reduced vs. oxidized) in soils via soil moisture. Controls on soil moisture are debated and likely vary from profile to profile [48-53], and pH (related to soil pore space saturation; often microbially-mediated) is a primary control on reduction/oxidation of Fe phases in soils (*e.g.*, [54]). Additionally, soil porewaters can serve as an intermediate step between recalcitrance and fluvial suspension for dissolved constituents (*e.g.*, [54, 55]). Exploring these relationships is key for understanding the likelihood of P mobilization under different moisture situations.

P and Fe in the geologic record

Geologists are interested in constraining many of the processes described above in ancient soils and ecosystems. Weathered P, transported to the oceans via fluvial networks and continental drainage, is typically invoked as a first-order control on marine primary productivity, which is associated with C sedimentation, atmospheric CO_2 drawdown, and oxygen production (*e.g.*, [10, 11, 56]). Like P, Fe can stimulate marine productivity on short timescales (*e.g.*, [57-60]), but it is of additional interest because in the past, it served as a P sorption site in marine

systems, effectively sequestering P so that it is not bioavailable (the so-called “Fe-P trap”) and limiting marine productivity [10].

With these processes in mind, geologists are interested in continent-to-ocean fluxes and mobility of Fe and P through time. However, the continent-to-ocean transport of P, although central to many biogeochemical models, is usually prescribed and not based on actual changes in fossil soil (paleosol) P values or weathering intensity data. Rather, it has been generalized based on crustal P values and fluxes controlled by large-magnitude changes, such as global glaciations or limited modern observations (*e.g.*, [61]). The value in providing robust constraints on the range and distribution of P in soils, as well as climatic and environmental controls on its mobility and bioavailability, will vastly improve the parameters for these models.

In addition to biogeochemical models, geologists are interested in how the evolution of terrestrial vegetation and mycorrhizae (fungal root symbionts) affected P bioavailability, terrestrial mobility, and fluxes to the oceans. Researchers have argued for both an increase [12, 56, 62, 63] and decrease [13,15] in P fluxes to the oceans following the spread of land plants. Constraining how modern vegetation relates to soil P mobility and distributions will help to answer this question.

Finally, the geochemical composition of fossil soils is used to reconstruct a range of climatic and environmental changes; however, these tools are primarily based on small datasets. This work provides ranges of reasonable values for soil chemistries under known environmental and atmospheric conditions, providing critical background information to improve our paleoclimate and paleoenvironment reconstructions.

This work

In the context of these concerns, several big-picture questions remain. Despite much research on P in modern soils, ecosystem (vegetation, anthropogenic impact) and climate (precipitation, weathering) controls on its concentration have not been quantified on landscape to continental scales for generalizable conclusions. Additionally, although P is known to have a strong affinity towards Fe (oxyhydr)oxides in soils, Fe species and soil redox conditions have not been considered as potential first-order controls on landscape-scale P bioavailability. Questions about how climate (precipitation, temperature), soil factors (drainage, soil moisture, clay content), and overall weathering intensity affect soil Fe-P associations needs to be interrogated,

to see if Fe species ultimately serves as a mediator for P bioavailability. And finally, once the distribution of and controls on soil P have been quantified, how do those new constraints affect (our understanding of) or (constraints on) biogeochemical P models in Earth's past?

We address these questions, along with hypotheses about P in the geologic record, using a large geochemical database of modern soils (n > 5000). The results can inform models of both past and future terrestrial biogeochemical cycles.

2.2 Materials and Methods

Sampling

Soil samples were collected in the field by the authors, and received from the USDA KSSL soil repository, and from contributors (total n = 404). A majority (n = 247) of these samples are B horizons and therefore reflect longer-term, stable pools of P (*e.g.*, P sorbed to clays or Fe (oxyhydr)oxides, which we test for here, or recalcitrant organic matter) and Fe. These soils include Entisols, Inceptisols, Alfisols, Ultisols, Histosols, Mollisols, and Aridisols and provide coverage from low (Hawaii) to high (Iceland) northern latitudes (Figure A1). Soils collected in the field or from repositories were screened for anthropogenic influence (*i.e.*, on developed or disturbed land), with anthropogenically-altered soils noted as such and binned separately in our treatments of the data here. To complement these soils, we used the USGS soil geochemistry interactive report [86] and collated geochemical data for the Top 5 cm, A horizons, and C horizons of all the soils included in that work (n = 4857). See Table A1 for summary descriptions of these two datasets, and Table A2 for complete sample information for the new dataset presented here. Geochemical data for the USGS dataset [64] are available at https://doi.org/10.3133/sir20175118.

Combining these soil databases yields excellent spatial, climatological, profile depth, drainage, vegetation (as plant functional type/generalized biome), and soil order coverage (Figure A1). While the samples are mostly from the United States, variation in soil forming factors across the continent reflect most of the potential global variation. The tropics are somewhat under-sampled, but data from Hawai'i are broadly reflective of those latitudes. While there are species-specific relationships between plants and soil geochemistry, generalized biome is acceptable for the continental scale of questions examined in this work, as well as the

relative/comparative nature of our inquiries (*e.g.*, [65-68]). Differences between plant functional types typically swamp differences within one plant functional type. Additionally, because biomes on sub-continental scales are typical for global biogeochemical models, and because more specific data are not available for the latitudinal scale of this work, generalizing by biome scale/plant functional type is appropriate.

Geochemical analyses

All analyses were performed on dry soils within the Sheldon lab, as were samples during the USGS analyses. Soils were dried per USDA APHIS regulations upon import and ground to <70μm for homogeneity during analyses; samples were stored dry in oxic (ambient room) conditions. (During experimental design, tests of pre- and post-drying, with drying temperatures varying between 25, 50, and 100°C showed no significant geochemical differences.) Bulk elemental geochemistry was performed at ALS Laboratories in Vancouver, BC, using a four-acid digestion and ICP-MS analysis. External precision was 0.01% for all major elements and 10 ppm for P_2O_5, analyzed at ALS. For samples from the USGS dataset, 1σ sample errors were 488 ppm and 1.39 wt% for P_2O_5 and total Fe, respectively) [64]. 1σ sample errors for total C and organic C were 4.6% (n.d. for inorganic C [64]).

To analyze Fe speciation in soils, we used a four-step sequential Fe extraction following Poulton and Canfield [69] and Raiswell et al. [70]. This extraction protocol separates operationally-defined pools as ascorbic acid (labile Fe; Fe_{asc}), dithionite- (crystalline Fe oxyhydroxides; Fe_{dith}), ammonium oxalate- (highly crystalline Fe oxyhydroxides; Fe_{ox}), and sodium acetate-extractable Fe (Fe in carbonates, analyzed separately from the sequential extraction; Fe_{acet}). Initially, we included a chromium-reducible sulfur (CRS; [71]) extraction separately to analyze for Fe sulfides (*e.g.*, pyrite), but those concentrations were below detection limit for all non-wetland soils. CRS was limited to wetland soils after the initial exploratory extractions, and raw values were normalized to average soil order densities to account for the large difference in density between Histosols and denser, more mineral-rich soil orders [72]. Sample supernatants were centrifuged and diluted 50x, and Fe was measured via ICP-OES and ICP-MS at the University of Michigan.

An internal standard of a local soil, dried at three different temperatures, was included in all runs for inter-run consistency checks and to determine reproducibility. The absolute standard

deviation for a sample's reproducibility depends on the concentration of each Fe species, so relative percent error ($(\sigma/\mu)*100$) is used instead. Repeated analyses show that Fe_{asc} is reliable within 3.7% of the mean, Fe_{dith}, within 1.7% of the mean, and Fe_{ox}, within 7.0% of the mean. Reproducibility on the Fe_{acet} samples was larger, at 15% of the mean, because the means in many of the samples we analyzed were near machine detection limits (~1000 ppm), where a difference of several hundred ppm yields far larger standard deviations than species with higher concentrations. The Fe_{asc} pool is considered to be a low constraint because a larger proportion of labile Fe may be in a soil's porewater (rather than solids). Because here we are primarily interested in relative differences between oxide and labile Fe species, and because species' concentrations tend to differ by orders of magnitude, we have deemed this approach acceptable. For further reading on nuances in sample preparation and extraction protocols, see two recent reviews by Raiswell et al. [73] and Algeo and Liu [74].

Fe speciation data were filtered for outliers by removing any samples where Fe_{spec} weight percent > total Fe weight percent (*i.e.*, the concentration of a measured Fe pool was higher than the measured total Fe). These discrepancies (n = 107, 95, 139, 106, for Fe_{asc}, Fe_{acet}, Fe_{dith}, and Fe_{ox}, respectively) likely arose from the 50x-dilution being insufficient, with high Fe concentrations overwhelming the ICP-OES, leading to erroneous measurements. Future work using Fe speciation on soils should consider using stronger dilution factors for high-Fe soils to circumvent instrument limitations.

Other data collated

Geochemical data for the Top 5 cm, A horizons, and C horizons from 4857 soils around the U.S. are available on an interactive portal [86]. Weathering-relevant cations (Al, Ca, Na, K) and the nutrients of interest (P, Fe) along with latitude and total clay content (clay: A and C horizons only) were compiled. For the USGS dataset, clay content was determined by XRD (for 10 and 14Å clays only). Organic, inorganic, and total carbon data were available for a majority of soils in A and C horizons in the USGS dataset (not all had inorganic carbon). It should be noted that a dry soil sample will have a higher relative weight percent organic carbon due to water loss during drying. Soil orders and drainage capability are not given for soils in this database, but because they span the conterminous U.S., it is a reasonable assumption that they include a variety of soil orders. Clay content as grain-size fraction, parent material, and soil

moisture regime were also gathered for the newly-collected dataset from USDA Soil Series reports when available (Table A2).

Climate data were gathered from Soil Series pages or, when not available, the PRISM 30-year averages (1981–2010) were used. If neither Soil Series nor PRISM climate data were available (*i.e.*, for non-US samples), country-specific governmental meteorological data or journal articles were used (see Table A2 for details).

The Chemical Index of Alteration (CIA)[75] was calculated to assess the degree of weathering for each soil, which reflects all of the soil-forming factors to some degree, but predominantly soil age and climate [14]. CIA is thought to reflect the weathering of feldspars to form clay minerals where high values represent more intense weathering. Molar oxide ratios are used (Equation 1). The CIA of an individual soil may not correspond directly with the CIA values of sediments in rivers (*e.g.*, [76]). However, because our soils' average CIA values (59 ±15, 42±32, and 57±21for A, B, and C horizons, respectively) are within 1σ of the North American rivers' average from that study (n = 7; mean CIA = 66 ±8.5, range 53–73) though with larger ranges (0.5 to 99 for all three horizons), we proceed with its use here.

$$CIA = (Al_2O_3/(Al_2O_3+CaO+NaO+K_2O)) * 100 \quad \text{(Eq 2.1)}$$

Statistical analyses

To examine how total Fe and P correlate with CIA (weathering intensity), a running average with a 10-CIA-unit window was used. Linear least-squares regressions were used to test for significant linear correlations where appropriate, based on the hypotheses that were being tested. Due to the large size of the USGS dataset, *p*-values are extremely low ($<10^{-16}$; essentially 0), meaning it is highly likely that the two variables are not randomly correlated. Strength of correlation should be primarily considered before taking any relationships to be predictive, but for simplicity's sake, coefficients of determination (R^2 values) are reported. Principle Components Analysis (PCA) was performed for USGS database soils by horizon (Top 5 cm, A, and C). These analyses are used to test expected relationships (*e.g.*, that Fe and P will be positively and linearly related), rather than to build predictive models. All of the statistical analyses were performed in Matlab.

2.3 Results

Complete sample information and all geochemical results are found in Supplemental Tables 2–5 and are available in the online version of this paper. For the larger USGS dataset [64], we have geochemical, drainage, and vegetation (generalized plant functional type) data, but no soil order or Fe speciation information. Results for soil order, drainage, parent material, and Fe speciation analyses are based only on the newly collected dataset (n = 404).

2.3.1 Fe and P: Concentrations, soil order, and vegetation

Phosphorus

The average total P concentration (referred to simply as "P" here onwards) in the continental crust is ca. 870 ppm P, and there is relatively little variation between bedrock lithologies [77]. The maximum soil P concentration in this compilation was >20,000 ppm (>2 wt%; C horizon of an anthropogenically-modified soil), an order of magnitude greater than the crustal average. Mean P concentrations for each horizon studied were depleted relative to the crustal average: Top 5 cm, A, and C horizons means were 660, 632 and 508 ppm P, respectively (USGS data), and B horizons from the new dataset had a mean of 937 ppm P. P concentrations vary spatially throughout the continental U.S. (Figure A2), with hotspots in a variety of different geologic, climatic, and biologic provinces. P concentrations varied among soil orders (Figure 2.1), with the highest concentrations in Inceptisols (Figure 2.1a), a relatively weakly-developed soil type.

The vegetation groups are Barren (lacking vegetation), Altered (*i.e.*, affected by human activity), Forest (no differentiation between deciduous and coniferous), Herbaceous/Grassland, Developed/Cultivated (*i.e.*, occupied or manicured), Shrubland, and Other (mostly including early-succession plants or microbial earths). For USGS samples, protocols dictated that roads, buildings, and industrial sites be avoided [64]. Among vegetation types, there is little variability between P concentrations and vegetation types (Figure 2.2); while Barren landscapes' B horizons show higher mean P, this is likely due to small bin size (n = 5; Figure 2.2c). Overall, variability in concentrations in different vegetation types and soil orders was minimal, with most soils being depleted in P relative to the crustal average. Vegetated soils (both natural and anthropogenically-altered) had higher ranges of P than unvegetated (Barren). There was a weak positive correlation with mean annual precipitation (Figure A3a), but the range of P values at a given precipitation

amount is typically too large (~1500 ppm) to be of predictive use. This trend could also be explained by related factors, such as vegetation coverage (cover versus bare ground) and weathering intensity, which are associated with precipitation.

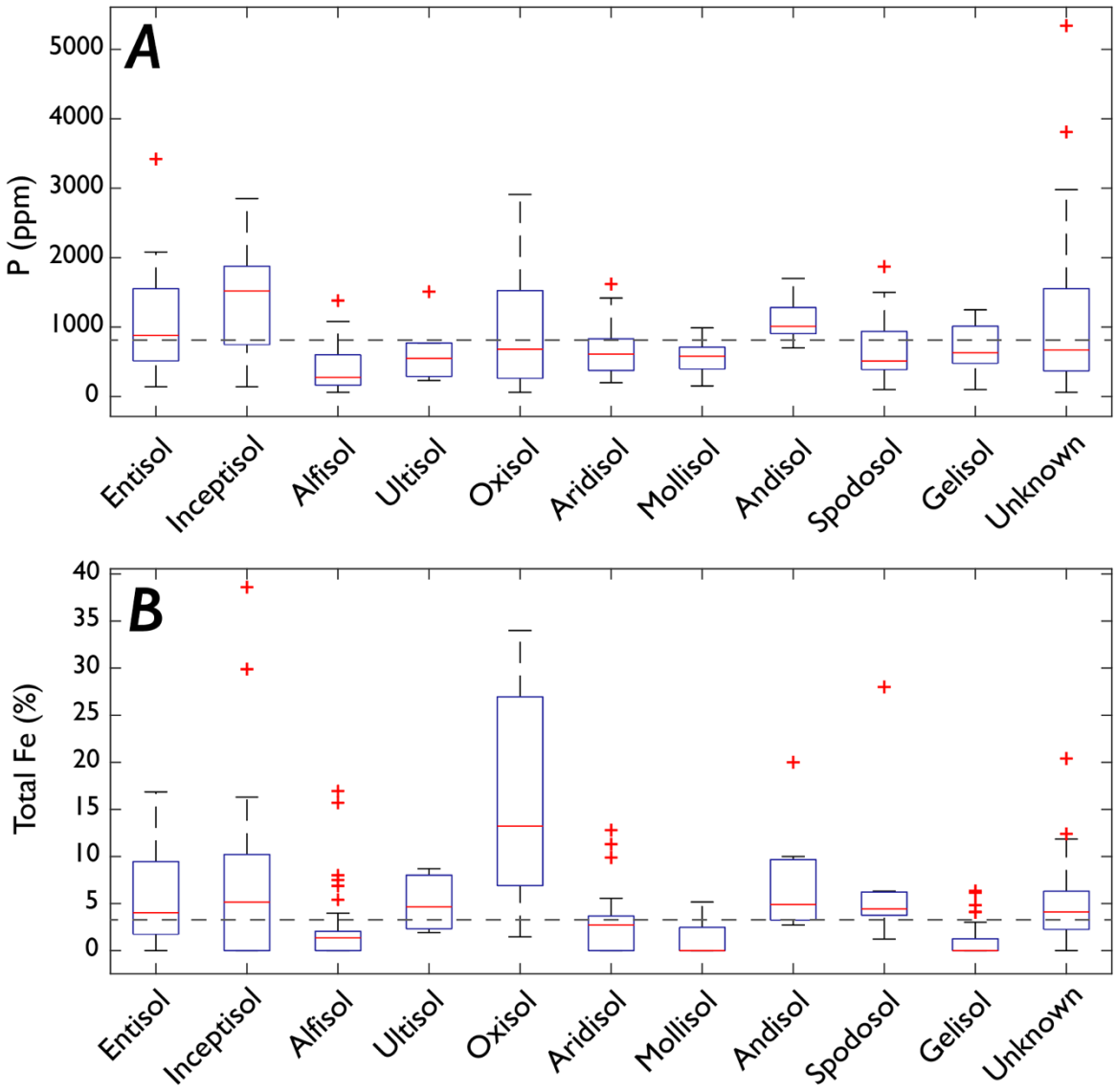

Figure 2.1. P and Fe in modern B horizons, by soil order.

P and Fe concentrations in modern soils' B horizons, binned by soil order. Red lines are median values, blue bins are 25th and 75th quartile, and red crosses are beyond the 75th quartile; the horizontal dashed gray line is the crustal average (870 ppm P and 3.5% Fe)[77]. (A) P concentrations, showing that younger soils (Entisols, Inceptisols) tend to have higher P than older soils (Alfisols, Ultisols). Oxisols have high ranges of P, but a much smaller bin size than other orders (n = 8). Andisols have high inherited P from volcanic parent materials. (B) Fe concentrations, showing consistent Fe concentrations between ca. 1 and 10 wt% with the exception of Oxisols, which are defined by their high rates of Fe oxide accumulation. Bin sizes:

Entisols (44), Inceptisols (75), Alfisols (42), Ultisols (6), Oxisols (8), Aridisols (76), Mollisols (60), Andisols (15), Spodosols (9), Gelisols (30), Unknown (39).

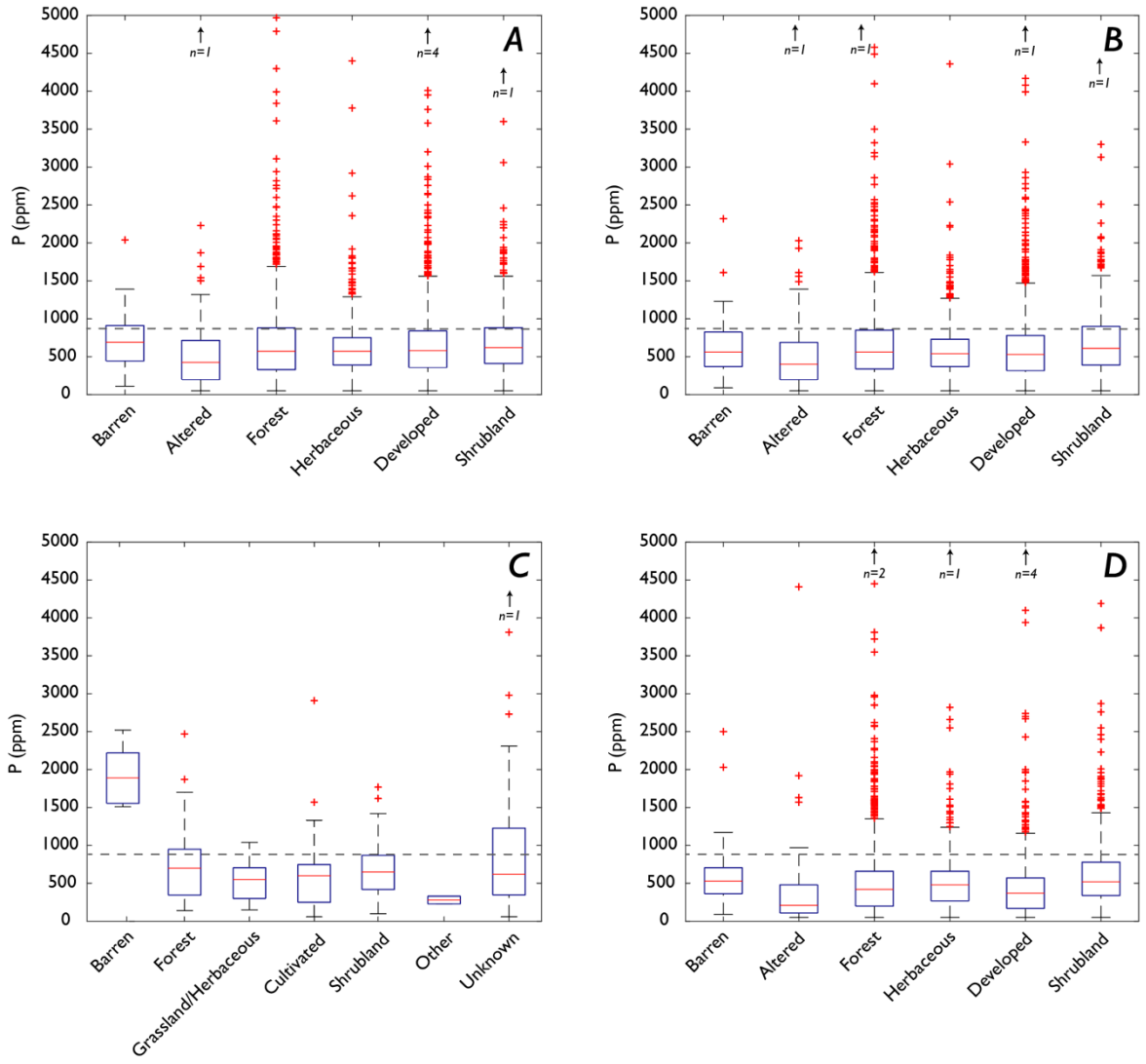

Figure 2.2. P in soils, by vegetation.

P concentrations in all horizons, binned by vegetation type. Dashed gray line in all is crustal average P (870 ppm)[77]. Arrows indicate off-plot values. (A) P in the Top 5 cm, where Barren (no vegetation) and Altered soils have the lowest range of P concentrations. (B) P in A horizons, with similar distributions to Top 5 cm. (C) P in B horizons, with much smaller bin sizes than other horizons. (D) P in C horizons. Bin sizes for (A), (B), and (D): Barren (68), Altered (209), Forest (1252), Herbaceous (815), Developed (1568), Shrubland (945). Bin sizes for (C): Forest (43), Grassland/Herbaceous (19), Shrubland (50), Barren (5), Cultivated (59), Unknown (74).

Fe

The crustal composition of total Fe (Fe_{tot}) is more variable than that of P because while P is sourced primarily by apatite-group minerals, Fe_{tot} can be present in a wide range of minerals

and lithologies. The Phanerozoic upper continental crust is estimated to have 3.5 wt% Fe [77]. Fe_{tot} averages in the soils studied here were 2.1 wt% for Top 5 cm, 1.6 wt% for A horizon, 2.6 wt% for C horizon, and 4 wt% for our dataset (primarily B horizons). Density-normalized Fe_{tot} varied slightly by soil order (Table A3), showing the expected trend of modest loss shifting to modest accumulation during the Alfisol-Ultisol transition (Figure 2.1b), but otherwise was relatively consistent. Oxisols had the highest values and range in Fe, with some variability among the other soil orders but generally consistent ranges (Figure 2.1b).

Fe_{tot} is generally consistent both within a given horizon and between different vegetation cover types (Figure 2.3). While most soil orders and most horizons had <3 wt% Fe_{tot}, values ranged up to >15% (Figure 2.3; Figure A2). The only notable variability in Fe concentrations among vegetation is in Cultivated soil B horizons (Figure 2.4c), which are depleted, and 'Other' soil B horizons that are substantially enriched relative to the other vegetation cover groups. 'Other' vegetation contains mostly basalt-parented soils from a limited geographical area (primarily Iceland), so this result is likely an artifact of our sampling. There was no strong correlation between Fe_{tot} in a soil and mean annual precipitation (R^2: 0.2; Figure A3b).

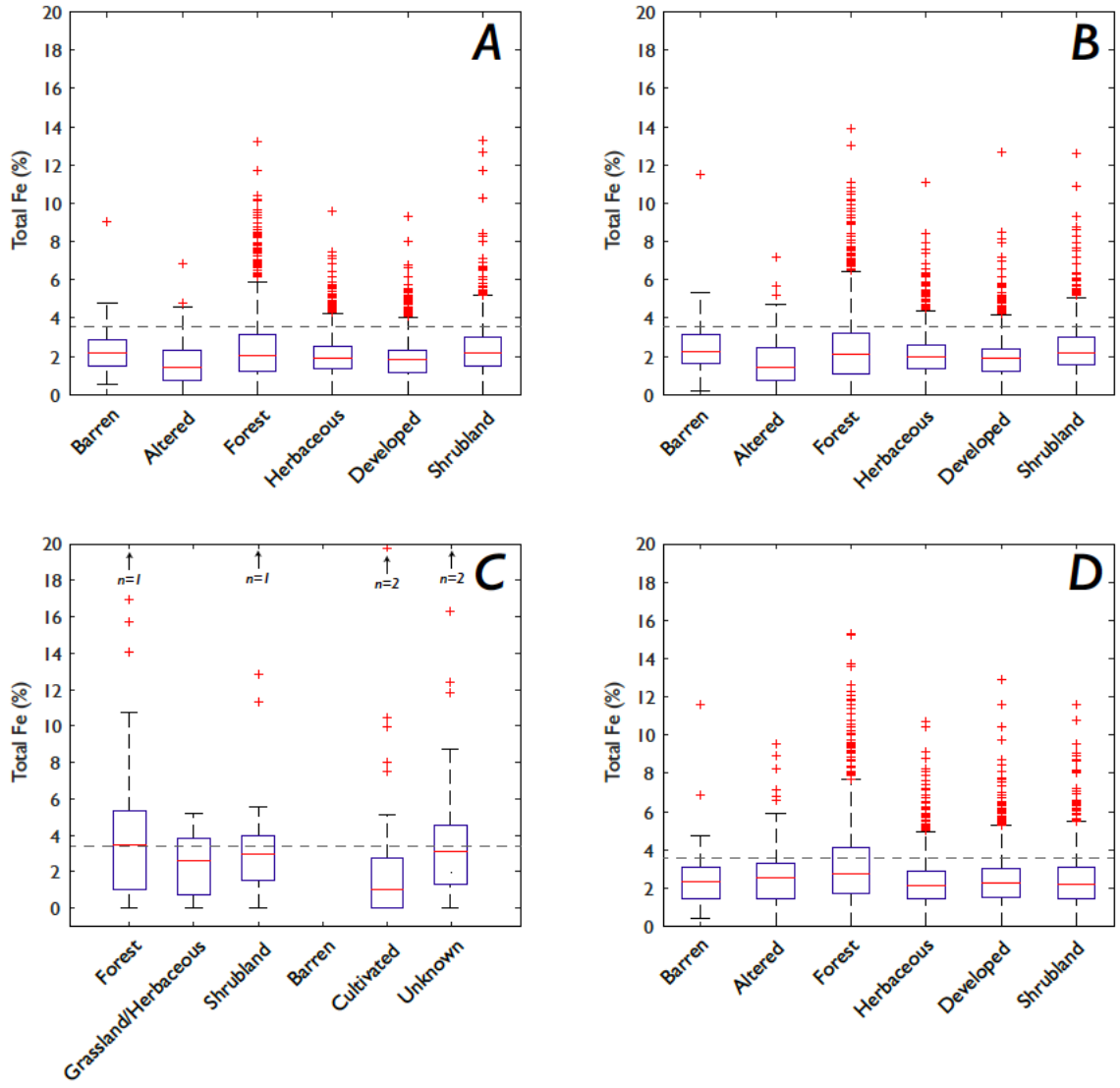

Figure 2.3. Fe in soils, by vegetation.

Fe concentrations in all horizons, binned by vegetation type. Dashed gray line in all is crustal average (3.5%)[77]. Arrows indicate off-plot values. (A) Fe in the Top 5 cm, where Barren and Altered soils have the lowest maximum Fe concentrations. (B) Fe in A horizons, with similar trends to Top 5 cm. (C) Fe in B horizons. There were no data for Barren B horizons' Fe. (D) Fe in C horizons. Bin sizes for (A), (B), and (D): Barren (68), Altered (209), Forest (1252), Herbaceous (815), Developed (1568), Shrubland (945). Bin sizes for (C): Forest (43), Grassland/Herbaceous (19), Shrubland (50), Barren (0), Cultivated (59), Unknown (74).

2.3.2 Fe and P: Latitude, weathering, soil order, and clay content

Latitude, weathering intensity, and clay content should each be associated with each other as well as with Fe (*e.g.*, [78]). Some of the trends described here could be influenced by latitudinal sampling bias, with most of the samples coming from the mid-latitudes (Figure A1;

Figure 2.4a). In the soils analyzed here, maximum weathering (as measured by CIA) decreases as latitude increases (Figure 2.4b), while clay content (a weathering product) does not show a strong trend with latitude (Figure 2.4c), with the exception of a weak mid-latitude (35–40°N) peak in clay content in some C horizons. Weathering trends between soil orders behave as expected, with CIA values increasing from Entisols to Ultisols/Oxisols (Figure 2.5). Clay content and weathering show a well-behaved and expected pattern of increase that matches the theoretical understanding of that metric [75, 79], with B horizons specifically showing the highest clay content until the highest CIA values are reached (Figure 2.4d, green points). Clay content and geochemical data were not available for the Top 5 cm subset of the USGS dataset, so that horizon is excluded from those comparisons.

Fe_{tot} content increases moderately with higher latitudes (Figure 2.6a), higher weathering (Figure 2.6c), and clay content (Figure 2.6e). P in soils behaves less linearly with respect to these variables: P increases moderately with latitude (Figure 2.6b), but rather than decreasing with weathering, as might be expected based on soil age-P relationships, average P concentrations in all horizons vary little, though there is a general increase in range at moderate weathering intensities (CIA ~40–70) (Figure 2.6d). P concentrations are weakly negatively correlated with clay content (Figure 2.6f). Fe_{tot} and P showed positive correlations with one another in all horizons, as expected (Figure A4).

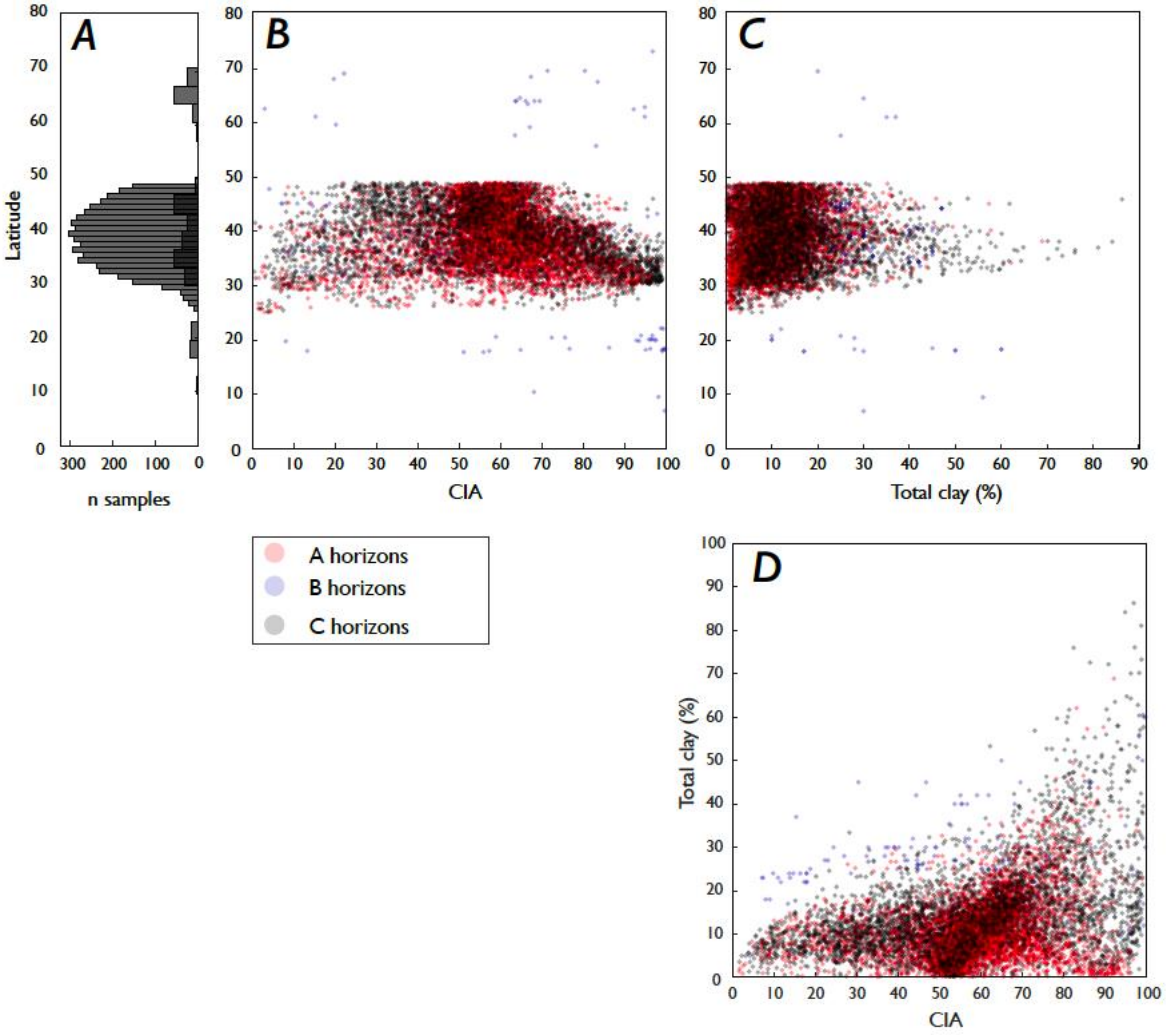

Figure 2.4. CIA and clay in soils, by latitude.

Latitudinal distribution of soils used in this study, where smaller bins represent the USGS dataset [64] and the wider bins are our soils. The range of latitudes covered here is 7° to 73°N, but most of the samples fall between 20 and 50°N. (B) Latitudinal trends in CIA. (C) Latitudinal trends in clay content. (D) Correlation between CIA and clay content (R2: 0.05, <0.01, and 0.19 for A, B, and C horizons, respectively). Overall, these results support common assumptions about the relationships between latitude and weathering.

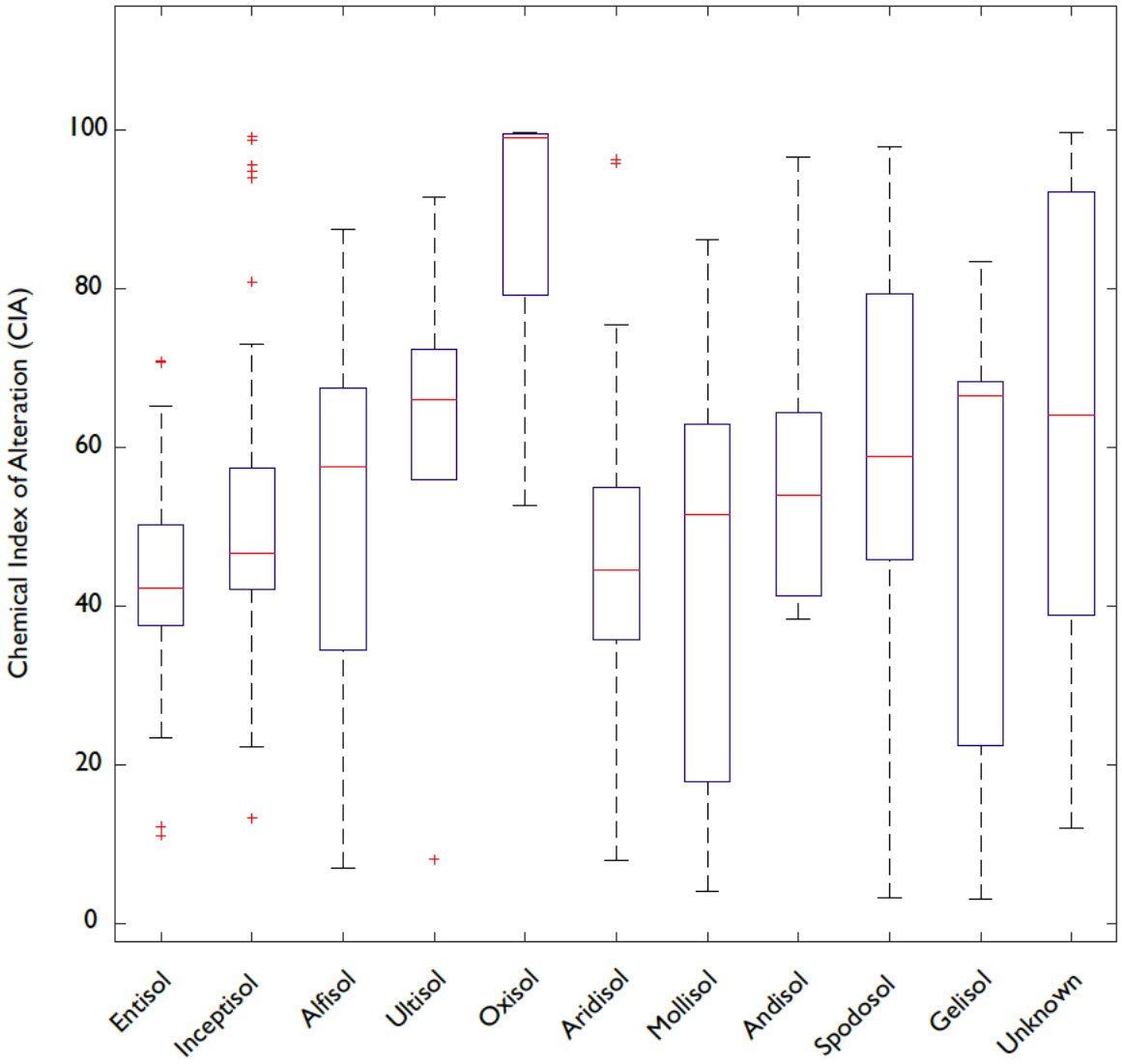

Figure 2.5. Boxplot of CIA in soils, by soil order.

Chemical Index of Alteration (CIA) binned by soil order. CIA increases through the Entisol-Ultisol soil development progression, as expected, and Oxisols have the highest CIA with a median near 100. Aridisols' median CIA falls between Entisols and Inceptisols. Bin sizes: Entisols (44), Inceptisols (75), Alfisols (42), Ultisols (6), Oxisols (8), Aridisols (76), Mollisols (60), Andisols (15), Spodosols (9), Gelisols (30), Unknown (39).

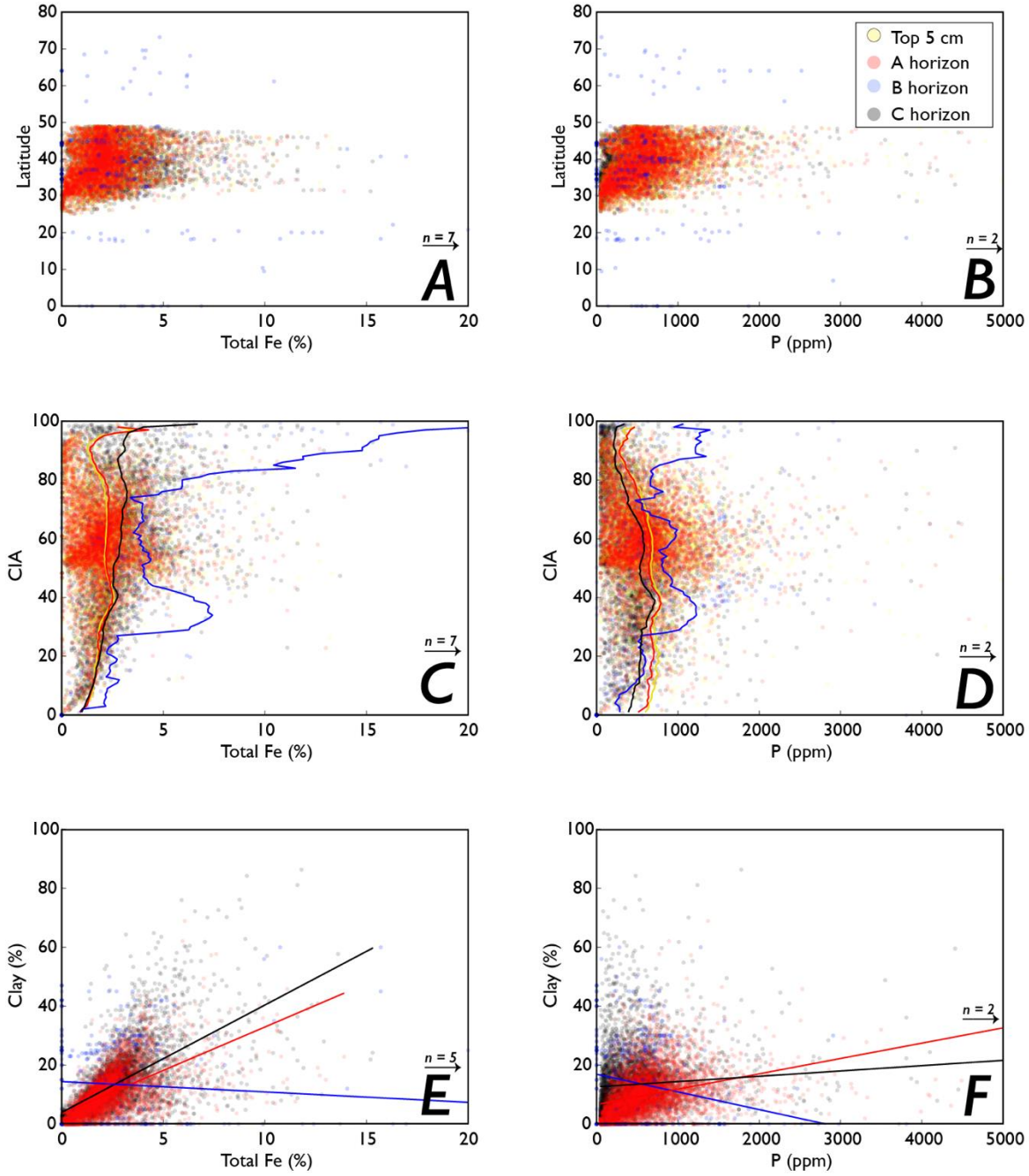

Figure 2.6. Fe, P, latitude, weathering, and clay trends.

Trends between latitude, weathering, and clay content and total Fe and P concentrations. Solid lines in (C) and (D) are running averages for Top 5 (yellow), A (red), B (blue), and C (black) horizons. Solid lines in (E) and (F) are linear least-squares regressions for A (red), B (blue) and C (black) horizons. (A) Fe in soils by latitude. (B) P in soils by latitude. (C) Fetot and weathering intensity. Solid lines are running averages (10-CIA-unit window) for each horizon; colors correspond to data colors. The B horizon average (blue line) is highest at very high CIAs due in part to lower sample density at very high CIA values, especially between 98–100. (D) P

concentrations and weathering intensity. (E) Fe and clay content (R2 is 0.34 and 0.37 for A and C horizons; 0.01 for B horizons, much smaller dataset; $p = 0.7$ for B horizon, $<<0.01$ for other horizons). Solid lines are linear least-squares regressions; B horizon (blue line) is skewed due to high-Fe, low-clay points off plot. (F) P and clay content. Solid lines are linear least-squares regressions (R2 is 0.11, 0.08, 0.01 for A, B, and C horizons respectively; $p<<0.01$ for all horizons).

2.3.3 Weathering, clay content, and vegetation

Between vegetation types, there is low variability in clay content, with Forests showing slightly lower values in B horizons than the other groups (Figure A5). Forests have the highest weathering in natural (unaltered/not developed) soils, followed by Grasslands and Shrublands (Figure 2.7).

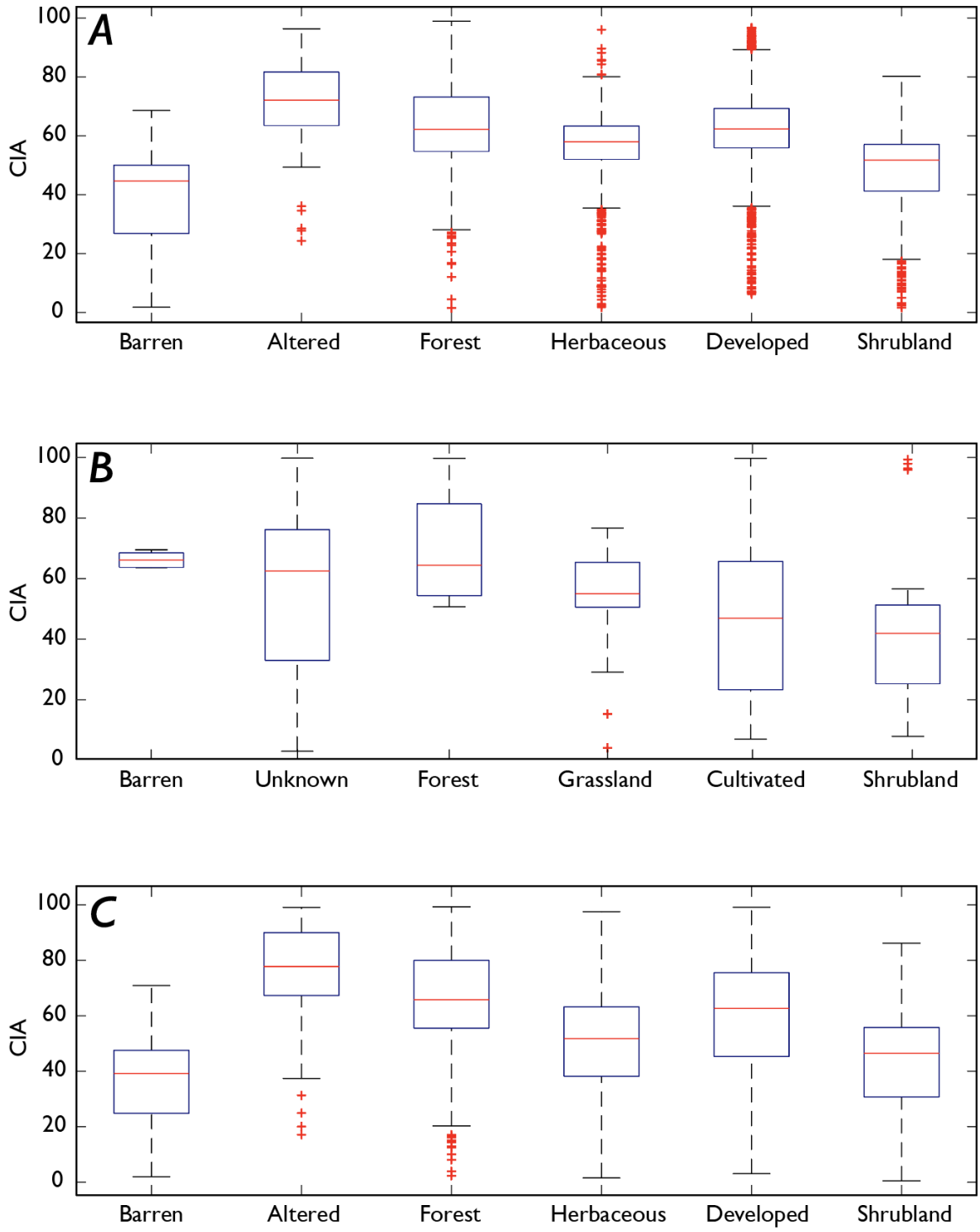

Figure 2.7. Boxplots of CIA by vegetation type and horizon.

Chemical Index of Alteration (CIA) binned by vegetation type, for horizons A, B, and C (bulk chemistry data for CIA were not available for the Top 5 cm horizon). (A) Altered soils have the highest CIA values overall, and Forest soils have the highest CIA for non-anthropogenically-affected soils, in A horizons. (B) Forests have the highest CIA values in B horizons, followed by

Grasslands and Shrublands. (Barren soils' small bin size, n=5, precludes it from analysis here.) (C) Altered soils also have the highest CIA in C horizons, followed by Forests.

2.3.4 Fe and P: Drainage and soil moisture

Moderately poorly-drained soils had higher Fe and P concentrations than the other degrees of drainage. Perudic moisture regimes had the highest Fe and P values (Figure 2.8); however, these samples were dominated by basalt-parented soils in Iceland, which may skew the results. Aside from that, Aquic and Xeric moisture regimes had high Fe, and Ustic and Udic soils had high P (Figure 2.8). Some trends emerge with relatively high Fe/low P (Aquic) and vice versa (Udic).

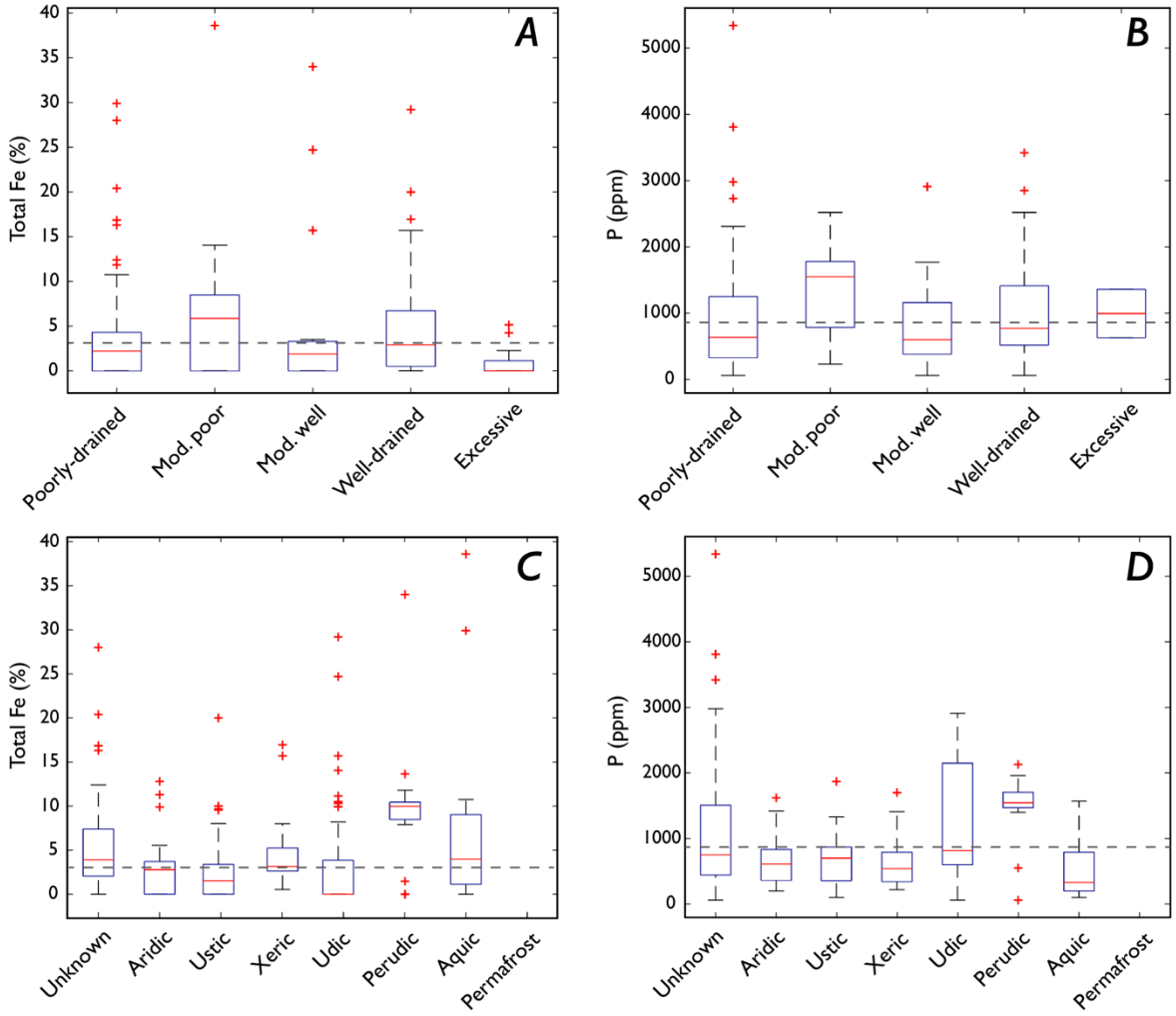

Figure 2.8. Fe and P in soils by soil moisture and drainage.

Variability in Fe concentrations (A,C) and P concentrations (B,D) in different soil drainage and moistures regimes. Dashed gray lines represent crustal averages for Fe and P in respective plots.

(A) Fe binned by drainage. (B) P binned by drainage. (C) Fe binned by moisture regime. (D) P binned by moisture regime. Some patterns emerge when comparing Fe and P between soil moisture regimes; e.g., Udic soils having low Fe/high P and Aquic soils having high Fe/low P. Perudic soils are dominated by basalt-parented soils, influencing their Fe and P concentrations and highlighting the importance of bedrock parent material. No data for Permafrost Fe or P concentrations. Bin sizes (A, B): Poorly-drained (166), Moderately poorly drained (25), Moderately well-drained (16), Well-drained (185), Excessively well-drained (12). Bin sizes for (C, D): Unknown (111), Aridic (73), Aquic (15), Udic (82), Perudic (27), Ustic (54), Xeric (21), Permafrost (N.D.).

2.3.5 Fe speciation

Fe speciation and P

Pyrite/Fe in sulfides, normalized to average soil order density, were above detection by titration in only 22 tested non-wetland soils out of 63 from around the continental U.S. (Supplemental Table 5), so that test was excluded from subsequent analyses. Density-normalized pyrite yields from all wetland sediments analyzed (n = 15) were measurable/above detection limit (>0.1 wt%), as opposed to non-wetland soils (Alfisols, Aridisols, and Mollisols), which typically fell below this limit after being density-normalized. In a non-perenially-waterlogged soil (*e.g.*, not wetlands), it is reasonable to assume that Fe in sulfides are negligible.

Contrary to expectations (see 4.3 below), Fe_{dith} and Fe_{ox} pools did not display stronger or more robust correlations with P (Figure 2.9) than the other Fe pools. There were no clear correlations between P and any Fe species (for all, R^2 <0.01). See Table A4 for all Fe species results and Fe^{3+}/Fe^{2+} ratios.

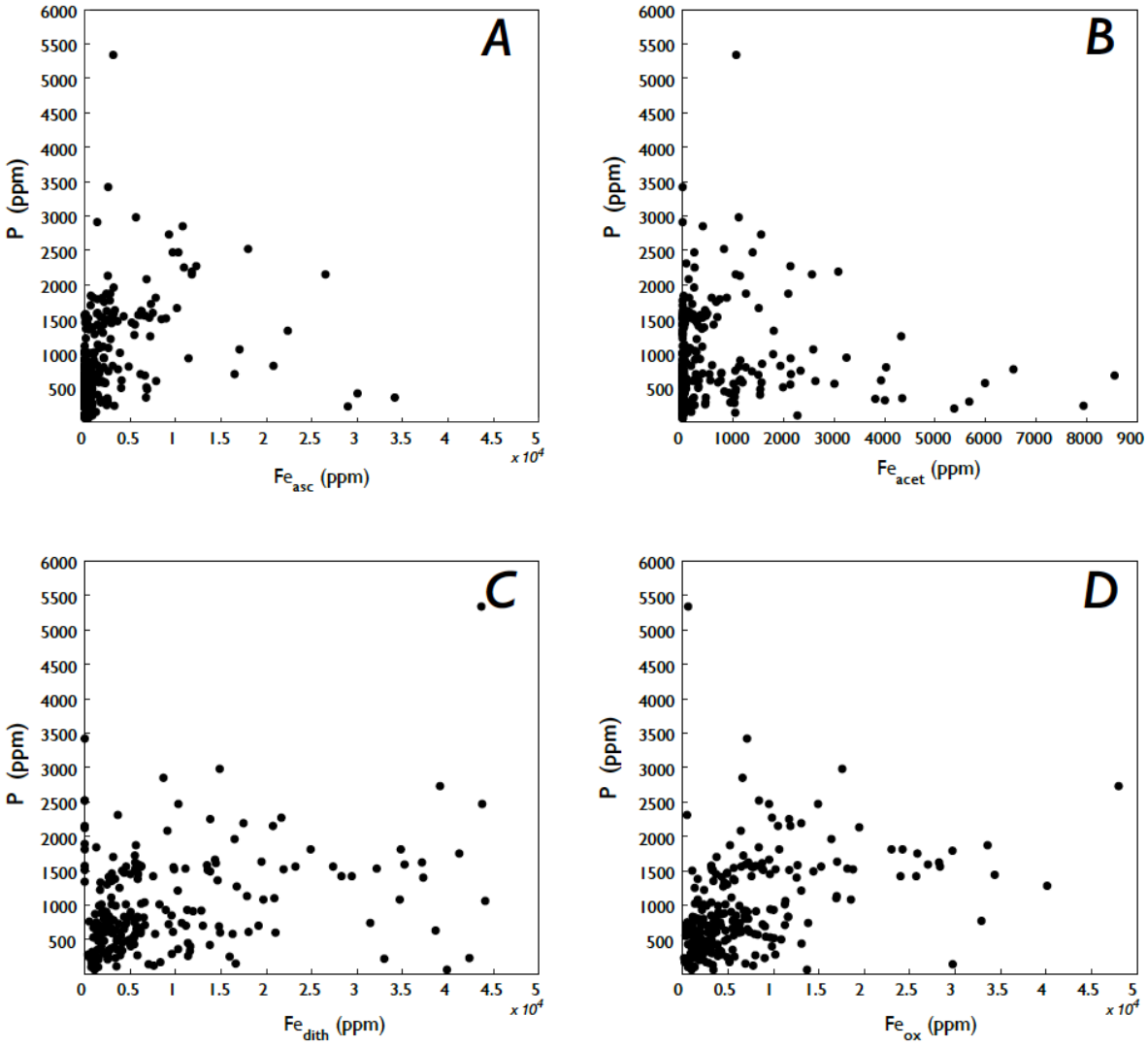

Figure 2.9. Fe species and P concentrations.

Relationships between Fe species and P concentrations, all with R2 values <0.1. Arrows indicate off-plot values. (A) No strong correlation between Fe_{asc} and P (p =10-6). (B) No significant correlation between Fe_{acet} and P (p = 0.2). Note different x-axis scale. (C) No strong correlation between Fe_{dith} and P (p = 0.003), where a positive correlation had been expected due to P's affinity to sorb to Fe (oxyhydr)oxides. (D) No strong correlation is present between Fe_{ox} and P (p = 10-9), again where a strong positive correlation might have been expected.

Fe speciation, precipitation, soil moisture, and drainage

Contrary to expectations (see 4.2.2 below), Fe speciation pools showed no strong predictive relationships (all R^2 <0.2) with mean annual precipitation (Figure 2.10), but there were differences between soil moisture regimes. Permafrost soils from the North Slopes of Alaska, high in organic matter and Fe, were dominated by labile Fe (Fe_{asc}). Aquic and Udic soils had

high Fe in carbonates (Fe_{acet}), and Perudic soils (primarily from Iceland, with basalt parent material) had high Fe_{ox} (Figure 2.11). Mean Fe_{dith} was consistent between soil moisture regimes but has an extremely high range in Aridic soils.

Poorly-drained soils had a high range of Fe_{asc} and Fe_{dith}, while well-drained soils had high amounts of Fe_{acet} (Figure 2.12a). The other Fe species and drainages were consistent. The role of slope was considered, but local, small-scale topographic relief was not readily determinable for most samples.

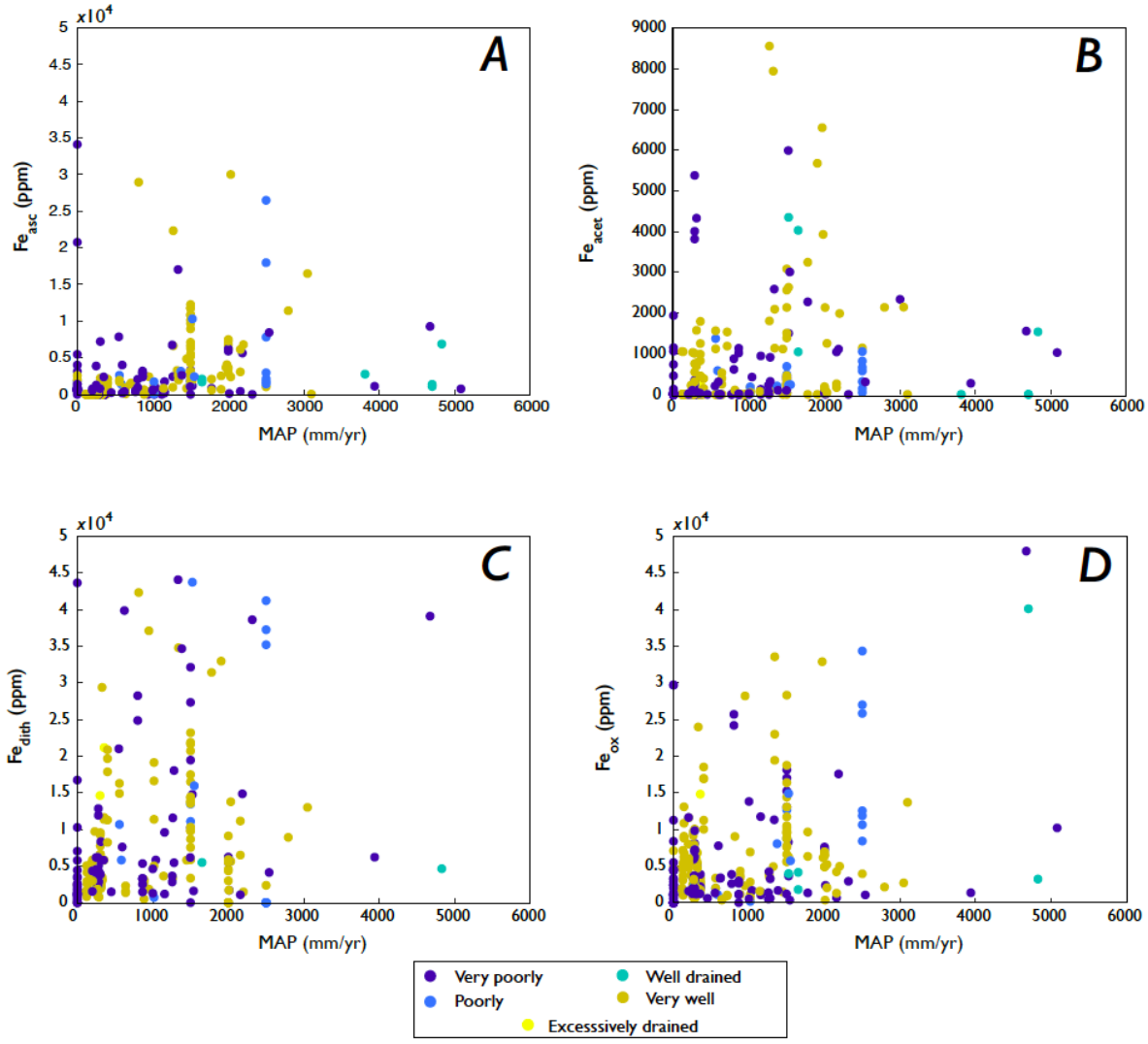

Figure 2.10. Fe species and MAP.

Relationships between mean annual precipitation (MAP; mm yr-1) and Fe species, colored by soil drainage. Arrows indicate off-plot values. (A) No correlation between MAP and Fe_{asc} (R^2 <0.1, p = 10-9). (B) No strong correlation between MAP and Fe_{acet} (R^2 <0.01; p = 0.0005) there could be a maximum MAP value beyond which Fe_{acet} is less kinetically favorable. Note different

y-axis scale. (C) No significant correlation between MAP and Fe_{dith} is present ($R^2 < 0.01$, $p = 0.7$). (D) Modest significant correlation between MAP and Fe_{ox}, ($R^2 = 0.16$, $p = 10\text{-}17$). For all Fe species, there are no strong predictive trends between Fe species concentration and MAP, and no patterns in drainage.

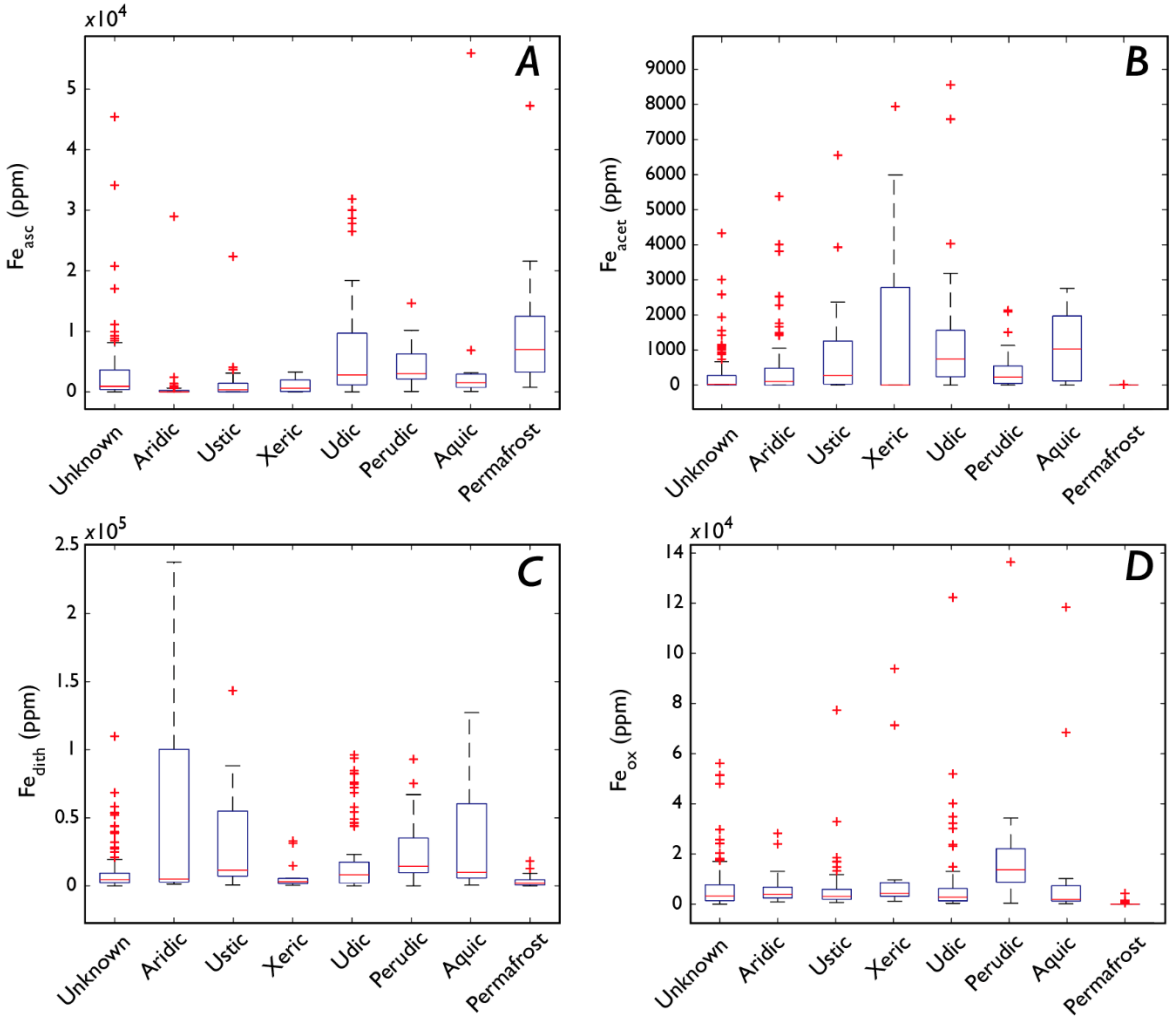

Figure 2.11. Fe species and soil moisture.

Fe species binned by soil moisture regime. (A) Udic, Perudic, and Permafrost soils have the highest median Fe_{asc}. (B) Fe_{acet} is quite low in most soils. Note different y-axis scale. (C) Aridic soils have high Fe_{dith}, but other moisture regimes show little variability. (D) Little variability in Fe_{ox} across soil moisture regimes. Bin sizes (slight variability between Fe species is due to extraction yields): (A) Unknown (106), Aridic (73), Aquic (15), Udic (82), Perudic (26), Ustic (53), Xeric (21), Permafrost (21). (B) Unknown (111), Aridic (73), Aquic (15), Udic (82), Perudic (27), Ustic (54), Xeric (21), Permafrost (18). (C) Unknown (111), Aridic (61), Aquic (14), Udic (78), Perudic (26), Ustic (48), Xeric (15), Permafrost (21). (D) Unknown (106), Aridic (73), Aquic (15), Udic (82), Perudic (27), Ustic (54), Xeric (21), Permafrost (21).

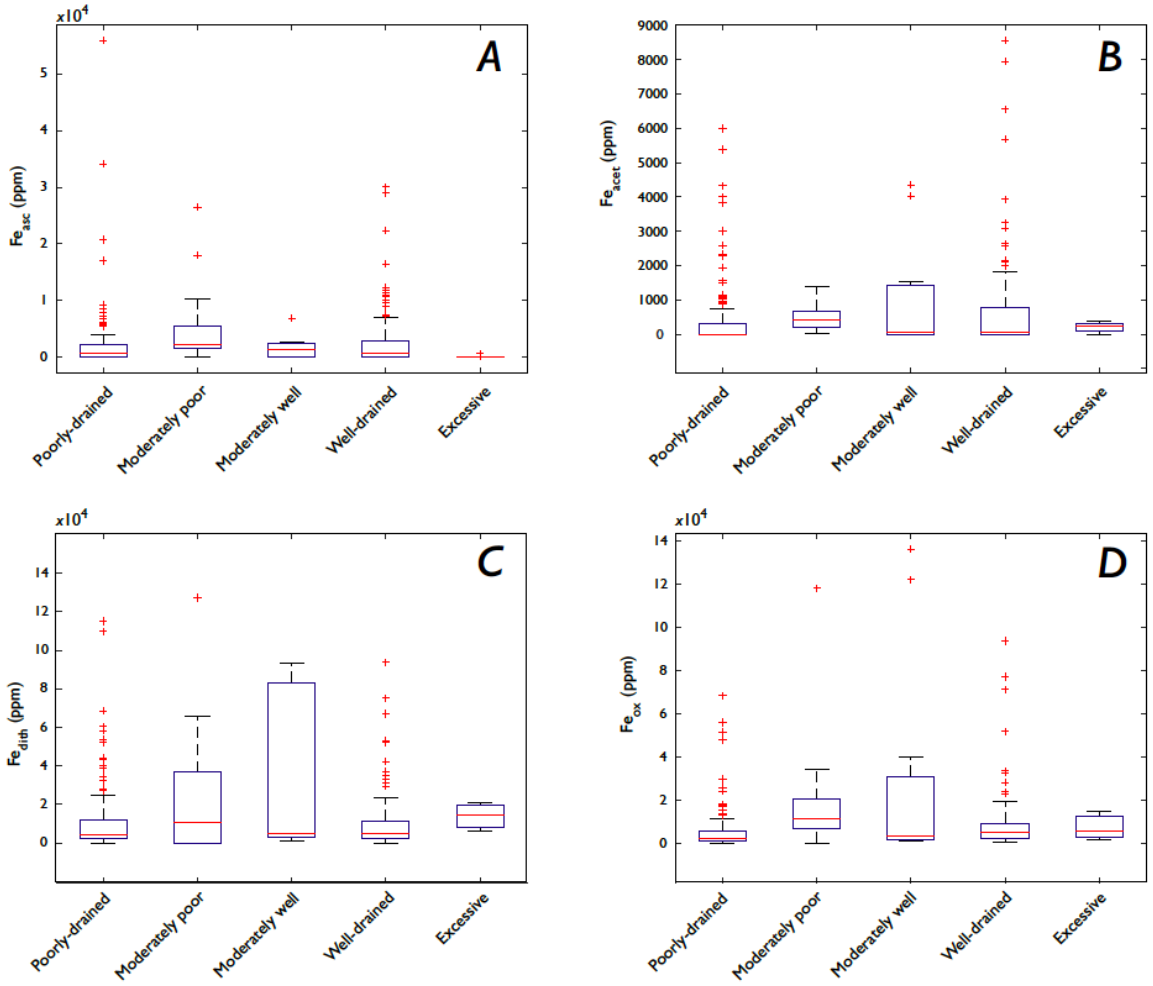

Figure 2.12. Fe species and soil drainage.
Fe species binned by soil drainage. (A) Excessively well-drained soils have very low Fe_{asc}. (B) Note different y-axis scale. Fe_{acet} is highest in well-drained soils, although poorly-drained soils show an unexpectedly high range as well. (C) Excessive soils show the lowest maximum Fe_{dith}, with the other drainages showing similar medians and ranges. (D) Fe_{ox} has similar patterns to Fe_{dith}, with three very high values for moderate drainages. Bin sizes: (A) Poorly-drained (104), Moderately poorly drained (16), Moderately well-drained (11), Well-drained (140), Excessively well-drained (3). (B) Poorly-drained (109), Moderately poorly drained (16), Moderately well-drained (11), Well-drained (142), Excessively well-drained (3). (C) Poorly-drained (101), Moderately poorly drained (15), Moderately well-drained (9), Well-drained (123), Excessively well-drained (3). (D) Poorly-drained (109), Moderately poorly drained (16), Moderately well-drained (11), Well-drained (142), Excessively well-drained (3).

Fe speciation, vegetation, and soil order

Forest soils had higher Fe_{acet} (Figure 2.13b) than the other vegetation groups, but Fe species concentrations were consistent otherwise. Oxisols had higher Fe_{dith} and Fe_{ox} than other soil orders (Figure 2.14c), but Fe species had little variability between soil orders otherwise.

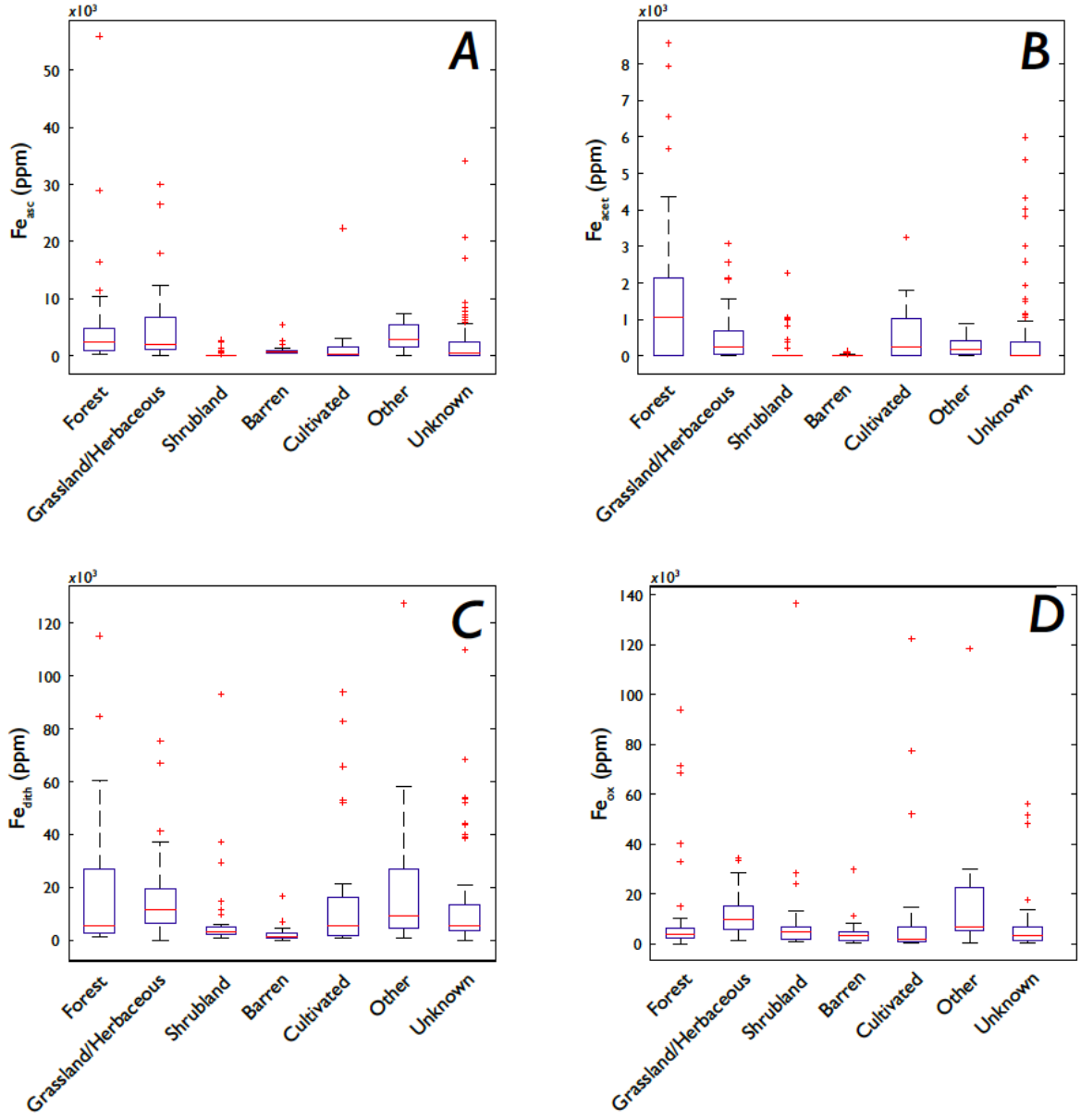

Figure 2.13. Fe species and vegetation.

Fe species binned by vegetation type. (A) Forests and Grasslands have higher Fe_{asc} than other vegetations (except for Unknown). (B) Forests have the highest Fe_{acet} values (median and range). (C) No pattern seen in Fe_{dith} and vegetation, except that Barren soils have low Fe_{dith}. (D) No patterns in Fe_{ox} and vegetation.

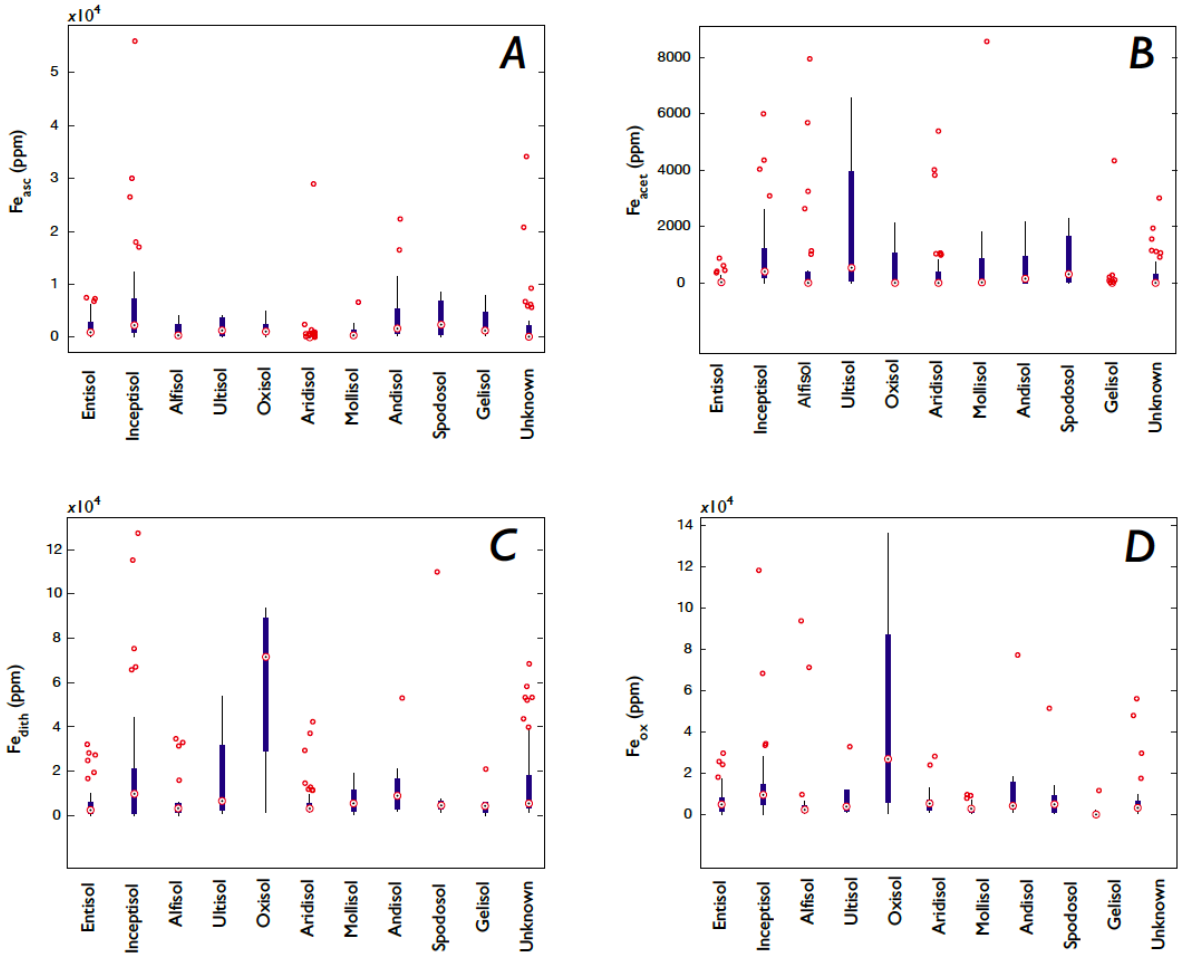

Figure 2.14. Fe species by soil order.

Boxplots of Fe species binned by soil orders, where centered red circles are the medians, the dark blue boxes are 25th inner quartiles, the whiskers are outer 25th quartiles, and the red circles are statistical outliers (outside 3σ). (A) No differences in Fe_{asc} between soil orders. (B) Ultisols have the highest Fe_{acet}, although Alfisols have high range of Fe_{acet} as well. (C) Oxisols have the highest Fe_{dith}, as expected. (D) Oxisols have the highest Fe_{ox}, as expected.

2.3.6 Organic carbon

Organic carbon (C_{org}) in A horizons ranged from 0 to 61 wt%, and in C horizons, ranged from 0 to 43 wt% [64]. The average C_{org}:P ratio for A horizons was 17.9:1, and for C horizons, 18.3:1. Relationships between C_{org} and CIA, P, Fe, and clay content were weak (Supplemental Figures 6,7). There were no strong correlations between inorganic C and Fe_{tot}, or between C_{tot} and Fe_{tot} (Figure A7).

2.3.7 Parent material

There is slight variability between Fe_{tot} and P concentrations and parent material, with igneous bedrock and ash/volcanics having the highest median values for Fe, and high P values as well (Figure A8). While limestone parent materials show high Fe, there are only two samples in this group and they are not included in this discussion. Parent material does not appear to be a predictive control on either Fe_{tot} or P (Figure A8). However, this could be due to the mixed provenance of many modern soils' parent material (*i.e.*, alluvium/colluvium, glacial deposits, etc. as opposed to compositionally homogeneous bedrock). A more targeted exploration into bedrock-parented soils, Fe_{tot}, and P could well show more well-behaved relationships.

2.3.8 Principle components analysis

Results from the principle components analyses (PCA) for the USGS data are shown in Figure A10. Principle components 1 and 2 explain ~60% of variance at a maximum. However, all eigenvalues are very low (<0.6) and data are essentially clustered about the origin, so while there are associations, they are very weak and should be interpreted conservatively. Latitude, P, Fe, and Al were associated with PC2 in the Top 5 cm and A horizons, and vegetation and CIA were associated with PC1. Groupings changed in the C horizons, with Fe and Al associated with PC2, but P and latitude associated with C_{org} along PC1. In all horizons, CIA and vegetation vectors are opposite to each other, and were orthogonal to subparallel to most other vectors.

2.4 Discussion

In this Discussion, we explore our results with a series of questions focused on constraining controls on Fe and total P in soils, defining their relationships on continental scales, and making inferences about how those relationships may impact terrestrial P fluxes. They are centered around key soil-forming factors, such as climate, vegetation, and weathering intensity, as well as soil redox-specific factors (*i.e.*, precipitation, moisture and drainage, and Fe species). Because a majority of samples come from between 20 and 50°N, the interpretations made here are most robust for those latitudes.

2.4.1 How do latitude, weathering, and clay content associate with P and Fe concentrations?

Most of the expected relationships between soil order, Fe_{tot} and P, weathering, and latitude were supported. As expected, weathering generally decreases with latitude, dropping from a maximum CIA of >95 at 30–35°N to a CIA ~75 at 50°N (the northern limit of the large USGS dataset). Farther north, some B horizons deviate from that pattern, with CIA values higher than might be expected based on their climatic regime [80,81]. Interpreting the latitudinal trends here should include a caveat for latitudinal sampling bias and limitations of the dataset to, mostly, between 20° and 50°N. While the PCA results (Figure A10) do not support a relationship between P and weathering, we interpret this discrepancy as being due to the complexities within the P-weathering relationship rather than negating the observations made between latitude, weathering, and P concentrations because the PCA eigenvalues are so low (most < ±0.2) and essentially, are clustered on the origin, which indicates not predictive value. P's relationship with weathering is complex and due to a variety of factors (climate, time, slope/erosion rate, etc.), and by looking only at the end product — which is what is left in the geologic record for analysis — we must inherently work around those limitations and draw the most robust conclusions possible from limited data on these large scales.

Fe_{tot} behaves as expected, accumulating in B horizons as soil weathering increases, while P accumulation in all horizons peaks at moderately-weathered soils (CIA ~60). The latter relationship is expected because a soil that has experienced moderate weathering and has developed somewhat (*e.g.*, Inceptisol, Alfisol) has had sufficient time to have P mobilized from the bedrock/substrate and biotically cycled, but not so long or such intense weathering that P is depleted from the substrate and removed via erosion and/or loss of biomass. An older and/or more intensely weathered soil (*e.g.*, Ultisol) will have a substrate more depleted of P and will have lost more P. In terms of terrestrial P transport, a moderately-weathered soil is the most likely to have a large pool of potential P to transport. An interesting next step, building off this work, could be to test these expected correlations by mapping soil P with soil age and collecting fluvial P loads.

P concentrations are, on average, far below the crustal average of 870 ppm P. Even if we account for bulk density differences between a typical soil (ca. 1.62 ± 0.2 g cm^{-3}; n = 659) [72] and continental crust (*e.g.*, granite, ca. 2.7 g cm^{-3}), all of the soil horizons are depleted in P relative to the crustal abundance. There is some variability between soil orders, but all but a small subset were below the crustal abundance (*i.e.*, recent basalt-parented soils). When

considering bulk density, total Fe concentrations show the opposite, with the soil Fe average of 4.4% being greater than the crustal average of 3.5%, again with some variability between soil orders but overall greater than the crustal average (Table A3). This has implications for biogeochemical modeling. While P concentrations could be expected to generally decrease with increased weathering intensity, a moderately-weathered soil is more likely to be at a mid-developmental stage (*e.g.*, Inceptisol, Alfisol) and supporting vegetation that can cycle P without being P-depleted (*e.g.*, [19]). This mid-CIA accumulation could be reflective of vegetation's impact on soil nutrients (*e.g.*, mycorrhizal P mobilization, P recycling through biomass/organic matter decomposition), pointing to a key balancing point in a soil's lifespan where the bedrock is being weathered enough to maximize fertility without yet being depleted. Forest and Altered/Cultivated soils have the highest CIA values (Figure 2.7), but P concentrations were relatively invariant between types of vegetation, suggesting that weathering intensity exerts a greater control on soil P than the type of vegetation.

Clay content (both percent of grain-size fraction and abundance of clay minerals) should increase with the degree of weathering a soil has undergone, and that is reflected in the results (Figure 2.4d). Consequently, there are secondary trends associated with clay content; *i.e.*, clay content peaks at lower latitudes where CIA values are the highest. Fe_{tot} and clay content show a strong positive correlation, as expected (Figure 2.6e), but P shows only a weak potential decrease as clay content increases, supporting traditional thinking that P is depleted as a soil is increasingly weathered and/or older (Figure 2.6f). While it is kinetically favorable for P to sorb to Fe and Al oxides (which accumulate in B horizons as a soil ages), clays (often with surficial Fe-Al oxides) may be equally as important for immobilizing P in soils [82].

Interestingly, our results indicate no positive correlations between Fe oxides (Fe_{dith} and Fe_{ox}) and clay content grain-size fraction (Figure A9) as would be expected based on soil development patterns (*i.e.*, higher weathering intensity leads to accumulation of clay minerals and Fe oxides), suggesting that while particle size may mediate Fe speciation due to varying degrees of reactivity, it is not a primary control. While the USGS database's clay content is based on mineralogy (determined by XRD), soils used in the Fe species work had clay content determined by settling, which would include both clay- and non-clay minerals that were clay-sized particles. This could explain at least partially the lack of expected trend. Further exploration of clay mineralogy-specific correlations (or lack thereof) with Fe speciation pools, in

the context of soil redox state, is warranted to explain this deviation from our expectations. Therefore, degree of weathering remains a primary control on soil P concentrations (*e.g.*, [19]).

Although dust deposition is a source of P, it is typically secondary to bedrock weathering, not really applicable on anthropogenic-change timescales, and is not rapid in most of our study area (primarily conterminous United States). Because it is not separately examined or included in this work, anyone using our results of soil P should take regional dust deposition and subsequent P replenishment into account when possible.

2.4.2 How do precipitation, soil moisture, and soil drainage affect P and Fe concentrations, and Fe species?

How does soil redox affect P?

The relationships between soil redox factors (precipitation, soil moisture, and soil drainage) and soil P contents suggest that moisture is not a dominant control on soil P. While there is a weak possible correlation between MAP and P (Figure A3a), the range of P concentrations for a given MAP is large (ca. 1500 ppm) and is not particularly predictive. Adding more climate data (*e.g.*, correlating continental climate data with the USGS sample locations) could improve this potential relationship. As with other possible relationships in soils, however, it could be mediated by an additional soil-forming factor (*i.e.*, precipitation is related to weathering intensity, and possibly to the presence of vegetation).

There exist only weak patterns between P and soil moisture or drainage. Udic soils have higher mean and ranges of P than other moisture regimes (Figure 2.8d), and poorly-drained soils can have higher P than well- or excessively-drained soils (Figure 2.8b). However, the bin sizes for these soil moisture regime types are relatively small; more data could clarify these trends. A relationship between soil P concentration and moisture regime would not necessarily be expected because soil moisture regimes are defined by the number of saturated days per year [83], but not necessarily if those days are linked by season (*i.e.*, they do not need to be consecutive). While soil redox state would affect the (short-term) phase of P adsorption sites (such as Fe oxides) and possibly the accumulation of organic matter, which can mediate P-oxide interactions [8,9], as well as sequester P in organic compounds, only precipitation and its links to weathering intensity would be expected to exert long-term control on P concentrations.

How does soil redox affect Fe concentrations and speciation?

Our primary hypothesis was that precipitation would exert control on soil moisture and therefore on redox conditions in the soil porewaters, controlling Fe speciation. However, mean annual precipitation did not correlate with total Fe and showed none of the expected correlations with the four Fe species. There was perhaps a maximum precipitation (ca. 2000 mm yr^{-1}) for most Fe in carbonates (Figure 2.10b), but little else. Turning to a more direct approach of constraining soil moisture - soil moisture regime – revealed one interesting correlation: although variability in total Fe was low across soil moisture regimes (Figure 2.9c,d), there are some patterns of trade-off between species within a moisture regime (Aquic, Udic). Similarly, variability between soil drainage was low, but a general pattern of moderately-drained soils having higher Fe in oxides and carbonate, whereas labile Fe (reduced) showed no trend. Based on these data, soil moisture, redox state, and associated chemistry are highly heterogeneous even within soil orders, moisture regimes, and drainage ability, and broad generalizations cannot be made.

Iron oxide mineralogy and soil magnetic properties have been linked to regional precipitation [84-87] and soil moisture [42, 43, 88, 89], but relatively few studies explore the links between soil iron oxide mineralogy and soil order [90, 91]. Cervi et al. [90] found parent material and climate to be primary controls on soil magnetic susceptibility. A recent survey of Australian soils explored 471 unaltered topsoils' magnetic properties [92], which was the only study we could find of a similar scale to the work presented here. Hu et al. [92] found parent material to be the strongest control on soil iron mineralogy, with climate (precipitation, temperature) showing weaker influence and vegetation effects on soil iron being regional.

In addition to using the large soil datasets that are increasingly available, more targeted studies on the influence of soil moisture and drainage on redox conditions – using larger datasets and including more detail of soil texture – could strengthen these trends and reveal additional patterns. Many of the soils included in this study were well- or very-well drained, with a smaller subset being poorly- or very poorly-drained. It is possible that relationships between Fe species and moisture are stronger in soil drainage regimes for which we have effectively too small datasets in this study. Additionally, highly localized slopes (along with the context of grain size composition) likely exert strong controls on soil moisture and redox state, but we were not able to expand this study to include those data. Doing so would help clarify potential relationships

between soil moisture and Fe species. Using high-resolution slope data (*e.g.*, fine-scale LiDAR/digital elevation models) could be useful for determining these relationships between local soil redox conditions and geochemistry.

2.4.3 How do Fe species associate with P?

We expected that Fe oxides, having been shown to efficiently sorb P onto their surfaces in other soils (*e.g.*, [8, 9, 44, 93]), would have a more robust correlation than between either labile Fe and P (in reducing microenvironments) or Fe in carbonates and P. However, no species showed a strong correlation with P (Figure 2.9). Overall, Fe_{tot} and P in all soils showed a positive correlation, suggesting that Fe species is not a dominant control on P concentration, and that no single species is more likely to be associated with P, at least on regional scales examined in this work. Because of the weak relationships between Fe species and assorted soil moisture proxies, as well as a surprising lack of correlation with clay content, there is no simple rule connecting Fe species, soil redox state, and P. However, an increase in any Fe-bearing species should correspond to an increase in P due to the general positive relationship (Figure A4). Fe (and Al) oxides in the clay fraction specifically may be most important for terrestrial P transport (both in soils and fluvial systems) (*e.g.*, [39, 44, 94]). We expect that repeated analyses within an individual profile or on a small local scale (*i.e.*, meters) would show stronger expected relationships, but they cannot be generalized to regional or continental scales.

2.4.4 How does vegetation affect P and Fe concentrations?

Biology – here, generalized as dominant vegetation on the soil surface (not considering microbial life and mesoscale organisms) – plays an important role in terrestrial P cycling. We found that Barren soils' B horizons had more P accumulation than other, vegetated soils' B horizons, reflecting plants' effectiveness at moving P from regolith to higher in the soil profile [15, 16]. The other vegetation types showed surprisingly little variability, but P does tend to increase up-profile, suggesting that once a landscape is vegetated – regardless of specific ecosystem type – P is efficiently mobilized by plants to the upper horizons and recycled and stored there. Additionally, vegetated soils had far higher ranges/maximum P concentrations than unvegetated soils, supporting the importance of plants' role in P mobilization and accumulation. Barren landscapes lack the rooting systems to mobilize and transport P, hence the increased

accumulation in B horizons. Halsted and Lynch [95] found essentially no discrimination in P uptake between C_3 and C_4 plants, which our results further support.

Aside from 'Other' vegetation (which was biased by Fe-rich parent material), Cultivated soils' B horizons were the only ones that showed depletion, suggesting that ecosystem variability is less important than parent material and soil mineral accumulation rates for Fe in soils. Deep tilling in agricultural practice could be an additional factor in lower-soil-profile nutrient depletion, but is less common than it used to be. Similarly, vegetation type does not appear to be a direct control on Fe species within soils; Forests did have greater Fe_{acet}, which is likely linked to the defined property of Alfisols of high cation exchange capacity and cation mobility, as well as their tendency to be well-drained.

Overall, the presence of vegetation - rather than differences in the type of vegetation - exerts the most control on P accumulation in soils (Figure 2). Although the mean P values were similar between vegetation types within a soil horizon (with the exception of B horizons in Barren soils), non-Barren (vegetated) soils had higher ranges of P than Barren soils. Forests also have higher CIA values than grasslands and shrublands (Figure 2.7), suggesting that the evolution and spread of different ecosystems could have changed the distribution of weathering intensity. This has interesting implications for the ongoing debate on land plants' influence on continental P fluxes.

Vegetation changes with latitude; the soils and ecosystems represented in this work span tropical and temperate forests, continental grasslands, dry shrublands, and high-latitude, little-vegetated landscapes. This inherently contributes to the observed latitudinal trend in weathering because different plants have different interactions with soil and bedrock. While there are ground-level differences between plants within a plant type (*e.g.*, grasses), the functional difference between plant functional types (*e.g.*, grasses vs. trees) are far larger and more meaningful on continental scales. While at local or regional scales high-resolution, species-specific studies on weathering and plant-soil relationships can be done, that level of analysis is neither possible nor necessary for continental-scale analysis of vegetation-weathering relationships. Global climate, biogeochemical, and environmental change models rely on continent-scale data; therefore, while locally, species variability within a plant functional type may lead to nuanced plant-soil geochemical relationships, the continental scale and umbrella vegetation type is appropriate for this style of inquiry.

2.4.5 Is soil order predictive of P and Fe concentrations?

Soil order is not quantitatively predictive of P and Fe concentrations. Soil order, Fe, and P are linked indirectly through the correlation between Fe/P and CIA; this relationship is stronger for Fe, which shows a clear Fe accumulation increasing with weathering (Figure 2.6a,c), which is also linked to the Inceptisol to Ultisol soil progression common in chronosequences. Soil order and weathering show a very well-behaved and expected relationship, with CIA values increasing from Entisols to Ultisols/Oxisols (Figure 2.5). An exception to this trend is high-latitude Gelisols, which have longer formation times and lower weathering rates. These results align with existing soil formation frameworks and support proxies that rely upon their use, such as the CIA-based mean annual precipitation proxy, the paleosol weathering index for mean annual temperature, and Bt thickness ([79] *and refs. therein*). However, because soil order depends on a variety of factors (*i.e.*, weathering stage, vegetation), quantitative relationships between soil order and either Fe_{tot} or P concentrations cannot be generalized, and samples within one soil order should not necessarily be used to predict Fe or P concentrations quantitatively for other samples of the same order. This is important to remember when using limited numbers of samples of fossil soils.

2.4.6 Implications for P in modern soils, climate change, and soil fertility/food security

Soil P, erosion and transport, and human activity

Aside from the geologically-recent uptick in anthropogenic influence on landscapes, continental scale-vegetation was relatively stable over the past millennium in North America (*e.g.*, [96]). Concern for changing P fluxes in terrestrial ecosystems largely stems from the occurrence of harmful algal blooms in rivers, lakes, and coastal areas, often linked to mass-production agriculture and nutrient-rich runoff. The implications for these fluxes from this work center on land use change and soil degradation, as well as climate change-driven shifts in vegetation (*e.g.*, grassland to barren). P would also be lost in that shift because vegetation loss exacerbates erosion and landscape degradation [97].

Human-induced changes (*e.g.*, industrial agriculture, extensive monoculture, unsustainable farming practices, etc.) can lead to natural P being lost through subsidence and erosion, P being added through fertilizer, and reduced plant P retention if natural, diverse

ecosystems are replaced with monoculture (*e.g.*, [98]). Land-use changes typically result in the removal of the upper portion of a soil profile (various, *e.g.*, [99]). Because P tends to accumulate in the upper horizons (O,A), our results suggest that this could lead to a noticeable loss in P and in agricultural soils, increased need for fertilizer (see 4.6.3). Land-use changes in vegetated soils could increase the P flux from land to lakes and coastal waters, leading to eutrophication. The spread of Aridisols through desertification could mean more regions experience erosion due to vegetation loss, but perhaps in turn lower weathering due to that loss of vegetation and to drier climatic conditions [100]. As desert regions expand, global dust volumes and distributions will change, which would change which areas see P removal (through increased erosion and P loss through dust) and which see P accumulation through dust deposition. Changes in atmospheric and soil CO_2 concentrations are likely to affect both plant and soil productivity (as well as mycorrhizal efficiency) under climate change, although the extent and duration of changes to productivity are debated [100-103].

Weathering, climate change, and soil P

In addition to changes in vegetation (ecosystem), climate change will impact weathering intensity and erosion, affecting global soil P reservoirs. As a consequence, soil fertility and food security risk will shift and vary depending on how different regions and biomes respond to climate change [104]. Currently, there is a general trend of intense, rapid weathering at lower latitudes as a consequence of high heat and precipitation. Higher latitudes tend to be cooler and drier, and therefore weathering intensity and rates are lower [14, 105]. While low-latitude areas are expected to undergo desertification (decreased precipitation, loss of vegetation), higher latitudes may experience an increase in precipitation and temperature. Therefore, the style and intensity of weathering will change regionally. Based on our results, where the range in P concentrations peaks at mid-intensity weathering (*i.e.*, CIA ~60; Figure 2.5) and decreases in older and/or more strongly-weathered soils (as expected), the climate change expected for higher-latitude regions may result in decreased soil fertility (limiting agricultural production, see 4.6.3) and increased risk of eutrophication in surrounding waters. The former effect could potentially be mediated by vegetation, which holds P and slows erosion.

Except for the increase in range at mid-intensity weathering, P concentrations were relatively consistent across weathering intensities, which was unexpected. We had hypothesized

that as older soils tend to be depleted in P, a higher weathering value would correspond to lower P. This was not demonstrated by our results. We interpret the lack of correlation as highlighting the significance of soil age — rather than weathering intensity (climate) — in controlling soil P, as some previous literature has suggested (*e.g.*, [19, 106]). A nuance that this large dataset could be missing is P speciation, which could still show P phase-specific variability with weathering intensity. The implication for P transport from soils remains unchanged from previous studies, where older soils would likely have smaller pools of P for mobilization. Mapping soil P with soil age on a large scale (such as the USGS dataset used here) would be a valuable new addition to the field and could elucidate the P-soil age-weathering puzzle. Additionally, exploring relationships between soils and weathering with species-level variability (on smaller, local scales) could help refine interpretations based on dominant regional plant functional type.

The difference in weathering intensity/CIA values between Forests and other natural vegetation types (Grasslands, Shrublands), as well as the high CIA values in Altered/Cultivated soils suggests that if more land is converted to farming (cultivated) from natural grasslands (*e.g.*, the Great Plains) or if agricultural intensity increases, weathering rates would increase, depleting the soils' nutrients more quickly and perhaps increasing P fluxes. To our knowledge, this is the first data-based demonstration of the principle on the continental scale rather than as a model result. Understanding how human activity and agricultural degradation of soils affects weathering and resulting P is crucial for predicting changes in terrestrial P.

Soil P, plants, and agriculture

Climate change is also likely to affect plant physiology and biological processes, such as P uptake (mediated by mycorrhizal fungi) and C storage, as a result of changing atmospheric carbon dioxide concentrations (pCO_2). Plants rely heavily on symbiotic relationships with mycorrhizae to mobilize and uptake recalcitrant mineral P and fix nitrogen [102, 107-109]. Mycorrhizal activity and P uptake can also be affected by soil moisture [110, 111], which depends on a number of factors (discussed in section 2.2) that could change in response to altered land use and climate change. P uptake efficiency also varies between species of symbiont [112], which may respond differently to climate stressors such as pCO_2 and temperature [110, 113, 114]. Some work suggests that increased atmospheric pCO_2 will be advantageous for plant growth, leading to greater terrestrial biomass and C storage [115, 116], though potentially with

an upper limit on pCO_2 vs. growth returns [117]. However, observations have shown that increases in pCO_2 during and after Industrialization did not always increase plant C richness or biomass growth [118-120], and the biomass increase effect can still be mediated by P (and N) limitation in soils [121-123] and mycorrhizal species [102, 114].

Ecosystem-specific C:N:P (Redfield) ratios vary, but throughout natural marine and terrestrial systems, P is the limiting nutrient [4,5]. For example, while the original marine phytoplankton-based Redfield ratio is 106:16:1, in soils, it is naturally higher at 186:13:1 [124]. The C:P ratios in both A and C horizons (16.7:1 and 14:1, respectively) were far lower than what is observed for O horizons (186:1 [124]) or inland streams/rivers (167:1 [125]), and are closer to ratios for microbial biomass in soils (~50:1; [124]). However, this ratio was derived with total P rather than organic P, and is therefore likely an overestimation. In these samples, the C_{org}:P_{org} may be closer to the expected value for soils, but further speciation work is needed. Additionally, it is reasonable to expect that mineral soil horizons (rather than organic-rich horizons, like O) would have lower C_{org} and nutrient concentrations. For developed soils (mean C_{org}:P = 15.25), this discrepancy could be linked to deep tilling removing nutrients from subsurface horizons and potentially increasing nutrient fluxes as compared to undisturbed or shallow-tilled soils. For natural soils with the potential for cultivation/deep tilling (*e.g.*, grasslands, mean C_{org}:P = 20.5), the lower C:P ratio in subsurface mineral horizons could be inferred as diminishing returns for deeper tilling. There were no strong correlations between C_{org}, C_{inorg}, or C_{tot} and variables of interest (CIA, clay content, P, Fe)(Supplemental Figures 6,7).

Complicating this response is the fact that increases in atmospheric pCO_2 could increase the rate of bedrock weathering (*e.g.*, [126]), which mediates P availability and biolimitation. Moderate increases in pCO_2 and weathering could lead to higher P availability and greater plant biomass, but if weathering increases too much, P in soils could be depleted while plant growth continues to increase. If high weathering rates lead to faster or premature depletion of P, especially exacerbated by anthropogenic activity (agriculture), crop stresses and regional food shortages could occur. Additionally, demand for P as fertilizer could increase; fertilizer P is ultimately sourced from bedrock which, on human timescales, is a nonrenewable material [127]. Without developing efficient P recycling methods or adding sources like bone char (*e.g.*, [128, 129]), P could run out in a matter of decades [130-132]. Therefore, when considering how climate change will affect agricultural yields, it is important to consider plant physiology and P

uptake mechanisms together with mineral/geochemical changes in the soil driven by natural and anthropogenic forces.

Overall, this work aids in predicting changes in terrestrial P fluxes primarily by linking soil P, weathering intensity, and the presence of vegetation. However, in this study, "vegetation" remains something of a black box; the mechanism by which the presence of vegetation affects soil P could be through slowing erosion, increasing biotic P cycling, retaining P via plant/microbial biomass, increasing bedrock apatite weathering, or – most likely – a combination of those factors. Exploring each of these factors at large spatial scales, and to the extent possible pairing those analyses with smaller-scale species-specific soil-plant relationships, is a critical next step in elucidating the potential for P fluxes in different terrestrial regions.

2.4.7 Implications for P in the fossil record of soils and its geologic use

Heterogeneity and paleosol representativeness

Fossilized soils (paleosols), which are present in the rock record as far back as at least 3.0 billion years ago, serve as important windows into Earth's terrestrial past [133]. They have been used to reconstruct ancient atmospheres (*e.g.*, [134-138]), climates ([79] *and refs. therein*), and terrestrial biology and biogeochemical cycling (*e.g.*, [139, 140]). The geochemical composition of fossil soils is used to reconstruct a range of climatic and environmental changes; however, these tools are primarily based on small modern soil datasets. This work provides ranges of reasonable values for soil chemistries under known environmental and atmospheric conditions, providing critical background information to improve our paleoclimate and paleoenvironment reconstructions. Based on the highly variable geochemical results in this work, we urge researchers using paleosols for these types of reconstruction to be cautious in assuming a single paleosol profile to be representative of an entire landscape or basin. More work on how representative a paleosol profile is, chemically and climatically, should be done to incorporate landscape-scale variability in soils (*e.g.*, [141]).

Paleosol Fe, atmospheric oxygen reconstructions, and microbial life

Because paleosols form at Earth's surface and in direct contact with the atmosphere, their Fe chemistry has been used to reconstruct atmospheric oxygen levels [134, 138, 142]. Across a range of soil orders, environments, and climates, non-wetland soils in this work reflect oxidizing

conditions (based on Fe^{3+}/Fe^{2+} ratios; Table A4). While Fe^{3+}/Fe^{2+} ratios are no longer the primary tool for reconstructing paleo-oxygen levels, these results indicate that that tool is qualitatively robust in the absence of other observations such Cr or S isotopes.

A concern with using fossil soils for reconstructing atmospheric oxygen is that these soils likely hosted microbial life, which could have affected the redox signal ('biosignature') left behind. Indeed, redox-sensitive metals have been proposed as biosignatures because they can be mobilized by biologic processes and redeposited within a soil profile [143]. However, if it is suspected that the soils have variable redox states due either to high moisture input or poor drainage, how reliably might they have recorded the atmospheric oxygen signal as opposed to microscale oxic/reducing conditions due to microbial activity? Modern biological soil crusts (BSC; or, cryptogamic soils) are symbiotic communities of microbes (predominantly cyanobacteria), algae, and fungi; these communities have been proposed as analogues for early life on Earth (and Mars) [143]. Here, we found that the soil redox state being recorded by BSCs was oxic (again, using Fe^{3+}/Fe^{2+} ratios and dominant Fe speciation; Table A4), despite BSCs' ability to retain water and temporarily shift to reducing conditions. It is unlikely that the microbial communities would have 'overprinted' the atmospheric oxygen signal even if they temporarily held water to cycle nutrients and leave behind biosignatures.

Continental weathering, nutrient fluxes, and the atmosphere

Geologists are interested in constraining many of the processes described above in ancient soils and ecosystems. Weathered P, transported to the oceans via fluvial networks and continental drainage, is typically invoked as a first-order control on marine productivity, which is associated with organic C and organic-associated and inorganic carbonate sedimentation, atmospheric CO_2 drawdown, and oxygen production [56]. Continental weathering, and therefore P flux, is a central control in many biogeochemical models of Earth's past. However, the continent-to-ocean transport of P is usually prescribed and not based on actual changes in fossil soil (paleosol) P values or weathering intensity data. Rather, it has been generalized based on crustal P values and fluxes controlled by large-magnitude changes, such as global glaciations [144, 145] or limited modern observations [61, 62].

Based on our results, continental weathering intensity and resulting elemental fluxes should vary with paleogeography (latitude effect), in addition to changes in climate and landmass

area. Clay content through time could be taken into account and paired with CIA to reconstruct actual weathering intensity where those data are available in the rock record [146]. Forests also have higher CIA values than grasslands and shrublands (Figure 2.7), suggesting that the evolution and spread of different ecosystems could have changed the distribution of weathering intensity. Biogeochemical models should take these differences into account as opposed to assuming uniform behavior spatially.

Continental sulfide weathering in the Precambrian (pre-540 Ma) has been invoked as a major source of sulfate to the oceans, affecting organic matter respiration rates, marine alkalinity and oxidation state, and ultimately the concentration of atmospheric oxygen [147-150]. At the Great Oxygenation Event (GOE) 2.45 billion years ago, pyrite burial and increased ocean sulfate concentrations are thought to have decreased atmospheric methane through microbial sulfate reduction, lowering the greenhouse effect and leading to global glaciations [151, 152]. Our results (Supplemental Table 5) constrain the amount of Fe-bound sulfides in modern soils, forming under an oxic atmosphere, and suggest the potential for a 'false positive' for a reducing atmosphere if a paleosol is not correctly identified as waterlogged (and therefore reducing) or histic. Although it should be noted that using the mere presence of minerals, such as pyrite or uraninite, in the rock record as reducing indicators [153] is simplistic and no longer widely-used in the field.

Vegetation and P in the Phanerozoic (542 Ma onwards)

The rise of land plants during the Devonian period (419–349 Ma) has been suggested as a major driver of change to the Phanerozoic P and C cycles, which could have affected atmospheric oxygen [15, 56,63, 154]. While B horizons in Barren vegetation had increased P retention, the lack of variability between other vegetation domains suggests a somewhat binary response - either soils are vegetated and mobilize/accumulate P, or they are not vegetated and are relatively depleted in P. Only soils with vegetation accumulated high ranges of P, supporting the need for biological mediation of P in terrestrial settings.

2.5 Conclusions

From this large-scale analysis of modern soils' physical and chemical properties, we draw conclusions about the relationships between modern soil biogeochemistry and climate, and link those to terrestrial P transport. We also describe implications about past terrestrial biogeochemistry and interpreting the terrestrial rock record.

In modern soils, some of the most well-defined (and expected) relationships were between soil composition and weathering. Latitude, clay content, and weathering correlate as expected, with higher latitudes corresponding with lower weathering intensity and clay content. Contrary to our expectations, average P concentrations are relatively consistent across weathering intensities but show a slight peak at middle weathering intensities, which supports commonly applied models of soil age and P loss. Specifically, it helps to clarify the conflation of time and weathering intensity that can occur, pointing to the importance of soil age as a control on soil P depletion. Maximum terrestrial P transport, then, would still likely occur at a midpoint in the weathering-P spectrum, where a soil is mature enough to have mobilized P from apatite and be linked to high erosion rates, but before soil P is too depleted due to age (which would be a lower P flux overall). Contrary to expectations, P in soils was not strongly associated with Fe (oxyhydr)oxides. The scale of such relationships may be much smaller than continental (*i.e.*, locally or per profile). Additionally, no strong, predictive relationships were present between Fe species and precipitation, soil moisture, or drainage, so predicting P transport based on climate or soil redox properties is not possible. Finally, the presence of vegetation (but not plant functional type or generalized ecosystem type) is important for P accumulation in soils, which has implications for how the rise of terrestrial plants may have changed P cycling through geologic history.

Based on modern relationships between soil P, weathering, and vegetation, the spread of land plants in the early Phanerozoic likely increased P accumulation in soils and on continents, rather than increasing the flux of P to the oceans. This would limit the role of terrestrial-marine P transport in marine productivity. Because of latitudinal variability in weathering intensity, biogeochemical models should take paleolatitude into account when using weathering intensity as a driver for P fluxes. Additionally, models should use density-normalized values for terrestrial P rather than bulk crustal values and should use the range of P in modern soils as a quantitative constraint. Finally, while we did not find the relationships between Fe species and climate that

we had expected, the overall Fe signature in soils (including microbially-colonized) was oxic despite analyzing a range of soil moistures and drainages, which supports the use of paleosol Fe/redox geochemistry for paleo-atmosphere reconstruction.

Acknowledgments

We thank NRCS KSSL for soil sample storage, preparation, and shipping; USGS Southwest Biological Science Center for assistance in soil crust sampling; soils from Adrianna Trusiak/Rose Cory lab; Catherine Seguin for her thesis work on biological soil crusts and lab assistance; Sonya Vogel, Bianca Gallina, and Jordan Tyo for assistance in lab; Emily Beverly for assistance in the field; and Kathryn Rico and Nikolas Midttun for helpful discussions. Thanks to our anonymous reviewers for their helpful comments and suggestions to improve our manuscript.

References

1. Froelich, P.N.; Bender, M.L; Luedtke. The marine phosphorus cycle. *Am. J. Sci.* **1982**, *282*, 474-511.

2. Du, E.; Terrer, C.; Pellegrini, A.F.A.; Ahlström, A.; van Lissa, C.J.; Zhao, X.; Xia, N.; Wu, X.; Jackson, R.B. Global patterns of terrestrial nitrogen and phosphorus limitation. *Nature Geoscience* **2020**, *13*, 221–226.

3. Correll, D.L. The role of phosphorus in the eutrophication of receiving waters: A review. *J. Env. Quality* **1998**, *27*, 261-266.

4. Filippelli, G.M. The global phosphorus cycle. *Rev. Mineralogy and Geochemistry* **2002**, *48*, 391-425.

5. Filippelli, G.M. The global phosphorus cycle: Past, present, and future. *Elements* **2008**, *4*, 89-95.

6. Peretyazhko, T.; Sposito, G. Iron(III) reduction and phosphorus solubilzation in humid tropical soils. *Geochimica et Cosmochimica Acta* **2005**, *69*, 3643-3652.

7. Chacon, N.; Silver, W.L.; Dubinsky, E.A.; Cusack, D.F. Iron reduction and soil phosphorus solubilization in humid tropical forests soils: The roles of labile carbon pools

and an electron shuttle compound. *Biogeochemistry* **2006**, *78*, 67-84.

8. Fink, J.R.; Inda, A.V.; Tiecher, T.; Barrón, V. Iron oxides and organic matter on soil phosphorus availability. *Ciência e Agrotecnologia* **2016**, *40*, 369-379.

9. Herndon, E.M.; Kinsman-Costello, L.; Duroe, K.A.; Mills, J.; Kane, E.S.; Sebestyen, S.D.; Thompson, A.A.; Wullschleger, S.D. *JGR Biogeosciences*, **2019**, *124*, 227-246.

10. Reinhard, C. T.; Planavsky, N. J.; Gill, B.C.; Ozaki, K.; Robbins, L. J.; Lyons, T. W.; Fischer, W. W.; Wang, C.; Cole, D.B.; Konhauser, K.O. Evolution of the global phosphorus cycle. *Nature*, **2017**, *541*, 386–389.

11. Lenton, T.M.; Daines, S.J.; Mills, B.J.W. COPSE reloaded: An improved model of biogeochemical cycling over Phanerozoic time. *Earth-Science Reviews*, **2018**, *178*, 1-28.

12. Guidry, M.W.; Mackenzie, F.T. Apatite weathering and the Phanerozoic phosphorus cycle. *Geology* **2000**, *28*, 631-634.

13. D'Antonio, M.P.; Ibarra, D.E.; Boyce, C.K. Land plant evolution decreased, rather than increased, weathering rates. *Geology* **2020**, *48*, 29-33.

14. Jenny, H.J. Factors in soil formation. 1941, McGraw-Hill, New York, United States.

15. Quirk J.; Leake J.R.; Johnson D.A.; Taylor L.L.; Saccone L.; Beerling D.J. Constraining the role of early land plants in Palaeozoic weathering and global cooling. *Proc. R. Soc. B* **2015**, *282*, 20151115.

16. Leake, J.R.; Read, D.J. Mycorrhizal symbioses and pedogenesis throughout Earth's history. In *Mycorrhizal Mediation of Soil: Fertility, Structure, and Carbon Storage.* Johnson, N.C.; Gehring, C.; Jansa, J.; **2017**, 9-33, Elsevier, New York, New York, United States.

17. Chadwick, O.A.; Derry, L.A.; Vitousek, P.M.; Huebert, B.J.; Hedin, L.O. Changing sources of nutrients during four million years of ecosystem development. *Nature* **1999**, *397*, 491-497.

18. Okin, G.S.; Mahowald, N.; Chadwick, O.A.; Artaxo, P. Impact of desert dust on the biogeochemistry of phosphorus in terrestrial ecosystems. *Global Biogeochemical Cycles*, **2004**, *18*, GB2005.

19. Walker, T.W.; Syers, J.K. The fate of phosphorus during pedogenesis. *Geoderma* **1976**, *15*, 1–19.

20. Wardle, D.AA.; Walker, L.R.; Bardgett, R.D. Ecosystem properties and forest decline in contrasting long-term chronosequences. *Science*, **2004**, *305*, 509-513.

21. Arvin, L.J.; Riebe, C.S.; Aciego, S.M.; Blakowski, M.A. Global patterns of dust and bedrock nutrient supply to montane ecosystems. *Science Advances*, **2017**, *3*, eaao1588, 1-10. DOI: 10.1126/sciadv.aao1588

22. Gu, C.; Hart, S.C.; Turner, B.L.; Hu, Y.; Meng, Y.; Zhu, M. Aeolian dust deposition and the perturbation of phosphorus transformation during long-term ecosystem development in a cool, semi-arid environment. *Geochimica et Cosmochimica Acta*, **2019**, *246*, 498-514.

23. Sherman, G.D. **1952**. The genesis and morphology of the alumina-rich laterite clays. *In* Problems of Clay and Laterite Genesis, Fredericksen, A.F., 154-161. New York: American Institute of Mining and Metallurgical Engineering.

24. Jobbagy, E.G; Jackson, R.B. The distribution of soil nutrients with depth: Global patterns and the imprint of plants. *Biogeochemistry*, **2001**, *53*, 51-77.

25. Riebe, C.S.; Kirchner, J.W.; Finkel, R.C. Erosional and climatic effects on long-term chemical weathering rates in granitic landscapes spanning diverse climate regimes. *Earth and Planetary Science Letters*, **2004**, *224*, 547-562.

26. Dixon, J.L.; Heimsath, A.M.; Amundson, R. The critical role of climate and saprolite weathering in landscape evolution. *Earth Surface Processes and Landforms*, **2009**, 34, 1507-1521.

27. Gabet, E.J.; Mudd, S.M. A theoretical model coupling chemical weathering rates with denudation rates. *Geology*, **2009**, *37*, 151-154.

28. Dixon, J.L.; Hartshorn, A.S.; Heimsath, A.M.; DiBiase, R.A.; Whipple, K.X. Chemical weathering response to tectonic forcing: A soils perspective from the San Gabriel Mountains, California. *Earth and Planetary Science Letters* **2012**, *323-324*, 40-49.

29. Hewawasam, T.; von Blanckenburg, F.; Bouchez, J.; Dixon, J.L.; Schuessler, J.A.; Maekeler, R. Slow advance of the weathering front during deep, supply-limited saprolite formation in the tropical Highlands of Sri Lanka. *Geochimica et Cosmochimica Acta*, **2013**, *118*, 202-230.

30. Uhlig, D.; Schuessler, J.A.; Bouchez,J.; Dixon, J.L.; von Blackenburg, F. Quantifying nutrient uptake as driver of rock weathering in forest ecosystems by magnesium stable isotopes. *Biogeosciences*, **2017**, *14*, 3111-3128. DOI: 10.5194/bg-14-3111-2017.

31. Eger, A.; Yoo, K.; Almond, P.C.; Boitt, G.; Larsen, I.J.; Condron, L.M.; Wang, X.; Mudd, S.M. Does soil erosion rejuvenate the soil phosphorus inventory? *Geoderma*, **2018**, *332*, 45-59.monta

32. Kurtz, A.C.; Derry, L.A.; Chadwick, O.A. Accretion of Asian dust to Hawaii soils: isotopic, elemental, and mineral mass balances. *Geochimica et Cosmochimica Acta* **2001,**

65 ,1971-1983.

33. Porder, S.; Hilley, G.E.; Chadwick, O.A. Chemical weathering, mass loss, and dust inputs across a climate by time matrix in the Hawaiian Islands. *Earth and Planetary Science Letters* **2007**, *258*, 414-427.

34. Swap, R.; Garstang, M.; Greco, S.; Talbot, R.; Kållberg, P. Saharan dust in the Amazon Basin. *Tellus B* **1992,** *44*, 133-149.

35. Bristow, C.S.; Hudson-Edwards, K.A.; Chappell, A. Fertilizing the Amazon and equatorial Atlantic with West African dust. *Geophysical Research Letters* **2010**, **37**, L14807.

36. Yu, H.; Chin, M.; Yuan, T.; Bian, H.; Remer, L.A.; Prospero, J.M.; Omar, A.; Winker, D.; Yang, Y.; Zhang, Y.; Zhang, Z.; Zhao, C. The fertilizing role of African dust in the Amazon rainforest: A first multiyear assessment based on data from cloud-aerosol lidar and infrared pathfinder satellite observations. *Geophysical Research Letters***, 2015,** *42***,** 1984-1991.

37. Bullard, J.E.; White, K. Dust production and the release of iron oxides resulting from the aeolian abrasion of natural dune sands. *Earth Surface Processes and Landforms* **2004,** *30*, 95-106.

38. Lafon, S.; Rajot, J.L.; Alfaro, S.C.; Gaudichet, A. Quantification of iron oxides in desert aerosol. *Atmospheric Environment* **2004**, *38*, 1211-1218.

39. Froelich, P.N. Kinetic control of dissolved phosphate in natural rivers and estuaries: A primer on the phosphate buffer mechanism. *Limnology and Oceanography*, **1988**, *33*, 649-668.

40. Karathanasis, A.D. Phosphate mineralogy and equilibria in two Kentucky Alfisols derived from Ordovician limestones. *Soil Sci. Soc. Am. J.*, **1991**, *55*, 1774-1782.
41. Turner, B.L.; Cade-Menun, B.J.; Westermann, D.T. Organic phosphorus composition and potential bioavailability in semi-arid arable soils of the western United States. *Soil Sci. Soc. Am. J.*, **2003**, *67*, 1168-1179.

42. Herndon, E.; AlBashaireh, A.; Singer, D.; Chowdhury, T.R.; Gu, B.; Grahan, D. Influence of iron redox cycling on organo-mineral associations in Arctic tundra soil, *Geochimica et Cosmochimica Acta* **2017**, *207*, 210-231.

43. Kuo S.; Mikkelsen D.S. Distribution of iron and phosphorus in flooded and unflooded soil profiles, and their relationship to phosphorus adsorption. *Soil Science* **1979**, *1*, 8-25.

44. Peña, F.; Torrent, F. Relationships between phosphate sorption and iron oxides in Alfisols from a river terrace sequence of Mediterranean Spain. *Geoderma*, **1984**, *33*, 283-

296.

45. Torrent, J.; Schwertmann, U.; Barrón, V. Fast and slow phosphate sorption by goethite-rich natural materials. *Clays and Clay Minerals*, **1992**, *40*, 14-21.

46. Jaisi, D.P.; Kukkadapu, R.K.; Stout, L.M.; Varga, T.; Blake, R.E. Biotic and abiotic pathways of phosphorus cycling in minerals and sediments: Insights from oxygen isotope ratios in phosphate. *Environmental Science & Technology*, **2011**, *45*, 6254-6261.

47. Prietzel, J.; Klysubun, W.; Werner, F. Speciation of phosphorus in temperate zone forest soils as assessed by combined wet-chemical fractionation and XANES spectroscopy. *J. Plant Nutrition and Soil Sci.*, **2016**, *179*, 168-185.

48. Coronato, F.R.; Bertiller, M.B. Climatic controls of soil moisture dynamics in an arid steppe of northern Patagonia, Argentina. *Arid Soil Research and Rehabilitation*, **1996**, *11*, 277-288.

49. Sandvig, R.M.; Phillips, F.M. Ecohydrological controls on soil moisture fluxes in arid to semiarid vadose zones. *Water Resources Research*, **2006**, *42*, W08422.

50. Vivoni, E.R.; Rinehard, A.J.; Mendez-Barroso, L.A.; Aragon, C.A.; Bisht, G.; Bayani Cardenas, M.; Engle, E.; Forman, B.A.; Frisbee, M.D.; Gutierrez-Jurado, H.A.; Hong, S.; Mahmood, T.H.; Tai, K.; Wyckoff, R.L. *Ecohydrology*, **2008**, *1*, 225-238.

51. Gaur, N.; Mohanty, B.P. Evolution of physical controls for soil moisture in humid and subhumid watersheds. *Water Resources Research*, **2013**, *49*, 1244-1258.

52. Fatichi, S.; Katul, G.G.; Ivanov, V.Y.; Pappas, C.; Paschalis, A.; Consolo, A.; Kim, J.; Burlando, P. Abiotic and biotic controls of soil moisture spatiotemporal variability and the occurrence of hysteresis. *Water Resources Research*, **2015**, *51*, 3505-3524.

53. Wang, T.; Wedin, D.A.; Franz, T.E.; Hiller, J. Effect of vegetation on the temporal stability of soil moisture in grass-stabilized semiarid sand dunes. *Journal of Hydrology*, **2015**, *521*, 447-459.

54. Surridge, B.W.J.; Heathwaite, A.L.; Baird, A.J. The release of phosphorus to porewater and surface water from river riparian sediments. *J. Environmental Quality*, **2007**, *36*, 1534-1544.

55. Kerr, J.G.; Burford, M.; Olley, J.; Udy, J. Phosphorus sorption in soils and sediments: implications for phosphate supply to a subtropical river in southeast Queensland, Australia. **2010** *Biogeochemistry*, **2010**, *102*, 73-85.

56. Berner, R.A. The carbon cycle and carbon dioxide over Phanerozoic time: The role of land plants. *Phil Trans Roy Soc B Biology* **1998**, 353.

57. Martin, J.H.; Fitzwater, S.E. Iron deficiency limits phytoplankton growth in the north-east Pacific subarctic. *Nature* **1988**, *331*, 431-343.

58. Martin, J.H.; Coale, K.H.; …; Tindale, N.W. Testing the iron hypothesis in ecosystems of the equatorial Pacific Ocean. *Nature* **1994**, *371*, 123-129.

59. Coale, K.H. Effects of iron, manganese, copper, and zinc enrichments on productivity and biomass in the subarctic Pacific. *Limnology and Oceanography* **1991**, *36*, 1851-1864.

60. Boyd, P.W.; Watson, A.J.; …; Zeldis, J. A mesoscale phytoplankton bloom in the polar Southern Ocean stimulated by iron fertilization. *Nature* **2000**, *407*, 695-702.

61. Berner, R.A.; Rao, J.L. Phosphorus in the sediments of the Amazon River and estuary: Implications for the global flux of phosphorus to the sea. *Geochimica et Comochimica Acta* **1994**, *58*, 2333-2339.

62. Moulton, K.L.; Berner, R.A. Quantification of the effect of plants on weathering: Studies in Iceland. *Geology*, **1998**, *26*, 895-898.

63. Lenton T.M.; Dahl, T.W; Daines, S.J.; Mills, B.J.W.; Ozaki, K.; Saltzman, M.R.; Porada, P. Earliest land plants created modern levels of atmospheric oxygen. *PNAS* **2016**, *113*, 9704-9709.

64. Smith, D.B.; Cannon, W.F.; Woodruff, L.G.; Solano, F.; Ellefsen, K.J. Geochemical and mineralogical maps for soils of the conterminous United States: U.S. Geological Survey Open-File Report **2014**, 386 p., *https://dx.doi.org/10.3133/ofr20141082*. ISSN 2331-1258 (online)

65. Box, E.O. Plant functional types and climate at the global scale. *J. Vegetation Sci.*, **1996**, *7*, 309-320.

66. Diaz S.; Cabido, M. Plant functional types and ecosystem function in relation to global change. *J. Vegetation Sci.*, **2009**, 8, 463-474.

67. DiMichele, W.A.; Montañez, I.P.; Poulsen, C.J.; Tabor, N.J. Climate and vegetational regime shifts in the late Paleozoic ice age Earth. *Geobiology* **2009**, 7, 200-226.

68. Diefendorf, A.F.; Mueller, K.E.; Wing, S.L.; Koch, P.L.; Freeman, K.H. Global patterns in leaf ^{13}C discrimination and implications for studies of past and future climate. *PNAS* **2010**, 107, 5738-5743.

69. Poulton, S.W.; Canfield, D.E. Development of a sequential extraction procedure for iron: implications for iron partitioning in continentally derived particulates. *Chemical Geology* **2005**, *214*, 209-221.

70. Raiswell, R.; Vu, H.P.; Brinza, L.; Benning, L.G. The determination of labile Fe in ferrihydrite by ascorbic acid extraction: Methodology, dissolution kinetics and loss of solubility with age and de-watering. *Chemical Geology* **2004**, *278*, 70-79.

71. Canfield, D.E.; Raiswell, R.; Westrich, J.T.; Reaves, C.M.; Berner, R.A. The use of chromium reduction in the analysis of reduced inorganic sulfur in sediments and shales. *Chemical Geology* **1986**, *54*, 149-155.

72. Sheldon, N.D.; Retallack, G.J. Equation for compaction of paleosols due to burial. *Geology* **2001**, *29*, 247-250.

73. Raiswell, R.; Hardisty, D.S; Lyons, T.W.; Canfield, D.E.; Owens, J.D.; Planavsky, N.J.; Poulton, S.W.; Reinhard C.T. The iron paleoredox proxies: A guide to the pitfalls, problems and proper practice. *Am J Sci* **2018**, 318, 491-526.

74. Algeo, T.J.; Liu, J. A re-assessment of elemental proxies for paleoredox analysis. *Chemical Geology* **2020**, 540, 119549.

75. Nesbitt, H.W.; Young, G.M. Early Proterozoic climates and plate motions inferred from major element chemistry of lutites. *Nature* **1982**, *299*, 715–717.

76. Li, C.; Yang, S. Is chemical index of alteration (CIA) a reliable proxy for chemical weathering in global drainage basins? *Am J Sci* **2010**, *310*, 111-127.

77. Taylor S.R.; McLennan S.M. The geochemical evolution of the continental crust. *Reviews of Geophysics* **1995**, *33*, 241-265.

78. Jobbagy, E.G; Jackson, R.B. The distribution of soil nutrients with depth: Global patterns and the imprint of plants. *Biogeochemistry*, **2001**, *53*, 51-77.

79. Sheldon, N.D.; Tabor, N.J. Quantitative paleoclimatic and paleoenvironmental reconstruction using paleosols. *Earth-Sci. Rev.* **2009**, *95*, 1–52.

80. Gallagher, T.M.; Sheldon, N.D. A new paleothermometer for forest paleosols and its implications for Cenozoic climate. *Geology*, **2013,** *41*, 647-650.

81. Stinchcomb, G.E.; Nordt, L.C.; Driese, S.G.; Lukens, W.E.; Williamson, F.C.; Tubbs, J.D. A data-driven spline model designed to predict paleoclimate using paleosol geochemistry. *Am. J. Sci.* **2016**, *316*, 746-777.

82. Gérard, F. Clay minerals, iron/aluminum oxides, and their contribution to phosphate sorption in soils – A myth revisited. *Geoderma* **2016**, *262*, 213-226.

83. Soil Survey Staff, Keys to Soil Taxonomy: Twelfth Edition. 2014, USDA-NRCS, United States.

84. Maher B. Magnetic properties of modern soils and Quaternary loessic paleosols: paleoclimatic implications. *Palaeogeography, Palaeoclimatology, Palaeoecology* **1998**, *137*, 25-54.

85. Maher, B.; Possolo, A. Statistical models for use of palaeosol magnetic properties as proxies of palaeorainfall. *Global and Planetary Change* **2013**, *111*, 280-287.

86. Hyland, E.G.; Sheldon, N.D.; Van der Voo, R.; Badgley, C.; Abrajevitch, A. A new paleoprecipitation proxy based on soil magnetic properties: implications for expanding paleoclimate reconstructions. *Geol. Soc. Am. Bull.* **2015**, *127*, 975–981.

87. Maxbauer, D.P.; Feinberg, J.M.; Fox, D.L. Magnetic mineral assemblages in soils and paleosols as the basis for Paleoprecipitation proxies: A review of magnetic methods and challenges. **2016** *Earth-Science Reviews*, **2016**, *155*, 28-48.

88. Prem, M.; Hansen, H.C.B.; Wenzel, W.; Heiberg, L.; Sørensen, H.; Kragholm, O. High spatial and fast changes of iron redox state and phosphorus solubility in a seasonally flooded temperate wetland soil. *Wetlands* **2015,** *35*, 237-246.

89. Valaee, M.; Ayoubi, S.; Khormali, F.; Lu, S.G.; Karimzadeh, H.R. Using magnetic susceptibility to discriminate between soil moisture regimes in selected loess and loess-like soils in northern Iran, *Journal of Applied Geophysics* **2016**, *127*, 23-30.

90. Cervi, E.C.; Maher, B.; Poliseli, P.C.; Junior, I.V.d.S.; da Costa, A.C.S. Magnetic susceptibility as a pedogenic proxy for grouping of geochemical transects in landscapes, *Journal of Applied Geophysics* **2019**, *169*, 109-117.

91. Chaparro, M.A.E.; Moralejo, M.d.P.; Bohnel, H.N.; Acebal, S.G. Iron oxide mineralogy in Mollisols, Aridisols and Entisols from the southwestern Pampean region (Argentina) by environmental magnetism approach. *Catena*, **2020**, *190*, 104534.

92. Hu, P.; Heslop, D.; Viscarra Rossel, R.A.; Roberts, A.P.; Zhao, X. Continental-scale magnetic properties of surficial Australian soils. *Earth-Science Reviews*, **2020**, *203*, 103028.

93. Borggaard O.K. The influence of iron oxides on phosphate adsorption by soils. *European J. Soil Sci.* **1983**, *34*, 333-341.

94. Stone, M.; Mudroch, A. The effect of particle size, chemistry and mineralogy of river sediments on phosphate adsorption. *Environmental Technology*, **1989**, *10*, 501-510.

95. Halsted, M.; Lynch, J. Phosphorus responses of C_3 and C_4 species. *J. Exp. Botany* **1996**, *47*, 497-505.

96. Griffith, D.M.; Cotton, J.M.; Powell, R.L.; Sheldon, N.D.; Still, C.J. Multi-century stasis in C_3 and C_4 grass distributions across the contiguous United States since the Industrial

revolution. *Journal of Biogeography* **2017**, *44*, 2564-2574.

97. Katra I.; Gross, A.; Swet, N.; Tanner, S.; Krasnov, H.; Angert, A. Substantial dust loss of bioavailable P from agricultural soils. *Scientific Reports* **2016**, *6*, 24736.
98. Ewel, J.J.; Mazzarino, M.J.; Berish, C.W. Tropical soil fertility changes under monocultures and successional communities of different structure. *Ecological Applications*, **1991**, *1*, 289-302.

99. Gregorich E.G.; Anderson D.W. Effects of cultivation and erosion on soils of four toposequences in the Canadian prairies. *Geoderma* **1985**, *36*, 343-354.

100. Cotton, J.M.; Jeffery, M.L.; Sheldon, N.D. Climate controls on soil respired CO_2 in the United States: Implications for 21st century chemical weathering rates in temperate and arid ecosystems. *Chemical Geology*, **2013**, *358*, 37-45.

101. Leakey, A.D.B.; Ainsworth, E.A.; Bernacchi, C.J.; Rogers, A.; Long, S.P.; Ord, D.R. Elevated CO2 effects on plant carbon, nitrogen, and water relations: six important lessons from FACE. *J. Exp. Botany*, **2009**, *60*, 2859-2876.

102. Terrer, C.; Vicca, S.; Hungate, B.A.; Phillips, R.P.; Prentice, I.C. Mycorrhizal association as a primary control of the CO_2 fertilization effect. *Science* **2016**, *353*, 72-74.

103. Obermeier, W.A.; Lehnert, L.W.; Kammann, C.I.; Muller, C.; Grunhage, L.; Luterbacher, J.; Erbs, M.; Moser, G.; Seibert, R.; Yuan, N.; Bendix, J. Reduced CO_2 fertilization effect in temperate C_3 grasslands under more extreme weather conditions. *Nature Climate Change* **2017**, *7*, 137-141.

104. Mearns, L. O.; Gutowski, W.J.; Jones, R.; Leung, L.Y.; McGinnis, S.; Nunes, A.M.B.; Qian, Y. A regional climate change assessment program for North America. *EOS*, **2009**, *90*, 311-312.

105. Maynard, J.B. Chemistry of modern soils as a guide to interpreting Precambrian paleosols. *The Journal of Geology* **1993**, *100*, 279-289.

106. Crews, T.E.; Kitayama, K.; Fownes, J.H.; Riley, R.H.; Herbert, D.A.; Mueller-Dombois, D.; Vitousek, P.M. Changes in soil phosphorus fractions and ecosystem dynamics across a long chronosequence in Hawaii. *Ecology*, **1995**, *76*, 1407-1424.

107. Schachtman, D.P.; Reid, R.J.; Ayling, S.M. Phosphorus uptake by plants: From soil to cell. *Plant Physiol.* **1998**, *116*, 447-453.

108. 50 Lynch, J.P.; Brown, K.M. Root strategies for phosphorus acquisition. *In* The Ecophysiology of Plant-Phosphorus Interactions. White, P.J.; Hammond, J.P., **2008**, Springer, Dordecht, Germany.

109. Smith, S.E.; Jakobsen, I.; Groønlund, M.; Smith, F.A. Roles of arbuscular mycorrhizas in plant phosphorus nutrition: Interactions between pathways of phosphorus uptake in arbuscular mycorrhizal roots have important implications for understanding and manipulating plant phosphorus acquisition. *Plant Physiol.* **2011**, *156*, 1050-1057.

110. Fitter, A.H.; Heinemeyer, A.; Husband, R.; Olsen, E.; Ridgway, K.P.; Staddon, P.L. Global environmental change and the biology of arbuscular mycorrhizas: gaps and challenges. *Can. J. Bot*. **2008**, *82*, 1133-1139.

111. Deepika, S.; Kothamasi, D. Soil moisture - a regulator of arbuscular mycorrhizal fungal community assembly and symbiotic phosphorus uptake. *Mycorrhiza* **2015**, *25*, 67-75.

112. Pearson, J.N.; Jakobsen, I. The relative contribution of hyphae and roots to phosphorus uptake by arbuscular mycorrhizal plants, measured by dual labelling with ^{32}P and ^{33}P. *New Phytologist* **1993**, *124*, 489-494.

113. Gavito, M.E.; Schweiger, P.; Jakobsen, I. P uptake by arbuscular mycorrhizal hyphae: Effect of soil temperature and atmospheric CO_2 enrichment. *Global Change Biology* **2003**, *9*, 106-116.

114. Treseder, K.K. A meta-analysis of mycorrhizal responses to nitrogen, phosphorus, and atmospheric CO_2 in field studies. *New Phytologist* **2004**, *164*, 347-355.

115. Kimball, B.A. Carbon dioxide and agricultural yield: An Assemblage and analysis of 430 prior observations. *Agron. J.* **1983**, *75*, 779-788.

116. Solomon, A.M.; Cramer, W. Biospheric implications of global environmental change. *In* Vegetation Dynamics and Global Change. Solomon, A.M.; Shugart, H.H.; Chapman and Hall, New York, United States, **1993**, 25-52.

117. Ehleringer, J. R.; Cerling, T. E. The earth system: biological and ecological dimensions of global environmental change. In *Encyclopedia of Global Environmental Change*; H. A. Mooney, J. G. Canadell; Chichester: John Wiley & Sons, Ltd., United Kingdom, **2002**, 186–190.

118. Girardin, M.P.; Bouriaud, O.; Hogg, E.H.; Kurz, W.; Zimmerman, N.E.; Metsaranta, J.M.; de Jong, R.; Frank, D.C.; Esper, J.; Büntgen, U.; Guo, X.J.; Bhatti, J. No growth stimulation of Canada's boreal forest under half-century of combined warming and CO_2 fertilization. *PNAS* **2016**, *113*, E8406-E8414.

119. Stein, R.A.; Sheldon, N.D.; Smith, S.Y. Rapid response to anthropogenic climate change by Thuja occidentalis: implications for past climate reconstructions and future climate predictions. *PeerJ* **2019**, *7*, e7378.

120. Sheldon, N.D.; Smith, S.Y.; Stein, R.A.; Ng, M. Carbon isotope ecology of gymnosperms and implications for paleoclimatic and paleoecological studies. *Global and Planetary Change* **2020**, *184*, 103060.

121. Norby, R.J.; Warren, J.M.; Iversen, C.M.; Medlyn, B.E.; McMurtrie, R.E. CO_2 enhancement of forest productivity constrained by limited nitrogen availability. *PNAS* **2010**, *107*, 19368-19373.

122. Ellsworth, D.S.; Anderson, I.C.; Crous, K.Y.; Cooke, J.; Drake, J.E.; Gherlenda, A.N.; Gimeno, T.E.; Macdonald, C.A.; Medlyn, B.E.; Powell, J.R.; Tjoelker, M.G.; Reich, P.B. Elevated CO_2 does not increase eucalypt forest productivity on a low-phosphorus soil. *Nat. Clim. Change* **2017**, *7*, 279-282.

123. Terrer, C.; Jackson, R.B.; Prentice, I.C.; … Franklin, O. Nitrogen and phosphorus constrain the CO_2 fertilization of global plant biomass. *Nature* **2019**, 9, 684-689.

124. Cleveland, C.C.; Liptzin, D. C:N:P stoichiometry in soils: is there a "Redfield ratio" for the microbial biomass? *Biogeochemistry* **2007**, 85, 235-252.

125. Maranger, R.; Jones, S.E.; Cotner, J.B. Stoichiometry or carbon, nitrogen, and phosphorus through the freshwater pipe. **2018,** *Limnology and Oceanography Letters*, **3**, 89-101.

126. Berner, R.A. Weathering, plants, and the long-term carbon cycle. *Geochimica et Cosmochimica Acta*, **1992**, *56*, 3225-3231.

127. Samreen, S.; Kausar, S. Phosphorus fertilizer: The original and commercial sources. In Phosphorus – Recovery and Recycling. Zhang, T. IntechOpen. DOI: 10.5772/intechopen.82240

128. Siebers, N.; Godlinski, F.; Leinweber, P. The phosphorus fertilizer value of bone char for potatoes, wheat, and onions: first results. *Agriculture and Forestry Research,* **2012**, *62*, 59-64.

129. Zwetsloot, M.J.; Lehmann, J.; Bauerle, T.; Vanek, S.; Hestrin, R.; Nigussie, A. Phosphorus availability from bone char in a P-fixing soil influenced by root-mycorrhizae-biochar interactions. *Plant and Soil* **2016**, *408*, 95-105.

130. Cordell, D.; Drangert, J.O.; White, S. The story of phosphorus: Global food security and food for thought. *Global Environmental Change*, **2009**, *19*, 292-305.

131. Dawson, C.J.; Hilton, J. Fertiliser availability in a resource-limited world: Production and recycling of nitrogen and phosphorus. *Food Policy*, **2011**, *36*, S14-S22.

132. Cordell, D.; White, S. Sustainable phosphorus measures: Strategies and technologies for achieving phosphorus security. *Agronomy*, **2013**, *3*, 86-116.

133. Retallack, G.J. Soils of the past: An introduction to paleopedology. 2001, Oxford, United Kingdom.

134. Rye, R.; Holland, H.D. Paleosols and the evolution of atmospheric oxygen: A critical review. *Am. J. Sci.* **1998**, *298*, 621-672.

135. Cerling, T.E. Carbon dioxide in the atmosphere: Evidence from Cenozoic and Mesozoic paleosols. *Am. J. Sci.* **1999**, *291*, 377-400.

136. Sheldon, N.D. Using paleosols of the Picture Gorge Basalt to reconstruct the Middle Miocene Climatic Optimum. *PaleoBios* **2006**, *26*, 27-36.

137. Driese, S. G.; Jirsa, M.A.; Ren, M.; Brantley, S.L.; Sheldon, N.D.; Parker, D.; Schmitz, M. Neoarchean paleoweathering of tonalite and metabasalt: Implications for reconstructions of 2.69 Ga early terrestrial ecosystems and paleoatmospheric chemistry. *Precambrian Res.* **2011**, *189*, 1–17.

138. Murakami, T.; Sreenivas, B.; Das Sharma, S.; Sugimori, H. Quantification of atmospheric oxygen levels during the Paleoproterozoic using paleosol compositions and iron oxidation kinetics. *Geochimica et Cosmochimica Acta* **2011**, *75*, 3982-4004.

139. Driese, S.G. Pedogenic translocation of Fe in modern and ancient Vertisols and implications for interpretations of the Hekpoort paleosol (2.25 Ga). *The Journal of Geology* **2004**, *112*, 543-560.

140. Retallack G.J. Criteria for distinguishing microbial mats and earths. *SEPM Special Publication* **2012**, 101.

141. Hyland, E.G.; Sheldon, N.D. Examining the spatial consistency of palaesol proxies: Implications for palaeoclimatic and palaeoenvironmental reconstructions in terrestrial sedimentary basins. *Sedimentology* **2016**, *63*, 959-971.

142. Beukes, N.J.; Dorland, H.; Gutzmer, J.; Nedachi, M.; Ohmoto, H. Tropical laterites, life on land, and the history of oxygen in the Paleoproterozoic. *Geology* **2002**, *30*, 491-494.

143. Beraldi-Campesi, H.; Hartnett, H.E.; Anbar A.; Gordon, G.W.; Garcia-Pichel, F. Effect of biological soil crusts on soil elemental concentrations: Implications for biogeochemistry and as traceable biosignatures of ancient life on land. *Geobiology* **2009**, *7*, 348-359.

144. Donnadieu, Y.; Goddéris, Y.; Ramstein, G.; Nédélec, A.; Meert, J. A 'snowball Earth' climate triggered by continental break-up through changes in runoff. *Nature* **2004**, *541*, 303–306.

145. Mills, B. J. W., Watson, A.J., Goldblatt, C., Boyle, R., Lenton, T.M. Timing of Neoproterozoic glaciations linked to transport-limited global weathering. *Nat. Geosci.* **2011**, *4*, 861–864.

146. Dzombak, R.M.; Sheldon, N.D. Three billion years of continental weathering and implications for marine biogeochemistry. *Proceedings of Goldschmidt Annual Geochemical Conference*, virtual, June 21-26, 2020; abstract number 635.

147. Canfield, D.E. A new model for Proterozoic ocean chemistry. *Nature* **1998**, *396*, 450-453.

148. Habicht, K.S.; Gade, M.; Thamdrup, B.; Berg, P.; Canfield, D.E. Calibration of sulfate levels in the Archean Ocean. *Science* **2002**, *298*, 2372-2374.

149. Halevy, I.; Peters, S.E.; Fischer, W.W. Sulfate burial constraints on the Phanerozoic sulfur cycle. *Science* **2012**, *337*, 331-334.

150. Fakhraee, M.; Hancisse, O.; Canfield, D.E.; Crowe, S.A.; Katsev, S. Proterozoic seawater sulfate scarcity and the evolution of ocean-atmosphere chemistry. *Nature Geoscience* **2019**, *12*, 375-380.

151. Cameron, E.M. Sulphate and sulphate reduction in early Precambrian oceans. *Nature* **1982**, *296*, 145-148.

152. Hoffman, P.F.; Kaufman, A.J.; Halverson, G.P.; Schrag, D.P. A Neoproterozoic Snowball Earth. *Science* **1998**, *281*, 1342-1346.

153. Prasad, N.; Roscoe, S.M. Evidence of anoxic to oxic atmospheric change during 2.45-2.22 Ga from lower to upper sub-Huronian paleosols, Canada. *Catena* **1996**, *27*, 105-121.

154. Algeo, T.G.; Scheckler, S.E. Terrestrial-marine teleconnections in the Devonian: Links between the evolution of land plants, weathering processes, and marine anoxic events. *Phil. Trans. Royal Soc. B* **1998**, *353*, 113-130.

Chapter 3
Three Billion Years of the Phosphorus Biogeochemical Cycle on Land[2]

3.1 Abstract

Phosphorus (P) is an essential nutrient for all organisms, ancient and modern, so constraining the timing and magnitude of P fluxes through geologic time is essential context for biological evolution. The timing and magnitude of P fluxes from continents to oceans have been implicated in critical transitions during Earth's history, such as rises in atmospheric oxygen and the evolution of complex life, but without better quantifying the terrestrial source of P in deep time, our ability to interpret trends in the marine shale P record is limited. Currently, our understanding of P biogeochemical cycling in a geologic sense is centered on the sediment sink—oceans—rather than the source. Paleosols (fossilized soils) and other terrestrial weathering products are sparser in the geologic record than marine shales, but they provide critical, direct insight into the P cycle on land. Here, we present a 3-billion-year record of P in paleosols, showing that the composition of terrestrial weathering products has been relatively unchanged since the rise of subaerially-exposed continents *ca.* 3 billion years ago. Notably, this stability persists through the rise of land plants, a biological innovation long thought to have caused a state change in terrestrial P cycling. The consistency of both P concentrations and mobilization from bedrock points to the importance of changes in continental land area as a primary baseline for potential P fluxes, with tectonics and climate change as secondary controls.

[2] *This chapter is in preparation for submission at Nature.*

3.2 Introduction: Phosphorus in ecosystems past and present

Phosphorus (P) is an essential nutrient and a critical driver of global primary productivity in modern ecosystems (Filippelli, 2002), and P was likely an essential nutrient in many ancient ecosystems as well. Changes in the timing and magnitude of P release from bedrock and transport between continents and the oceans are thought to have contributed to major events in Earth's biogeochemical past, such as changes in the atmospheric and marine oxygen content throughout the Proterozoic and the evolution of complex life during the Neoproterozoic (Guidry and Mackenzie, 2000; Paytan and McLoughlin, 2007; Kipp and Stueken, 2017; Reinhard et al., 2017; Laakso and Schrag 2018; Lenton et al., 2018; Hao et al., 2020a,b; Reinhard et al., 2020). P movement from the source to sink has been invoked as a first-order control on marine primary productivity, which would have provided O_2 and increased CO_2 drawdown. Atmospheric composition changes are also connected to the silicate weathering cycle, with positive feedbacks between atmospheric CO_2 (pCO_2) and weathering intensity. Increased weathering intensity on the continents, in turn, has been hypothesized to have increased the magnitude of P being delivered to the oceans, further stimulating primary productivity and increasing pO_2. Weathering intensity is also a control on P concentration in soils (e.g., Walker and Syers, 1976).

As the oceans became oxygenated (likely in the Neoproterozoic; Lyons et al., 2014), rates of scavenging and burial between P, Fe, and organic C are thought to have changed, affecting bioavailable P for marine primary producers particularly during the Neoproterozoic (Reinhard et al., 2017). An increase in marine shale P coincides approximately with the evolution of complex animal life (metazoan) in the Neoproterozoic. Later, in the Phanerozoic, the evolution of rooting land plants and symbiotic fungi has been hypothesized to cause a state change in the degree of weathering intensity on land, consequently affecting P fluxes. Arguments for both an increase (Lenton and Watson, 2004) and decrease (D'Antonio et al., 2020) in weathering intensity have been made, with the former increasing P fluxes to oceans and the latter decreasing P fluxes. Those potential changes in P delivery could have had an effect on Phanerozoic pO_2 levels (e.g., Lenton and Watson, 2004).

In each of these major biogeochemical transitions—oxygenation of the atmosphere and oceans, the evolution of animals, and the rise of land plants—the concentration P in soils and its movement from bedrock to soils, and from soils to oceans (source to sink), is a critical variable. However, records from the P sink (marine shales) are more readily available and more widely

studied than the source (Figure 3.1a), leaving biogeochemical models to make assumptions about the critical parameter of terrestrial P. This fundamental knowledge gap can be bridged by using existing paleosol geochemical data in the literature to quantify terrestrial P concentrations and test hypotheses about changes in terrestrial P through geologic time. Those same data can also help answer outstanding questions about how similar ancient soils' P cycling may have been to modern soils.

An additional motivation for this work is the potential for the paleosol record of P to reflect the development of a terrestrial biosphere. While some argue that a terrestrial biosphere did not evolve until the Neoproterozoic, there is evidence that life on land existed as early as life in the oceans, including physical structures likely made by microbial communities, C and N isotopes, molecular clocks, and elemental enrichments indicative of biotic cycling (Lenton and Daines, 2017; Finke et al., 2019; de Kock et al., 2020; Wellman and Strother, 2015; Noffke et al., 2008, Noffke et al., 2013; Sheldon 2012; Rye and Holland, 2000; Driese et al., 2011; Beaty and Planavsky, 2021; Homann et al., 2018; Homann, 2019; Jabłonska and Tawfik, 2021). A terrestrial biosphere would likely have affected the terrestrial P cycle, and likely would have mediated the source-to-sink movement of P.

The evolution of a widespread terrestrial biosphere in the Neoproterozoic and the evolution of vascular land plants and roots in the Devonian are two critical transition periods in biogeochemical history (e.g., Knauth and Kennedy 2009; Beraldi-Campesi et al. 2009; Wellman and Strother 2015). Both periods have been argued as causes for increased P fluxes and resulting biogeochemical shifts (*e.g.,* Lenton and Watson, 2004; Knauth and Kennedy, 2009; D'Antonio et al., 2020). Knauth and Kennedy (2009) argued for a Neoproterozoic "greening" of the continents as the terrestrial biosphere dramatically expanded, resulting in the Neoproterozoic oxygenation event (NOE). In the Phanerozoic, the advent of rooting plants and mycorrhizal fungi could have increased targeted P weathering and mobilization from bedrock (Guidry and Mackenzie, 2000; Lenton and Watson, 2004; Berner, 2004). Alternatively, the evolution of rooting plants and mycorrhizal fungi could have led to greater soil retention and increased biotic P cycling in soils, ultimately stabilizing or even decreasing P fluxes to the oceans (D'Antonio et al., 2020).

In modern soils, biogeochemical processes largely control P mobilization, movement, and loss in terrestrial ecosystems. Rooting plants with symbiotic fungi (mycorrhizae) facilitate P mobilization from bedrock via acid weathering (e.g., Lenton, 2001; Neaman et al., 2005). The

balance of these processes determines whether there is a net depletion or retention of P within a soil. Previous work has shown that deviations from bedrock P concentrations, either depletion or retention, can be associated with a biosphere that is actively using and cycling P, serving as a semi-quantitative biosignature in ancient soils (Beaty and Planavsky, 2021). Therefore, the paleosol P record can be used to check for terrestrial P cycling as an additional line of evidence for early life on land.

In modern soils, P retention relative to the parent material is a key indicator of biotic activity, from microbes and mesoscopic organisms to roots and plants. Organic acids from plants and fungi weather apatite (and other P-bearing minerals) to mobilize P from bedrock or regolith. P can then be taken up into the plant and enter the biosphere, being recycled as organic matter decomposes. Most of this occurs either in the rhizosphere or in the O horizon, which is the layer of active organic matter accumulation in modern soils; however, C, N, and other nutrients like P also accumulate down-profile, though typically in decreasing concentrations (Walker and Syers, 1976; Smeck, 1985; Jobbágy and Jackson, 2001). In a mature soil, these processes create a characteristic P trend through the vertical soil profile, with P accumulation at the surface and typically decreasing deeper in the soil as biotic activity becomes more limited (Walker and Syers, 1976). P accumulation has also been found on microbial scales, with biological soil crusts (BSCs; symbiotic communities of cyanobacteria, fungi, and algae) showing enriched P concentrations relative to soils without BSC (e.g., Beraldi-Campesi et al., 2009). The enrichment pattern in BSCs is important for early terrestrial biospheres, as they would have been composed of microbial and, later, algal mats, with fungi coming into the scene much later in the latest Neoproterozoic (e.g., Labandeira 2005; Wellman and Strother, 2015; Gomes et al., 2020; Thomazo et al., 2020).

The geologic P record

Current understanding is that fluvial systems were the primary mode of P transport in Earth's past, moving weathered material from continents to oceans (Filippelli 2002). These transport processes are recorded by marine sediments (*e.g.*, shales, Figure 3.1a, Reinhard et al., 2017). An increase in P in marine sediments in the Neoproterozoic has been connected to the rise of atmospheric oxygen (primary productivity stimulation) and evolution of early animals (removal of a nutrient limitation) (e.g., Lenton and Watson, 2004; Planavsky et al., 2010; Lyons

et al., 2014; Reinhard et al., 2017; Lenton and Daines, 2018; Guilbaud et al., 2020; Laakso et al., 2020). This increase has been primarily attributed to two possible mechanisms: a rapid onset and expansion of a terrestrial biosphere (Knauth and Kennedy, 2009) or an increase in the efficiency of P recycling by marine ecosystems (Reinhard et al., 2017).

Deep-time biogeochemical models commonly make the additional assumption that the P concentration of the exported weathered product would have been approximately equal to the average of P in continental crust. (Other workers have suggested P concentrations in terrestrial sediments would have been lower than modern; Lyons et al., 2014). However, the assumption that weathering products had similar P concentration to the continental crust has not yet been quantitatively demonstrated, potentially affecting the accuracy of our models of critical transitional periods in Earth's history.

Here, we compile a new ca. 3-billion-year record of P in paleosols and Precambrian weathering profiles (Figure 3.1b), along with fluvial sandstones and glacial diamictites (Gaschnig et al., 2015). We provide quantitative constraints on the range and distribution of P concentrations in weathering products through time. By comparing that record to crustal P composition (Cox et al., 2018) and the marine P sink (Reinhard et al., 2017), we provide a more robust conceptual perspective on P source-to-sink cycling through geologic time. Additionally, we examine P retention/depletion in bedrock-parented paleosols through time to test the hypotheses (a) that a Neoproterozoic terrestrial biosphere expansion led to greater P mobilization, and (b) that the early Phanerozoic evolution of land plants changed terrestrial P cycling.

3.3 Results: Three billion years of terrestrial P

Our new record shows that terrestrial P (paleosols, fluvial sandstones, and diamictites) has been at approximately the crustal average P value through time (ca. 0.2 wt %; Figure 3.1b; Figure B1). While the crustal record shows a slight and gradual increase through time (Figure 3.1c), the change over time is small relative to the range of P concentrations in paleosols. Paleosol and weathering profile P values all fall within the P range of modern soils (green bar in Figure 3.1b). Diamictites show little change in P (Figure 3.2). In contrast to the stable paleosol P record, P in shales increases around 600–700 Ma (Figure 3.1a), and bootstrapped means of

shales show a slight increase in mean P in the Phanerozoic (Figure B3a; Reinhard et al. 2017). (Building on Reinhard et al. (2017), Laakso et al. (2020) argue against a statistical change in P in marine sedimentary rocks. Our analysis supports a slight but significant increase in shale P.) Bootstrapping the Precambrian/Phanerozoic P_2O_5 means in paleosols shows a slight decrease in Phanerozoic paleosols (Figure B3b). Quantile-quantile plots demonstrate that for paleosols in both the Precambrian and Phanerozoic, data are approximately log-normally distributed and behave similarly, with heavy right-skewed long-tail distributions (Figure B4). Additional discussion of statistical methods is in Appendix B.

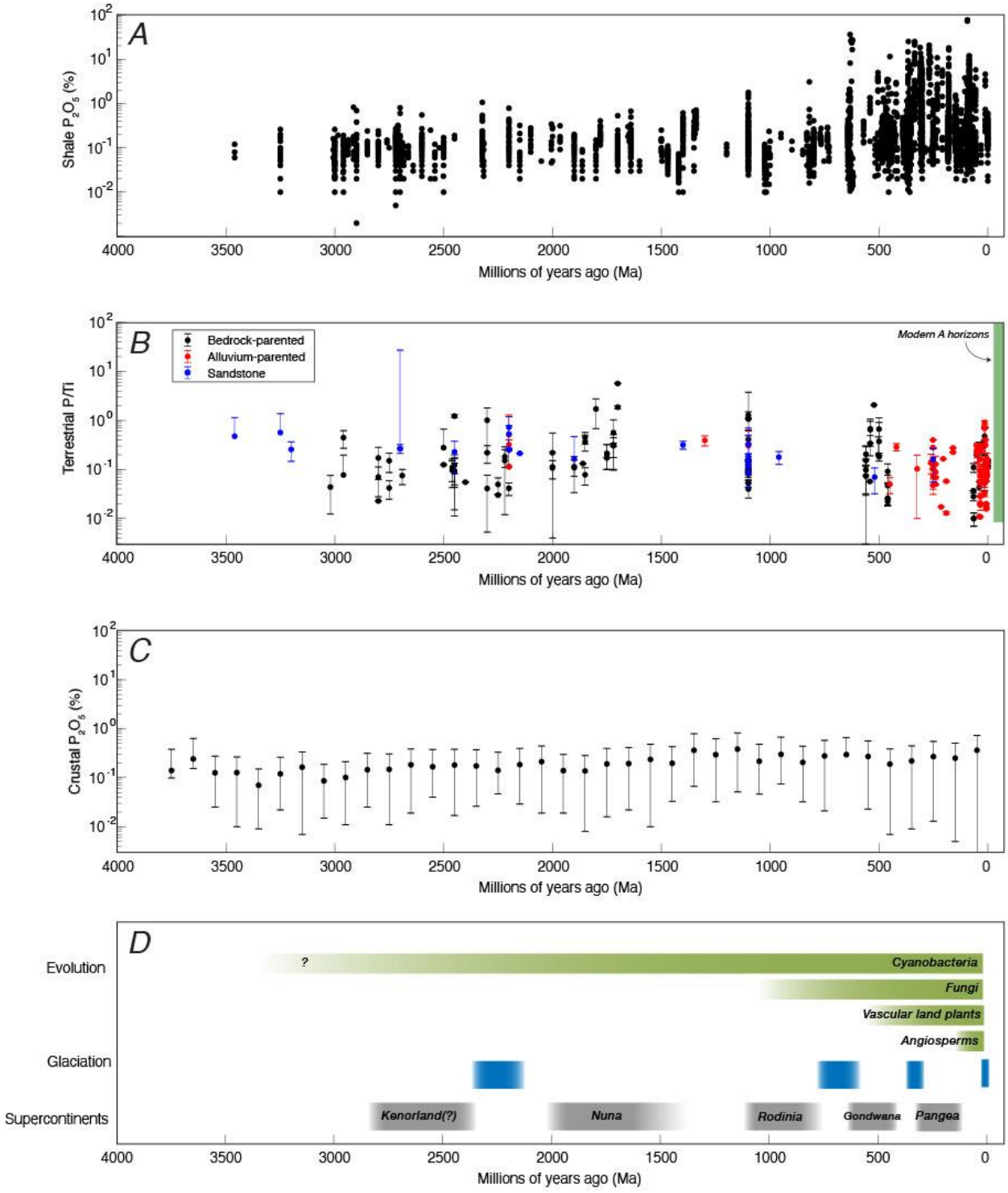

Figure 3.1. P in shales, paleosols, and continental crust through time.

(A) Marine shale P record (Reinhard et al. 2017). (B) Paleosol/weathering profile P/Ti record, newly-compiled in this work, with bedrock-parented paleosols as black dots, alluvium-parented paleosols as red dots, and massive fluvial sandstones as blue dots. Dots are upper paleosol/profile

means (e.g., A, B horizons), and error bars represent the standard deviation of the mean. Green shaded box at the right shows the range of modern P/Ti distribution. Ages for profiles are as reported in the literature. (C) Crustal P record of time-binned, bootstrapped averages (Cox et al., 2018). Error bars are the reported 5/95% confidence intervals. (D) Major evolutionary events are represented by green bars. Glacial periods and supercontinents marked in blue and black background bars, respectively. Supercontinent age estimates from Domeier et al. (2018).

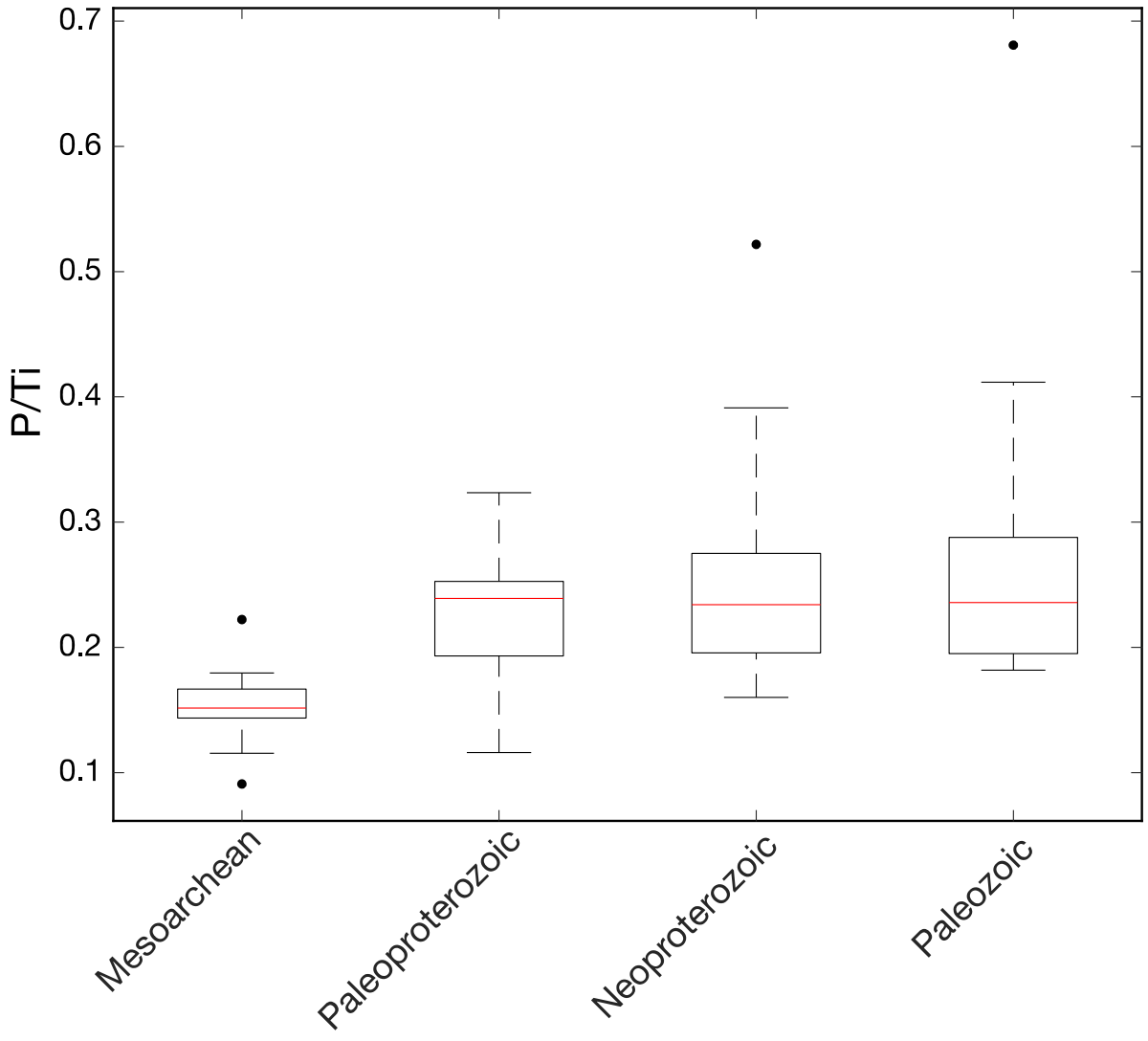

Figure 3.2 P/Ti in glacial diamicites through time.

Boxplot of glacial tillite P/Ti values (not relative to bedrock) through time (Gaschnig et al., 2014). Red line is median, box edges are 25th and 75th percentiles, respectively, and whiskers contain all non-outlier points. Statistical outliers are represented by black dots. Bin sizes are: Mesoarchean (n=13), Paleoproterozoic (n=44), Neoproterozoic (n=51), and Paleozoic (n=16).

The record of P retention/depletion from bedrock-parented paleosols and weathering profiles shows that paleosols and weathering profiles throughout the entire timespan can be either enriched or depleted in P relative to the bedrock parent within error (Figure 3.3a). Bedrock-parented paleosols had higher ranges of retained P than alluvium-parented paleosols (Figure 3.3b). There is no statistically significant difference between the distribution of Precambrian and Phanerozoic profiles' P retention/depletion (Figure 3.3c), similar to the study of Al retention across the Precambrian/Phanerozoic boundary (Beaty and Planavsky, 2021). Additionally, modern soils and paleosols' P distributions are similar throughout a range of comparisons (Figure 3.4).

Temporal coverage of the paleosol record is generally good, with most gaps on the order of tens of millions of years. As in many other geologic records from the time, the paleosol record from ca. 1500 to 600 Ma is relatively sparse, corresponding in part with Neoproterozoic glaciations. (See Discussion for a brief exploration of preservation biases.) We do not believe that these gaps do not preclude us from drawing long-term conclusions about the state of terrestrial P.

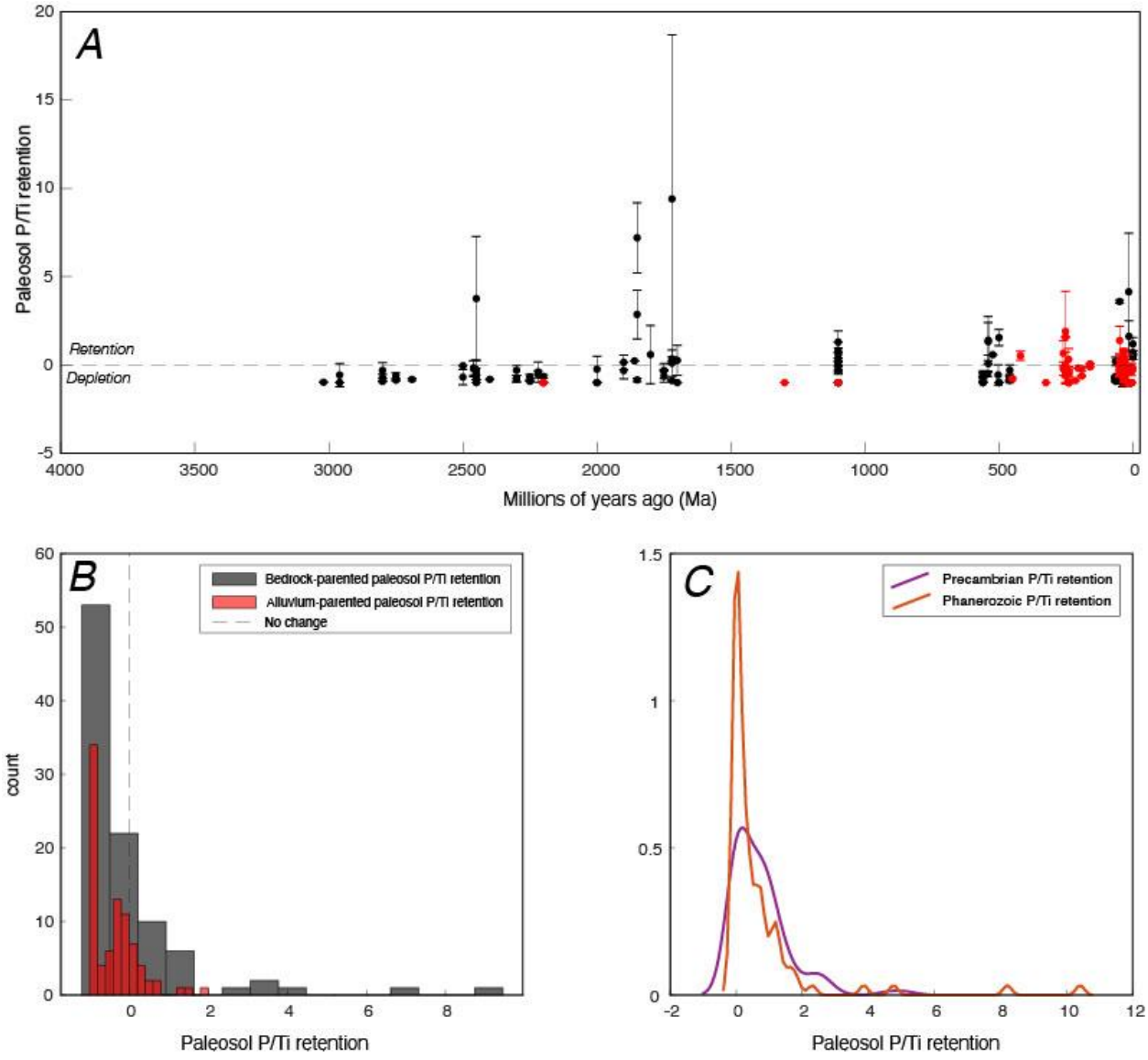

Figure 3.3. P retention in paleosols through time.

(A) Retention/depletion of P normalized to Ti through geologic time. Black dots are bedrock-parented paleosols/weathering profiles, red dots are alluvium-parented. Error bars are the propagated uncertainty of the ratio (see Supplemental Methods). Dashed line indicates no retention or depletion in the paleosol relative to the parent. Two profiles, Thelon and Denison, have high P/Ti values driven by high parent Ti concentrations. (B) Histogram comparing P/Ti retention/depletion in bedrock-parented paleosols (black bars) to that of alluvium-parented paleosols (red bars), with dashed line showing no retention or depletion. (C) Smoothed kernel density plot comparing paleosol P/Ti retention/depletion in the Precambrian (purple line) and the Phanerozoic (orange line).

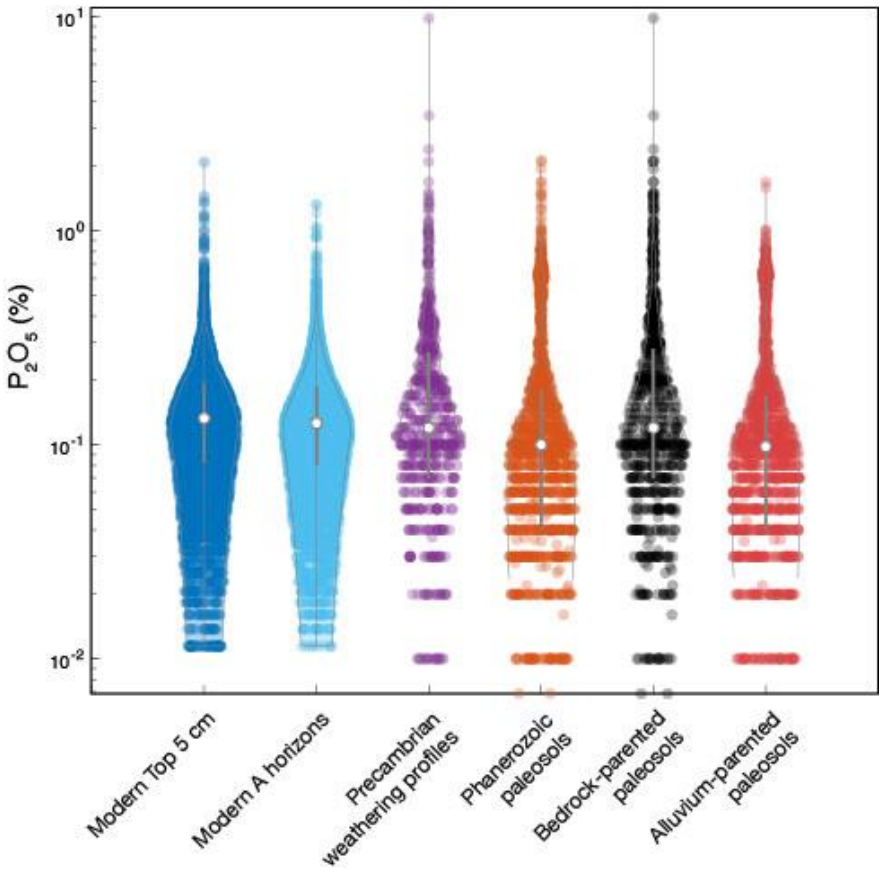

Figure 3.4. Distribution of P in modern soils and paleosols.

Violin plots showing distributions of P in (from left to right): top 5 cm of modern soils, modern A horizons, Precambrian upper weathering profiles, Phanerozoic paleosols, bedrock-parented paleosols, and alluvium-parented paleosols. Center white dot is median value and grey vertical lines are 25/75th percentiles. Violin plots were made using Bechtold (2016), see Supplemental Methods (Appendix B).

3.4 Discussion

The consistency in the paleosol P record prompts a reconsideration of assumptions around the magnitude of P fluxes driving major biogeochemical transitions in Earth's history. If the concentration of P in paleosols and other terrestrial weathering-product sediments is relatively stable through time, several possibilities for P driving biogeochemical change exist. Changes in the area of subaerially-exposed (and therefore weatherable) continent could have exerted a first-order control on the volume of sediment generated by weathering, therefore controlling the "baseline" magnitude of a P flux from continents to oceans. Deviations from that

baseline could have occurred on shorter timescales than the paleosol P record here captures, still providing a rapid spike in P and primary productivity. However, long-term changes in terrestrial P concentrations alone are unlikely to have caused the Neoproterozoic oxygenation or evolution of complex life around the same time. Finally, stability in the P/Ti ratio of paleosols over 3 Ga ago supports previous work that interpreted that signal as evidence for an early (Paleoproterozoic) terrestrial biosphere. That stability also fails to resolve the question of whether the evolution of land plants would have increased or decreased P mobilization and transport to the oceans. Below, we expand on these central ideas and discuss best approaches to terrestrial P sources going forward.

3.4.1 Exposed land area as a key control on P

Because the range of P concentrations recorded in terrestrial weathering materials is relatively constant through time, it is necessary to consider mechanisms aside from state changes in P concentrations for controlling the magnitude of P fluxes from continents to oceans. With little change in average crustal P concentrations relative to the range in paleosol P (Figure 3.1c), crustal evolution cannot be considered a main driver of potential increases in P sedimentary sinks. (Average paleosol P concentrations are similar to crustal P averages through time, but vary due, in part, to biotic activity; see section 3.4.3 for discussion.) As the sediment source, subaerially-exposed continental area is a key variable in considering biogeochemical evolution, and it has changed through time in response to planetary evolution, sea level change, and tectonic activity.

The amount of weatherable area has previously been argued to be a primary control on the global P cycle (e.g., Hao et al, 2020). While the timing of the exposure of continents and development of continental crust in early Earth remains debated, most workers agree that continental crust was consistently exposed by at least ca. 2.5 Ga ago based on both geologic and geochemical evidence and model results (Table B4). There is some evidence for localized sub-aerial weathering by 3.46 Ga (Buick et al., 1995), which would support some of the earlier estimates for continental emergence. The combined possibilities of continental emergence and a terrestrial biosphere prior to 3 Ga ago suggest that a version of the terrestrial P cycle could have been active at 3 Ga ago, when the paleosol record presented here begins. This could explain the stability in P through time, up to the Phanerozoic.

As subaerially-exposed continental area increased, the potential volume of sediments being generated would have increased to some degree as well. Holding the average P concentration of weathering products constant, as our new record here suggests, those changes in area and sediment generation would likely correlate with P release from bedrock and transportation. While other processes (e.g., tectonic activity, biotic influence, climate) affect the magnitude of sediment generation via continental weathering, the area of subaerially-exposed continent remains the primary control, setting a "baseline" for the potential magnitude of P fluxes from source to sink.

As weatherable area changed, the magnitude and intensity of silicate weathering would have changed in the carbon cycle feedback (Berner, 1998); while pCO_2 generally decreased through time, the sedimentary record reflects relatively little change in weathering intensity following the GOE (Sheldon et al., 2021). Tectonic activity (e.g., the supercontinent cycle; Figure 3.1d), generally corresponds to changes in relief, sediment supply, and continental erosion rates, and so could increase P flux from soils to ocean, affecting marine biogeochemical cycles (e.g., Campbell and Allen, 2008; Campbell and Squire, 2010; Och and Shields-Zhou, 2012). The degree of relief on early-emerging continental landmasses would have affected erosion rates as well, but remains poorly constrained, especially for the Archean when creating high topography was more difficult (e.g., Korenaga et al., 2017; Lee et al., 2018) or where early continents were largely submerged (Dong et al., 2021). Innovations in marine nutrient use efficiency likely played a critical mediating role in oxygenation and Fe-P burial rates (e.g., Reinhard et al., 2017, 2020). Weathering intensity (which may also be considered stable on 100 Ma and longer timescales; e.g., Sheldon et al., 2021; Chapter IV in this dissertation), evolution of terrestrial geomorphology (e.g., Davies and Gibling, 2010), and changes in marine nutrient burial (e.g., Reinhard et al., 2017; Kipp and Stueken, 2017) are important, but ultimately secondary to subaerially-exposed continental area, in the global P biogeochemical cycle.

Geologically short-term perturbations, such as glacial/interglacial cycles, abrupt climatic transitions, and some tectonic activity (Figure 3.1d), could have affected both the magnitude and timing of P fluxes. Glaciers would have affected the timing and rate of continental erosion, and therefore of P fluxes to the oceans and marine productivity (Föllmi, 1995; Planavsky et al., 2010; Hawkings et al., 2016; Dubnick et al., 2017; Martin et al., 2020). The temporal extent of glaciations' impact on P flux would have been on the order of $10^{6\text{-}7}$ years (Donnadieu et al.,

2004; Mills et al., 2011), a short enough timeframe to be potentially absent from our record. However, within the constraints of the data (i.e., gaps), there are no clear changes in either the continental (Figure 3.1b; Figure 3.2) or marine (Figure 3.1a) P concentrations associated with the Paleoproterozoic, Neoproterozoic, or Paleozoic ice ages (Figure 3.1d). The gaps during ice ages likely reflect both a lack of soil formation and rapid removal of terrestrial sediments globally.

Rapid climatic extremes on short (e.g., the K–Pg boundary, the Paleocene–Eocene Thermal Maximum) to intermediate (e.g., Early Eocene Climatic Optimum) timescales are known to have affected terrestrial weathering rates (e.g., Sheldon, 2006; Schaller et al., 2014; Cao et al., 2019), which in turn could have affected the magnitude of P transported from continents to oceans. However, as the relationship between continental weathering intensity and P fluxes remains debated (Lenton and Watson, 2004; D'Antonio et al., 2020), it is unclear whether P fluxes would have increased in these abrupt transitions. (There would also likely have been a lag effect due to mismatch between the timescales of soil formation vs. climate change.)

3.4.2 Implications for Neoproterozoic biogeochemistry

The Neoproterozoic is one of the primary periods in geologic history where an increase in P flux has been posited as driving biogeochemical change (i.e., evolution of complex life, rise in atmospheric oxygen). Our result of stable terrestrial P through the Neoproterozoic does not support a discrete expansion of the terrestrial biosphere during that time. Rather, the lack of variability in P highlights the importance of other factors, such as glacially-driven erosion and subsequent P fluxes in tandem with biological innovations in marine nutrient use efficiency and nutrient (Fe-P) burial, as possible controls on the NOE (e.g., Lenton et al., 2014; Reinhard et al., 2017). These results also highlight the importance of constraining other P flux-mediating factors in biogeochemical models during critical intervals of atmospheric oxygenation. Because we use land area as the primary control on potential P fluxes, quantifying changes in subaerially-exposed land area through time is a critical step for then quantifying continent-to-marine P fluxes (Hao et al., 2020). The average concentrations of terrestrial P allow that in a way not previously available, although crustal composition-based estimates remain reasonable. While records of (super)continents and tectonic activity are more certain for the Phanerozoic, the late Neoproterozoic is relatively recent and should be a primary target for this type of analysis given its changing continental configuration. Additionally, efforts to quantify past weathering-driven

fluxes should consider geomorphology-informed models of terrestrial weathering and erosion as a modifier for basic land-area when possible (i.e., when lateral landscapes are preserved and local tectonic environments are well-constrained).

3.4.3 P record supports Precambrian active terrestrial biosphere

Together with the physical, geochemical, and genomic evidence outlined above, our stable P and P/Ti records suggest that the expansion of the terrestrial biosphere continents occurred essentially at the same time that continents emerged, rather than being delayed until the Neoproterozoic as has been hypothesized (Knauth and Kennedy 2009). Together, the hypothesized presence of a terrestrial biosphere and consistently-weatherable continents (Figure 3.4) as early as the Neoarchean provides a baseline potential P flux, perturbed by shorter-timescale events. The style of biosphere has certainly evolved since the earliest microbial terrestrial biospheres, and the impacts of the evolution from microbially-dominated biospheres to more diverse biospheres (plants, fungi, arthropods) merits further detailed investigation, as does P cycling in modern analogues to early terrestrial biospheres. The transition to land plants is discussed briefly in the next section.

The concept of a terrestrial biosphere as early as the Archean (pre-2.5 Ga) is relatively well-accepted. Evidence for life on land sufficient to impact at least localized biogeochemical cycling (Lenton and Daines, 2017; Finke et al., 2019; de Kock et al., 2020; Beaty and Planavsky, 2021) and potentially the atmosphere (Zhao et al., 2017; Dick et al., 2018) is present back to at least the Mesoarchean (*see* Wellman and Strother, 2015). Microbially-induced sedimentary structures provide some of the earliest evidence of life on land (pre-3 Ga, Noffke et al., 2008, Noffke et al., 2013; Mesoproterozoic, Sheldon 2012). Some Archean paleosols indicate complex biological processes including methanogenesis (Rye and Holland, 2000) and organic acid weathering (Driese et al., 2011; Beaty and Planavsky, 2021). Geochemical evidence as early as 3.2 Ga reflects C and N isotopic fractionation from microbial mats in fluvial environments (Homann et al., 2018; Homann, 2019). Recent genomic work analyzing oxygen-utilizing and -producing enzymes estimated that both terrestrial and marine phylogenies diverged around 3.1 Ga, supporting the potential for Neoarchean life on land (Jabłonska and Tawfik, 2021).

Adding to this body of evidence, we interpret the lack of a statistically-significant shift in paleosol P/Ti retention versus loss relative to parent material (Figure 3.3c) as supporting a robust

terrestrial biosphere prior to the Neoproterozoic, similar to the Al/Ti approach in Beaty and Planavsky (2021). We also suggest that the similarity in paleosols' P distribution to modern soils (Figure 3.4), which are all biotically active, could be additional evidence that paleosols have hosted a biosphere throughout the duration of the paleosol record. If paleosols were reflecting only time-related weathering and compaction, rather than biotic influence on top of that, we might expect that signal to reflect only loss relative to bedrock in abiotic soils. Mechanisms for abiotic P retention relative to bedrock are limited, with preferential apatite dissolution as one potential explanation.

Under a high pCO_2 and hotter Precambrian atmosphere, apatite dissolution kinetics have been modeled as occurring more readily than today (Guidry and Mackenzie, 2000; Hao et al., 2020a). Hao et al. (2020a) reported both depletion and enrichment of P/Ti (their Figure S4) in many of the same Precambrian weathering profiles used in this work, but only compared those results to a single early Phanerozoic profile (Arisaig) rather than considering the Phanerozoic P record as a whole or the modern distribution of P enrichment/depletion in bedrock-parented soils. Therefore, we argue that it is possible to interpret the P depletion in Precambrian weathering profiles as a consequence of biotic P cycling rather than strictly abiotic processes (i.e., pCO_2-enhanced apatite dissolution), especially considering the ample evidence of a terrestrial biosphere during this time. While their model assumed Archean P concentrations in soils was half of modern values, similar P concentrations in modern soils (Dzombak and Sheldon, 2020) and the new paleosol P record indicate that this assumption is not necessarily valid (Figure 3.1b; Figure 3.4). However, regardless of the exact composition of the continental weathering product, we agree that continental emergence is a primary control on global rates of P transport.

3.4.4 Phosphorus and land plants in the Phanerozoic

In the early Paleozoic, our record weakly supports the potential for decreased P fluxes due to biological innovation (i.e., the evolution of land plants and root-fungi symbiosis), as D'Antonio et al. (2020) argued and contrary others (e.g., Lenton and Watson, 2004), but it requires closer examination going forward. While there is no discrete change in average P retention/release, there is an increase in the number of highly P-retaining soils towards the present (Figure 3.3c). Additionally, because our record comprises mineral horizons only (lacking O horizons), the record may not represent horizons that are both reflective of plant biomass

accumulation and likely to have high P concentrations and P/Ti values. Expanding the Phanerozoic record to include more O horizons and coal deposits will improve our understanding of how the evolution of land plants affected terrestrial P cycling. It is also possible that the increase in P towards the modern is related to exposure time and modernity, as soils tend to become P-depleted with time (Walker and Syers, 1976; Smeck, 1985; Jobbágy and Jackson, 2001). Therefore, while our record provides a baseline understanding for terrestrial P in geologic time, the potential for the evolution of vascular land plants and rooting systems to either increase or decrease P erosional fluxes requires a close examination of Phanerozoic soils, including O-horizons and coals.

The Phanerozoic soil geochemical record should also be interpreted in the context of the dramatic geomorphological changes that plants brought to terrestrial ecosystems, including increased sediment residence time (e.g., Davies and Gibling, 2010 and refs. therein). Soil shielding can also decrease continental chemical weathering as a stable soil mantle forms (Hartmann et al. 2014). Together, these geomorphic processes have been hypothesized to affect terrestrial weathering and subsequent P release, serving important mediator roles particularly in the Phanerozoic (Davies and Gibling, 2010). A higher-resolution Phanerozoic P retention/depletion record, along with weathering intensity, could help shed light on these processes in the geologic past.

3.5 Conclusions

The new compilation of paleosol, weathering profile, fluvial sandstone, and diamictite P concentrations presented here provides critical quantitative constraints on the composition of weathering P product through time. Across the nearly 3 billion years, the P composition of weathering product is approximately stable around the crustal P average, validating a baseline assumption commonly made in deep-time biogeochemical models. The pattern of P retention/depletion through geologic time—that is, soils' ability to both retain and lose P—supports an active terrestrial biosphere prior to the Neoproterozoic. Hypothesized Phanerozoic P cycling changes linked to the evolution of land plants remain obscure. Because the P concentration of weathering products through time does not change, the area of subaerially-exposed, weatherable landmass through time provides a first-order control on the potential

magnitude of P fluxes, with processes such as glacial/interglacial cycles, shorter-term tectonic activity, and other terrestrial changes likely playing a secondary role in controlling P erosional fluxes.

Acknowledgments

Parts of this work were funded by NSF 1050760 to N.D.S. The authors acknowledge E.A. Hetland for helpful comments and discussions in early versions of this work, and N.C. Midttun for assistance with Matlab.

References

1. Beaty, B.J. & Planavsky, N.J. A 3 b.y. record of a biotic influence on terrestrial weathering. *Geology* **49**, 407-411 (2021).

2. Beraldi-Campesi, H., Hartnett, H.E., Anbar, A., Gordon, G.W., Garcia-Pichel, F. Effect of biological soil crusts on soil elemental concentrations: implications for biogeochemistry and as traceable biosignatures of ancient life on land. *Geobiology* **7**, 348-359 (2009).

3. Berner, R. A. The carbon cycle and CO_2 over Phanerozoic time: The role of land plants. *Philos. Trans. R. Soc. B Biol. Sci.* **353**, 75–82 (1998).

4. Berner, R.A. The Phanerozoic Carbon Cycle: CO_2 and O_2. Oxford University Press, Oxford, UK (2004).

5. Buick, R., Thornett, J., McNaughton, N. *et al.* Record of emergent continental crust ~3.5 billion years ago in the Pilbara craton of Australia. *Nature* **375,** 574–577 (1995).

6. Campbell, I. H. & Allen, C. M. Formation of supercontinents linked to increases in atmospheric oxygen. *Nat. Geosci.* **1**, 554–558 (2008).

7. Campbell, I. H. & Squire, R. J. The mountains that triggered the Late Neoproterozoic increase in oxygen: The Second Great Oxidation Event. *Geochim. Cosmochim. Acta* **74**, 4187–4206 (2010).

8. Cox, G. M., Lyons, T. W., Mitchell, R. N., Hasterok, D. & Gard, M. Linking the rise of atmospheric oxygen to growth in the continental phosphorus inventory. *Earth Planet. Sci.*

Lett. **489**, 28–36 (2018).

9. Crews, T.E., Kitayama, K., Fownes, J.H., Riley, R.H.;,Herbert, D.A., Mueller-Dombois, D., Vitousek, P.M. Changes in soil phosphorus fractions and ecosystem dynamics across a long chronosequence in Hawaii. *Ecology* **76**, 1407-1424 (1995).

10. D'Antonio, M.P., Ibarra, D.E., Boyce, C.K. Land plant evolution decreased, rather than increased, weathering rates. *Geology* **48**, 29-33 (2020).

11. Davies, N.S. & Gibling, M.R. Cambrian to Devonian evolution of alluvial systems: The sedimentological impact of the earliest land plants. *Earth-Sci. Rev.* **98**, 171-200 (2010).

12. Dick, G. J., Grim, S. L. & Klatt, J. M. Controls on O2 production in Cyanobacterial mats and implications for Earth's oxygenation. *Annu. Rev. Earth Planet. Sci.* **46**, 123–147 (2018).

13. Domeier, M., Magni, V., Hounslow, M.W., Torsvik, T.H. Episodic zircon age spectra mimic fluctuations in subduction. *Scientific Reports* **8**, 17471 (2018).

14. Dong, J., Fischer, R.A., Stixrude, L.P., Lithgow-Bertelloni, C.R. Constraining the volume of Earth's early oceans with a temperature-dependent mantle water storage capacity model. *AGU Advances* **2**, e2020AV000323 (2021).

15. Donnadieu, Y., Goddéris, Y., Ramstein, G., Nédélec, A., Meert, J. A 'snowball Earth' climate triggered by continental break-up through changes in runoff. *Nature* **541**, 303–306 (2004).

16. Driese, S. G., Jirsa, M.A., Ren, M., Brantley, S.L., Sheldon, N.D., Parker, D., Schmitz, M. Neoarchean paleoweathering of tonalite and metabasalt: Implications for reconstructions of 2.69Ga early terrestrial ecosystems and paleoatmospheric chemistry. *Precambrian Res.* **189**, 1–17 (2011).

17. Dubnick, A., Wadham, J., Tranter, M., Sharp, M., Orwin, J., Barker, J., Bagshaw, E., Fitzsimons, S. Trickle or treat: The dynamics of nutrient export from polar glaciers. *Hydrol. Process.* **31**, 1776–1789 (2017).

18. Filippelli, G.M. The global phosphorus cycle. *Rev. Min. Geochem.* **48**, 391-425 (2002).

19. Finke, N., Simister, R.L., O'Neil, A.H., Monosatryo, S., Henny, C., MacLean, L.C., Canfield, D.E., Konhauser, K.O., Lalonde, S.V., Fowle, D.A., Crowe, S.A. Mesophilic microorganisms build terrestrial mats analogous to Precambrian microbial jungles. *Nat. Commun.* **10**, 1–11 (2019).

20. Föllmi, K.B. 160 m.y. record of marine sedimentary phosphorus burial: Coupling of climate and continental weathering under greenhouse and icehouse conditions. *Geology*

23, 503-506 (1995).

21. Gaschnig, R. M., Rudnick, R.L., McDonough, W.F., Kaufman, A.J., Hu, Z., Gao, S. Onset of oxidative weathering of continents recorded in the geochemistry of ancient glacial diamictites. *Earth Planet. Sci. Lett.* **408**, 87–99 (2014).

22. Gomes, M.L., Riedman, L.A., O'Reilly, S., Lingappa, U., Metcalfe, K., Fike, D.A., Grotzinger, J.P., Fischer, W.W., Knoll, A.H. Taphonomy of biosignatures in microbial mats on Little Ambergris Cay, Turks and Caicos. *Frontiers in Earth Sci.* **8**, 576712 (2020).

23. Guidry, M.W. & Mackenzie, F.T. Apatite weathering and the Phanerozoic phosphorus cycle. *Geology* **28**, 631-634 (2000).

24. Guilbaud, R., Poulton, S.W., Thompson, J. *et al*. Phosphorus-limited conditions in the early Neoproterozoic ocean maintained low levels of atmospheric oxygen. *Nat. Geosci.* **13,** 296–301 (2020).

25. Hao, J., Knoll, A.H., Huang, F., Hazen, R.M., Daniel, I. Cycling phosphorus in the Archean Earth: Part I. Continental weathering and riverine transport of phosphorus. *Geochim. Cosmochim. Acta* **273**, 70-84 (2020a).

26. Hao, J., Knoll, A.H., Huang, F., Schieber, J., Hazen, R.M., Daniel, I. Cycling phosphorus in the Archean Earth: Part II. Phosphorus limitation on primary production in Archean ecosystems. *Geochim. Cosmochim. Acta* **280**, 360-377 (2020b).

27. Hartmann, J., Moosdorf, N., Lauerwald, R., Hinderer, M., West, A.J. Global chemical weathering and associated P-release—The role of lithology, temperature, and soil properties. *Chem. Geo.* **363**, 145-163 (2014).

28. Hawkings, J., Wadham, J., Tranter, M., Telling, J. & Bagshaw, E. The Greenland Ice Sheet as a hot spot of phosphorus weathering and export in the Arctic. *Global Biogeochem. Cycles* **30**, 191–210 (2016).

29. Homann, M. Earliest life on Earth: Evidence from the Barberton Greenstone Belt, South Africa. *Earth-Sci. Rev.* **196**, 102888 (2019).

30. Homann, M., Sansjofre, P., Van Zuilen, M., Heubeck, C., Gong, J., Killingsworth, B., Foster, I.S., Airo, A., Van Kranendonk, M.J., Ader, M., Lalonde, S.V. Microbial life and biogeochemical cycling on land 3,220 million years ago. *Nature Geosci* **11,** 665–671 (2018).

31. Jabłońska, J., Tawfik, D.S. The evolution of oxygen-utilizing enzymes suggests early biosphere oxygenation. *Nat Ecol Evol* **5,** 442–448 (2021).

32. Jobbágy, E. G. & Jackson, R. B. The distribution of soil nutrients with depth: Global patterns and the imprint of plants. *Biogeochemistry* **53**, 51–77 (2001).

33. Kipp, M. A. & Stüeken, E. E. Biomass recycling and Earth's early phosphorus cycle. *Sci. Adv.* **3**, 1–7 (2017).

34. Knauth, L.P. & Kennedy, M.J. The Late Precambrian greening of the Earth. *Nature* 460, 728-732. (2009)

35. Korenaga, J., Planavsky, N.J., Evans, D.A.D. Global water cycle and the coevolution of the Earth's interior and surface environment. *Phil. Trans. Royal Soc. A.* **375**, 20150393 (2017).

36. Laakso, T. A. & Schrag, D. P. Limitations on Limitation. *Global Biogeochem. Cycles* **32**, 486–496 (2018).

37. Laakso, T.A., Sperling, E.A., Johnston, D.T., Knoll, A.H. Ediacaran reorganization of the marine phosphorus cycle. *PNAS* **117**, 11961-11967 (2020).

38. Labanderia, C.C. Invasion of the continents: cyanobacterial crusts to tree-inhabiting arthropods. *Trends in Ecol. & Ev.* **20**, 253-262 (2005).

39. Lenton, T. M. & Daines, S. J. Matworld – the biogeochemical effects of early life on land. *New Phytol.* **215**, 531–537 (2017).

40. Lenton, T. M. & Watson, A. J. Biotic enhancement of weathering, atmospheric oxygen and carbon dioxide in the Neoproterozoic. *Geophys. Res. Lett.* **31**, L05202 (2004).

41. Lenton, T. M. The role of land plants, phosphorus weathering and fire in the rise and regulation of atmospheric oxygen. *Glob. Chang. Biol.* **7**, 613–629 (2001).

42. Lenton, T. M., Daines, S. J. & Mills, B. J. W. COPSE reloaded: An improved model of biogeochemical cycling over Phanerozoic time. *Earth-Science Rev.* **178**, 1–28 (2018).

43. Lenton, T.M. & Daines, S.J. The effects of marine eukaryote evolution on phosphorus, carbon, and oxygen cycling across the Proterozoic-Phanerozoic transition. *Emerging Topics in Life Sci.* **2**, 267-278 (2018).

44. Lyons, T.W., Reinhard, C.T., Planavsky, N.J. The rise of oxygen in Earth's early ocean and atmosphere. *Nature* **506,** 307-315 (2014).

45. Martin, J.B., Pain, A.J., Martin, E.E., Rahman, S., Ackerman, P. Comparisons of nutrients exported from Greenlandic glacial and deglaciated watersheds. *Glob. Biogeochem. Cycles* **34**, e2020GB006661 (2020).

46. Mills, B. J. W., Watson, A.J., Goldblatt, C., Boyle, R., Lenton, T.M. Timing of Neoproterozoic glaciations linked to transport-limited global weathering. *Nat. Geosci.* **4**, 861–864 (2011).

47. Neaman, A., Chorover, J., Brantley, S.L. Implications of the evolution of organic acid moieties for basalt weathering over geologic time. *Am. J. Sci.* **302**, 147-185 (2005).

48. Noffke, N., Beukes, N., Bower, D., Hazen, R.M., Swift, D.J.P. An actualistic perspective into Archean worlds – (cyano-)bacterially induced sedimentary structures in the siliciclastic Nhlazatse Section, 2.9 Ga Pongola Supergroup, South Africa. *Geobiology* 6, 5-20 (2008).

49. Noffke, N., Christian, D., Wacey, D., Hazen, R.M. Microbially induced sedimentary structures recording an ancient ecosystem in the ca. 3.48 Ga Dresser Formation, Pilbara, Western Australia. *Astrobiology* **13**, 1103-1124 (2013).

50. Och, L. M. & Shields-Zhou, G. A. The Neoproterozoic oxygenation event: Environmental perturbations and biogeochemical cycling. *Earth Sci. Rev.* **110**, 26–57 (2012).

51. Paytan, A. & McLaughlin, K. The oceanic phosphorus cycle. *Chem. Rev.* **107**, 563-576 (2007).

52. Planavsky, N. J., Rouzel, O.J., Bekker, A., Lalonde, S.V., Konhauser, K.O., Reinhard, C.T., Lyons, T.W. The evolution of the marine phosphate reservoir. *Nature* **467**, 1088–1090 (2010).

53. Reinhard, C. T., Planavsky, N.J., Gill, B.C., Ozaki, K., Robbins, L.J., Lyons, T.W., Fischer, W.W., Wang, C., Cole, D.B., Konhauser, K.O. Evolution of the global phosphorus cycle. *Nature* **541**, 386-389 (2017).

54. Reinhard, C. T., Planavsky, N.J., Ward, B.A., Love, G.D., Hir, G.L., Ridgwell, A. The impact of marine nutrient abundance on early eukaryotic ecosystems. *Geobiology* **00**, 1–13 (2020).

55. Rye, R. & Holland, H. D. Life associated with a 2.76 Ga ephemeral pond?: Evidence from Mount Roe #2 paleosol. *Geology* **28**, 483–486 (2000).

56. Sheldon, N.D. & Tabor, N.J. Quantitative paleoenvironmental and paleoclimatic reconstruction using paleosools. *Earth-Sci. Rev.* **95**, 1-52 (2009).

57. Sheldon, N.D. Abrupt chemical weathering increase across the Permian-Triassic boundary. *Palaeogeo., Palaeoclim., Palaeoec.* **231**, 315-321 (2006).

58. Sheldon, N.D. Microbially induced sedimentary structures in the ca. 1100 Ma terrestrial midcontinent rift of North America. *SEPM* Special Publication No. 101, 153-162 (2012).

59. Sheldon, N.D., Mitchell, R.L., Dzombak, R.M. Reconstructing Precambrian pCO_2 and pO_2 using paleosols. Cambridge Elements, Oxford, UK. 2021.

60. Smeck, N. E. Phosphorus dynamics in soils and landscapes. *Geoderma* **36**, 185–199 (1985).

61. Thomazo, C., Couradeau, E., Giraldo-Silva, A., Marin-Carbonne, J., Brayard, A., Homann, M., Sansjofre, P., Lalonde, S.V., Garcia-Pichel, F. Biological soil crusts as modern analogs for the Archean continental biosphere: Insights from carbon and nitrogen isotopes. *Astrobiology* **20**, 815-819 (2020).

62. Walker, T.W., Syers, J.K. The fate of phosphorus during pedogenesis. *Geoderma* **15**, 1–19 (1976).

63. Wellman, C. H. & Strother, P. K. The terrestrial biota prior to the origin of land plants (embryophytes): A review of the evidence. *Palaeontology* **58**, 601–627 (2015).

64. Zhao, M., Reinhard, C. T. & Planavsky, N. J. Terrestrial methane fluxes and Proterozoic climate. *Geology* **46**, 1–4 (2017).

Chapter 4
Three Billion Years of Continental Weathering and Preservation Biases in the Paleosol Record

4.1 Abstract

Although continental weathering intensity has been invoked as a primary control on biogeochemistry, tectonics, and the carbon cycle throughout geologic history, it remains poorly quantified over Earth's history. As a direct product of continental weathering, paleosols (fossil soils) offer unique insight into surface conditions, but they have been underused in attempts to constrain past weathering trends. Here, we compile the largest terrestrial weathering record to date, spanning three billion years, and analyze a suite of weathering indices to test common hypotheses around state-changes in terrestrial weathering intensity due to atmospheric changes and terrestrial biosphere expansion. Contrary to commonly invoked assumptions, we find that these weathering indices reflect consistent average terrestrial weathering intensity through time. No unidirectional state changes in weathering intensity are present in the record, as has been previously hypothesized.

We interpret this weathering record through lenses of preservation biases and the evolution of soils and soil-forming processes (e.g., climate, tectonics, geomorphology, biology) through time. The temporal distribution of paleosols is uneven, correlating approximately with the supercontinent cycle. Paleosol occurrences and soil order diversity also increase during the Phanerozoic, a pattern that could be attributable in part to land plant-driven pedogenesis (soil formation) and landscape stabilization, which affect both soil formation and preservation. The stable weathering record likely reflects the baseline level of weathering from which the Earth system can deviate during periods of perturbation (i.e., major climate transitions, rapid tectonic activity) and can be used to improve models of deep-time biogeochemistry.

Finally, while average weathering intensity is stable, there is an increase in the total range of Chemical Index of Alteration (CIA) values preserved during the Phanerozoic, with the increased CIA range driven by the appearance of high-CaO paleosol samples. The appearance of

high-Ca soils suggests that as land plants and terrestrial ecosystems diversified, facilitating the formation and retention of carbonate minerals, soils became an increasingly important inorganic C sink that could contribute to a more stable C cycle. The record presented here is the first to demonstrate this previously hypothesized relationship quantitatively.

4.2 Introduction

Subaerial weathering of continents has been invoked as both a cause and consequence of multiple major biogeochemical transitions throughout geologic time, as outlined below (see Figure 4.1 for periods of interest). However, how the intensity and style of weathering changed remains poorly understood due to a relative dearth of direct evidence. Marine sediment geochemical records can reflect terrestrial weathering (e.g., Fedo et al., 1995; Blum et al., 1998; Bahlburg and Dobrzinski, 2011) and provide useful proxies for the timing and magnitude of continental weathering and erosion, but as the sediment sink, they are limited in their ability to reflect surface conditions directly. Marine records are also linked to the biogeochemical changes that are posited to result from, at least in part, changes in continental weathering. Disentangling the two is crucial for understanding the co-evolution of the terrestrial geosphere, marine biosphere, and the atmosphere. To do that, continental weathering intensity through time must be directly quantified using the rock record of weathering products—the sediment source.

Several key periods in Earth's history have been linked to changing continental weathering, which likely began when widespread continents permanently emerged and were exposed to the atmosphere between ca. 3–2.5 Ga (billion years ago)(see references in Table B4, and Korenaga 2018). As atmospheric oxygen increased during the Neoarchean and Paleoproterozoic, weathering shifted from abiotic CO_2 acid weathering to both oxidative and acid weathering (e.g., Anbar et al., 2007; Reinhard et al., 2009; Kendall et al., 2015; Somelar et al., 2020; Sheldon et al., 2021; Lipp et al., 2021). Throughout the Proterozoic, continental weathering-derived fluxes (e.g., C, Fe, P) from the continents are thought to have contributed to changing ocean chemistry (e.g., Berner, 2004; Anbar and Knoll, 2002; Lenton and Watson, 2004; Mills et al., 2011; Sahoo et al., 2012; Lyons et al., 2014; Cermeño et al., 2015; Laakso et al., 2020).

The Neoproterozoic is one of the transitions in geologic history in which continental weathering has been invoked as a driver of biogeochemical change. The Neoproterozoic saw global glaciations, the formation and breakup of supercontinents, and the evolution of complex life (see Och and Shields-Zhou, 2012), all of which can be tied to weathering, erosion, and terrestrial-to-marine nutrient fluxes. In particular, weathering-driven fluxes of phosphorus (P) have been hypothesized as a control on marine productivity, oxygenation, climate, and atmospheric composition (Donnadieu et al., 2004; Campbell and Squire, 2010; Planavsky et al., 2010; Mills et al., 2011; Och and Shields-Zhou, 2012; Brocks et al., 2017; Reinhard et al., 2017; Reinhard et al., 2020). But constraining that critical P flux depends, in part, on quantifying terrestrial weathering. The evolution of rooting vascular land plants in the Devonian and a resulting change in weathering intensity has been hypothesized as a driver of change in oxygenation and climate, ultimately culminating in the late Paleozoic ice age (e.g., Algeo et al., 1995; Berner, 1998; Lenton, 2001; Lenton and Watson, 2004; Algeo and Scheckler, 1998; Porada et al., 2016; D'Antonio et al., 2020).

In the Cenozoic, links between the rate of continental silicate weathering and a cooling climate have been proposed, but whether weathering causes cooling or vice versa remains debated (e.g., Molnar and England 1990; Raymo and Ruddiman, 1992; Willenbring and von Blanckenburg, 2010; Caves et al., 2016). Links between Cenozoic erosion and marine productivity have also been proposed (e.g., Cermeño et al., 2015). Finally, the emplacement of large igneous provinces (LIPs) and volcanic arcs have been invoked as drivers for weathering and climate (e.g., Cohen and Coe, 2002; Lee et al., 2015; Cox et al., 2016); however, more data are needed to quantify the relationship between these events, soils, and weathering intensity. Despite the central role continental weathering plays in many basic questions around climate, tectonics, and the biosphere, weathering intensity through time remains poorly understood, with an imbalance of data and analysis between the sources (i.e., paleosols, terrestrial sediments) and sinks (i.e., shales, from which the source is commonly inferred).

Efforts to constrain and quantify continental weathering through time have typically focused on several tools: mass-balance and kinetic modeling approaches based on sedimentology, mineralogy, and atmospheric composition (e.g., Francois and Walker, 1992; Rye and Holland, 1998; Murakami et al., 2004; Berner, 2006; Fabre et al., 2011; Lyons et al., 2014; Kendall et al., 2015; Hao et al., 2017, 2020); Sr and Nd isotopes (e.g., Brass, 1975; Martin and

Macdougall, 1995; Blum et al., 1998; Theiling et al., 2012; Bayon et al., 2021); weathering indices like CIA and clay mineralogy in shale and glacial records (Fedo et al., 1996; Kelly et al., 2005; Bahlburg and Dobrzinski, 2011; Gaschnig et al., 2014; Lipp et al., 2021); and most recently, efforts using large community-built datasets like MacroStrat and the Sedimentary Geochemistry and Paleoenvironments Project (Lipp et al., 2021).

Paleosols offer a unique, direct record of climatic, biologic, and atmospheric conditions at Earth's surface while pedogenesis was occurring. They have been used in a relatively limited sense to address weathering through geologic time, with work typically focusing on a small suite of elements of interest (e.g., Colwyn et al., 2019), individual paleosol profiles as case studies for areas or environments of interest, or a high-resolution transect of paleosols through geologically short periods of time (e.g., Bestland et al., 1997; Sheldon et al., 2002; Kraus and Riggins, 2007; Hyland et al., 2017). Compilations of longer records (billions of years) have been limited to a small number (ca. 15) of very well-studied, primarily bedrock-parented profiles through time (e.g., Rye and Holland, 1998; Sheldon, 2006a; Colwyn et al., 2019; Beaty and Planavsky, 2021). This approach allowed a baseline to be established, as not all weathering profiles (particularly in the Precambrian) can be used for comparative paleosol/parent geochemistry due to post-depositional alteration. However, to begin to understand global biogeochemical changes at the scope of geologic time, a higher-resolution record that extends beyond only the handful of intensely studied profiles is necessary. We can do this by broadening the terrestrial record to include select alluvium-parented paleosols, which can be compared to underlying sediments and can undergo similar, if not identical, quality-control checks (i.e., establishing reasonable parent material, avoiding diagenetically-influenced profiles, only including profiles with multiple samples) as bedrock-parented paleosols. This also provides critical new constraints for the terrestrial sediment supply as a counterpart to the well-studied marine weathering sink represented by shales.

Here, we compile the largest ca. 3-billion-year record of weathering intensity in paleosols and use it to test hypothesized changes in weathering intensity, as well as to explore the nature of pedogenesis and the paleosol record itself through geologic history. By considering the distribution of paleosols through time in the context of soil formation (e.g., changing controls on soil formation; depositional environments), preservation biases (i.e., what time periods, climates,

etc. are represented by the record?), and sampling biases, we can more accurately interpret the geochemical paleosol record and identify critical knowledge gaps moving forward.

With this compilation, we can begin to address some of the outstanding questions in weathering and biogeochemistry mentioned above. Specifically, we address the following questions: Are there state changes in weathering intensity at key points (i.e., rise of oxygen, the Neoproterozoic, land plant evolution) over the past 3 billion years, as have been hypothesized? What is the distribution of paleosols through time, and how does that relate to the supercontinent cycle? And how does the paleosol record reflect changes in soil-forming processes through time (i.e., terrestrial biosphere evolution, climate, tectonics)?

4.3 Methods

Bulk oxide geochemical data and descriptive information for paleosols and weathering profiles (n profiles = 261; bedrock-parented = 117, alluvium-parented = 144; total n samples = 2849) were collected from the literature as described in Chapter III (Tables C1, C2). For the analyses in this chapter, soil/weathering profile thicknesses were gathered or estimated as available (Table C3). Profile thickness was taken from the uppermost horizon or part of the profile to parent rock or the appearance of corestones (individual pieces of parent material above the massive parent material surface). Soil orders were noted when available but are not quantitatively considered in this work due to sample size limitations and sampling bias; see supplemental methods in Appendix C.

Geochemical analyses for this work focused on established weathering indices: the Chemical Index of Alteration (CIA; Nesbitt and Young, 1982), CIA without potash (CIA-K; Maynard, 1992), and Mafic Index of Alteration (MIA; Babechuk et al., 2014). Equations for each of these indices are below, with possible values ranging from 1–100 (low to high weathering intensity) for both CIA(-K) and $MIA_{ox,red}$. CIA and CIA-K reflect plagioclase weathering, where the latter excludes K to account for K metasomatism (Maynard, 1992). MIA was created to reflect weathering of mafic substrates (e.g., basalt, a common parent material through time; Babechuk et al., 2014). Because MIA includes Fe and Mg, which are common in high-temperature silicates in mafic rocks, it is perhaps better equipped to reflect weathering on mafic parent materials. By comparing patterns in these indices through time, we can see if patterns in pedogenesis vary or are stable.

$$CIA = Al_2O_3 / (Al_2O_3 + CaO + Na_2O + K_2O) * 100 \quad [Eq. 1]$$

$$CIA\text{-}K = Al_2O_3 / (Al_2O_3 + CaO + Na_2O) * 100 \quad [Eq. 2]$$

$$MIA(ox.) = (Al_2O_3 + Fe_2O_3) / (Al_2O_3 + Fe_2O_3 + MgO + CaO + Na_2O + K_2O) * 100 \quad [Eq. 3]$$

$$MIA(red.) = Al_2O_3 / (Al_2O_3 + Fe_2O_3 + MgO + CaO + Na_2O + K_2O) * 100 \quad [Eq. 4]$$

While weathering index values were calculated for all samples, only values from the upper portion of a paleosol or weathering profile (i.e., A/B horizon for Phanerozoic paleosols, above corestones or weakly-weathered parent material for Precambrian weathering profiles) are used for comparisons to parent material. Individual samples (rather than profile averages) were used for bootstrap resampling or in other analyses where overall variation in paleosol geochemistry was of interest. Because CaO concentration tends to be a primary driver of variability in CIA(-K) and use of the proxy requires CaO screening, we explored CIA both with and without CaO screening (exclusion of samples with CaO >5%; Prochnow et al., 2006; Michel et al., in prep; Dzombak et al., in review).

We also calculated enrichment/depletion in the ratio of Al/Ti in paleosols relative to their parent material [Eq. 5], following Beaty and Planavsky (2021). Al is mobilized primarily by organic acids in soils, so examining its relative mobility through time can be a test for weathering due to the presence of an active terrestrial biosphere. Al/Ti retention values were calculated using the same subdivisions of paleosol profiles as in Chapter III where complete bulk geochemical data were available. (See Chapter III for bootstrap resampling methods.)

$$Al/Ti\ retention = Al/Ti_{paleosol\text{-}avg} / Al/Ti_{parent\text{-}avg} \quad [Eq. 5]$$

To contextualize both this ratio and other weathering indices, and to test for possible influences of secular evolution in the composition of continental crust, we also calculated Ti/Al for each individual profile (to test for single profile provenance; Sheldon and Tabor, 2009) and ran time-binned bootstrap resampling for Ti, Al, and Al/Ti through time (Figure C3).

To place the paleosol record into wider geologic record context and to explore paleosol preservation biases, we compare it to the global zircon record through time (Figure 4.1a; Voice et al., 2011) and to passive margin lengths through time (Figure 4.1b; Bradley 2008). The distribution of zircon ages (Figure 4.1a) is generally thought to represent the supercontinent cycle, although which stage of that cycle (i.e., assembly, stable middle period, breakup) remains debated (e.g., Pastor-Galán et al., 2018; Domeier et al., 2018; and refs. therein). Because passive margins typically represent the latter half of the supercontinent cycle and may correspond to changes in total exposed land area, the total length of passive margins through time provides supplemental context for interpreting the occurrence of paleosols and potential Sadler-effect type preservation biases (Figure 4.1b through time, along with the zircon record and its implications for the supercontinent cycle. Soils are the largest terrestrial carbon sink today, so to explore how this role may have evolved, we also examine the increase in CaO in Phanerozoic paleosols and its coincidence with the evolution of rooted, vascular plants (Krissansen-Totton et al., 2015; Nordt et al. 2016; Figure 4.2b). Finally, glacially-derived sediments (i.e., tillites, diamictites) can provide terrestrial weathering records during glacial periods when paleosols may be less likely to be formed and/or preserved. We include a weathering record from tillites through time (Figure C5; Gaschnig et al., 2014) to fill in gaps in the terrestrial weathering record from paleosols. Together, these records (Figure 4.1 and 4.2) create a robust and interconnected picture of terrestrial weathering—and its tectonic context—for the past three billion years.

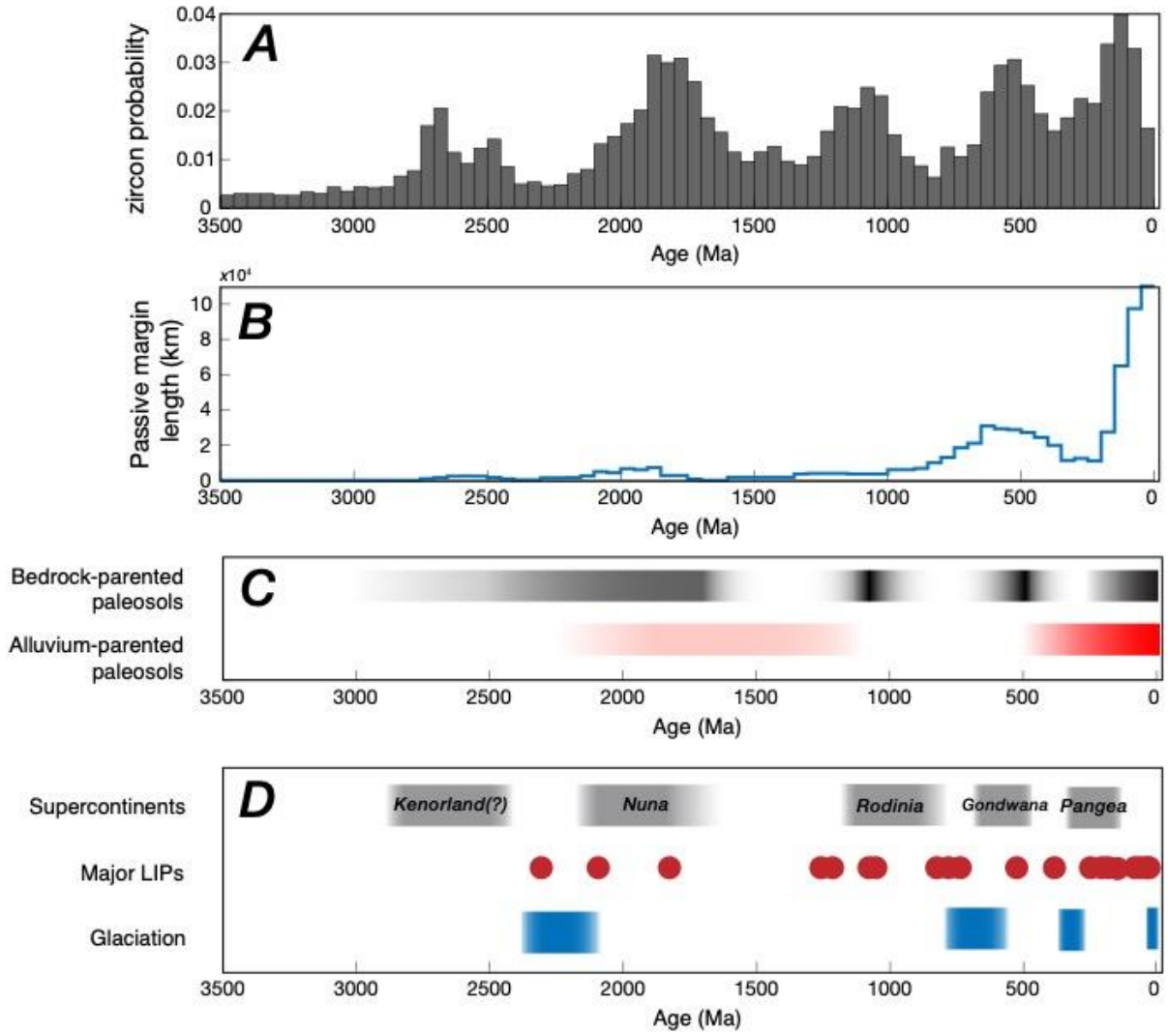

Figure 4.1. Major tectonic and climatic events.

(A) Zircon occurrence through time (Voice et al., 2011), normalized to probability. (B) Cumulative length of passive margins through time (Bradley et al., 2008), using a 50 million year time bin. The record shows a strong increase towards the present and is not corrected for potential preservation biases. (C) Occurrence of paleosols in this record, where saturation reflects relative density (i.e., darker = more paleosols preserved). Black bar represented bedrock-parented paleosols, red bar represents alluvium-parented paleosols. (D) General geologic and biologic context for this work. Supercontinents are grey bars, with fading to represent uncertainty around ages of assembly and breakup (Pastor-Galán et al., 2019; Domeier et al., 2018). Red dots represent major Large Igneous Province (LIP) emplacement with volumes >1 Mkm^3 (Ernst et al., 2021). Green bars show general timelines for major biological innovations.

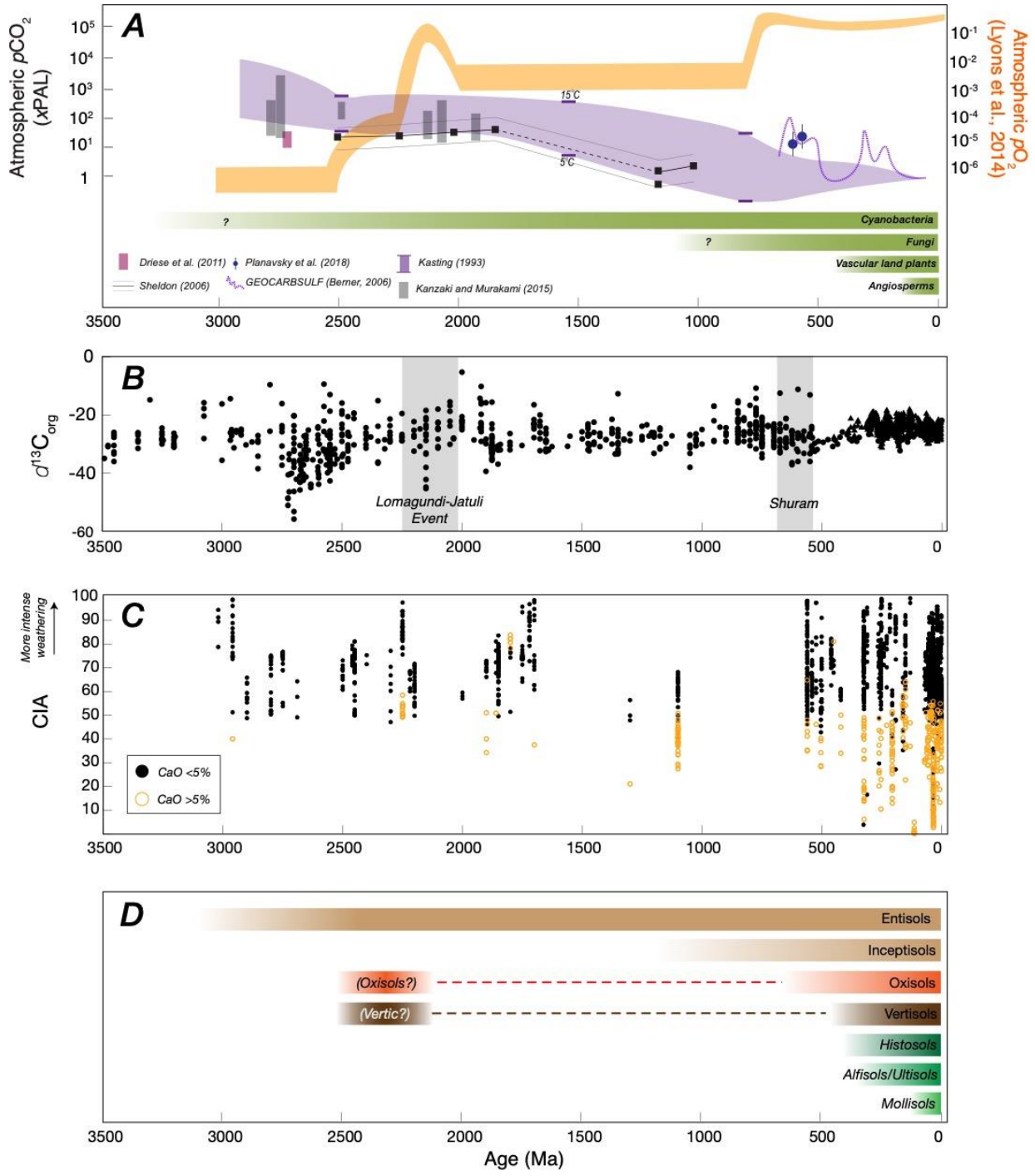

Figure 4.2. Atmosphere, C, and the biosphere through time.

(A) Generalized evolution of atmospheric composition, with pCO_2 from multiple sources (legend on plot) and pO_2 in orange (Lyons et al., 2014). Modified from Sheldon et al. (2021). Major terrestrial biological innovations are shown in green bars. (B) Organic C through time (Krissansen-Totton et al., 2015; Nordt et al., 2016). Krissansen-Totton et al. values (circles) are $\delta^{13}C_{org}$ average values for each formation included. Nordt et al. values (triangles) come from a

variety of terrestrial C_{org} sources. (C) CIA in paleosols (individual samples) through time, with samples with CaO >5 % marked by hollow orange circles (Sheldon et al., 2002; Prochnow et al., 2006). (D) Semi-quantitative schematic depicting the appearance of soil orders (as defined by modern USDA soil taxonomy) in geologic time (based on Retallack 2001). Soil order names in italics have few samples in the present compilation, so their appearances are inferred based on known terrestrial biosphere evolutions. Soil order names in italics and parentheses (Vertic) represents a designation made in the literature that remains debated. Not all orders are included. See Supplemental Text/Appendix C for more on soil orders through time.

4.4 Results

Weathering through time. Continental weathering intensity has been posited to have undergone state changes (increases) at several points in Earth's history as outlined in the Introduction. Two key periods commonly proposed to have experienced changes in weathering intensity are around the Great Oxidation Event (GOE), as pCO_2 decreased and pO_2 increased (ca 2.4–2.2 Ga) (Lyons et al., 2014), and in the Phanerozoic during the evolution of land plants with roots, mycorrhizal fungi, and organic acid weathering (Horodyskyj et al., 2012; Neaman et al., 2005). However, at neither of these periods is there a significant increase in weathering indices examined here (Figure 4.3, Figures C1,2) or by bootstrap resampling of their means (Figure 4.4a,b, Figure C2). Paleosols and weathering profiles do not show a statistically significant shift in average weathering intensity through time (Figures 4.3, 4.4). Both raw distributions and bootstrap resampled means' distributions overlap, indicating that the means are within standard error of each other and therefore statistically similar. (The Phanerozoic increase in CIA range is geologically meaningful, but not statistically significant; see section 4.5.3). Compared to the distribution of CIA values in modern soils, distribution seen in Phanerozoic paleosols' CIA is similar but with fewer low weathering intensity values preserved during the Precambrian (Figure 4.5). Between paleosols and modern soils, paleosols have higher median CIA values by ca. 10 CIA units, and bedrock-parented paleosols in particular have a smaller range, with almost no CIA values <30 (Figure 4.5).

In paleosols, Al/Ti is relatively constant and enriched relative to parent material through time (Figure 4.6), supporting the results of Beaty and Planavsky (2021) who found similar stability with a smaller set of paleosols. Modern soils have a larger range of Al/Ti retention (higher values) than in paleosols, but all paleosol Al/Ti retention values fall within that range (Figure 4.7). Resampled means for Al/Ti in paleosols decrease between the Precambrian and Phanerozoic, while still reflecting retention rather than depletion as the dominant mode (Figure

4.8a). The resampled means for TiO_2 show no meaningful change between the Precambrian and Phanerozoic (Figure 4.8a), and resampled means for Al_2O_3 decrease in the Phanerozoic from ca. 17.75 to 13.75% Al_2O_3 (Figure 4.8b,c; Figure C3).

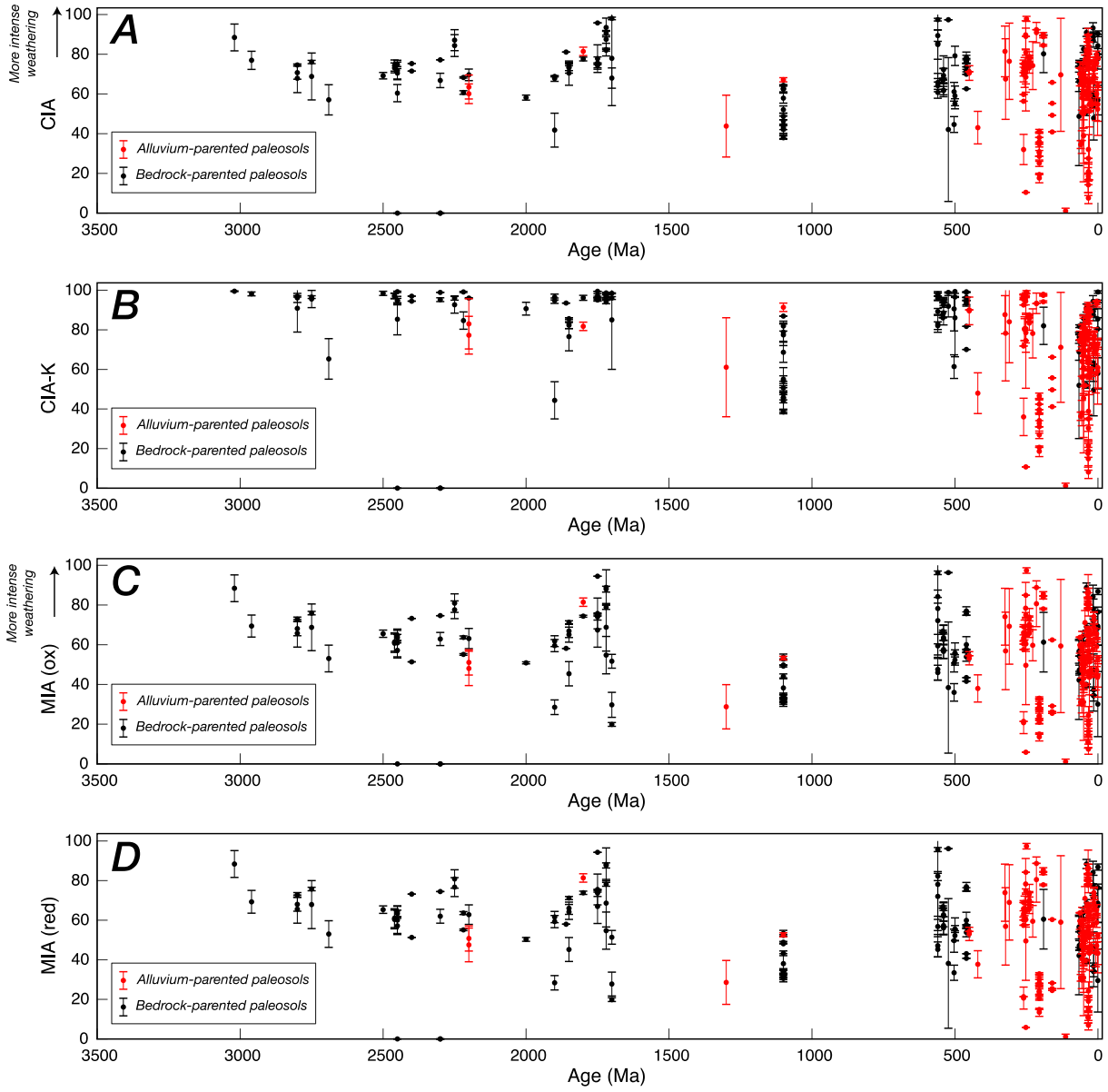

Figure 4.3. Weathering indices in paleosols.

Weathering indices in paleosols (profile averages) through time, where black dots are bedrock-parented paleosols and red dots are alluvium-parented paleosols. Error bars represent 1σ within an individual profile. (A) CIA, (B) CIA-K, (C), MIA (oxic), and (D) MIA (reducing).

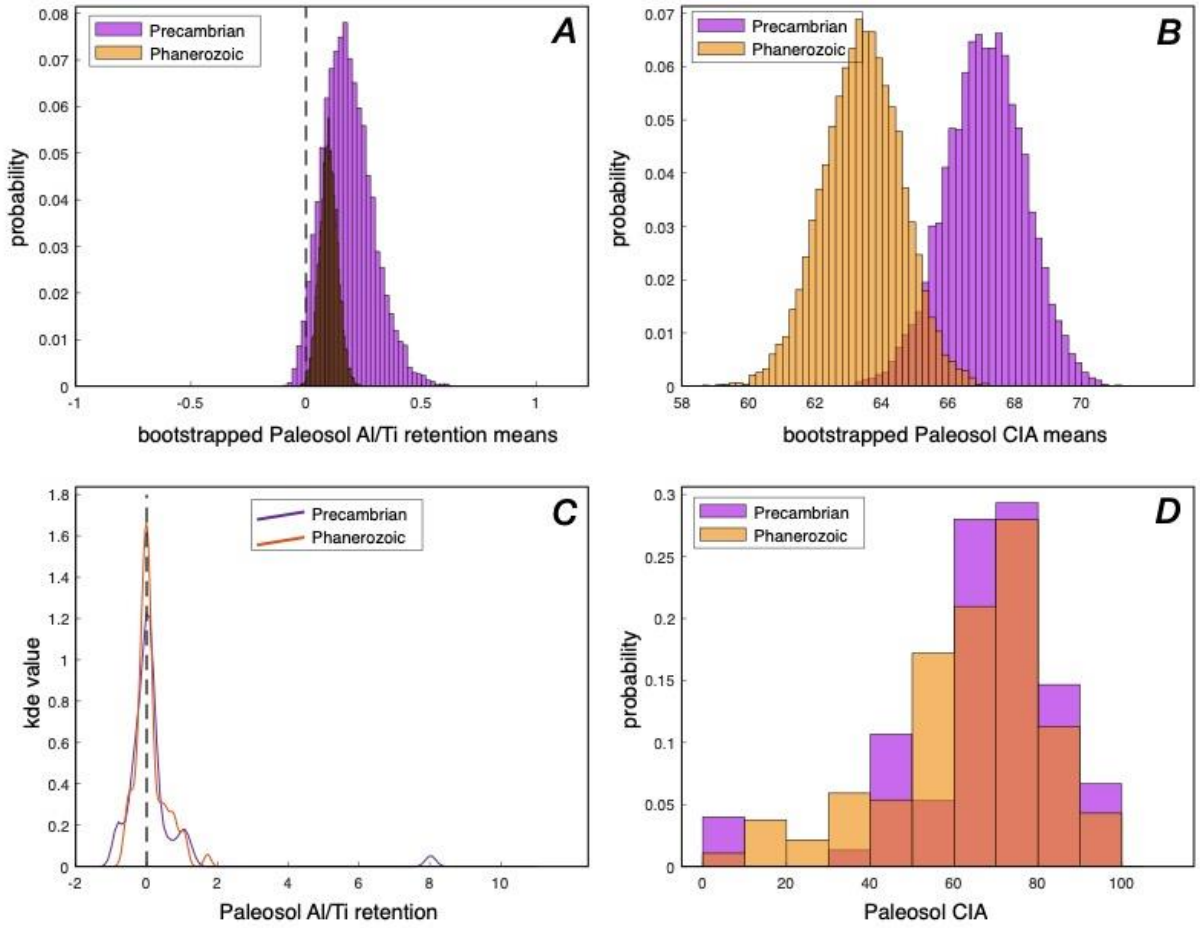

Figure 4.4. Al/Ti retention and CIA distributions in paleosols.

Bootstrap resampled means of (A) Al/Ti retention and (B) CIA values in paleosols (individual samples), binned into Precambrian (purple) and Phanerozoic samples (orange). Note x-axis scale for (B) is 58–72. (C) Kernel density estimates for Al/Ti retention in paleosols (individual samples) in Precambrian (purple) and Phanerozoic (orange) time bins, with both distributions centered on 0 (dashed line; no retention/loss). (D) Histograms of Precambrian (purple) and Phanerozoic (orange) CIA values in paleosols (individual samples), normalized to probability.

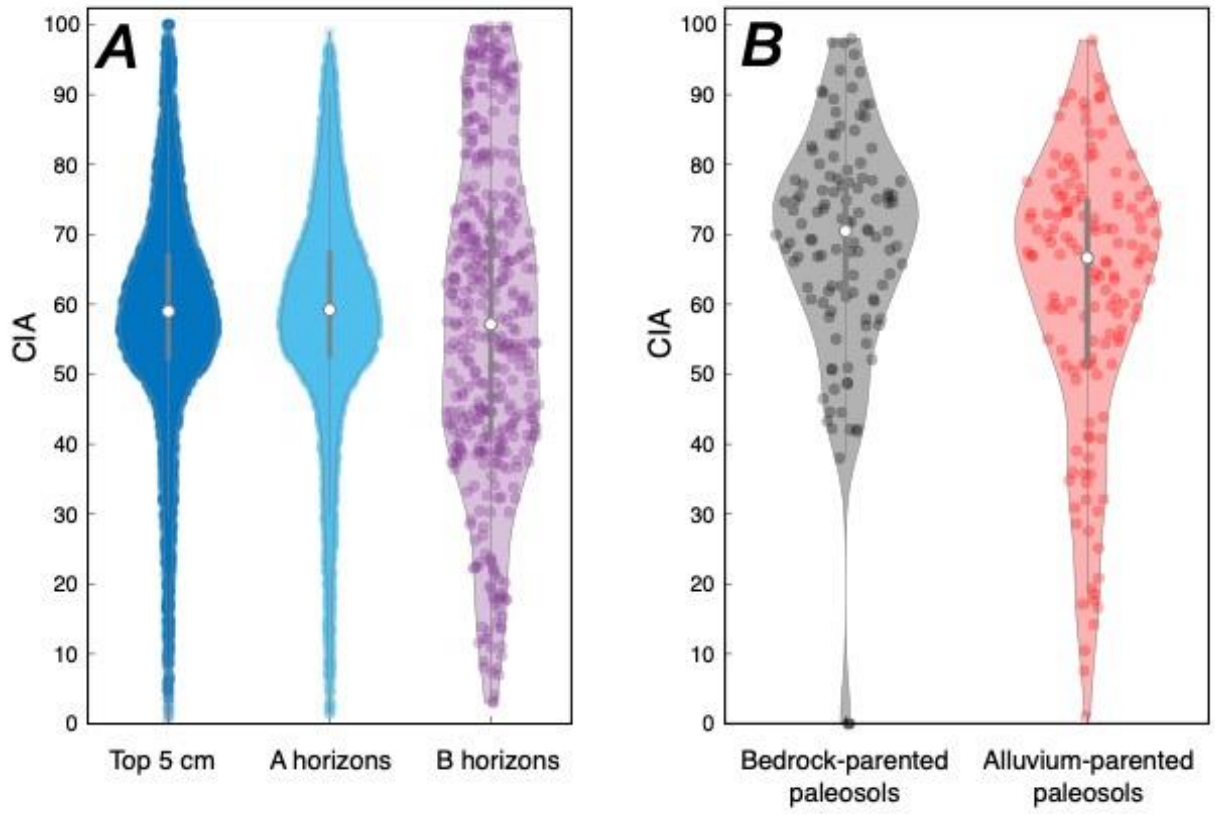

Figure 4.5. CIA in modern soils and paleosols.

Distributions of CIA values in (A) modern soils and (B) combined Precambrian and Phanerozoic paleosols (profile averages). In all plots, white dot represents median value and grey bars are first and third quartiles. The plots' shapes overall suggest normal distributions, with modern B horizons somewhat closer to uniform (Hintze and Nelson, 1998). (Modern soils are compiled in Chapter II.)

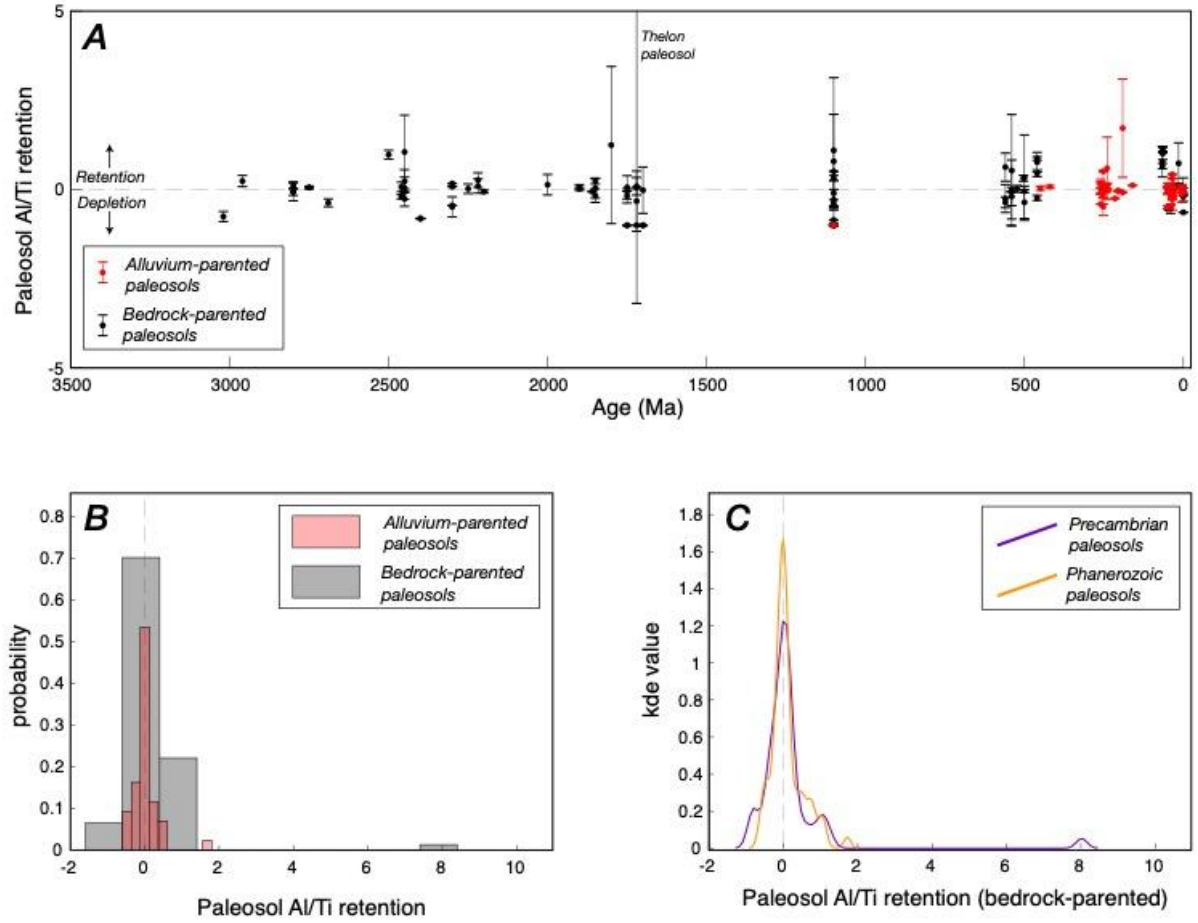

Figure 4.6. Al/Ti retention in paleosols thru time and time-binned distributions.

(A) Al/Ti retention/depletion in paleosols (profile averages) through time, showing similar results as in Beaty & Planvsky (2021). Dashed line at 0 represents no change between Al/Ti in paleosols vs. parent material. Error bars represent 1σ of Al/Ti in an individual profile. One profile (Thelon, bedrock-parented) is not shown at Al/Ti ~8. (B) Probability-normalized histogram of Al/Ti retention in paleosols, binned by parent material. (C) Kernel density estimates for Al/Ti retention in Precambrian (purple line) and Phanerozoic (orange line) paleosols.

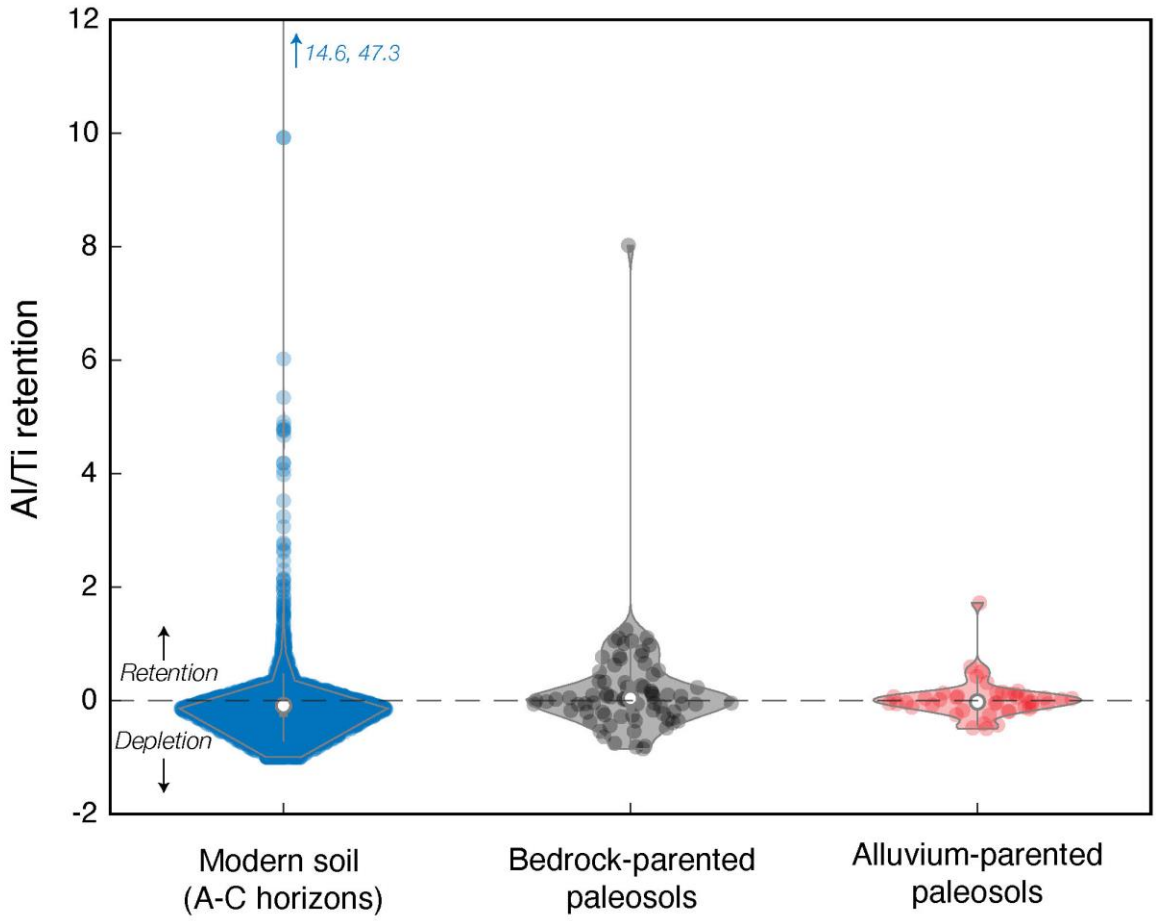

Figure 4.7. Distribution of Al/Ti retention in modern soils and paleosols.

Al/Ti retention in modern soils (leftmost violin plot), bedrock-parented paleosols (middle plot), and alluvium-parented paleosols (rightmost plot). Dashed line at 0 represents no change in Al/Ti between paleosol and parent material. Paleosol points are individual samples.

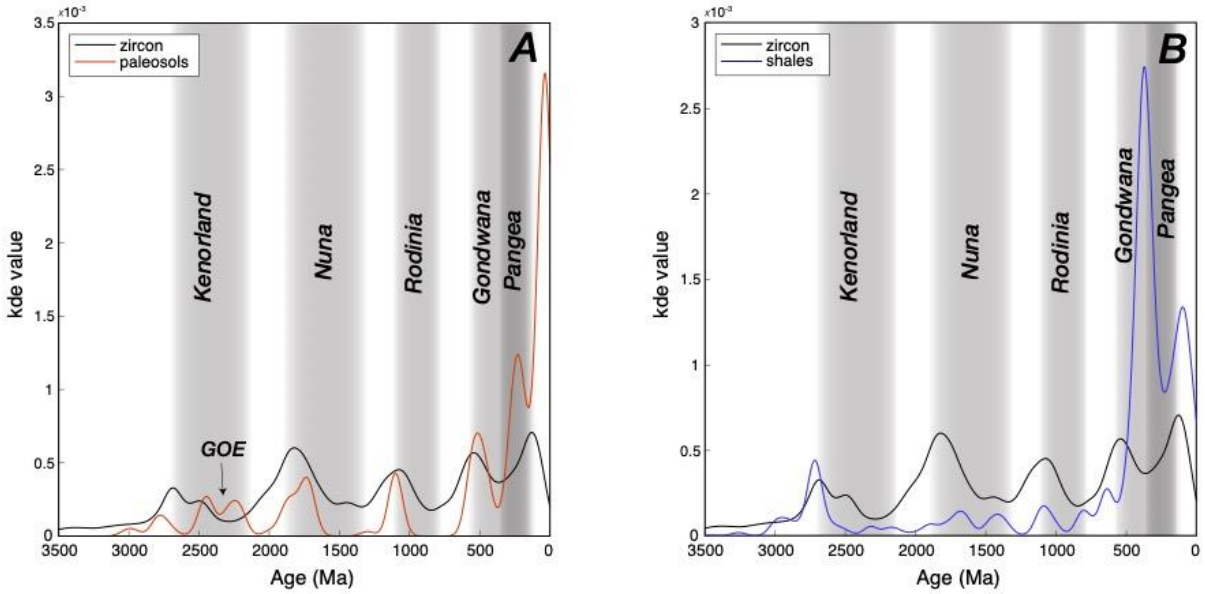

Figure 4.8. Comparison of distributions between paleosols, shales, and zircon ages.

(A) Kernel density estimates for the occurrences of paleosols (individual samples; orange line) and zircons (black line; Voice et al., 2011) through time, with supercontinents marked by vertical grey bars in the background. GOE: Great Oxygenation Event. (B) Kernel density estimates for the occurrences of shales (blue line) and zircons (black line) through time.

Distribution through time. Paleosols are not preserved evenly throughout the geologic record, with longer temporal gaps between profiles from ca. 1.7 Ga to 600 Ma (Figure 4.1c). The number of paleosols generally increases towards the present, with an increase in alluvium-parented paleosols in the Phanerozoic (Figure 4.1c). Compared to the zircon record, paleosols tend to occur approximately synchronously with zircon peaks, with lower numbers of paleosols during zircon low points (Figure 4.8a). The shale record (Reinhard et al., 2017) is more continuous, suffering fewer gaps, but still correlates with some peaks in the zircon record (Figure 4.8b), but not others. Both the distribution of paleosols and total passive margin length through time increase towards the present (Figure 4.1b). In this compilation, the maximum thickness in Precambrian weathering profiles is higher than Phanerozoic paleosol profiles, which have a larger overall range but lack very thick profiles (Figure C4); however, see supplemental text in Appendix C.

4.5 Discussion

4.5 What does a stable weathering paleosol record actually mean?

It has been assumed that the intensity of continental weathering has substantially changed throughout Earth's history as the atmosphere (e.g., high pCO_2), climate (e.g., hothouse conditions), tectonics (e.g., supercontinent cycle), and biosphere (e.g., rooted plants) changed. In contrast to common expectations, the weathering indices analyzed here (CIA, MIA, Al/Ti) reflect stable weathering intensity in different pedogenic processes through the past 3 Ga, with a Phanerozoic appearance of low-CIA driven by the evolution of pedogenesis and appearance of pedogenic carbonate rather than solely by weathering intensity (Figures 4.3, 4.4; Figure C1). The terrestrial weathering records compiled here do not reflect such discrete, stepped transitions in weathering intensity. Stability in the paleosol weathering record supports previous findings of long-term, stable weathering intensity in a smaller paleosol compilation (Beaty and Planavsky, 2021) and in marine sedimentary rocks (Lipp et al., 2021).

An additional consideration in interpreting the record of CIA through time is the difference in average CIA value between modern soils and paleosols (around 10 CIA units, Figure 4.5). This lower modern mean could be explained by increased preservation of carbonate minerals in very modern soils; it could also be due to a postglacial bias in the dataset of modern soils, with most representing ca. 100ky at most and many likely reflecting tens of thousands of years. Relatively short periods of soil formation could result in modern soils being less intensely weathered or developed, biasing the CIA record slightly lower. Higher pCO_2 throughout most of geologic time than in the Quaternary could also contribute to this pattern (Sheldon et al., 2021). As the Phanerozoic paleosol weathering record is filled in to be more complete, closer examinations of possible correlations between variability in pCO_2 and terrestrial weathering intensity would be useful in testing the role atmosphere plays in modern-style pedogenesis, as well as how tectonic activity and the creation of accommodation space affect preservation.

We interpret the paleosol weathering records in three contexts: the timescale of perturbations in weathering intensity, the shift of dominant control on weathering intensity through time, and biases in terrestrial geologic records. We suggest that a baseline level of terrestrial weathering was reached once continents were subaerially exposed and the atmosphere was consistently oxidizing. Once continental weathering was established, perturbations in global weathering intensity occurred but did not lead to discrete, unidirectional state changes as

hypothesized. Rather, the weathering record reflects the variability in and evolution of soil-forming factors over time (biosphere, climate, tectonics), with continental area controlling the magnitude of weathering-driven sediment fluxes. Soil formation times and preservation biases obfuscate potential shorter-timescale changes in weathering intensity (e.g., rapid climate change, soils during glacial periods). Additionally, the Phanerozoic increase in the range of CIA values preserved (due to a change in style of pedogenesis, rather than solely reflecting weathering intensity) suggests the value of examining multiple weathering indices. As in Chapter III, we point to the importance of the area of subaerially exposed continent as a key baseline control on potential weathering-driven elemental fluxes.

4.5.1 Timescales of weathering intensity events and the geologic baseline

There are numerous, well-constrained, rapid changes in continental weathering intensity throughout the Phanerozoic recorded by paleosols (e.g., Bestland et al., 1997; Sheldon 2006b; Sheldon et al., 2012; Schaller et al., 2015; Hyland et al., 2017), demonstrating that such events can be captured by paleosols with their relatively short formation times (ca. <100 ka). In the context of the geologic timescale, however, the weathering signatures of such events effectively get swamped by the long-term signal, which is, for the Phanerozoic, the full range of possible weathering intensity. Although these events do not appear to affect the long-term trend in terrestrial weathering significantly, they remain important when considered in their relative timescale of interest (typically hundreds of thousands to millions of years) and in the context of other major perturbations at the time (e.g., icehouse/hothouse transition, mass extinction, flood basalts, etc.). As with any index or proxy application, considering apparent changes in the context of uncertainty and background levels of variability is the most robust approach to paleosol geochemistry. The same logic can apply to other perturbations in weathering intensity (tectonic, biotic, etc.) where there is a mismatch between rates of those processes, pedogenesis, and soil preservation

We interpret the paleosol weathering record (as represented here) to reflect the global 'background' weathering intensity for most of geologic history, setting the baseline for potential sediment fluxes on long timescales. This 'long-term baseline' interpretation is in line with the findings of Lipp et al. (2021), who used CO_2 mass-balance and a global compilation of shales (the sediment sink) to estimate weathering intensity over 4 Ga. Their CO_2 sequestration-based

calculations found weathering to be in a steady state on timescales of ca. 0.5 Ga and longer, with weathering fluxes driven by total amount of erosion (rather than changes in weathering intensity) on long timescales. On shorter timescales (ca. millions of years), weathering and erosion fluxes may have been influenced by more discrete perturbations (e.g., carbon cycle/pCO_2 fluctuations, climate transitions, tectonics). Such perturbations could have been both spatially and temporally localized. Very short perturbations (<1 Ma) may not be captured by paleosols due to soil formation times, which at their longest typically span the order of 100 ka. (Markewich et al., 1990; Sheldon and Tabor, 2009), or by shales, where time-averaging and seafloor erosion could obfuscate the signal that might be better recorded by carbonates.

It is important to note that since at least the beginning of the Phanerozoic, the modern range of weathering intensity is represented in the paleosol CIA record (Figures 4.2–4.4). This supports arguments for 'modern' pedogenesis beginning in the Phanerozoic, when vascular, rooting plants evolved and pedogenic carbonate consistently appears in the rock record. It is also possible that the Precambrian record suffers from preservation biases leading to low-weathering intensity paleosols (and likely thin or unrecognized as weathering surfaces) being omitted (see section 4.5.3). The MIA record reflects a modern range ca. 1.7 Ga ago, earlier than the CIA record (Figures 4.4c,d), and is less heavily CaO-influenced than CIA because it considers more elements. Having this context is necessary for interpreting potential changes in weathering intensity (e.g., up-section variability in CIA) and points to the importance of high-resolution sampling and consideration of error and uncertainty (e.g., Heimsath and Burke, 2013; Hyland et al., 2016; Amorosi et al., 2021; Dzombak et al., in review/Chapter V of this dissertation), to avoid over-interpreting a relatively small change in a weathering index. A broader context and preservation biases should always be considered and looking at relative (rather than absolute) changes may be a more appropriate approach to small-scale questions of weathering changes (Bahlburg and Dobrzinski, 2011; Sheldon et al., 2012; Chapter V).

The dominant control or controls on weathering intensity likely varied through time, as the atmosphere evolved, the terrestrial biosphere expanded, and tectonic activity waxed and waned. For example, on the Archean Earth, under high pCO_2 and with relatively little terrestrial biosphere, terrestrial weathering could have been largely controlled by CO_2-dominated weathering (Sheldon, 2006a). Pedogenesis is generally considered to have changed as these weathering variables evolved through time, shifting first from abiotic CO_2 acid weathering to

both acid and oxidative weathering at the Great Oxygenation Event around 2.4–2.2 Ga (Figure 1.2). There is evidence that by the end of the Archean, organic acid weathering was occurring due to the presence of a terrestrial (microbial) biosphere, contributing to early leaching and weathering profile formation (Rye and Holland, 2000; Driese et al., 2011; Beaty and Planavsky, 2021). An increase in the total diversity of redox-sensitive minerals (i.e., clays, oxides, and oxyhydroxides) has also been used as evidence for changes in oxidative weathering through time (Hazen et al., 2008; Kennedy et al., 2006).

Once weathering mechanisms stabilized as the atmosphere was dominantly oxic and continents were consistently emerged, transient or shorter-term shifts in the driver of weathering intensity would have changed over both space and time. As pCO_2 dropped from bars of CO_2 to thousands of ppm of CO_2 (Kasting, 1993; Kanzaki and Murakami, 2015; Sheldon et al., 2021) and tectonic activity increased, tectonics may have begun to play a more important role in weathering rate than pCO_2 by delivering high volumes of readily-weatherable material to the surface. Similarly, as the terrestrial biosphere expanded and global climates alternated between glacial and hothouse periods, those may have increased their contribution to the global weathering intensity signature, trading off as one waxed and the other waned. Climate and relief would also have played different roles in weathering intensity (and therefore soil production) and soil erosion through space and time, contributing variability in paleosol geochemistry, thickness, and distribution and preservation (e.g., Dixon et al., 2009; Dixon et al., 2012; West, 2012; Cao et al., 2019). The overall effect of this continuous interplay of factors could have resulted in the seemingly stable weathering intensity reflected in this compilation. Lipp et al. (2021) posit that transient perturbations in the carbon cycle, with returns to a balanced system, explain the stability of weathering as recorded in shales. The stability in our paleosol record supports the idea of long-term dynamic stability in the carbon cycle with varying strength of silicate weathering-carbon feedbacks (e.g., Caves et al., 2016).

4.5.3 Distribution through time and biases in the paleosol record

Several biases related to paleosol soil formation and preservation complicate the interpretation of weathering records on geologic timescales. We note that while this compilation is the largest to date, it is not exhaustive and is biased towards paleosols with bulk geochemical data available. (In the Phanerozoic, paleosol studies with isotope data, rather than bulk

geochemistry, are more common.) These biases are evident in the gaps in the distribution of paleosols as well as trends in paleosol geochemistry, and we discuss each potential source of bias here.

4.5.3.1 Paleosol bias, supercontinents, and LIPs

Paleosols in this record are most likely to be preserved during times with zircon peaks (Figures 4.1c and 4.8), with significant gaps during the Mesoproterozoic and Neoproterozoic; the Paleoproterozoic mismatch between zircon peaks and paleosol occurrences coincides with the GOE, which we interpret as over-sampling bias (Figure 4.8a; see section 4.5.3.4). Zircon peaks are generally thought to be associated with the assembly of supercontinents, although other zircon-forming events not associated with supercontinent assembly can contribute to the record (Domeier et al., 2018; Pastor-Galán et al., 2018, and refs. therein). The paleosol-zircon correlation could reflect optimal conditions for both soil formation (i.e., larger land area, increased sediment supply, climate shifts) and preservation (i.e., basin formation, depositional environments), although the latter is more logical in a stable continental setting or even in the beginning of breakup (i.e., rifting) rather than during continental assembly. However, the distribution of zircon ages could also be a result of preservation bias within the zircon record itself (Cawood et al., 2013; Pastor-Galán et al., 2018), so the paleosol-zircon correlation should be revisited if our understanding of the zircon record changes.

From the zircon record, the most important implication for interpreting the paleosol record is that paleosol preservation is more likely at some points in the supercontinent cycle, likely during the tail end of assembly and the stable middle period. If supercontinent assembly and increased tectonic uplift led to increased erosion and global cooling (as has been posited in the past, e.g., Molnar and England, 1990; Raymo and Ruddiman, 1992), and paleosols are more likely to be preserved from that syn- or post-orogenic cool period, it is possible that paleosols from those times would have a cool bias. Additionally, if paleosols tend to represent periods of maximum land area, they might be strongly affected by a continentality climate effect (i.e., arid interiors) which could affect both the geochemical and climatic signals as well as spatial preservation bias (i.e., less likely to preserve arid paleosols due to low vegetation and slow weathering rates). Testing the continentality and preservation of paleosols on regional scales during well-constrained periods of tectonic activity (e.g., Sheldon, 2009) would be useful for

elucidating the potential climate-preservation biases in the paleosol record related to the supercontinent cycle.

Total passive margin lengths correlate somewhat with the zircon record as well, although not as strongly as either paleosols or shales do with zircon ages. Starting in the Neoproterozoic, higher cumulative passive margin lengths overlap with zircon peaks, with the strongest correlation during Pangea. Although cumulative lengths during the Precambrian are low compared to the Phanerozoic, the average 'lifespan' of a passive margin was longer. Bradley (2008) credits these longer-lived passive margins to sluggish plate tectonics with longer-lived continents, which could have allowed some of the earliest weathering profiles to form. Passive margin lengths also qualitatively correlate with paleosol occurrences (both increasing in the Phanerozoic) and the ages of supercontinents, with the most recent peak related to the breakup of Pangea and the formation of today's passive margins. Additionally, Evenick (2021) analyzed the global distribution of basins through the Phanerozoic, finding an increase in the number of basins during the Mesozoic (Pangea). Together, the passive margin record and the increased likelihood for basin formation and preservation support the concept of depositional environment-driven preservation bias in paleosols during the supercontinent cycle.

The emplacements of LIPs occur steadily throughout the geologic record (Figure 4.1d; Ernst et al., 2021). Because of their consistent distribution, and along with the steadiness of the paleosol weathering record (as well as the shale record; Lipp et al., 2021), we consider LIPs to contribute to the baseline of weathering intensity through time, creating transient perturbations in weathering intensity during extreme events (e.g., mass extinctions associated with LIP emplacement; Sheldon, 2006b,c; Gastaldo et al., 2014; Sayyed, 2014; Schaller et al., 2015; van de Schootbrugge et al., 2020). However, the relationship between LIPs and global weathering (along with climate and the biosphere) remains debated. While some key LIP events such as the Deccan Traps (e.g., Dzombak et al., 2020a), CAMP (e.g., Schaller et al., 2011), and Columbia River Flood Basalt Province (e.g., Sheldon 2006c) preserve intra-basaltic paleosols that can be used to examine relationships between weathering intensity and climate directly (see Sayyed, 2014), adding additional paleosols during other Phanerozoic LIPs could help settle the debate about whether the LIPs enhanced weathering through direct greenhouse gas emissions or enhanced weathering by increasing the size the of the C sink available for silicate weathering.

4.5.3.2 Paleosol bias and climate

Changes in climate (temperature, precipitation, seasonality) can cause perturbations in global weathering and erosion intensity (e.g., Jenny, 1941, 1995; Bluth and Kump, 1994; Cao et al., 2019). As a primary driver of weathering, climate can facilitate or slow pedogenesis directly (e.g., increased temperature/precipitation) and indirectly (e.g., facilitating terrestrial biosphere). The distribution of climates globally, and the variability of that distribution, fluctuates through time (i.e., the latitudinal temperature gradient in transitional/icehouse conditions vs. stable greenhouse). Based on the weathering records presented here, these changes likely occurred on geologically short timescales (e.g., the Paleocene-Eocene Thermal Maximum, mass extinction events, etc.) or in spatially limited settings (e.g., basin-wide), making such discrete events unlikely to be captured by paleosols broadly (c.f., Hyland et al., 2017) even if they may be captured locally (e.g., at the scale of a single basin). Climate would also have affected soil preservation through weathering-erosion relationships (see supplemental text in Appendix C).

Global glaciations and icehouse-greenhouse transitions are the primary exception to the short-term impact of climate on soil formation and preservation, as evidenced by the significant gap in the paleosol record during Neoproterozoic glaciations, although some weathering can still occur during glacial periods (Figure 4.1d). While weathering likely slows during global glacial periods, studies of modern glacial environments suggest that chemical weathering at the surface would have continued, even if those terrestrial records were ultimately lost (e.g., Dubnick et al., 2017; Graly et al., 2020; Martin et al., 2020). Glacial tillites can help fill in those gaps, with compositions in similar distributions to paleosols (Figure C3; Gaschnig et al., 2014).

4.5.3.3 Paleosol bias from the biosphere, and implications for carbon cycling

Prior to the advent of land plants and fungi, the terrestrial biosphere consisted of microbial life, similar to microbial mats and early-stage biological soil crusts present today (e.g., Beraldi-Campesi et al., 2009; Wellman and Strother, 2015). While those communities would have influenced early pedogenesis through organic acid weathering, chemolithotrophy, and landscape stabilization, fossilized terrestrial microbial communities are rare and must be accompanied by other lines of evidence to establish biogenicity (see Retallack, 2012). Overall, the terrestrial fossil microbial record is biased towards fluvial and aquatic systems rather than paleosols *sensu stricto* (e.g., Gutzmer and Beukes, 1998; Mitchell and Sheldon, 2009; Noffke

and Amwarak, 2013; Homann et al., 2018), although whether this reflects optimal environments or taphonomic bias is unclear. A similar bias may be present in paleosols, as floodplain deposits are among the most common in the paleosol record and is a commonly preserved, non-lacustrine terrestrial facies in Macrostrat (Peters et al., 2018). Paleosols remain underrepresented in major databases relative to marine records, and expanding their representation will help build a more complete picture of terrestrial-marine links in weathering and biogeochemical cycling.

In the Phanerozoic, paleosol preservation increases, and the number of alluvium-parented paleosols increases as well. Both increases could be due to a combination of preservation bias in which younger rocks are more likely to be preserved than older rocks and fluctuations in sedimentation rate over geologic time (Sadler, 1999; Schumer and Jerolmack, 2009; Meyers and Peters, 2011; Peters and Husson, 2017; Paola et al. 2018). If sedimentation and accumulation rates are presumed to fluctuate over time, rather than secularly increase or decrease, the stability of the record remains robust. With more paleosols preserved towards the present and with those paleosols tending to have a wider range of weathering intensities (i.e., retaining the low-CIA values), it is reasonable to expect that if more paleosols were preserved in earlier periods, they would be more likely to capture a wider range of weathering conditions as well. However, preservation biases and the lack of carbonate prior to the Phanerozoic (either from a lack of rooting land plants, higher pCO_2, or both) create the CIA record presented here. All geologic records suffer from some gaps, and the community works to fill in those gaps and continually revise best interpretations. Based on available data, then, multiple indices of terrestrial weathering reflect a broad stability in weathering through the past 3 billion years despite temporal gaps.

Stacked or composite paleosols also become dominant during the Phanerozoic (see Table C2). Beyond a background/overall preservation bias towards the modern, which is present in essentially all geologic records, this could reflect changes in terrestrial geomorphology (i.e., the influence of plants on forming meandering rivers; Davies and Gibling, 2010) and a potential overall increase in the global volume of sediments beginning in the Neoproterozoic (Husson and Peters, 2017). The rise of deeper rooting by vascular plants during the early Phanerozoic could well have played a role in increasing preservation, especially of thinner profiles that could otherwise be readily eroded, serving as a landscape-stabilizing mechanism.

Rooted plants have also been hypothesized to have both increased (e.g., Algeo et al., 1995; Algeo and Scheckler, 1998; Lenton and Watson, 2004; Algeo and Twitchett, 2010) or decreased (e.g., D'Antonio et al., 2020) the intensity of terrestrial weathering. They could increase weathering by organic acid weathering (Horodyskyj et al, 2012; Driese et al., 2011) and physical weathering by roots, or decrease weathering by increasing the volume of soil mantle (therefore shielding bedrock from further weathering; see Appendix C)(e.g., Burke et al., 2007; Stockmann et al., 2014; Hartmann et al., 2014). Our weathering records (and P record in Chapter III) and previous work (Beaty and Planavsky 2021; Lipp et al., 2021) show no state change during the rise of land plants in the Silurian/Devonian—at first glance a surprising result, but one that is likely explained by the number of competing factors controlling the global weathering intensity signature at the time and a tendency of global biogeochemical systems (including the carbon cycle) to return to steady-state (see 4.5.2). Some modern soil scientists view soil profiles as existing in a state of plant-stabilized 'dynamic equilibrium' (e.g., Lucas, 2001) which lends support to the stability of this record.

The Phanerozoic mean Al_2O_3 decrease in the upper portions of paleosols (Figure C3) may reflect increased Al mobility due to plant- and fungi-mediated dissolution (Hausrath et al., 2009; Beaty and Planavsky, 2021) or a change in the composition of continental crust. The latter is an unlikely explanation; multiple studies have found relatively little change in Archean vs. bulk continental crust, with Al_2O_3 estimates for between 14–15.2% Al_2O_3 throughout geologic history (Taylor & McLennan, 1995; Rudnick and Gao, 2003; Lipp et al., 2021). Paleosol Al compositions are approximately centered around the continental crust average, supporting the interpretation of long-term stability at the surface with transient weathering perturbations, and potentially an increase in Al mobility with the advent of rooting land plants. Geochemical evidence of element mobilization via organic acids is taken as support for fungi-mediated terrestrial weathering due to fungal production of organic acids (e.g., Lenton and Watson, 2004; Horodyskyj et al., 2012). However, differentiating between fungal acid weathering and plant organic acid weathering (e.g., in the Al/Ti record) without other evidence for the presence of fungi is difficult. Terrestrial fungus species tend to be highly specialized (i.e., forming a symbiosis with a single plant species) due to different plant nutrient needs. To see changes in terrestrial biogeochemistry due to fungi, then, considering plant-specific metal incorporation on a smaller scale might be more appropriate than bulk changes in soil P, regardless of vegetation

type. The increase in Al in the Phanerozoic likely reflects an increase in clay mineral (aluminosilicates) mobility as well. Because clay minerals tend to carry nutrients, an increase in their mobility could have increased marine productivity; however, that increased mobility could also have negatively impacted marine primary productivity by increasing turbidity and reducing light penetration.

The evolution of global C sinks during the Phanerozoic has been established based on global C isotope records in terrestrial and marine settings (e.g., Ekart et al., 1999; Berner, 2004; Nordt et al., 2016), but this is the first time the Phanerozoic increase in pedogenic carbonate has been quantitatively demonstrated with a large dataset, supporting previous hypotheses about that concept (e.g., Sheldon and Tabor, 2009; Cantine et al., 2020; Sheldon et al., 2021). Global organic C isotopes (Figure 4.2b) in the Phanerozoic decrease in variability compared to the Precambrian, suggesting that the growing C sink in soils and pedogenic carbonate helped to stabilize the global C cycle (although perturbations still occurred). In our record, CaO in paleosols increases during the Phanerozoic (Figure 4.2c), providing support for this hypothesis. Soil compaction is unlikely to explain an increase in CaO through time, as most soil aside from Histosols have similar bulk densities (Sheldon and Retallack, 2001), and the composition of the continental crust is not thought to have experienced a discrete increase in crustal Ca at the onset of the Phanerozoic (Taylor and McLennan, 1985). This could be explained by plants (particularly in more arid environments; Retallack, 2001) facilitating the formation of pedogenic carbonate, contributing to CO_2 drawdown and greatly expanding the magnitude of the soil C sink both by limiting terrestrial erosion and storing C in soil horizon and pedogenic carbonate. The increase in CaO and low CIA values also corresponds to the variability of soil orders increasing, supporting an increase in geochemical variability as ecosystems and pedogenic processes grew more complex and varied (Figure 4.2c,d). Rooting and the evolution of symbiotic relationships with fungi allowed plants to colonize drier environments with more difficult to access nutrients, contributing to the spread of more intense pedogenesis in more varied environments (Algeo and Scheckler, 1998). Altogether, the presence of vascular land plants in the Phanerozoic facilitated pedogenesis, likely increased the probability of paleosol preservation and expanded the range of environments that could be preserved.

4.5.3.4 Sampling biases in paleosol research

Finally, sampling biases—both in space and time—obfuscate true trends in the paleosol record, as with any field-based sampling. As seen during the GOE, certain time periods of interest may be over-sampled relative to the number of profiles that exist during that timeframe. Certain soil orders of interest may also be overrepresented; for instance, Vertisols account for nearly a quarter of Phanerozoic profiles in this record, despite forming in limited environments (Vertisols cover only about 2.4% of ice-free land area today). In the Precambrian, weathering profiles with low weathering intensities may be under-sampled due to low profile thicknesses or simply due to our failure to recognize them as weathering profiles. This could contribute to the narrower range of weathering intensities in Precambrian profiles. Paleosols yielding pedogenic carbonate (i.e., arid and semi-arid regions) may also be over-sampled for carbon and oxygen isotope analysis, whereas tropical areas may be unsampled. Globally, access to field sites and a history of high-resolution geologic mapping varies widely, typically biasing our knowledge of paleosols to areas with good access. Not all types of data are available for every paleosol or weathering profile, limiting the conclusions that can be drawn from different subsets of a compilation. For example, many paleosol studies focusing on carbonate isotope geochemistry report only those values rather than also reporting bulk oxides, so the record here may under-represent carbonate-bearing paleosols, which would also lead to under-sampling of low CIA values. Considering sampling biases is useful when comparing different types of records (i.e., are they biased in similar ways?) and can make interpretations more robust.

4.5.4 Implications for reconstructing past climates and biogeochemical cycling

As discussed in Chapter III, biogeochemical models inherently include assumptions about the timing, rates, and magnitude of continental weathering and resultant sediment fluxes to oceans; however, until now, no quantitative record has existed to inform model parameters. Despite the gaps in the paleosol record, this compilation provides a baseline for weathering, suggesting that an essentially modern range of weathering intensities could have occurred at most points during Earth's history. Perhaps because the record reflects this background variability, some transient events that are known to have been captured by paleosols (e.g., the EECO; Gallagher and Sheldon, 2013; Hyland et al., 2017) are not reflected. Therefore, the weathering intensity record could be used as a baseline distribution, with known perturbations essentially shifting the distribution of weathering values higher only for a short time. Models

should not necessarily rely on secular or discrete increases in terrestrial weathering as a driver for long-term, biogeochemical state changes. Biogeochemical models should also take the Phanerozoic increase in paleosol CaO into account when modeling Phanerozoic carbon cycling and other connected biogeochemical systems.

An important implication for the practical application of paleosol geochemistry in reconstructing past climates and biogeochemical changes is the need to quantify background variability on the temporal and spatial scales of interest. If, at any given time from 3 Ga onwards, a paleosol CIA value could be 0–100, individual profiles are of little use unless they are placed in environmental and tectonic context. Including multiple profiles in space and time, as well as comparing paleosol geochemistry to other proxies (e.g., Tabor et al., 2008; Gulbranson et al., 2015; Hyland and Sheldon, 2016; Hyland et al., 2017; Chapter V) constrains local to regional geochemical variability and allows more robust interpretation of paleosol geochemical trends. Additionally, considering relative rather than absolute changes may be appropriate if other external factors can only be poorly constrained (e.g., Hyland et al., 2017; Chapter V).

4.5.5 Next steps for the field

The compilation presented here will hopefully serve as a starting point for the paleosol community to create a collaborative and comprehensive paleosol database that will allow some outstanding "big questions" in the field to be addressed. Shale compilations tend to be high resolution, but are a more indirect weathering product than paleosols, limiting the terrestrial interpretations and conclusions that can be drawn from them. The Phanerozoic record in particular should be filled in to robustly test hypotheses related to the rise of land plants and the distribution of soil orders though (relatively recent) geologic time, which would shed light on the distribution of terrestrial ecosystems and depositional environments through time as well. Without such a database, questions around the evolution of pedogenesis, biogeochemical transitions, and preservation bias will remain unanswered. Additionally, constraining modern soils globally in a similar approach—profile thicknesses, weathering intensity, geochemical composition, etc.—is necessary to provide a baseline or point of reference for interpreting potential trends or changes in the paleosol record.

While this compilation focused on bulk geochemistry (i.e., major oxides), assembling a similar dataset including trace metals and REE in paleosols over time could be helpful for

biogeochemical modeling and improving our understanding of the evolution of the terrestrial biosphere and its connections to marine productivity. Additionally, exploring individual elements in detail—particularly for the Phanerozoic record—could provide unique insights into specific biogeochemical cycles.

4.6 Conclusions

In contrast with common assumptions about how terrestrial weathering intensity has changed through geologic time, our new compilation of paleosols/weathering profiles shows consistent weathering intensity in a suite of weathering indices (CIA(-K), MIA, and Al/Ti), providing support for two recent long-term weathering records that were stable on long timescales. While indices' averages are similar over the past three billion years, one—CIA—exhibits an increase in range in the Phanerozoic due to the increased presence of low-CIA paleosols. This suggests that preservation biases affect the paleosol record, as in other parts of the geologic record, where more recent rocks are more likely to be preserved. The Phanerozoic increase in the presence of low-CIA paleosols also likely reflects an appearance of pedogenic carbonate—a primary source of Ca aside from feldspars—which has been previously posited, but never quantitatively demonstrated until now. We interpret the ~10-unit difference in mean CIA between modern soils and paleosols as a preservation bias placed by North American glaciation. Overall, these stable records reflect the long-term baseline of terrestrial weathering intensity, which can be perturbed on shorter timescales (e.g., climate transitions, tectonic events) before returning to its steady state. As in Chapter III, we point to factors other than weathering intensity as controlling terrestrial erosional fluxes, such as overall land area. These quantitative metrics of weathering through time can be applied to improve constraints for biogeochemical models.

This record also highlights a concern throughout geology: preservation bias. By connecting the distribution of paleosols through time with other long-term records (i.e., zircons, shales, passive margins) as well as geochemical trends through time, we suggest that the occurrence of taphonomically-preferable depositional environments, sediment supply, climate, and the biosphere vary through time and change the likelihood of paleosol formation and preservation. Therefore, paleosol records may be more likely to represent certain environments, climates, or periods within the supercontinent cycle, and interpretations of paleosol geochemistry should take this into account. Communally building a more comprehensive database of paleosol

geochemistry, particularly in the Phanerozoic, should aid in interpreting paleosol geochemistry as well as gaps in the paleosol record.

Acknowledgments

Funding during this work was partially provided by NSF #1812949 to N.D.S and others. Thanks to Jordan Tyo, Katie Seguin, Bianca Gallina, and Sonya Vogel for help in assembling this dataset.

References

1. Algeo, T. J. & Twitchett, R. J. Anomalous Early Triassic sediment fluxes due to elevated weathering rates and their biological consequences. *Geology* **38**, 1023–1026 (2010).

2. Algeo, T. J., Berner, R. A., Maynard, J. B. & Scheckler, S. E. Late Devonian Oceanic Anoxic Events and Biotic Crises: 'Rooted' in the Evolution of Vascular Land Plants? *GSA Today* **5**, 1,45,64-66 (1995).

3. Algeo, T. J. & Scheckler, S. E. Terrestrial-marine teleconnections in the Devonian: links between the evolution of land plants, weathering processes, and marine anoxic events. *Philos. Trans. R. Soc. London B* **353**, 113–130 (1998).

4. Amorosi, A., Bruno, L., Campo, B., Di Martino, A. & Sammartino, I. Patterns of geochemical variability across weakly developed paleosol profiles and their role as regional stratigraphic markers (Upper Pleistocene, Po Plain). *Palaeogeogr. Palaeoclimatol. Palaeoecol.* in press, 110413 (2021).

5. Anbar, A. D. *et al.* A whiff of oxygen before the great oxidation event? *Science* **317**, 1903–1906 (2007).

6. Anbar, A. D. & Knoll, A. H. Proterozoic Ocean Chemistry and Evolution: A Bioinorganic Bridge? *Science* **297**, 1137–1142 (2002).

7. Babechuk, M. G., Widdowson, M. & Kamber, B. S. Quantifying chemical weathering intensity and trace element release from two contrasting basalt profiles, Deccan Traps, India. *Chem. Geol.* **363**, 56–75 (2014).

8. Bahlburg, H. & Dobrzinski, N. A review of the Chemical Index of Alteration (CIA) and its application to the study of Neoproterozoic glacial deposits and climate transitions. In: The Geological Record of Neoproterozoic Glaciations, eds. Arnaud, E., Halverson, G.P. & Shields-Zhou, G. *Geol. Soc. Mem.* **36**, 81–92 (2011). London.

9. Bayon, G. *et al.* A global survey of radiogenic strontium isotopes in river sediments. *Chem. Geol.* **559**, 119958 (2021).

10. Beaty, B. J. & Planavsky, N. J. A 3 b.y. record of a biotic influence on terrestrial weathering. *Geology* **49**, 407–411 (2021).

11. Beraldi-Campesi, H., Hartnett, H. E., Anbar, A. D., Gordon, G. W. & Garcia-Pichel, F. Effect of biological soil crusts on soil elemental concentrations: Implications for biogeochemistry and as traceable biosignatures of ancient life on land. *Geobiology* **7**, 348–359 (2009).

12. Berner, R. A. The carbon cycle and CO_2 over Phanerozoic time: The role of land plants. *Philos. Trans. R. Soc. B Biol. Sci.* **353**, 75–82 (1998).

13. Berner, R.A. The Phanerozoic Carbon Cycle: CO_2 and O_2. Oxford University Press, Oxford, UK (2004).

14. Berner, R. A. GEOCARBSULF: A combined model for Phanerozoic atmospheric O_2 and CO_2. *Geochim. Cosmochim. Acta* **70**, 5653–5664 (2006).

15. Bestland, E. A., Retallack, G. J. & Swisher, C. C. Stepwise climate change recorded in Eocene-Oligocene paleosol sequences from Central Oregon. *J. Geol.* **105**, 153–172 (1997).

16. Blum, J. D., Gazis, C. A., Jacobson, A. D. & Chamberlain, C. P. Carbonate versus silicate weathering in the Raikhot watershed within the High Himalayan Crystalline Series. *Geology* **26**, 411–414 (1998).

17. Bluth, G. J. S. & Kump, L. R. Lithologic and climatologic controls of river chemistry. *Geochim. Cosmochim. Acta* **58**, 2341–2359 (1994).

18. Bradley, D. C. Passive margins through earth history. *Earth-Science Reviews* **91**, 1–26 (2008).

19. Brass, G. W. The effect of weathering on the distribution of strontium isotopes in weathering profiles. *Geochim. Cosmochim. Acta* **39**, 1647–1653 (1975).

20. Brocks, J. J. *et al.* The rise of algae in Cryogenian oceans and the emergence of animals. *Nature* **548**, 578–581 (2017).

21. Burke, B. C., Heimsath, A. M. & White, A. F. Coupling chemical weathering with soil production across soil-mantled landscapes. *Earth Surf. Process. Landforms* **32**, 853–873 (2007).

22. Campbell, I. H. & Squire, R. J. The mountains that triggered the Late Neoproterozoic increase in oxygen: The Second Great Oxidation Event. *Geochim. Cosmochim. Acta* **74**,

4187–4206 (2010).

23. Cantine, M. D., Knoll, A. H. & Bergmann, K. D. Carbonates before skeletons: A database approach. *Earth-Science Reviews* **201**, 103065 (2020).

24. Cao, Y. *et al.* Intensified chemical weathering during the Permian-Triassic transition recorded in terrestrial and marine successions. *Palaeogeogr. Palaeoclimatol. Palaeoecol.* **519**, 166–177 (2019).

25. Caves, J. K., Jost, A. B., Lau, K. V. & Maher, K. Cenozoic carbon cycle imbalances and a variable weathering feedback. *Earth Planet. Sci. Lett.* **450**, 152–163 (2016).

26. Cawood, P. A., Hawkesworth, C. J. & Dhuime, B. The continental record and the generation of continental crust. *Bull. Geol. Soc. Am.* **125**, 14–32 (2013).

27. Cermeño, P., Falkowski, P. G., Romero, O. E., Schaller, M. F. & Vallina, S. M. Continental erosion and the Cenozoic rise of marine diatoms. *Proc. Natl. Acad. Sci. U. S. A.* **112**, 4239–4244 (2015).

28. Cohen, A.S. & Coe, A.L. New geochemical evidence for the onset of volcanism in the Central Atlantic magmatic province and environmental change at the Triassic-Jurassic boundary. *Geology* **30**, 267-270 (2002).

29. Colwyn, D. A. *et al.* A paleosol record of the evolution of Cr redox cycling and evidence for an increase in atmospheric oxygen during the Neoproterozoic. *Geobiology* **17**, 579–593 (2019).

30. Cox, G. M. *et al.* Continental flood basalt weathering as a trigger for Neoproterozoic Snowball Earth. *Earth Planet. Sci. Lett.* **446**, 89–99 (2016).

31. Davies, N. S. & Gibling, M. R. Cambrian to Devonian evolution of alluvial systems: The sedimentological impact of the earliest land plants. *Earth Sci. Rev.* **98**, 171–200 (2010).

32. Dixon, J. L. & Blanckenburg, F. Von. Soils as pacemakers and limiters of global silicate weathering. *Comptes rendus - Geosci.* **344**, 597–609 (2012).

33. Dixon, J. L., Heimsath, A. M., Kaste, J. & Amundson, R. Climate-driven processes of hillslope weathering. *Geology* **37**, 975–978 (2009).

34. Domeier, M., Magni, V., Hounslow, M. W. & Torsvik, T. H. Episodic zircon age spectra mimic fluctuations in subduction. *Sci. Rep.* **8**, 17471 (2018).

35. Donnadieu, Y., Godderis, Y., Ramstein, G., Nedelec, A. & Meert, J. A ‘snowball Earth’’ climate triggered by continental break-up through changes in runoff. *Nature* **541**, 303–306 (2004).

36. Driese, S. G. *et al.* Neoarchean paleoweathering of tonalite and metabasalt: Implications for reconstructions of 2.69Ga early terrestrial ecosystems and paleoatmospheric chemistry. *Precambrian Res.* **189**, 1–17 (2011).

37. Dubnick, A. *et al.* Trickle or treat: The dynamics of nutrient export from polar glaciers. *Hydrol. Process.* **31**, 1776–1789 (2017).

38. Dzombak, R. M., Sheldon, N. D., Mohabey, D. M. & Samant, B. Stable climate in India during Deccan volcanism suggests limited influence on K–Pg extinction. *Gondwana Res.* **85**, 19–31 (2020).

39. Ekart, D. D., Cerling, T. E., Montañez, I. P. & Tabor, N. J. A 400 million year carbon isotope record of pedogenic carbonate: Implications for paleoatmospheric carbon dioxide. *American Journal of Science* **299**, 805–827 (1999).

40. Ernst, R. *et al.* Part I. The temporal record of large igneous provinces (LIPs). in *Large Igneous Provinces: A Driver of Global Environmental and Biotic Changes* (eds. Ernst, R. E., Dickson, A. J. & Bekker, A.) American Geophysical Union and John Wiley & Sons, Inc., D.C. 2021.

41. Evenick, J. C. Glimpses into Earth's history using a revised global sedimentary basin map. *Earth-Science Rev.* **215**, 103564 (2021).

42. Fabre, S., Berger, G. & Nédélec, A. Modeling of continental weathering under high-CO2 atmospheres during Precambrian times. *Geochemistry, Geophys. Geosystems* **12**, 1–23 (2011).

43. Fedo, C. M., Eriksson, K. A. & Krogstad, E. J. Geochemistry of shales from the Archean (~3.0 Ga) Buhwa Greenstone Belt, Zimbabwe: Implications for provenance and source-area weathering. *Geochim. Cosmochim. Acta* **60**, 1751–1763 (1996).

44. Francois, L. M. & Walker, J. C. G. Modelling the Phanerozoic carbon cycle and climate: constraints from the $^{87}Sr/^{86}Sr$ isotopic ratio of seawater. *American Journal of Science* **292**, 81–135 (1992).

45. Gallagher, T. M. & Sheldon, N. D. A new paleothermometer for forest paleosols and its implications for Cenozoic climate. *Geology* **41**, 647–650 (2013).

46. Gaschnig, R. M., Rudnick, R. L., Mcdonough, W. F. & Kaufman, A. J. Onset of oxidative weathering of continents recorded in the geochemistry of ancient glacial diamictites. *Earth Planet. Sci. Lett.* **408**, 87–99 (2014).

47. Gastaldo, R. A., Knight, C. L., Neveling, J. & Tabor, N. J. Latest Permian paleosols from Wapadsberg Pass, South Africa: Implications for Changhsingian climate. *Geol. Soc. Am. Bull.* **126**, 665–679 (2014).

48. Graly, J. A., Licht, K. J., Bader, N. A. & Bish, D. L. Chemical weathering signatures from Mt. Achernar Moraine, Central Transantarctic Mountains I: Subglacial sediments compared with underlying rock. *Geochim. Cosmochim. Acta* **283**, 149–166 (2020).

49. Gulbranson, E. L., Montañez, I. P., Tabor, N. J. & Oscar Limarino, C. Late Pennsylvanian aridification on the southwestern margin of Gondwana (Paganzo Basin, NW Argentina): A regional expression of a global climate perturbation. *Palaeogeogr. Palaeoclimatol. Palaeoecol.* **417**, 220–235 (2015).

50. Gutzmer, J. & Beukes, N. J. Earliest laterites and possible evidence for terrestrial vegetation in the Early Proterozoic. *Geology* **26**, 263–266 (1998).

51. Hao, J., Knoll, A. H., Huang, F., Hazen, R. M. & Daniel, I. Cycling phosphorus on the Archean Earth: Part I. Continental weathering and riverine transport of phosphorus. *Geochim. Cosmochim. Acta* **273**, 70–84 (2020).

52. Hao, J., Sverjensky, D. A. & Hazen, R. M. A model for late Archean chemical weathering and world average river water. *Earth Planet. Sci. Lett.* **457**, 191–203 (2017).

53. Hartmann, J., Moosdorf, N., Lauerwald, R., Hinderer, M. & West, A. J. Global chemical weathering and associated P-release — The role of lithology, temperature and soil properties. *Chem. Geol.* **363**, 145–163 (2014).

54. Hausrath, E. M., Neaman, A. & Brantley, S. L. Elemental release rates from dissolving basalt and granite with and without organic ligands. *Am. J. Sci.* **309**, 633–660 (2009).

55. Hazen, R. M. *et al.* Mineral evolution. *Am. Mineral.* **93**, 1693–1720 (2008).

56. Heimsath, A. M. & Burke, B. C. The impact of local geochemical variability on quantifying hillslope soil production and chemical weathering. *Geomorphology* **200,** 75-88 (2013).

57. Hintze, J.L & Nelson, R.D. Violin plots: A box plot-density trace synergism. *The American Statistician* **52**, 181-184 (1998).

58. Homann, M. *et al.* Microbial life and biogeochemical cycling on land 3,220 million years ago. *Nat. Geosci.* **11**, 665–671 (2018).

59. Horodyskyj, L. B., White, T. S. & Kump, L. R. Substantial biologically mediated phosphorus depletion from the surface of a Middle Cambrian paleosol. *Geology* **40**, 503–506 (2012).

60. Husson, J. M. & Peters, S. E. Atmospheric oxygenation driven by unsteady growth of the continental sedimentary reservoir. *Earth Planet. Sci. Lett.* **460**, 68–75 (2017).

61. Hyland, E. G. & Sheldon, N. D. Examining the spatial consistency of palaeosol proxies: Implications for palaeoclimatic and palaeoenvironmental reconstructions in terrestrial sedimentary basins. *Sedimentology* **63**, 959–971 (2016).

62. Hyland, E. G. & Sheldon, N. D. Coupled CO2-climate response during the Early Eocene Climatic Optimum. *Palaeogeogr. Palaeoclimatol. Palaeoecol.* **369**, 125–135 (2013).

63. Hyland, E. G., Sheldon, N. D. & Cotton, J. M. Constraining the early Eocene climatic optimum: A terrestrial interhemispheric comparison. *Bull. Geol. Soc. Am.* **129**, 244–252 (2017).

64. Hyland, E. G., Sheldon, N. D. & Fan, M. Terrestrial paleoenvironmental reconstructions indicate transient peak warming during the early Eocene climatic optimum. *Bull. Geol. Soc. Am.* **125**, 1338–1348 (2013).

65. Jenny, H.J. Factors in soil formation. 1941, McGraw-Hill, New York.

66. Jenny, H. & Amundson, R. Factors of soil formation: A System of Quantitative Pedology. (1994).

67. Kanzaki, Y. & Murakami, T. Estimates of atmospheric CO_2 in the Neoarchean-Paleoproterozoic from paleosols. *Geochim. Cosmochim. Acta* **159**, 190–219 (2015).

68. Kasting, J. F. Earth's Early Atmosphere. *Science* **259**, 920–926 (1993).

69. Kelly, D. C., Zachos, J. C., Bralower, T. J. & Schellenberg, S. A. Enhanced terrestrial weathering/runoff and surface ocean carbonate production during the recovery stages of the Paleocene-Eocene thermal maximum. *Paleoceanography* **20**, 1–11 (2005).

70. Kendall, B., Creaser, R. A., Reinhard, C. T., Lyons, T. W. & Anbar, A. D. Transient episodes of mild environmental oxygenation and oxidative continental weathering during the late Archean. *Sci. Adv.* **1**, e1500777 (2015).

71. Kennedy, M. J., Droser, M., Mayer, L. M., Pevear, D. & Mrofka, D. Late Precambrian Oxygenation: Inception of the Clay Mineral Factory. *Science* **311**, 1446–1450 (2006).

72. Korenaga, J. Crustal evolution and mantle dynamics through Earth history. *Philos. Trans. R. Soc. A Math. Phys. Eng. Sci.* **376**, (2018).

73. Kraus, M. J. & Riggins, S. Transient drying during the Paleocene-Eocene Thermal Maximum (PETM): Analysis of paleosols in the bighorn basin, Wyoming. *Palaeogeogr. Palaeoclimatol. Palaeoecol.* **245**, 444–461 (2007).

74. Krissansen-Totton, J., Buick, R. & Catling, D. C. A statistical analysis of the carbon isotopic record from the Archean to Phanerozoic and implications for the rise of oxygen.

Am. J. Sci. **315**, 275–316 (2015).

75. Laakso, T. A., Sperling, E. A., Johnston, D. T. & Knoll, A. H. Ediacaran reorganization of the marine phosphorus cycle. *Proc. Natl. Acad. Sci.* **117**, 11961–11967 (2020).

76. Lee, C. T. A., Thurner, S., Paterson, S. & Cao, W. The rise and fall of continental arcs: Interplays between magmatism, uplift, weathering, and climate. *Earth Planet. Sci. Lett.* **425**, 105–119 (2015).

77. Lenton, T. M. The role of land plants, phosphorus weathering and fire in the rise and regulation of atmospheric oxygen. *Glob. Chang. Biol.* **7**, 613–629 (2001).

78. Lenton, T. M. & Watson, A. J. Biotic enhancement of weathering, atmospheric oxygen and carbon dioxide in the Neoproterozoic. *Geophys. Res. Lett.* **31**, (2004).

79. Lipp, A. G. *et al.* The composition and weathering of the continents over geologic time. *Geochemical Perspect. Lett.* **17**, 21–26 (2021).

80. Lucas, Y. The Role of Plants in Controlling Rates and Products of Weathering: Importance of Biological Pumping. *Annu. Rev. Earth Planet. Sci.* **29**, 135–163 (2001).

81. Lyons, T. W., Reinhard, C. T. & Planavsky, N. J. The rise of oxygen in Earth's early ocean and atmosphere. *Nature* **506**, 307–15 (2014).

82. Markewich, H. W., Pavich, M. J. & Buell, G. R. Contrasting soils and landscapes of the Piedmont and Coastal Plain, eastern United States. *Geomorphology* **3**, 417–447 (1990).

83. Martin, E. E. & Macdougall, J. D. Sr and Nd isotopes at the Permian/Triassic boundary: A record of climate change. *Chem. Geol.* **125**, 73–99 (1995).

84. Martin, J. B., Pain, A. J., Martin, E. E., Rahman, S. & Ackerman, P. Comparisons of nutrients exported from Greenlandic glacial and deglaciated watersheds. *Geobiology* **34**, e2020GB006661 (2020).

85. Maynard, J. B. Chemistry of modern soils as a guide to interpreting Precambrian paleosols. *J. Geol.* **100**, 279–289 (1992).

86. Meyers, S.R. & Peters, S.E. A 56 million year rhythm in North American sedimentation during the Phanerozoic. *Earth and Planetary Science Letters* **303**, 174-180 (2011).

87. Michel, L.A., Sheldon, N.D., Myers, T.S., Tabor, N.J., (in review), Paleoprecipitation estimates from paleosols: reassessment after nearly 20 years of research. *Chemical Geology.*

88. Millot, R., Gaillardet, J., Dupré, B. & Allègre, C. J. The global control of silicate weathering rates and the coupling with physical erosion: New insights from rivers of the

Canadian Shield. *Earth Planet. Sci. Lett.* **196**, 83–98 (2002).

89. Mills, B. J. W., Watson, A. J., Goldblatt, C., Boyle, R. & Lenton, T. M. Timing of Neoproterozoic glaciations linked to transport-limited global weathering. *Nat. Geosci.* **4**, 861–864 (2011).

90. Mitchell, R. L. & Sheldon, N. D. Weathering and paleosol formation in the 1.1 Ga Keweenawan Rift. *Precambrian Res.* **168**, 271–283 (2009).

91. Molnar, P. & England, M. H. Late Cenozoic uplift of mountain ranges and climate: chicken or egg? *Nature* **346**, 29–34 (1990).

92. Murakami, T. *et al.* Anoxic dissolution processes of biotite: Implications for Fe behavior during Archean weathering. *Earth Planet. Sci. Lett.* **224**, 117–129 (2004).

93. Neaman, A., Chorover, J. & Brantley, S. L. Implications of the evolution of organic acid moieties for basalt weathering over geological time. *Am. J. Sci.* **305**, 147–185 (2005).

94. Nesbitt, H. W. & Young, G. M. Early Proterozoic climates and plate motions inferred from major element chemistry of lutites. *Nature* **299**, 715–717 (1982).

95. Noffke, N. & Awramik, S. M. Stromatolites and MISS-Differences between relatives. *GSA Today* **23**, 4–9 (2013).

96. Nordt, L., Tubbs, J. & Dworkin, S. Stable carbon isotope record of terrestrial organic materials for the last 450 Ma yr. *Earth-Science Rev.* **159**, 103–117 (2016).

97. Nott, J. The Influence of Deep Weathering on Coastal Landscape and Landform Development in the Monsoonal Tropics of Northern Australia. *J. Geol.* **102**, 509–522 (1994).

98. Och, L. M. & Shields-Zhou, G. A. The Neoproterozoic oxygenation event: Environmental perturbations and biogeochemical cycling. *Earth-Science Rev.* **110**, 26–57 (2012).

99. Pastor-Galán, D., Nance, R. D., Murphy, J. B. & Spencer, C. J. Supercontinents: Myths, mysteries, and milestones. *Geol. Soc. Spec. Publ.* **470**, 39–64 (2019).

100. Peters, S.E. & Husson, J.M. Sediment cycling on continental and oceanic crust. *Geology* **45**, 323-326 (2017).

101. Peters, S.E., Husson, J.M., and Czaplewski, J. Macrostrat: A platform for geological data integration and deep-time Earth crust research. *Geochem., Geophys., Geosys.* **19**, 1393-1409 (2018).

102. Planavsky, N. J. *et al.* A case for low atmospheric oxygen levels during Earth's middle history. *Emerg. Top. Life Sci.* **2**, 149–159 (2018).

103. Planavsky, N. J. *et al.* The evolution of the marine phosphate reservoir. *Nature* **467**, 1088–1090 (2010).

104. Porada, P. *et al.* High potential for weathering and climate effects of non-vascular vegetation in the Late Ordovician. *Nat. Commun.* **7**, 12113 (2016).

105. Prochnow, S. J., Nordt, L. C., Atchley, S. C. & Hudec, M. R. Multi-proxy paleosol evidence for middle and late Triassic climate trends in eastern Utah. *Palaeogeogr. Palaeoclimatol. Palaeoecol.* **232**, 53–72 (2006).

106. Raymo, M. E. & Ruddiman, W. F. Tectonic forcing of late Cenozoic climate. *Nature* **359**, 117–122 (1992).

107. Reinhard, C. T. *et al.* The impact of marine nutrient abundance on early eukaryotic ecosystems. *Geobiology* **18**, 139–151 (2020).

108. Reinhard, C. T., Raiswell, R., Scott, C., Anbar, A. D. & Lyons, T. W. A Late Archean Sulfidic Sea Stimulated by Early Oxidative Weathering of the Continents. *Science* **326**, 713–716 (2009).

109. Reinhard, C. T. *et al.* Evolution of the global phosphorus cycle. *Nature* **541**, 386–389 (2017).

110. Retallack, G. J. Cenozoic Expansion of Grasslands and Climatic Cooling. *J. Geol.* **109**, 407–426 (2001).

111. Retallack, G. J. Criteria For Distinguishing Microbial Mats and Earths. in *Microbial Mats in Silicilastic Depositional Systems Through Time* 139–152. SEPM Society for Sedimentary Geology, 2012.

112. Rudnick, R. L., Gao, S. in The Crust (ed. Rudnick, R. L.). Treatise in Geochemistry, Vol. 3, p. 1-64. Elsevier, Amsterdam. 2003.

113. Rye, R. & Holland, H. D. Life associated with a 2.76 Ga ephemeral pond?: Evidence from Mount Roe #2 paleosol. *Geology* **28**, 483–486 (2000).

114. Rye, R. & Holland, H. D. Paleosols and the evolution of atmsopheric oxygen: a critical review. *Am J Sci* **298**, 621–672 (1998).

115. Sadler, P. M., Bruns, P. & Haas, H. C. The Influence of Hiatuses on Sediment Accumulation Rates On the Determination of Sediment Accumulation Rates. *GeoResearch Forum* **5**, 15-40 (1999).

116. Sahoo, S. K. *et al.* Ocean oxygenation in the wake of the Marinoan glaciation. *Nature* **489**, 546–549 (2012).

117. Sayyed, M. R. G. Flood basalt hosted palaeosols: Potential palaeoclimatic indicators of global climate change. *Geosci. Front.* **5**, 791–799 (2014).

118. Schaller, M. F., Wright, J. D. & Kent, D. V. Atmospheric pCO_2 Perturbations Associated with the Central Atlantic Magmatic Province. *Science* **331**, 1404–1410 (2011).

119. Schaller, M. F., Wright, J. D. & Kent, D. V. A 30 Myr record of late Triassic atmospheric pCO_2 variation reflects a fundamental control of the carbon cycle by changes in continental weathering. *Bull. Geol. Soc. Am.* **127**, 661–671 (2014).

120. Schumer, R. & Jerolmack, D.J. Real and apparent changes in sediment deposition rates through time. *J. Geophys. Res.: Earth Surface* **114** F00A06 (2009).

121. Sheldon, N. D. Precambrian paleosols and atmospheric CO_2 levels. *Precambrian Res.* **147**, 148–155 (2006).

122. Sheldon, N. D. Using paleosols of the Picture Gorge Basalt to reconstruct the middle Miocene climatic optimum. *PaleoBios* **26**, 27–36 (2006).

123. Sheldon, N. D. Abrupt chemical weathering increase across the Permian-Triassic boundary. *Palaeogeogr. Palaeoclimatol. Palaeoecol.* **231**, 315–321 (2006).

124. Sheldon, N. D. Causes and consequences of low atmospheric CO_2 in the Late Mesoproterozoic. *Chem. Geol.* **362**, 224–231 (2013).

125. Sheldon, N. D. Nonmarine records of climatic change across the Eocene-Oligocene transition. *Spec. Pap. Geol. Soc. Am.* **452**, 241–248 (2009).

126. Sheldon, N.D. & Retallack, G.J. Equation for compaction of paleosols due to burial. *Geology* **29**, 247-250 (2001).

127. Sheldon, N. D., Costa, E., Cabrera, L. & Garcés, M. Continental Climatic and Weathering Response to the Eocene-Oligocene Transition. *J. Geol.* **120**, 227–236 (2012).

128. Sheldon, N. D., Mitchell, R. L. & Dzombak, R. M. Reconstructing Precambrian pCO_2 and pO_2 Using Paleosols. Cambridge University Press, 2021.

129. Sheldon, N. D., Retallack, G. J. & Tanaka, S. Geochemical Climofunctions from North American Soils and Application to Paleosols across the Eocene-Oligocene Boundary in Oregon. *J. Geol.* **110**, 687–696 (2002).

130. Sheldon, N. D. & Tabor, N. J. Quantitative paleoenvironmental and paleoclimatic reconstruction using paleosols. *Earth-Science Rev.* **95**, 1–52 (2009).

131. Somelar, P. *et al.* CO_2 drawdown and cooling at the onset of the Great Oxidation Event recorded in 2.45 Ga paleoweathering crust. *Chem. Geol.* **548**, 119678 (2020).

132. Stockmann, U., Minasny, B. & Mcbratney, A. B. How fast does soil grow? *Geoderma* **216**, 48–61 (2014).

133. Tabor, N. J., Montañez, I. P., Scotese, C. R., Poulsen, C. J. & Mack, G. H. Paleosol archives of environmental and climatic history in paleotropical western Pangea during the latest Pennsylvanian through Early Permian. *Geol. Soc. Am. Spec. Pap.* **2441**, 291–303 (2008).

134. Taylor, S.R. & McLennan, S.M. The continental crust: Its composition and evolution. Blackwell, United States. 1985.

135. Taylor S.R.; McLennan S.M. The geochemical evolution of the continental crust. *Reviews of Geophysics* 1995, *33*, 241-265.

136. Theiling, B. P., Elrick, M. & Asmerom, Y. Increased continental weathering flux during orbital-scale sea-level highstands: Evidence from Nd and O isotope trends in Middle Pennsylvanian cyclic carbonates. *Palaeogeogr. Palaeoclimatol. Palaeoecol.* **342**–**343**, 17–26 (2012).

137. van de Schootbrugge, B. *et al.* Catastrophic soil loss associated with end-Triassic deforestation. *Earth-Science Rev.* **210**, 103332 (2020).

138. Voice, P. J., Kowalewski, M. & Eriksson, K. A. Quantifying the Timing and Rate of Crustal Evolution: Global Compilation of Radiometrically Dated Detrital Zircon Grains. *J. Geol.* **119**, 109–126 (2011).

139. Wellman, C. H. & Strother, P. K. The terrestrial biota prior to the origin of land plants (embryophytes): A review of the evidence. *Palaeontology* **58**, 601–627 (2015).

140. West, A. J. Thickness of the chemical weathering zone and implications for erosional and climatic drivers of weathering and for carbon-cycle feedbacks. *Geology* **40**, 811–814 (2012).

141. Willenbring, J. K. & Von Blanckenburg, F. Long-term stability of global erosion rates and weathering during late-Cenozoic cooling. *Nature* **465**, 211–214 (2010).

Chapter 5
Incorporating Lateral Variability and Extent of Paleosols Into Proxy Uncertainty[3]

5.1 Abstract

Paleosols (fossil soils) are valuable records of terrestrial climate and environments, and paleosol-based proxies are commonly used to reconstruct past climates and ecosystems. Results from relatively small outcrops or transects or from single vertical sections are frequently scaled up to represent basin-scale processes and conditions, and reconstructions are relied on for temporal changes in those basins. However, uncertainty arising from limited outcrop extent is not currently considered in the standard application of paleosol-based proxies. To explore uncertainty arising from lateral paleosol heterogeneity, we performed a random subsampling analysis on a newly-collected 2.9 km paleosol transect from SW Wyoming, along with two previously-published paleosols. We demonstrate the importance of sampling multiple paleosol profiles, considering lateral geochemical variability, and focusing on relative rather than absolute changes when outcrop-based uncertainty may require it.

5.2 Introduction

Paleosols provide critical, unique insight into the interactions in the 'critical zone' where the atmosphere, biosphere, and geosphere meet at Earth's surface (Brantley et al., 2007; Nordt and Driese, 2014). Because they form at the surface, in constant contact with and in response to regional climates and whatever life is present, paleosols can be used to reconstruct past climates, environments, and chemical conditions of the continents (Jenny, 1941; Harnois, 1988; Maynard, 1992; Cerling, 1984; Rye and Holland, 1998; Retallack 2001; Sheldon and Tabor, 2009; Sheldon, 2018; Tabor and Myers, 2015). Geochemical proxies derived from soil chemistry are powerful tools for understanding the planet's history, but they remain imperfect. Some baseline

[3] *This paper is in review at Palaeo3 as an invited submission.*

limitations for paleosol-based proxies include preservation of their original composition (e.g., Retallack 1991; Fedo et al., 1995; Rye and Holland, 1998), outcrop exposure, soil order identification (Mack et al., 1993; e.g., Sheldon et al., 2002; Nordt and Driese 2010; Gallagher and Sheldon, 2013), and their calibration based on modern soil conditions, processes, and datasets. These in turn limit our ability to interpret and extrapolate results beyond the calibration datasets. While the community is continually working to improve paleosol-based proxies, one limitation–outcrop exposure–remains a relatively unaddressed source of statistical uncertainty in paleoclimate reconstructions.

Many paleosol-based proxies are applied to a limited number of paleosol profiles, as determined by outcrop exposure and quality. Because of common proxy development methods and field applications, paleosol-based proxies are not well-constrained at landscape or basin-wide scales, which are often the scales of interest for paleoclimate and paleoenvironmental reconstruction. The field is left with a number of uncertainty sources in these proxies based on outcrop exposure and extent that are not taken into consideration when interpreting results. The ultimate effect of this omission is an overstatement of certainty.

While statistical uncertainty in paleosol-based proxies could be improved in several ways (e.g., focusing on improvements in the calibration datasets and moving away from fixed standard error as in Lukens et al. (2019)), lateral variability in paleosols' geochemistry is one of the key targets for improvement. Modern landscapes host varied microclimates, vegetation, hydrology, and sedimentary architectures, leading to geochemical variability. The same can be assumed to be true for ancient landscapes following the advent of land plants. Sampling practices are inherently limited by outcrop exposure, but no one has yet quantified or demonstrated how this limitation should affect the certainty of paleosol-based climate reconstructions. If, for example, a paleosol has a 50 m laterally-continuous exposure and three profiles are sampled, how should the statistical uncertainty of those paleoclimate reconstructions be treated as opposed to if ten profiles were sampled in that same section? How large a lateral exposure, or multiple exposures, should be used to represent basin-wide climate or ecosystems? At a fundamental level, the base geochemical variability within a paleosol outcrop should be considered as part of proxy uncertainty, rather than relying solely on the fixed proxy error, but this is not currently standard practice.

Some previous work has considered lateral variability in paleosol-based proxies, such as Kraus (1999) and Hyland and Sheldon (2016), which focused on quantifying sedimentological and geochemical variability in paleosols at km-scale, respectively. Kraus' work in the 1980s and 1990s pushed forward the concept of pedofacies and soils' spatial relationships with basin-wide sedimentological processes (Bown and Kraus 1987, Kraus 1997, Kraus 1999). Hyland and Sheldon (2016) found that geochemical variability across a 1 km single-paleosol transect of the Wasatch Fm. was relatively low and proxies were reliable. Similarly, Stiles et al. (2001) found no lateral variability within a single pedon for their Fe nodule-based MAP reconstruction. Driese and Ashley (2016) sampled four paleosols with <1 km of each other and found geochemical consistency. More work exists constraining the variability of paleosol types and environmental variability within a basin in a tectonic/sedimentological context (see Tabor and Myers, 2015). Tabor et al. (2006) examined general paleosol variability (not a single paleosol transect) across 15 km in the Ischigualasto-Villa Union basin in Argentina, where they found uneven paleosol distributions and thicknesses derived from geomorphic heterogeneity, as well as variability in the pedogenic carbonates' oxygen isotope values. Rosenau et al. (2013a,b) observed basin-scale variability in paleosol type, linked primarily to the degree of marine influence. Thus, while a number of studies have examined lateral paleosol variability as a first step toward considering local environmental variability. Here we identify an opportunity for proxy improvement by explicitly quantifying how lateral variability translates to certainty or uncertainty in proxy reconstructions.

Additional efforts for improving the treatment of uncertainty have included developing proxies based on individual soil orders and soil functional types, which is critical because different soils have distinct chemical traits/processes (e.g., Sheldon, 2006; Nordt and Driese, 2010; Gallagher and Sheldon 2013). Several researchers have focused on modifying the statistical treatment of proxies (e.g., Breecker, 2013; Stinchcomb et al., 2016; Lukens et al., 2019). For pedogenic carbonate-based proxies, understanding what part of the year a proxy represents has been shown to be critical for accurate interpretation of carbon and oxygen isotopes (Passey et al., 2010; Gallagher and Sheldon, 2016; Gallagher et al., 2019; Kelson et al., 2020) and different workers have also improved the interpretation of carbonate isotope geochemistry by using both inorganic and organic isotopes (Tabor et al., 2013; Tabor et al, 2017; Sheldon, 2018). Constraining lateral geochemical variability in paleosols provides essential background

information for each of those techniques and the methods discussed in this work could easily be applied to other approaches (e.g., C isotopes in organic matter, pedogenic carbonate) and likely has implications for the taphonomy of phytoliths as well (e.g., Hyland 2014).

The presence of pedogenic carbonates, whether authigenic or diagenetic, can strongly influence many paleosol-based proxies, to the point that some proxies define acceptable levels of carbonate (e.g., Sheldon et al., 2002; Nordt and Driese, 2010; Michel et al., 2016). Authigenic pedogenic carbonate is linked to precipitation and soil saturation, with proxies such as depth to Bk horizon relying on that relationship (Jenny, 1941; Retallack, 2005). Secondary or diagenetic carbonate, which does not reflect original soil formation conditions, can therefore skew paleosol proxy results (e.g., Retallack 1991; Michel et al., in review). Treatment of samples, either in sample preparation or processing/analysis, can also affect Ca concentrations and therefore impact proxy-based reconstructions (Michel et al., in review). For example, with the CIA-K precipitation proxy, an anomalously high Ca concentration leads to an underestimation of precipitation; the accidental removal of authigenic carbonate through non-conservative pre-treatment (such as 20% H_2O_2), on the other hand, would lead to overestimating precipitation (Michel et al., in review). Therefore, paleosol Ca content merits careful consideration, particularly in the context of spatial variability and the representativeness of any given paleosol profile.

By quantifying baseline geochemical heterogeneity and testing the robustness of select paleosol-based proxies at basin scales, ideally at multiple sites in a range of environments and soil orders, we can improve our understanding of km-scale processes in paleosols, make our proxies more statistically robust, and ultimately strengthen certainty in basin-wide paleoclimate and paleoenvironment reconstructions. Basins with good exposure and relatively flat-lying, continuous terrestrial strata are ideal testing grounds for the effects outcrop extent have on proxy uncertainty. Here, we examine the lateral variability of two Eocene paleosol transects and make a first attempt at quantifying the magnitude of uncertainty associated with km-scale outcrop resampling.

5.3 Field site and geologic context

With its flat-lying deposits, ample exposures, and high-resolution age constraints, the Eocene Green River Basin in SW Wyoming, USA (Figure 1) has been the subject of many

paleoclimate and paleoenvironmental studies, including some previous work on lateral geochemical variability (e.g., Hyland and Sheldon, 2016). These strata record a lacustrine to fluvial floodplain environment during a relatively warm and wet period and span the early Eocene climatic optimum (EECO; Braunagel and Stanley, 1977; Clyde et al., 1997; Clyde et al., 2001; Smith et al., 2008). The basin received sediment inputs from the proximal Wind River Range during the Eocene (Chetel and Carroll, 2010; Hyland and Sheldon, 2013) and is relatively well-dated due to stratigraphic correlation to dated tuffs, paleomagnetic records, and land mammal stratigraphy (Clyde et al., 2001; Smith et al., 2008). The floodplain deposits outside of paleo-Lake Gosiute are represented in part by the Eocene Wasatch Formation. These laterally-extensive outcrops are striking red, orange, yellow, and purple stripes on the tan-to-white backdrop of lacustrine deposits and stretch across basins, making them ideal targets for testing lateral heterogeneity and constraining statistical uncertainty in proxies.

Within the Wasatch Fm. of Wyoming, we focus on two sites of approximately the same age: previously sampled paleo-Alfisols of Honeycomb Buttes (HB; 42.237 °N, 108.533 °W, as reported), the site of Hyland and Sheldon (2016)'s work, and the new site presented here, Jack Morrow Hills (JMH), which is characterized by paleo-Inceptisols. The two sites are ca. 35 km apart (Figure 5.1). The JMH transect is within the Main Body of the Wasatch Fm. and is overlain by the Tipton Member of the Green River Fm. (Sutherland and Luhr, 2011). The excellent exposures at JMH and HB are thanks in part to their position within the uplifted and incised northern extent of the Laramide-age Rock Springs Uplift (Mederos et al., 2005). Physically, they differ primarily in apparent redox condition: while Honeycomb Buttes is dominated by red-orange paleosols (oxidized), the JMH transect quickly transitioned from red-orange to dominantly purple (reduced) paleosols with grey, green, and yellow reduction mottles. Because of this difference, comparing the resampling results between the two sites is informative of broad soil conditions (i.e., not limited to either reduced or oxic paleosol or to a single soil order).

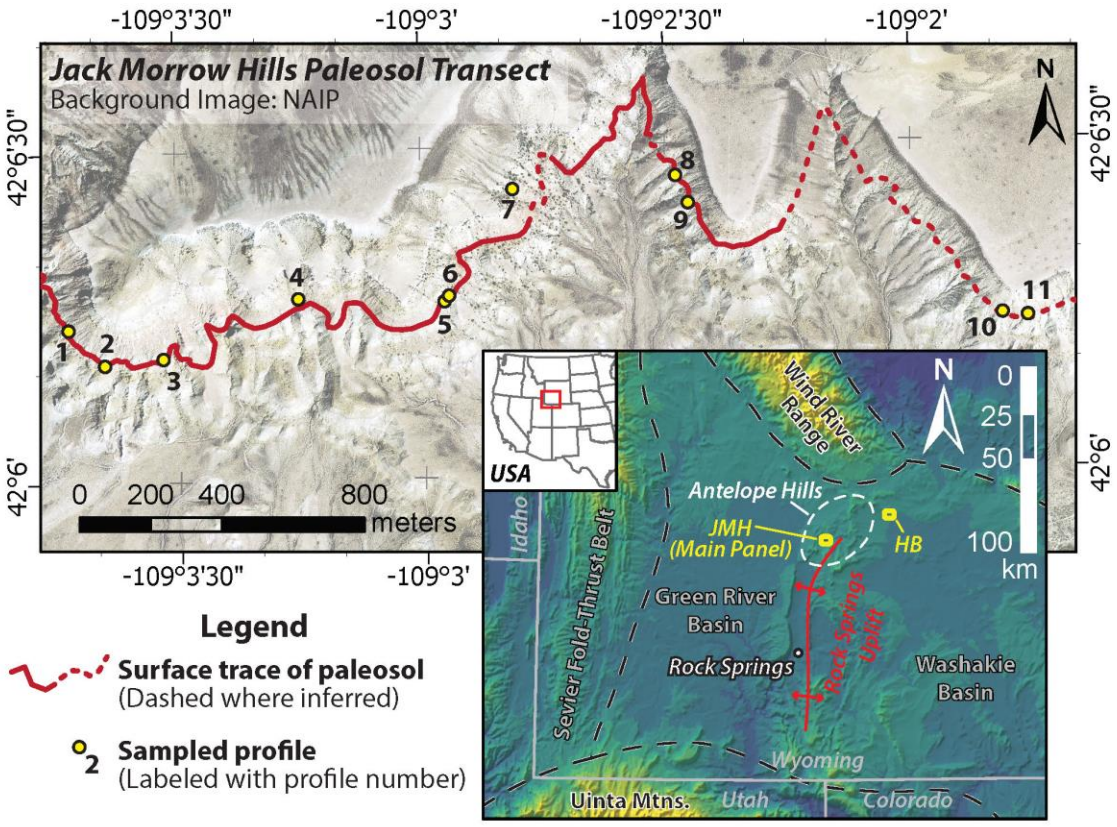

Figure 5.1 Map of Jack Morrow Hills sampling

Map of sampling locations. JMH=Jack Morrow Hills (new paleosols in this work), HB=Honeycomb Buttes (Hyland and Sheldon, 2016). Lower panel shows regional geography, with the two sampling sites marked in yellow nearby the Rock Springs Uplift (red lines). Top panel shows the JMH paleosol transect; yellow dots mark sampled paleosol profiles. Dashed red line indicates inferred trace due to access limitation (e.g., too steep or too vegetated to reach).

5.4 Methods

Access and sampling

The Jack Morrow Hills (JMH) transect (42.104 °N, 109.055 °W; ca. 2225 m) is located in Sweetwater County, WY, north of Jack Morrow Creek in the broader Antelope Hills area (Figure 5.1). It is federal land managed by the BLM. It was accessed off of Hwy 28 between Farson and South Pass City, via county roads 21 and 83.

A lateral transect of a continuous paleosol was followed over 2.9 km, identified by its stratigraphic position above interspersed thick channel deposits and as part of a two-paleosol

couplet (Figure 5.2). Within the transect, ten profiles were sampled, and one profile was sampled from an overlying paleosol (red star in Figure 5.3; Paleosol 7 in Figure 5.4). At each profile, trenches (at least ca. 20 cm deep) were dug until fresh rock, unaffected by modern surface processes, was reached. Modern vegetation and roots were avoided during sampling. Within each profile, samples were taken to represent each color or horizon change, and multiple samples within most B horizons to ensure intra-horizon replicability of results. One stretch of the transect (2–3 km) had steep slopes and more vegetation, so we were unable to sample the paleosol at the ca. 2.5 km mark. After ~3 km, the paleosol couplet became less distinct and the butte was more eroded, effectively limiting the transect length to ca. 3 km. Sample locations and descriptions are found in Table D1.

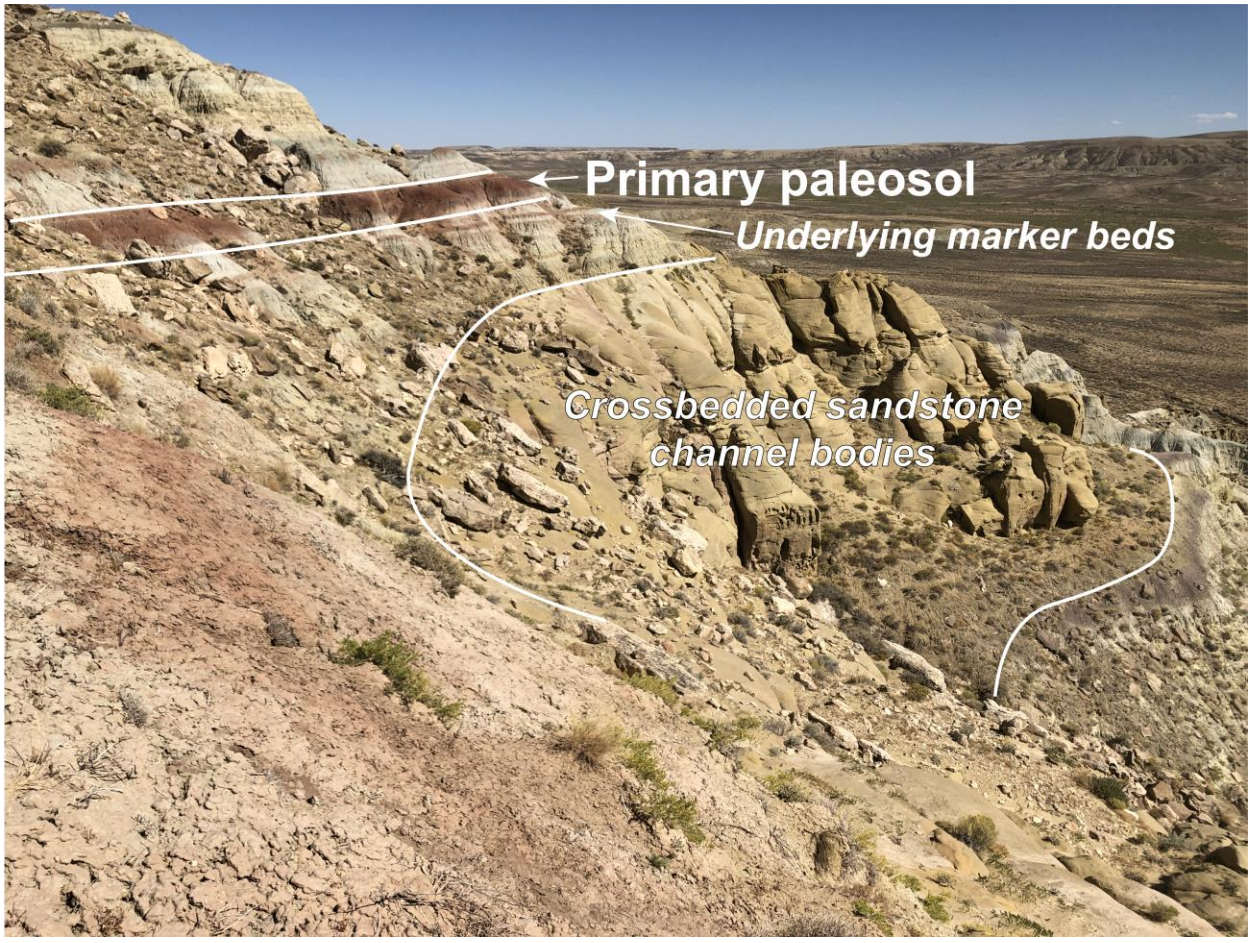

Figure 5.2 Side view of JMH outcrop

Full JMH section in profile, with massive fluvial sandstone underlying stacked paleosol successions. The distinctive paired dark-red paleosols were present for nearly 3 km, despite a transition from red to purple dominant hue. Channel sandstones were intermittently present at the same relative stratigraphic level.

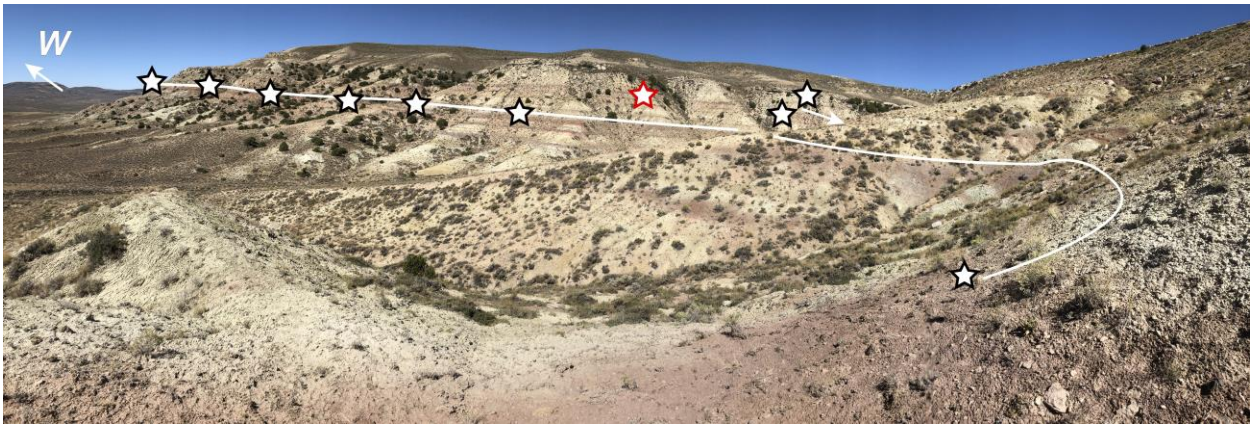

Figure 5.3 Overview of JMH sampling transect

JMH site overview, with sampling locations marked by stars. Red star indicates a profile (#7) accidentally sampled from overlying paleosol.

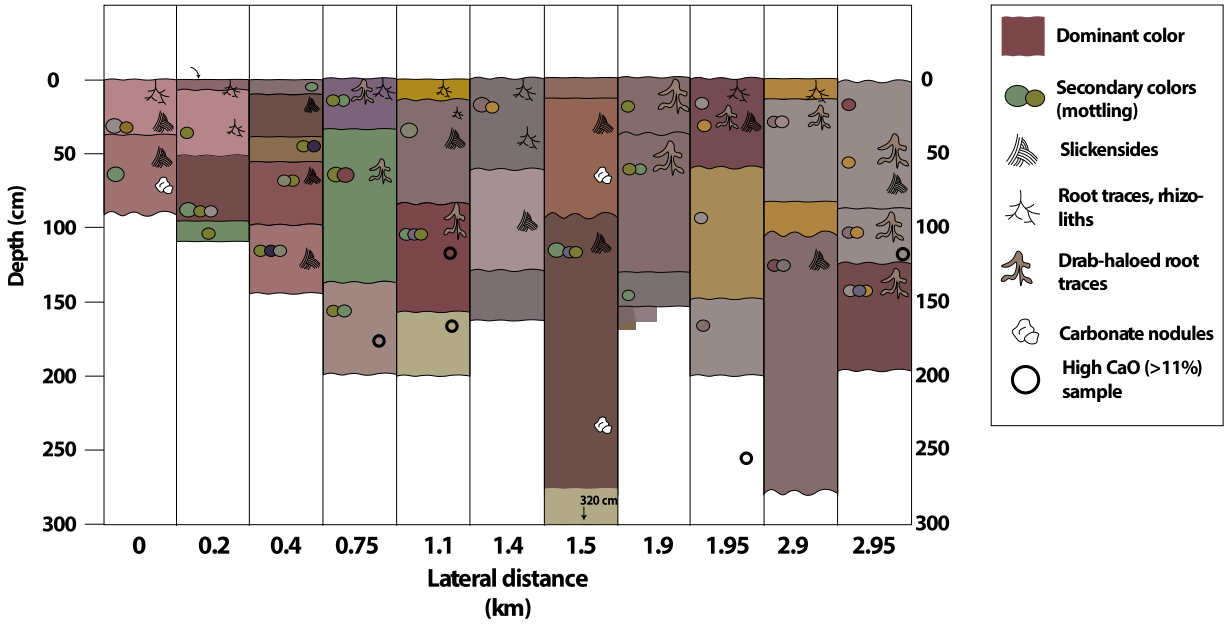

Figure 5.4 JMH paleosol profiles

Cartoon of each JMH paleosol profile, from W to E (left to right). A general shift from oxic to reducing conditions is apparent based on paleosol color, as well as an increase in profile thickness. Along with a decrease in channel sandstones on the eastern end of the transect, this

change could reflect more distal, ponded conditions. Carbonates and rootlets were sparse across the transect, with slickensides as the most common pedogenic feature.

Sample preparation and analysis

Samples were crushed in a Shatterbox, dried at room temperature, and ground to <2 μm. Samples were not acidified in order to preserve Ca content. Bulk geochemistry was performed at ALS Minerals in Vancouver, BC via conservative four-acid digestion and ICP-MS analysis. Instrument error is <0.01% for major elements. Bulk geochemical data are reported in Table D2; extended CaO data are in Table D3.

Proxies

To test paleoclimate reconstructions, we used the Chemical Index of Alteration minus potash (CIA-K; Harnois, 1988; Maynard, 1992)-derived mean annual precipitation (MAP) proxy (Sheldon et al., 2002; Sheldon and Tabor, 2009). CIA-K is calculated on a molar basis following Eq. 1, and MAP from CIA-K in Eq. 2. The error for CIA-K-based MAP, ±182 mm yr^{-1}, is the standard error of the regression from Sheldon et al. (2002).

CIA-K equation $Al_2O_3/(Al_2O_3 + CaO + Na_2O)$ [Eq. 1]

MAP equation $MAP = 221e^{0.0197(CIA\text{-}K)}$, ±182 mm yr^{-1} [Eq. 2]

To test our resampled uncertainty on an unrelated paleosol, we also included in our statistical analysis a previously-sampled ~1.5 km Vertisol paleocatena from Kenya (Kisaaka; reported as ca. 0.84 °S, 34.15 °E, ca. 1170 m) which, with only 4 profiles' bulk geochemistry available over that distance but robust intra-paleosol sampling, provides a good point of comparison (Beverly et al., 2015, 2017). Because that transect contained Vertisols, we used the CALMAG MAP proxy, which was calibrated on and intended for application on Vertisols (Nordt and Driese, 2010). CALMAG is similar to other Al/base cation ratios but includes CaO and MgO, as the two cations with the strongest correlations with MAP (Nordt and Driese 2010) rather than Na_2O and CaO (e.g., CIA-K). While some users have treated the CIA-K and CALMAG proxies as interchangeable, CALMAG would be inappropriate for quantitative use

with JMH and HB paleosols (Inceptisols/Alfisols). Instead, we use a comparison between proxies to consider the role of paleosol taxonomy in increasing or decreasing reconstruction uncertainty.

$$CALMAG = Al_2O_3 / (Al_2O_3 + CaO + MgO) \times 100 \quad \text{[Eq. 3]}$$

$$MAP_{CM} = 22.69 \times CALMAG - 435.8, \text{ RMSE} = \pm 108 \text{ mm yr}^{-1} \quad \text{[Eq. 4]}$$

Additionally, we checked two mean annual air temperature (MAAT) proxies (SAL, PWI) for lateral continuity (Figure D1) (Retallack, 1991; Sheldon et al., 2002; Gallagher and Sheldon, 2013). To test for intra- and inter-paleosol geochemical variability, MAP and MAAT proxies were explored both within single profiles and across the transect.

$$PWI = [(4.20 \times Na) + (1.66 \times Mg) + (5.54 \times K) + (2.05 \times Ca)] \times 100 \quad \text{[Eq. 5]}$$

$$MAAT_{PWI} = -2.74 \ln(PWI) + 21.39, \text{ SE of regression} = \pm 2.1\ ^\circ C \quad \text{[Eq. 6]}$$

$$SAL = (K_2O + Na_2O) / Al_2O_3 \quad \text{[Eq. 7]}$$

$$MAAT_{SAL} = -18.5 \times SAL + 17.3, \text{ SE of regression} = \pm 4.4\ ^\circ C \quad \text{[Eq. 8]}$$

Holdridge life zones provide a semi-quantitative means of matching climate with vegetation and provide the underpinnings for other modern approaches to soil energy models (Holdridge, 1947; Lugo et al., 1999). Mean annual precipitation and the ratio of estimated evapotranspiration to MAP (ET/MAP) are plotted on a ternary diagram, with classes (as defined by the International Institute for Applied Systems Analysis) overlaid based on modern vegetation maps. For paleosols, paleo-ET is estimated based on the difference between reconstructed MAP and soil effective precipitation (P_{eff}) (Rasmussen et al., 2005; Rasmussen and Tabor, 2007; Gulbranson et al., 2011). In modern environments, P_{eff} is a linear function of MAP and ET (Gulbranson et al. 2011). This empirically-derived relationship can be used to estimate P_{eff} values for a MAT range of 10–13°C using Equations 9, 10 (Gulbranson et al. 2011):

$$P_{eff} = 0.924(MAP) - 19.221 \quad \text{[Eq. 9]}$$

and related to ET through Equation 10 (Gulbranson et al., 2011):

$$ET = MAP_{CIA\text{-}K} - P_{eff} \quad \text{[Eq. 10]}$$

Data for Holdridge calculations can be found in Table D4.

Statistical analysis

To demonstrate how the number of profiles sampled can affect paleoclimate reconstruction uncertainty, average MAP values from primarily North American B horizons (which are used for paleoclimate reconstruction due to their longer formation times) were calculated from random subsamples of all profiles from each paleosol horizon. For JMH (profile n=11), the 11 profiles were subsampled in 11 rounds that each used an increasing number of randomly selected profiles, starting with a single profile and ending with all 11 profiles. Each round of subsampling consisted of 10,000 trials, during each of which the average MAP values from the 1-11 randomly selected profiles were recorded. Each of the 10,000 mean values were then nudged by a normally-distributed random value based on standard error of the proxy regression, originally 182 mm yr^{-1} (Sheldon et al., 2002; Prochnow et al., 2006). Because the original reported error is the standard error of the regression, which is approximately similar to 2σ, we nudged the resampled mean by ±91 mm yr^{-1}. Deviation from the mean, as 95% confidence intervals, were also calculated to represent the convergence towards $\mu+2\sigma$. The final result of each round of subsampling was a distribution of 10,000 mean MAP values that could result from only using the number of profiles (1-11) prescribed in that round of subsampling and accounting for the proxy error. At HB (profile n = 10), resampling used permutations of 1-10 randomly selected profiles, and at Kisaaka paleosol (profile n = 4), permutations of 1-4 profiles.

All 11 profiles were included in the JMH resampling regardless of geochemistry or stratigraphic location, to most accurately reflect the possibility of mis-sampling during fieldwork. Resampling tests were repeated with (a) all B-horizon samples, (b) only samples with <5% CaO (Prochnow et al., 2006; Sheldon and Tabor, 2009), and (c) only samples with <11% CaO, a threshold determined by the distribution of CaO in modern Inceptisols as described below. The resampling with samples <5% CaO, as the most conservative proxy, are in main text

figures; others are presented in the supplement for comparison. No HB samples fell outside the 5% CaO threshold, so no repeat resampling tests were necessary for those profiles. We also resampled data from the 4 profiles from the Kisaaka paleosols, with a nudge of 108 mm yr^{-1}, the original RMSE. No Kisaaka samples fell outside the 10% CaO limit for CALMAG to be considered applicable.

First, to quantify a baseline for soil CaO concentrations, we used the USGS database of modern soil geochemistry, including A and C horizons and the top 5 cm of the soil, across a range of soil orders (Smith et al., 2014; n = 4857). For B horizons, which were not included in the USGS database, we used the Marbut (1935) dataset (n = 46), a dataset our lab compiled for previous work (Dzombak and Sheldon, 2020; n = 195), and the Vertisol transect used to calibrate CALMAG (Nordt and Driese, 2010). Soil orders included in this Ca analysis are Andisols, Alfisols, Aridisols, Gelisols, Histosols, Inceptisols, Oxisols, Mollisols, Spodosols, Vertisols, and Ultisols, though the resulting dataset is dominated by Mollisols (n=60), Ultisols (n=57), Aridisols (n=55), Alfisols (n=44), and Vertisols (n=42). For all horizons, CaO data are log-normally distributed, with long right tails (Figure D2, D3). Based on the USGS data, CaO values in the 95th percentile in Top 5 cm/A horizons are about 8.5%, and in C horizons around 14.5% (Table D3). For B horizons, the 95th percentile in all soil orders' CaO was 17% CaO (n = 325). The 95th percentile of CaO for modern Inceptisols only (the designation of JMH paleosols) and B horizons only (used for paleoclimate reconstructions) is 11% (Table D3). Both 5% and 11% were used as thresholds for Ca screening at JMH and HB. To improve Ca screening in paleosols, future work should constrain modern Ca distributions more robustly for each soil order. (This could also improve geochemical paleosol designations.)

Code for subsampling is available in the supplemental materials online at DOI: 10.17632/kpdngx4m2f.1.

5.5 Results

Paleosol description

Complete descriptive features for each horizon are found in Table D1. Profiles were typically between 1–2 m thick with a B and C horizon; A horizons were typically truncated or present as A/AB transitions, denoted primarily by textural changes (e.g., sandy vs. silty/clayey) accompanied by the presence of root traces (Figure 5.4). Root traces were sparsely present, and

slickensides were pervasive throughout (Figure 5.5d). Only two profiles (Paleosols 1 and 7) yielded pedogenic carbonate nodules (Figure 5.5e), despite several other profiles having anomalously high Ca concentrations in certain samples (white circles in Figure 5.4). Hydromorphic features (e.g., drab-haloed root traces and redoximorphic mottling) were consistently present across the transect. Based on the degree of horizon development but lack of other diagnostic features, the paleosols were identified as paleo-Inceptisols, some with Vertic features (i.e., slickensides). They are designated as paleo-Inceptisols rather than -Alfisols or -Vertisols because no other Vertic features were present and B horizons were not clay-rich enough to qualify as Bt horizons. Paleosol profiles for the complete transect are depicted in Figure 5.5.4. From west to east, the paleosol thickened and changed dominant color scheme, and the interspersed large channel bodies became smaller and sparser.

One profile was mistakenly sampled in the overlying paleosol (Paleosol 7; red star in Figure 5.3), but yielded similar geochemical results, providing a temporal/vertical point of comparison.

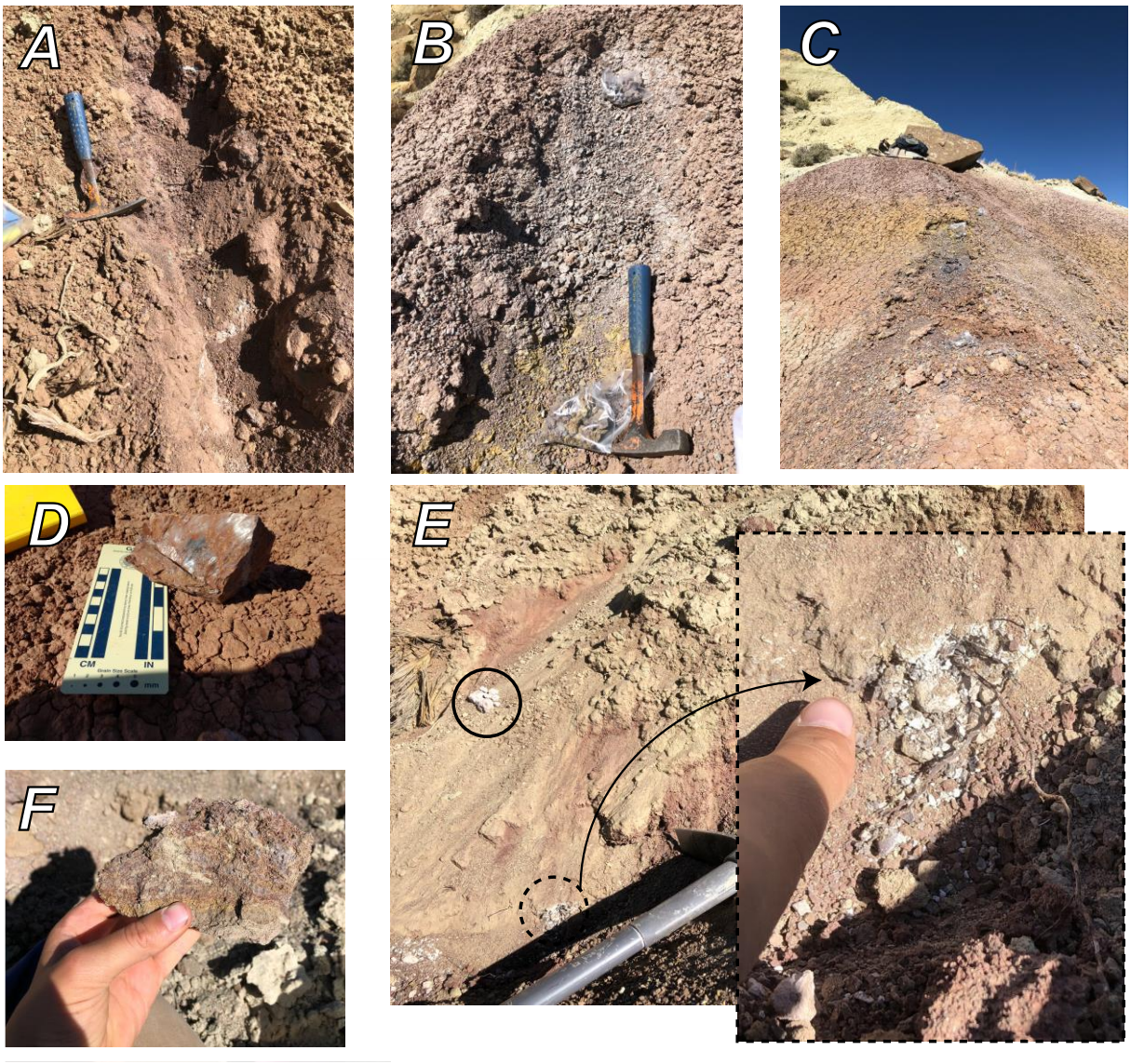

Figure 5.5 Paleosol detail photos.

(A) Trench of oxic paleosol on western end of transect; hammer for scale. (B) Trench of transitional, purple-dominant paleosol; hammer for scale. (C) Trench of far eastern paleosol, with purple, red, and mottled yellow horizons present; backpack and field shovel at top of ridge for scale. (D) Slickenside on paleosol ped. (E) Examples of carbonates, with collected nodules marked with the black circle. Dashed circle and zoomed-in dashed rectangle show modern roots using paleo-carbonate as nutrient hotspot. Because nodules were in float rather than in place, and in-situ carbonate was influenced by modern roots, analyses of carbonates were not possible for this transect. (F) Hand sample of mottled paleosol.

Physical and geochemical variability

Across the transect, the primary physical change in the paleosol was a shift from dark red to purple as the dominant color, with reduction mottling and drab-haloed root traces increasing as the paleosol became dominantly purple/grey eastward (Figure 5.5.4). The JMH transect had more color variability than the transect at HB. The sediment distribution also gained some silt in the easternmost samples, but we did not see sandy channels directly interfingered with this particular paleosol at our sampling sites.

Overall, paleosol geochemistry for most elements within paleoclimate proxies (Al, Na, K) was consistent across the transect, despite apparent shifts in redox conditions (color change; Table D2). Redox-sensitive elements (Fe, Cr, Mn) generally showed consistency across the transect, despite a shift from red-orange to purple-dominant claystone (Figure D4). Down-profile trends in Ti/Al (Figure D5b) reflect steady, minimal detrital input during soil formation, and down-profile trends in CIA-K (Figure D5a) reflect typical within-profile weathering patterns (e.g., Sheldon and Tabor, 2009).

However, CaO concentrations did vary notably in several profiles (Paleosols 4, 5, 9, 11 in Figure 5.5.4), despite the absence of obvious sources like pedogenic carbonate nodules or grain coatings. Because these high CaO values directly affected proxy reconstructions, we tested how excluding CaO values above different thresholds would affect the MAP reconstructions for individual profiles (and in resampling, see below). For JMH samples, 10 B-horizon samples exceeded the 5% threshold, and 3 B-horizon samples exceeded the 11% threshold. For HB samples, no B-horizon samples exceeded the 5% CaO threshold. In JMH B horizons, CaO correlates significantly with Mn, but less strongly with Fe and Cr (Figure D6).

Proxy variability

Across the transect, MAP and the other indices were bimodally distributed about the mean, with one cluster of values around the mean and another, lower cluster present in paleosols with high Ca values (*e.g.*, Paleosol 4; Figure 5.6). Reconstructed MAP values from JMH B horizons averaged 1038 ± 182 mm yr^{-1} with high-CaO samples and 1185 ± 182 mm yr^{-1} excluding high-CaO samples. The magnitude of the increase in mean MAP value is within the standard error of the proxy, making it statistically insignificant. However, the individual MAP values of the high-CaO samples are significantly lower than the mean, with the 5% and 11% threshold samples resulting in reconstructed MAP values from 300–500 mm yr^{-1}. This range is

statistically significantly different from the overall mean; additionally, such MAP values would represent a different terrestrial biome that is not supported by other paleoclimate and paleoenvironmental work in this region.

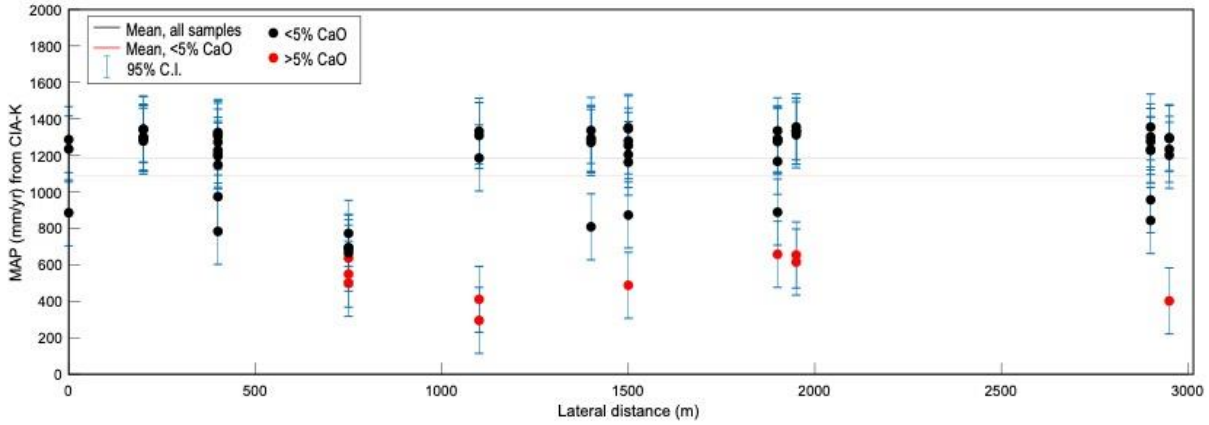

Figure 5.6 Reconstructed MAP across the transect

Lateral variability in MAP reconstructed from CIA-K. Each dot is one B-horizon sample. Black dots are under the 5% CaO threshold, red dots exceed 5% CaO. The error bars are 95% confidence intervals, based on CIA-K regression error. The solid black horizontal line is the average MAP including only samples with CaO <5%; the red horizontal line is the mean including all samples. Excluding samples >5% CaO results in a higher overall average MAP.

For the JMH transect, MAAT reconstructions from B-horizon PWI and SAL averaged 12.7 ± 2.1 and 11.7 ± 4.4 °C, respectively. (Including samples from all horizons lowers those values to 12.6 and 11.5 °C, respectively; the change is within each proxy's error but still demonstrates the effect including the incorrect horizons has on the proxies.) These temperatures are lower than MAATs derived from leaf-margin analysis of several penecontemporaneous Green River Basin early Eocene localities (>20 °C, Wilf, 2000; Fricke and Wing, 2004; Hyland et al., 2018; see *Discussion*).

Within Holdridge life zone space, each paleosol profile plotted in the wet forest biome with the exception of Paleosol 4, which plotted as a wet tundra (Figure D7). For comparison, the nearby HB also plotted as wet forest. We plotted the modern southwestern Wyoming climate as a check, and it fell appropriately within the dry scrub biome.

The Kisaaka paleosol had moderate geochemical variability, with two of the four profiles' reconstructed MAP ranges and standard deviations being larger than the others (Figure

D8). As with the JMH paleosols, CaO content is the primary driver of variability across that transect.

Resampling and statistical constraints

Our random resampling showed that the distribution of MAP reconstructions narrows as more profiles are added to the sampling, with the final iteration (all profiles and samples included) effectively representing the standard error of the distribution about the mean (Figure 5.7). At JMH, deviations from the mean (Figure 5.7b) show diminishing improvement in MAP variance after more than 4–5 profiles are included, as well as asymmetry in the distribution of resulting MAP values for small numbers of included profiles. These results were repeated in the HB transect, which lacked samples with exceptionally high CaO (Figure D9). Resampling the JMH profiles with samples exceeding the 5% CaO threshold resulted in a similar result (Figure D10). There was no discernible difference between the 5% and 11% threshold resampling, as only three samples exceeded the 11% CaO threshold. Resampling for the Kisaaka paleosol, with four profiles but no clear outlier as at JMH, had muted results in a similar pattern, with uncertainty decreasing after two profiles (Figure D11).

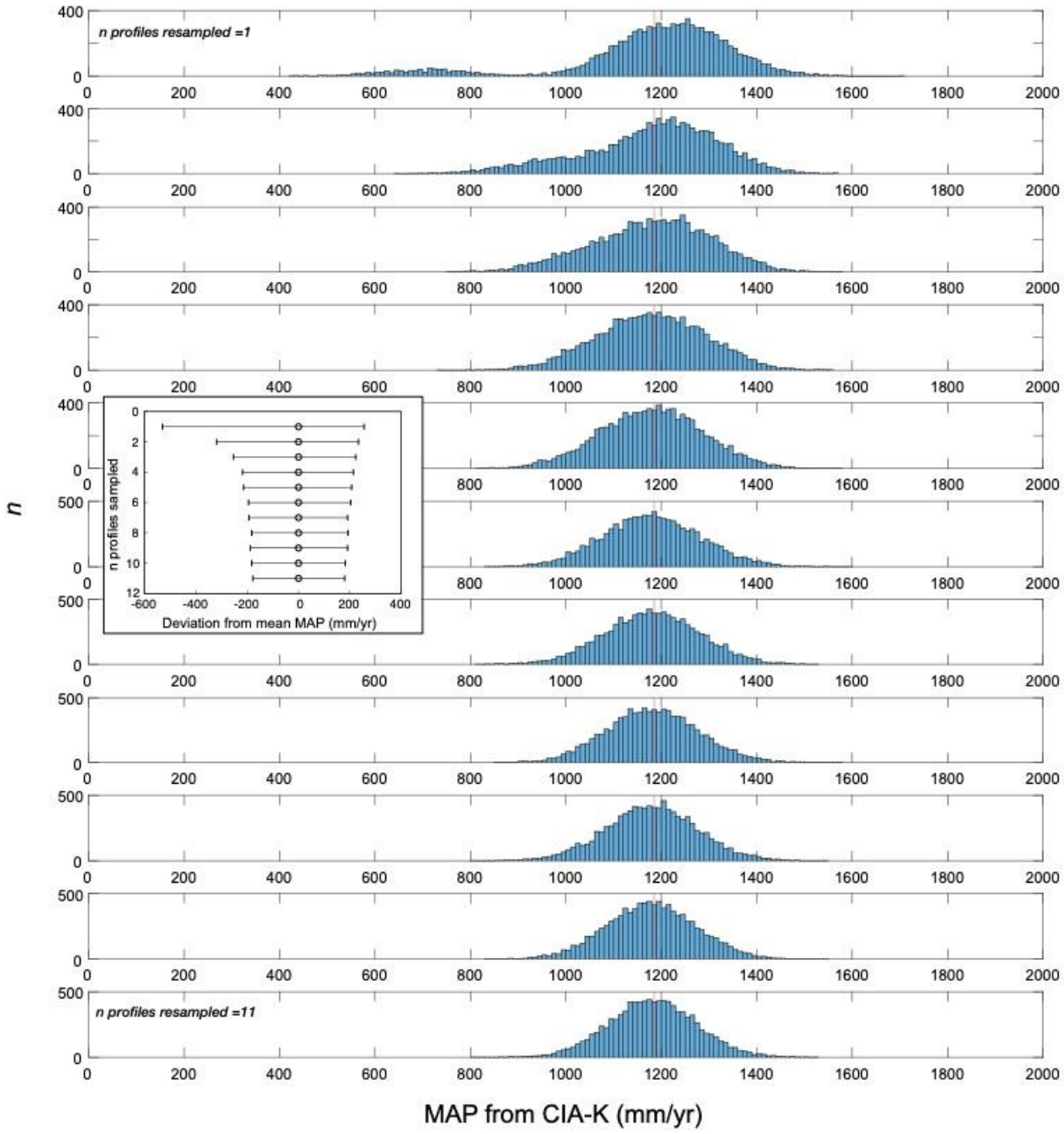

Figure 5.7 Resampling MAP results from JMH.

Resampling results for JMH transect (B horizons with CaO <5%). From top to bottom, the number of profiles included in the resample increases by one (i.e., top panel resamples one profile, bottom panel resamples all 11 profiles). The vertical red line is the average MAP from the dataset. All panels show results from 10,000 trials. The bottom panel effectively represents the mean ± standard error of the regression. (Inset panel) From top to bottom, the deviation from the average MAP value for 1 to 11 profiles resampled, demonstrating how results become more certain with more profiles sampled.

5.6 Discussion

Ecosystem and climate reconstruction

Overall, our climatological results agree with proxies from approximately the same geologic time and place. Paleosol-based MAP reconstructions of 1185 ± 182 mm yr^{-1} are comparable to physiognomic reconstructions of the Green River Basin (1160 ± 58 mm yr^{-1}; Wing and Greenwood, 1993), though Wilf et al. (1998) revised this value to be lower, around 840 mm yr^{-1}. MAP and MAAT results are also consistent with penecontemporaneous results from nearby Honeycomb Buttes (~1100 mm yr^{-1}, ~11 °C) (Hyland and Sheldon, 2016). However, later reconstructions of the Honeycomb Buttes paleosols based on clumped isotope analyses place 11 °C as representative of transitional seasons (e.g., MAM, OND), while the average air temperature from PPM1.0 was higher at 15.2 °C ± 1.3 °C (1σ; Hyland et al. 2018). Recent researchers have found that pedogenic carbonates accumulated in B-horizons of soils are not recording mean annual temperature, and instead are seasonally biased (Passey et al., 2010; Quade et al., 2013; Gallagher and Sheldon, 2016; Gallagher et al., 2019; Kelson et al. 2020); it would be reasonable to expect that other B horizon processes (e.g., weathering) could be subject to similar seasonal effects.

The proximity to sandy channels, color hues, and presence of hydromorphic soil features (mottling, drab-haloed root traces; lack of carbonate nodules) suggests a frequently wet floodplain environment for these paleo-Inceptisols, with some wet/dry cycles indicated by the presence of slickensides. The Holdridge life-zone designation of wet forest is reasonable in this context, as well as with the proxy-based paleoclimate reconstructions. (The 'wet tundra' designation for Paleosol 4 is driven by high CaO and should not be considered robust.) Ecosystem results based on our data align with findings from nearby ecosystems (e.g., Hyland et al., 2013; Hyland et al., 2018; Stein et al., in prep/review). Paleobotanical evidence from the proximal (in space and time) Bridger Formation includes trees, understory and climbing ferns consistent with subtropical forest conditions (Allen 2017a,b). Paleocene Eocene Thermal Maximum (PETM) and early Eocene climatic optimum estimates from the Bighorn Basin to the northeast plot as wet forest conditions (Wing et al., 2005; Wing and Currano, 2013), as do early Eocene estimates from the Bridger Formation (e.g., Blue Rim, WY; Allen, 2017a,b; Stein et al., in review). Although southwest Wyoming today is a cold, dry-scrub/desert, the early Eocene was

equable and latitudes as far north as British Columbia have fossil evidence that supports the presence of subtropical species (Greenwood et al., 2005; Smith et al., 2009), so it is reasonable that the area would have been warm, wet, and forested at the time.

Geochemical variability, Ca effect, and proxies

The primary source of geochemical variability in the JMH transect was Ca, with high-CaO samples decreasing the MAP reconstruction for its paleosol profile (Figure D12). Otherwise, geochemistry and proxies were relatively consistent, similar to previous work on a shorter (1 km) transect (Hyland and Sheldon 2016). Because the three studies analyzed several different proxies, had different redox regimes, were different maturity levels, and differed in the degree of CaO variability, it is noteworthy that overall heterogeneity in proxies was low in the transects. New intra-horizon sampling presented here also reflects low heterogeneity. That variations in color do not necessarily reflect statistically significant variations in geochemistry or proxy values is a key and encouraging result.

With Ca being a main source of variability in North American soils (which encompass a wide range of climatic and environmental settings; Figure D12), screening for Ca prior to reconstructions is critical. In modern soils, the distribution of B horizon geochemistry suggests that most soils have <5% CaO (Table D4; Figure D2). If a paleosol exceeds that value, care should be taken to check for diagenesis or other secondary alteration. A site with paleosols exceeding the CaO threshold would be a good situation to consider using relative rather than quantitative change. Because most proxies (except CALMAG, which has an upper threshold of 10% CaO; Nordt and Driese 2010) were developed on noncalcareous or weakly calcareous parent materials, future work should develop more proxies for carbonate-parented non-Vertic soils.

Profiles in different redox regimes yield similar paleoclimate results, suggesting that while redox variation indicates small-scale hydrology, paleoclimate results remain robust. One redox-indicator trace element, Mn (e.g., Driese and Sim, 1995), correlates strongly to CaO content in B horizons ($r^2 = 0.95$, $p < 0.001$, n = 90; Figure D6a). Mn was more variable in the JMH transect than in either the HB or Kisaaka transects. Other redox indicators explored (Fe, Cr) had less linear negative correlations with CaO (Figure D6b,c; $r^2 = 0.21$, $p < 0.001$ and $r^2 = 0.48$, $p < 0.001$, n = 90 for both). The strong correlation between Mn and CaO could be indicative of

Ca– Mn replacement in dispersed carbonates or exchangeable clays during periods in which the paleosol was waterlogged and the redox regime became strongly reducing. The suggested Mn–Ca relationship could be a fruitful path of investigation in future work, and given long-standing interest in paleosol Fe (e.g., Sheldon et al., 2021) and Cr (e.g., Colwyn et al., 2019) as redox indicators in geologic history, the weaker relationships identified here may also be worth further investigation.

Time and weathering intensity are two soil-forming factors which are important to consider. As a soil evolves from an immature or weakly-weathered stage (i.e., Entisol/Inceptisol) to a more mature or intensely-weathered stage (i.e., Alfisol, Ultisol), there could be a systemic change in geochemical variability. By applying a random resampling analysis to transects with Inceptisols, Alfisols, and Vertisols, respectively, we demonstrate that this basic principle of outcrop extent-based sampling uncertainty applies to a variety of soil orders and maturity levels. Future research could improve on this work by resampling in an expanded range of soil orders, as well as more varied environments; JMH and HB effectively represent the same wet forested biome, and the Kisaaka paleosol formed in a tropical savanna (Beverly et al., 2015, 2017). Future work could also explore more explicitly the effect of time or paleosol maturity (i.e., from Entisol to Ultisol), as well as vegetative cover type (e.g., grasslands/paleo-Mollisols), on tendencies for geochemical heterogeneity and proxy uncertainty.

The resampling results highlight the benefits of including more profiles from a single horizon, including increased confidence that sampled profiles are in fact representative of the entire horizon, as well as decreased uncertainty in the absolute proxy outputs. Increasing the number of profiles included narrows the resulting distribution of possible MAP values, but with diminishing impact after 4–5 profiles (Figure 5.7b). The distribution begins to converge around 4–5 profiles for our JMH site, with limited ‘return on investment’ of including more profiles beyond that point (Figure 5.7b). Similarly, HB begins to converge at 3–4 profiles sampled because it has less geochemical variability (Figure D9). The Kisaaka paleosol is more difficult to compare at 1.5 km with 4 profiles, but it still shows the decrease in uncertainty at 3 profiles (Figure D11). Practically as well as logically, then, sampling at least three profiles for a transect of any extent is a robust baseline practice. Beyond that point, the number of profiles that should be sampled scales with extent and the apparent degree of variability.

Paleosols as stratigraphic markers

Kraus and colleagues identified early on paleosols' strengths and shortcomings as recorders of environment and placemarkers in basin-wide stratigraphy. Considering spatial (horizontal) as well as temporal (vertical) distribution variability in paleosols is important to be able to best use paleosols in interpreting basin-scale changes in hydrology and environment, as well as using them as relative markers. Relying on a paleosol designation from a single profile, or from multiple profiles closely grouped together within a basin, for basin-wide or regional correlation should be done carefully, given that — as with modern soils — relatively small changes in topography, biosphere, and hydrology can affect both the type of paleosol and whether or not it would be preserved at all. It is common for a basin to have multiple pedotypes present, with their particular distribution dependent in part on basin-wide fluvial processes (e.g., Kraus, 1999; Tabor et al., 2006; Hamer et al., 2007; Rosenau et al., 2013a,b; Weissmann et al., 2013).

Many paleosol studies effectively examine vertical/temporal variability when looking at paleosol sequences through time, but it is imperative to understand the geochemical variability *within* a paleosol—both internally and laterally—so we can know if the temporal changes are within error, essentially, of the lateral distribution, or if the observed/reconstructed changes are larger and therefore significant, representing meaningful, actual change in climate or environment. Additionally, interpreting a paleosol accurately depends on understanding its paleotopographic context, which can only be done through examining its lateral extent (Adams et al., 2011). More broadly, to most accurately interpret a paleosol, its position in a basin-wide context should be known (e.g., proximal, distal, different inputs; Kraus, 1987; Bown and Kraus, 1987; Kraus, 1999), and the preservation bias for flat or low-lying floodplains should be considered.

Paleosols are useful chemostratigraphic indicators because of their distinctive weathering patterns that become particularly evident in stacked paleosol successions (Kraus 1999). By tracking vertical/temporal changes in multiple geochemical proxies/weathering indices (e.g., CIA, isotopic changes, provenance indicators), such successions have been used to track global shifts in climate on a basin-wide scale (e.g., Sheldon and Retallack 2004; Baczynski et al., 2013; Hyland et al., 2017). These relative changes in weathering should be consistent throughout the

basin if similar paleosols/pedotypes are compared (i.e., similar pedofacies and order), but correlations could fail if the basin has tectonic/sedimentary regimes that are substantially different at one end from the other. Like other climate-change tools, chemostratigraphic tools are best used in conjunction with other dating and relative stratigraphic markers.

Under-sampling a paleosol weakens its physiochemical description (making it harder to correlate across larger scales) and limits certainty of paleoclimate/paleoenvironmental proxies. The contributions in this work towards improving paleoclimate proxy uncertainty primarily improve paleosols' use as chemostratigraphic markers in vertical sections because at basin or larger scales, it is often unlikely that a single paleosol transect would be present uninterrupted. By refining an approach to proxy uncertainty, the chemostratigraphic marker becomes better defined. Sampling fewer profiles in building a chemostratigraphic record minimizes the ability to confidently correlate trends in paleoclimate proxies across regional scales. Sampling fewer profiles in a well-defined transect could also lead to erroneous interpretations of climatic or environmental change when the observed variability is, in fact, due to synchronous variability. Redox variability in the physical appearance of paleosols in the JMH transect serves as an example of this.

Implications for uncertainty and analyses

Because both JMH and HB had relatively consistent geochemistry and a clear climate signal, our findings support the use of paleosol-based proxies—with the important caveat that sampling multiple profiles affects reconstruction uncertainty. Sampling a single paleosol profile, even with multiple samples per horizon within that profile, does not provide sufficient information on how representative of the whole paleosol extent, let alone the landscape-scale, that profile might be. Our resampling exercise demonstrates that without considering the uncertainty associated with outcrop limitations, paleosol-based reconstructions are falsely precise, perhaps leading to overinterpretation of individual outcrops or in the context of time-series changes (i.e., climate change). It is particularly important to consider as many sources of uncertainty/variability as possible when taking reconstructions a step further (e.g., to paleoaltimetry), as any unaccounted-for uncertainty could compound in the next level of work.

Based on our results, paleosol reconstructions that do not incorporate outcrop-based uncertainty may have over-interpreted the significance of apparent climate change based on

paleosol geochemical proxies. That is, without quantifying the true lateral variability of an outcrop, we cannot definitively say whether there has been significant temporal change unless it greatly exceeds the proxy calibration error. By increasing the lateral and/or vertical sampling coverage, we can address this uncertainty. It could also be prudent to think in terms of relative, rather than absolute/quantitative, changes for outcrops with limited extent, both in terms of magnitude and climate/environment. This more conservative approach still allows interpreting large-scale climate and environmental shifts that we're interested in and that could be linked to broader/global trends, as is currently the case with global chemostratigraphic correlations in carbon cycle disturbances/the C isotope record (Sahy et al., 2015; Cotton et al., 2015; Gallagher et al., 2019). Relative changes in weathering in paleosol successions have been used (e.g., Sheldon et al., 2012; Hyland et al., 2013), but this is not common practice. At the least, relative changes should be considered along with quantitative changes, and in the context of both proxy- and outcrop-based uncertainties. For profiles and outcrops with limited lateral sampling opportunities (and therefore lower confidence in their representativeness), we encourage placing more weight on relative changes than absolute values.

Finally, we note that paleosols' lateral geochemical variability could influence local taphonomy. For example, mesoscale topographic changes can influence plant growth, water ponding, and redox state, which together can influence preservation likelihood (e.g., Demko et al., 1998; Trueman 1999; Behrensmeyer et al. 2000; Gastaldo and Demko 2010). Little work has been done on paleosol geochemical variability and taphonomy, and what potential biases this introduces into terrestrial paleobotanical/palynological records (e.g., Hyland 2014) or to studies that seek to "fingerprint" fossil remains by comparing their chemistry to the paleosol chemistry (e.g., Metzger et al., 2004). This area merits further investigation.

Implications for fieldwork

Outcrop limitations are the foremost constraint on paleosol fieldwork. A single, small outcrop is statistically not that informative unless coupled with other nearby outcrops; this may limit the number of sites where we can do paleosol-based reconstructions, but it is necessary to acknowledge this fundamental constraint. Rather than being prescriptive, this resampling exercise generally demonstrates the uncertainty inherent in using a single paleosol profile to represent a landscape rather than a lateral outcrop. Practically, there is no set number of paleosol

profiles that should be sampled per some given distance. At a minimum, three paleosol profiles should be sampled for basic repeatability testing, ideally with multiple samples from within each horizon to constrain any internal variability (i.e., Ca hotspots). Beyond that, the number of profiles to sample essentially scales with extent and degree of apparent variability. An additional 'best practice' is to report outcrop lateral extents (in addition to profiles' vertical thickness), along with the variability in their exposure quality and features.

When determining how many profiles to sample either vertically or laterally, it is crucial to consider the needs and limitations of the relevant scientific questions. Defining a transition from a forest to a desert over a 5 my record requires a lower-resolution record than capturing a smaller-magnitude shift in climate. The latter case, then, also calls for a better description of the uncertainty in paleoclimate proxies than in the former. Nuanced changes in climate (e.g., a change in MAP of 200 mm yr^{-1}) is more defensible with robust sampling that allows a well-defined range of uncertainty. Quantitative proxy changes that far exceed calibration errors can be confidently interpreted as change; when the change is smaller in magnitude, a more conservative interpretation may be more appropriate.

5.7 Conclusions

The primary conclusion from this work is that sampling strategy affects the uncertainty on paleosol-based proxies, and that uncertainty should be taken into account both when planning sampling/fieldwork and analyzing paleoclimate reconstruction data. In general, as we constrain different types of uncertainty around paleosol-based proxies that are currently underestimated or not accounted for, we should be more conservative in interpreting paleoclimate reconstructions as absolute. Relying solely on calibration-based fixed standard error underestimates the true uncertainty of the reconstructed value; until these other sources of error are incorporated into reconstructions, we recommend analyzing relative changes, particularly for shorter timescale or higher-resolution datasets with relatively few profiles sampled.

This study lays the groundwork for improving the statistical uncertainty on paleosol-based proxies that stems from lateral variability and the hurdles to reliably scaling single outcrop-based reconstructions to basin-wide and regional scales. Carrying out more multiple km-scale transect analyses, such as the work presented here, would improve our understanding of these uncertainty effects in a range of environments and soil orders. Ideally, the community will

work towards having multiple such transects from single large basins, like the Green River Basin, that record critical transition periods in Earth's history. Including varied data (e.g., regular and clumped isotopes, phytoliths, mineralogical indicators such as Goethite/Hematite) could improve understanding of how different terrestrial biogeochemical processes are linked at landscape scales, and how their different preservation biases could affect our interpretation of their records. Finally, carrying out these statistical analyses in a variety of soil orders and environments would make landscape-scale paleoclimate and paleoenvironmental reconstructions more robust.

Acknowledgements

This work funded by NSF Award #1812949 to N. Sheldon and others. Thanks to B. Gallina and S.M. Vogel for assistance with sample preparation and Munsell color identification in the lab.

References

1. Adams JS, Kraus MJ, Wing SL. Evaluating the use of weathering indices for determining mean annual precipitation in the ancient stratigraphic record. Palaeogeography, Palaeoclimatology, Palaeoecology 309 (2011), pp. 358-366.

2. Allen SE. Reconstructing the local vegetation and seasonality of the Lower Eocene Blue Rim site of southwestern Wyoming using fossil wood. International Journal of Plant Sciences 178 (2017a), pp. 689-714.

3. Allen SE. The Uppermost Lower Eocene Blue Rim Flora from the Bridger Formation of Southwestern Wyoming: Floristic Composition, Paleoclimate, and Paleoecology. Doctoral Dissertation, University of Florida. 2017b.

4. Baczynski AA, McInerney FA, Wing SL, Kraus MJ, Block JI, Boyer DM, Secord R, Morse PE, Fricke HC. Chemostratigraphic implications of spatial variation in the Paleocene-Eocene Thermal Maximum carbon isotope excursion, SE Bighorn Basin, Wyoming. Geochem., Geophys., Geosys. 14 (2013), pp. 4133-4152.

5. Behrensmeyer AK, Kidwell SM, Gastaldo RA. Taphonomy and paleobiology. Paleobiology 26 (2000), pp. 103-147.

6. Beverly EJ, Driese SG, Peppe DJ, Arellano LN, Blegen N, Faith JT, Tryon CA. Reconstruction of a semi-arid late Pleistocene paleocatena from the Lake Victoria region, Kenya. Quaternary Research 84 (2015), pp. 368-381.

7. Beverly EJ, Peppe DJ, Driese SG, Blegen N, Faith JT, Tryon CA, Stinchcomb GJ. Reconstruction of late Pleistocene paleoenvironments using bulk geochemistry of paleosols from the Lake Victoria region. Frontiers in Earth Science (2017), pp. 368-381.

8. Bown TM, Kraus MJ. Integration of channel and floodplain suites. I. Developmental sequence and lateral relations of alluvial paleosols. J. Sediment. Petrol. 57 (1987), pp. 587–601

9. Brantley SL, Goldhaber MB, Ragnarsdottir KV. Crossing disciplines and scales to understand the critical zone. Elements 3 (2007), pp. 307-314.

10. Braunagel LH and Stanley KO. Origin of variegated redbeds in the Cathedral Bluffs tongue of the Wasatch Formation (Eocene), Wyoming. J. Sed. Res. 47 (1977), pp. 1201-1219.

11. Breecker DO. Quantifying and understanding the uncertainty of atmospheric CO_2 concentrations determined from calcic paleosols. Geochem., Geophys., Geosys. 14 (2013), pp. 3210-3220.

12. Cerling TE. The stable isotopic composition of modern soil carbonate and its relationship to climate. Earth and Planetary Science Letters 71 (1984), pp. 229-240.

13. Chetel LM and Carroll AR. Terminal infill of Eocene Lake Gosiute, Wyoming, U.S.A. J. Sed. Res. 80 (2010), pp. 492-514.

14. Clyde W C, Sheldon ND, Koch PL, Gunnell GF, Bartels WS. Linking the Wasatchian/Bridgerian boundary to the Cenozoic Global Climate Optimum: new magnetostratigraphic and isotopic results from South Pass, Wyoming. Palaeogeography, Palaeoclimatology, Palaeoecology, 167 (2001), pp. 175-199.

15. Clyde WC, Zonnevold JP, Stamatakos J, Gunnel GF, Bartels WS. Magnetostratigraphy across the Wasatchian/Bridgerian NALMA boundary (Early to Middle Eocene) in the Western Green River Basin, Wyoming. J. Geology 105 (1997), pp. 657-669.

16. Colwyn DA, Sheldon ND, Maynard JB, Gaines R, Hofmann A, Wang X, Gueguen B, Asael D, Reinhard CT, Planavsky NJ. A paleosol record of the evolution of Cr redox cycling and evidence for an increase in atmospheric oxygen during the Neoproterozoic. Geobiology 17 (2019), pp. 579-593.

17. Cotton JM, Sheldon ND, Hren MT, Gallagher TM. Positive feedback drives carbon release from soils to atmosphere during Paleocene/Eocene warming. Am. J. Sci. 315 (2015), pp. 337-361.

18. Demko TM, Dubiel RF, Parrish JT. 1998. Plant taphonomy in incised valleys: Implications for interesting paleoclimate from fossil plants. Geology 26(12), pp. 1119-

1122.

19. Driese SG and Ashley GM. Paleoenvironmental reconstruction of a paleosol catena, the Zinj archaeological level, Olduvai Gorge, Tanzania. Quaternary Research 85 (2016), pp. 133-146.

20. Driese SG and Sim EL. Redoximorphic paleosols in alluvial and lacustrine deposits, 1.8Ga Lochness Formation, Mount Isa, Australia: Pedogenic processes and implications for paleoclimate. J. Sed. Res. 65A (1995), pp. 675-689.

21. Dzombak RM and Sheldon ND. Weathering intensity and presence of vegetation are key controls on soil phosphorus concentrations: Implications for past and future terrestrial ecosystems. Soil Systems 4 (2020), 73. doi:10.3390/soilsystems4040073

22. Fedo CM, Nesbitt HW, Young GM. Unraveling the effects of potassium metasomatism in sedimentary rocks and paleosols, with implications for paleoweathering conditions and provenance. Geology 23 (1995), pp. 921–924.

23. Fricke HC, Wing SL. Oxygen isotope and paleobotanical estimates of temperature and $\delta^{18}O$–latitude gradients over North America during the early Eocene. American Journal of Science 304 (2004), pp. 612-635.

24. Gallagher TM and Sheldon ND. Combining soil water balance and clumped isotopes to understand the nature and timing of pedogenic carbonate formation. Chemical geology 435 (2016), pp. 79-91.

25. Gallagher TM, Cacciatore CG, Breecker DO. Interpreting the difference in magnitudes of PETM carbon isotope excursions in paleosol carbonate and organic matter: Oxidation of methane in soils versus elevated soil respiration rates. Palaeoceanography and Paleoclimatology 34 (2019), pp. 2113-2128.

26. Gallagher TM, Hren M, Sheldon ND. The effect of soil temperature seasonality on climate reconstructions from paleosols. Am. J. Sci. 319 (2019), pp. 549-581.

27. Gallagher TM, Sheldon ND. A new paleothermometer for forest paleosols and its implications for Cenozoic climate. Geology 41 (2013), pp. 647–650.

28. Gastaldo RA and Demko TM. The relationship between continental landscape evolution and the plant-fossil record: Long term hydrologic controls on preservation. Chapter in: Taphonomy, pp 249-285. Aims & Scope Topics in Geobiology Book Series, Volume 32. Springer. 2010.

29. Greenwood DR, Archibald SB, Matthews RW, Moss PT. Fossil biotas from the Okanagan Highlands, southern British Columbia and northeastern Washington State: climates and ecosystems across an Eocene landscape. Canadian Journal of Earth

Sciences 42 (2005), pp. 167-185.

30. Gulbranson EL, Montanez IP, Tabor NJ, A proxy for humidity and floral province form paleosols: The Journal of Geology 119 (2011), pp. 559-573.

31. Hamer JMM, Sheldon NH, Nichols GJ, Collinson ME. Late Oligocene-Early Miocene paleosols of distal fluvial systems, Ebro Basin, Spain. Palaeo3 247 (2007), pp. 220-235.

32. Harnois 1988 CIW (CIA-K) The CIW Index: A new chemical index of weathering. Sed. Geo. 55 (1988), pp. 319-322.

33. Holdridge, L.R. Determinations of world plant formations from simple climatic data. Science 105 (1947), pp. 367-368.

34. Hyland EG and Sheldon ND. Examining the spatial consistency of palaeosol proxies: Implications for palaeoclimatic and palaeoenvironmental reconstructions in terrestrial sedimentary basins. Sedimentology 63 (2016), pp. 959-971.

35. Hyland EG, Huntington KW, Sheldon ND, Reichgelt T. Temperature seasonality in the North American continental interior during the Early Eocene Climatic Optimum. Clim. Past. 14 (2018), pp. 1391-1404.

36. Hyland EG, Sheldon ND, Cotton JM. Constraining the early Eocene climatic optimum: A terrestrial interhemispheric comparison. GSA Bulletin 129 (2017), pp. 244-252.

37. Hyland EG. Phytoliths as tracers of recent environmental change. *Chapter in* Experimental Approaches to Understanding fossil organisms, pp. 207-225. Springer, UK. 2014.

38. Hyland, E. G., & Sheldon, N. D. Coupled CO_2-climate response during the early Eocene climatic optimum. Palaeogeography, Palaeoclimatology, Palaeoecology 369 (2013), pp. 125-135.

39. Jenny HJ. Factors in Soil Formation; McGraw-Hill: New York, NY, USA, 1941.

40. Kelson JR, Huntington KW, Breecker DO, Burgener LK, Gallagher TM, Hoke GD, Petersen SV. A proxy for all seasons? A synthesis of clumped isotope data from Holocene soil carbonates. Quat. Sci. Rev. 234 (2020), 106259.

41. Kraus, MJ. Integration of channel and floodplain suites, II. Vertical relations of alluvial paleosols. J. Sed. Petrology 57 (1987), pp. 602-612.

42. Kraus MJ. 1997. Lower Eocene alluvial paleosols: pedogenic development, stratigraphic relationships, and paleosol-landscape association. Palaeogeography, Palaeoclimatology, Palaeoecology 129 (1997), pp. 387–406.

43. Kraus MJ. Paleosols in clastic sedimentary rocks: their geologic applications. Earth Sci. Rev. 47 (1999), pp. 41–70.

44. Lugo AE, Brown SL, Dodson R, Smith TS, Shugart HH. The Holdridge life zones of the conterminous United States in relation to ecosystem mapping. J. Biogeography, 26 (1999), pp. 1025-1038.

45. Lukens WE, Stinchcomb GE, Nordt LC, Kahle DJ, Driese SG, Tubbs JD. Recursive partitioning improves paleosol proxies for rainfall. Am. J. Sci. 319 (2019), pp. 819-845.

46. Mack GH, James WC, Monger HC. Classification of paleosols. Geol. Soc. Am. Bull. 105, (1993), pp. 129–136.

47. Marbut, C. F. 1935. Atlas of American agriculture. III. Soils of the United States. Washington, D.C., Government Printing Office.

48. Maynard JB. Chemistry of Modern Soils as a Guide to Interpreting Precambrian Paleosols. J. Geol. 100 (1992), pp. 279–289.

49. Mederos S, Tikoss B, Bankey V. Geometry, timing, and continuity of the Rock Springs uplift, Wyoming, and Douglas Creek arch, Colorado: Implications for uplift mechanisms in the Rocky Mountain foreland, U.S.A. Rocky Mountain Geology 40 (2005), pp. 167-191.

50. Metzger CA, Terry, Jr. DO, Grandstaff DE. Effect of paleosol formation on rare earth element signatures in fossil bone. Geology 32 (2004), pp. 497-500.

51. Michel LA, Tabor NJ, Montanez, IP. Paleosol diagenesis and its deep-time paleoenvironmental implications, Pennsylvanian-Permian Lodève Basin, France. J. Sed. Res. 86 (2016), pp. 813-829.

52. Michel, L.A., Sheldon, N.D., Myers, T.S., Tabor, N.J., (in review), Assessment of pretreatment methods on CIA-K and CALMAG indices and the effects on paleoprecipitation estimates. Palaeogeography, Palaeoclimatology, Palaeoecology.

53. Nordt LC and Driese SG. Application of the critical zone concept to the deep-time sedimentary record. The Sedimentary Record 11 (2014), 4-9.

54. Nordt LC, Driese SD. 2010. New weathering index improves paleorainfall estimates from Vertisols. Geology 38 (2010), pp. 407–410.

55. Passey BH, Levin NE, Cerling TE, Brown FH, Eiler JM. High-temperature environments of human evolution in East Africa based on bond ordering in paleosol carbonates. Proc. Nat. Acad. Sci. 107 (2010), pp. 11245–11249.

56. Prochnow SJ, Nordt LC, Atchley SC, Hudec MR. 2006. Multi-proxy paleosol evidence for middle and late Triassic cliamte trends in eastern Utah. Palaeo3, 232(1), pp.53-72.

57. Quade J, Eiler J, Daeron M, Achyuthan H. The clumped isotope geothermometer in soil and paleosol carbonate. Geochim. Et Cosmochim. Acta 105 (2013), pp.92-107.

58. Rasmussen C, Southard RJ, Horwath WR. Modeling energy inputs to predict pedogenic environments using regional environmental databases. Soil Science Society of America Journal 69 (2005), pp. 1266-1274.

59. Rasmussen C. and Tabor N.J. Applying a quantitative pedogenic energy model across a range of environmental gradients: Soil Science Society of America Journal 71 (2007), pp. 1719-1729.

60. Retallack GJ. Pedogenic carbonate proxies for amount and seasonality of precipitation in paleosols. Geology 33 (2005), pp. 333-336.

61. Retallack GJ. Soils of the Past. Blackwell, Oxford. 2001. 600pp.

62. Retallack GJ. Untangling the effects of burial alteration and ancient soil formation. Ann. Rev. Earth Planet. Sci. 19 (1991), pp. 183-206.

63. Rosenau NA, Tabor NJ, Elrick SD, Nelson WJ. Polygenetic history of paleosols in Middle-Upper Pennsylvanian cyclothems of the Illinois Basin, USA. Part I: Characterization of paleosol types and interpretations of pedogenic processes. J. Sediment. Res. 83 (2013a), pp. 606–636.

64. Rosenau NA, Tabor NJ, Elrick SD, Nelson WJ. Polygenetic history of paleosols in Middle-Upper Pennsylvanian cyclothems of the Illinois Basin, USA. Part II: The impacts of geomorphology, climate, and glacioeustasy. J. Sediment. Res. 83 (2013b), pp. 637–668.

65. Rye R and Holland H. Paleosols and the evolution of atmospheric oxygen: A critical review. Am. J. Sci. 298 (1998), pp.621-672.

66. Sahy D, Condon DJ, Terry Jr. DO, Fischer AU, Kuiper KF. Synchronizing terrestrial and marine records of environmental change across the Eocene-Oligocene transition. Earth and Plan. Sci. Letters 427 (2015), pp. 171-182.

67. Sheldon ND and Retallack GJ. Regional Paleoprecipitation records from the Lake Eocene and Oligocene of North America. J. Geol. 112 (2004), pp. 487-494.

68. Sheldon ND, Mitchell RL, Dzombak RM. Reconstructing Precambrian pCO_2 and pO_2 using paleosols. Cambridge University Press, Cambridge, UK. (2021)

69. Sheldon ND, Retallack GJ, Tanaka S. Geochemical climofunctions from North American soils and application to paleosols across the Eocene-Oligocene boundary in Oregon. J. Geol. 110 (2002), pp. 687–696.

70. Sheldon ND, Tabor NJ. Quantitative paleoclimatic and paleoenvironmental reconstruction using paleosols. Earth Sci. Rev. 95 (2009), pp. 1–52.

71. Sheldon ND. Quaternary glacial-interglacial climate cycles in Hawaii. J. Geol. 114 (2006), pp. 367–376.

72. Sheldon ND, Costa E, Cabrera L, Garcés M. Continental climatic and weathering response to the Eocene-Oligocene transition. J. Geol. 120 (2012), pp. 227-236.

73. Sheldon ND. Using carbonate isotope equilibrium to screen pedogenic carbonate oxygen isotopes: Implications for paleoaltimetry and paleotectonic studies. Geofluids (2018), Article ID 5975801.

74. Smith DB Cannon WF, Woodruff LG, Solano F, Ellefsen KJ. Geochemical and Mineralogical Maps for Soils of the Conterminous United States; U.S. Geological Survey Open-File Report; United States Geological Survey: Denver, CO, USA, 2014; 386p, ISSN 2331-1258.

75. Smith ME, Carroll AR, Singer BS. Syoptic reconstruction of a major ancient lake system: Eocene Green River Formation, western United States. GSA Bulletin 120 (2008), pp. 54-84.

76. Smith RY, Basinger JF, Greenwood DR. Depositional setting, fossil flora, ad paleoenvironment of the Early Eocene Falkland site, Okanagan Highlands, British Columbia. Canadian J. Earth Sci. 46 (2009), pp. 811-822.

77. Stein RA, Sheldon ND, Dzombak RM, Smith ME, Allen SE. A Comprehensive Approach to Climate & Ecology in the Eocene Rocky Mountain Interior. Accepted, Climate of the Past.

78. Stiles CA, Mora CI, Driese SG. Pedogenic iron-manganese nodules in Vertisols: a new proxy for paleoprecipitation? Geology 29 (2001), pp. 943–946.

79. Stinchcomb GE, Nordt LC, Driese SG, Lukens WE, Williamson FC, Tubbs JD. A data-driven spline model designed to predict paleoclimate using paleosol geochemistry. Am. J. Sci. 316 (2016), pp. 746–777.

80. Sutherland WM and Luhr SC. (2011) Preliminary bedrock geologic map of the Farson 30' x 60' quadrangle, Sweetwater, Sublette and Fremont Counties, Wyoming. Wyoming State Geological Survey. 1:100,000. Accessible online at https://ngmdb.usgs.gov/Prodesc/proddesc_95798.htm

81. Tabor NJ, Montanez IP, Kelso KA, Currie B, Shipman T, Colombi C. A Late Triassic soil catena: landscape and climate controls on paleosol morphology and chemistry across the Carnian-age Ischigualasto-Villa Union basin, northwestern Argentina. Geol. Soc. Am. Spec. Pap. 416 (2006), pp. 17–41.

82. Tabor NJ, Myers TS. Paleosols as indicators of paleoenvironment and paleoclimate. Ann. Rev. Earth and Planetary Sci. 43 (2015), pp. 333-361.

83. Trueman CN. Rare earth element geochemistry and taphonomy of terrestrial vertebrate assemblages. Palaios 14 (1999), pp. 555-568.

84. Weissmann GS, Hartley AJ, Scuderi LA, Nichols GJ, Davidson, SK, Own A, Atchley SC, Bhattacharyya P, Chakraborty T, Ghosh P, Nordt LC, Michel L, Tabor NJ. Prograding distributive fluvial systems–geomorphic models and ancient examples. *Chapter in* New Frontiers in Paleoped. And Terrestrial Paleoclimatology (2013), pp. 131-147. Tulsa, OK, USA.

85. Wilf P, Wing SL, Greenwood DR, Greenwood CL. Using fossil leaves as paleoprecipitation indicators: an Eocene example. Geology 26 (1998), pp. 203-206.

86. Wilf P. Late Paleocene–early Eocene climate changes in southwestern Wyoming: Paleobotanical analysis. Geological Society of America Bulletin 112 (2000), pp. 292-307.

87. Wing SL, Currano ED. Plant response to a global greenhouse event 56 million years ago. American Journal of Botany 100 (2013), pp. 1234-1254.

88. Wing SL, Harrington GJ, Smith FA, Bloch JI, Boyer DM, Freeman KH. Transient floral change and rapid global warming at the Paleocene-Eocene boundary. Science 310 (2005), pp. 993-996.

89. Wing SL, Greenwood DR. Fossils and fossil climate: the case for equable continental interiors in the Eocene. Philosophical Transactions of the Royal Society of London. Series B: Biological Sciences 341 (1993), pp. 243-252.

Chapter 6
Conclusions and Future Work

6.1 Modern soils improve our interpretations of paleosol geochemistry

Across a range of spatial scales, modern soils exhibit highly variable chemical composition in response to factors like climate, vegetation, and parent material. On continental scales—the primary scale of interest for deep-time biogeochemical modeling—environmental and climatic conditions are often poor predictors of soil chemistry. However, a number of key correlations between environmental factors and soil chemistry are still discernable in the modern soil compositions. The presence of rooting vegetation (but not plant functional type) correlates with increased soil weathering intensity. Weathering intensity appears exerts moderate control on the concentration of P in soils, with intensely-weathered soils losing P compared to less-weathered soils. Removal of P from soils during periods of intense weathering has been hypothesized to cause an increase in P flux from continents to oceans, however, well-constrained and high-resolution weathering and P records are needed to test that relationship. (The record here, particularly in the Phanerozoic, is not dense enough to explicitly test temporally-limited weathering perturbations that would likely have supplied short-term nutrient fluxes.)

The geochemical compositions of modern soils across a continent display the full range of possible weathering intensities. Chemical variability within these soils is a natural consequence of variability in parent material, ecosystem, and climate across a continent (the atmospheric composition, at least, is consistent). Interpretations of deep-time weathering records and biogeochemical models are prone to over-generalization of the complex controls on soil chemistry, in part due to a need to simplify models, but more importantly due to a lack of quantitative constraints on many of these important input variables. Building a better understanding of modern soil parameters—including geochemistry, responses to external factors, thickness, etc.—has the potential to significantly improve our ability to interpret the paleosol geochemical record.

Paleosols are likely just as geochemically complex and varied as modern soils, particularly in the Phanerozoic when the rise of land plants effectively established modern

terrestrial ecosystems. To diminish the possibility of biasing results through under-sampling the highly variable paleosol record, studies of paleosols should include multiple profiles, constrain intra-paleosol geochemical variability, and focus on relative changes in proxies as opposed to absolute precipitation or temperature estimates. Biogeochemical models and work interpreting paleosol geochemistry should shift perspective to assume the same degree of variability in paleosol geochemistry as is observed in modern soils. The data presented in this dissertation are examples of the kinds of quantitative paleosol data that emphasizes spatial variability and reflects continental-scale patterns in soil geochemical variability that should serve as the basis for estimates of model input parameters.

6.2 Some major hypothesized changes in terrestrial biogeochemistry and weathering intensity need to be reconsidered

This dissertation addresses two major hypotheses related to terrestrial biogeochemical cycling: that the amount of P retained or lost on land (in soils) has changed through time, and that the degree of continental weathering intensity has changed through time. On long geologic timescales, the records presented here do not support those two hypotheses.

6.2.1 P in soils has not significantly changed through time

The hypothesis that terrestrial P has changed over geologic time has been proposed based on several research contexts, including marine records (e.g., Fe-P burial; changes in marine productivity, with P as an assumed limiting nutrient; e.g., Reinhard et al., 2017), records of crustal geochemical evolution (e.g., Cox et al., 2018), and assumptions about how land plants would have influenced P weathering and mobility (e.g., Lenton and Watson, 2004). However, paleosols reflect remarkably stable P compositions, essentially reflecting the crustal average of P (ca. 0.2%). Relative to the variability in soil P concentrations, the crustal evolution component of P is negligible. Additionally, P enrichment in paleosols (relative to bedrock/parent material) is varied through time, with soils capable of both retaining and losing P present throughout the record. The stability in the P record does not preclude shorter-term perturbations in terrestrial P cycling; such events may not have been captured at the temporal resolution of this record. Additionally, while fungi would likely have altered plant nutrient acquisition, the geochemical signature of that process would have varied between species and so may simply result in noise in

the record. Soil P stability can be interpreted as reflecting a tendency for ecosystems to establish geochemical equilibrium.

That the terrestrial P record is largely stable points to the importance of factors besides weathering intensity and natural P abundance in controlling the flux of P (and possibly other nutrients/elements) from continents to oceans. The total area of subaerially-exposed (and therefore weatherable) land would likely have been a key control on establishing a baseline potential for P fluxes; if only a small continental area were emerged, the total possible P flux would have been small as well. Secondarily, controls on erosion rate (e.g., tectonics, climate) would have modulated those fluxes once the continent was emerged. These relationships also point to the importance of marine nutrient use efficiency and burial for marine productivity and oxygen production, as has been previously suggested (e.g., Reinhard et al., 2017).

6.2.2 Continental weathering intensity has not significantly changed through time

The intensity of continental weathering has been hypothesized to change over time, particularly in relation to the composition of the atmosphere (i.e., pCO_2; Berner, 1998; Lipp et al., 2021), tectonic activity (e.g., Raymo and Ruddiman 1992, Molnar and England 1990), and the evolution of rooting, vascular land plants (e.g., Berner, 1998; Algeo and Scheckler, 1998; Lenton and Watson, 2004; D'Antonio et al., 2020). On long geologic timescales, the paleosol record of weathering does not support discrete state changes in weathering intensity. Rather, the record is consistent through time, with paleosols in the Phanerozoic reflecting the entire range of possible weathering intensities—as seen in modern soils at a continental scale today. As with P, this stability does not preclude perturbations in weathering intensity on shorter timescales or smaller spatial scales, but likely reflects a dynamic equilibrium in weathering and continental and atmospheric processes, with weathering intensity reverting to the mean after a disturbance (e.g., the emplacement of major flood basalts coinciding with a mass extinction; Sheldon, 2006; Schaller et al., 2015) or even after a major evolutionary change like the appearance of land plants. The stability of this weathering intensity record on long timescales again points to other factors (e.g., land area, tectonics) as key drivers of sediment fluxes from continents to oceans.

6.2.3 Land plants did change the C cycle

The Precambrian paleosol weathering record tends to reflect more intense weathering than in the Phanerozoic. This pattern is likely due to a combination of preservation bias (see section 6.3) and a shift in pedogenic process during the Phanerozoic, when rooting plants facilitated the retention of Ca in soils and formation of pedogenic carbonate ($CaCO_3$). As CaO is a major oxide included in weathering indices and tends to be more variable in soils than other index elements (Al, Na, K; Chapter V), Ca variability can drive variability in weathering index values (specifically, higher Ca results in lower CIA and MIA). Therefore, the observed increased range in Phanerozoic weathering index values can be partially attributed to an increase in pedogenic carbonate.

Today, pedogenic carbonate plays an important role in the global C cycle, with soils serving as the largest terrestrial C sink. As land plants evolved, they likely increased landscape stability and may have facilitated the formation and retention of soils, increasing the potential for a soil C sink. As pedogenic carbonate became more abundant and soil CO_2 concentrations rose to exceed the atmosphere, the overall soil C sink would have grown. Rooting and vasculature also allowed plants to colonize drier environments, leading to soils both form and be preserved in areas that may have been less likely to host and preserve soils previously. Rooting plants may have also increased clay mobility, providing greater nutrient fluxes to marine ecosystems while also increasing turbidity, which can negatively affect primary productivity. Therefore, while the rise of land plants certainly affected both terrestrial and marine biogeochemical cycles, it may not have been in the ways that have been commonly hypothesized.

6.3 Biases in the paleosol record need to be better understood before we meaningfully interpret long-term trends

Surviving paleosols in the rock record are not evenly distributed in time. They occur more frequently towards the present, and the record suffers from the same Meso–Neoproterozoic gap that other geologic records (particularly terrestrial) reflect. Peaks in paleosol occurrence coincide with peaks in the zircon record and, in the Phanerozoic, with maximums in global length of passive margins and global rate of basin formation. Together, these trends suggest that paleosols are not forming during all stages of the supercontinent cycle equally in part due to pedogenic formation conditions. For example, if paleosols are biased towards the relatively stable middle period of the supercontinent cycle when basins are forming due to rifting and

previously-uplifted mountains are eroding, collectively those paleosols may look very different from paleosols preserving a later supercontinent stage when sediment inputs from high-relief erosion are lower and continentality-climate effects may be less pronounced. Additionally, the interplay between large continents, the potential for soil formation and preservation, and continent-scale climate (e.g., orographic effects, continentality) mean that although soils could *form* broadly, they may still be biased towards being *preserved* in certain depositional environments (e.g., floodplains). Paleosols may therefore be biased towards representing certain tectonic and depositional environments, a crucial factor that should be considered when interpreting apparent changes in terrestrial settings via paleosols.

Part of the bias in the paleosol record is likely due to preservation or taphonomic bias, which would also skew the record towards representing different depositional environments. Studying the distribution of soil orders and environments (both ecosystems and tectonic settings) from which paleosols are preserved (possibly in the Cenozoic when the record is likely the densest) would help provide the context necessary for interpreting the paleosol record. Sampling bias by geologists also likely contributes to gaps and periods of over-representation, as well as uneven data distribution. Studies using paleosol geochemistry could limit potential biases by including small-scale (e.g., km) transects that capture basin-scale geochemical variability more reliably than relying on individual paleosol profiles.

While the paleosol record in this dissertation is still incomplete, it is the largest compilation of paleosol geochemistry to date. The observed stability in weathering intensity and soil geochemistry in this record provides a baseline for weathering intensity in biogeochemical modeling as well as identifying meaningful trends in paleosol-based geochemical proxies.

6.4 Directions for future work

This dissertation hopefully highlights the need for a collaborative effort by those in the field to create an accessible, comprehensive database of paleosol bulk geochemistry (including major oxides used in many indices as well as minor elements that are biologically relevant, like Mn, Ni). Similar efforts to this point have focused on the marine sediments (e.g., Lipp et al., 2021) or limited to isotope geochemistry over shorter time periods (e.g., Nordt et al., 2016; Paleo-CO_2 Project). Paleosols are less common in the rock record than other terrestrial

sedimentary rocks, but they merit attention because they represent the paleo-critical zone and can provide great insight into the past on Earth's surface.

Modern soil geochemistry should be more heavily relied upon to inform our interpretations of paleosols; as part of that, collaborations with the modern soil science community to quantify continental-scale trends in soils (which would be relevant for interpreting deep-time terrestrial geochemistry) could be fruitful. Additionally, creating modern maps of soil surface age and profile thickness, perhaps in collaboration with the geomorphology community, would provide valuable insight into soil formation and preservation likelihood, which could be used to model 'backwards' and predict the distribution of preservable soils through time. Being able to better assess how 'representative' a paleosol or suite of paleosols from any given time truly are will profoundly improve the accuracy of our interpretations of the paleosol record.

References

1. Algeo, T. J. & Scheckler, S. E. Terrestrial-marine teleconnections in the Devonian: links between the evolution of land plants, weathering processes, and marine anoxic events. *Philos. Trans. R. Soc. London B* **353**, 113–130 (1998).

2. Berner, R. A. The carbon cycle and CO_2 over Phanerozoic time: The role of land plants. *Philos. Trans. R. Soc. B Biol. Sci.* **353**, 75–82 (1998).

3. Cox, G. M., Lyons, T. W., Mitchell, R. N., Hasterok, D. & Gard, M. Linking the rise of atmospheric oxygen to growth in the continental phosphorus inventory. *Earth Planet. Sci. Lett.* **489**, 28–36 (2018).

4. D'Antonio, M. P., Ibarra, D. E. & Boyce, C. K. Land plant evolution decreased, rather than increased, weathering rates. *Geology* **48**, 29–33 (2020).

5. Lenton, T. M. & Watson, A. J. Biotic enhancement of weathering, atmospheric oxygen and carbon dioxide in the Neoproterozoic. *Geophys. Res. Lett.* **31**, (2004).

6. Lipp, A. G. *et al.* The composition and weathering of the continents over geologic time. *Geochemical Perspect. Lett.* **17**, 21–26 (2021).

7. Nordt, L., Tubbs, J. & Dworkin, S. Stable carbon isotope record of terrestrial organic materials for the last 450 Ma yr. *Earth-Science Rev.* **159**, 103–117 (2016).

8. Paleo-CO_2 is an NSF-funded collaboration to create a quality-controlled dataset for Cenozoic pCO_2. Accessible online at https://paleo-co2.org.

9. Reinhard, C. T. *et al*. Evolution of the global phosphorus cycle. *Nature* **541**, 386–389 (2017).

10. Schaller, M. F., Wright, J. D. & Kent, D. V. A 30 Myr record of Late Triassic atmospheric pCO_2 variation reflects a fundamental control of the carbon cycle by changes in continental weathering. *Bull. Geol. Soc. Am.* **127**, 661–671 (2015).

11. Sheldon, N. D. Abrupt chemical weathering increase across the Permian-Triassic boundary. *Palaeogeogr. Palaeoclimatol. Palaeoecol.* **231**, 315–321 (2006).

Appendices

Appendix A

Supplemental Figures for Chapter II

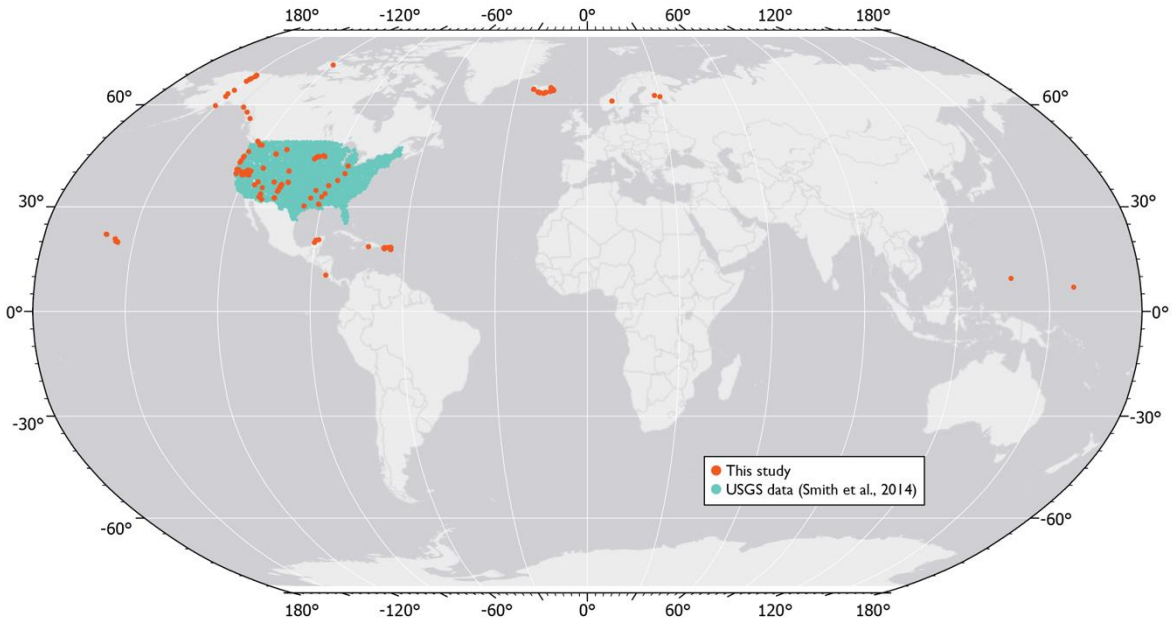

Figure A 1. Map of modern soils in Chapter II.

Map of soils used in this study, with newly-collected and compiled soils in orange and soils collated from the USGS database in turquoise.

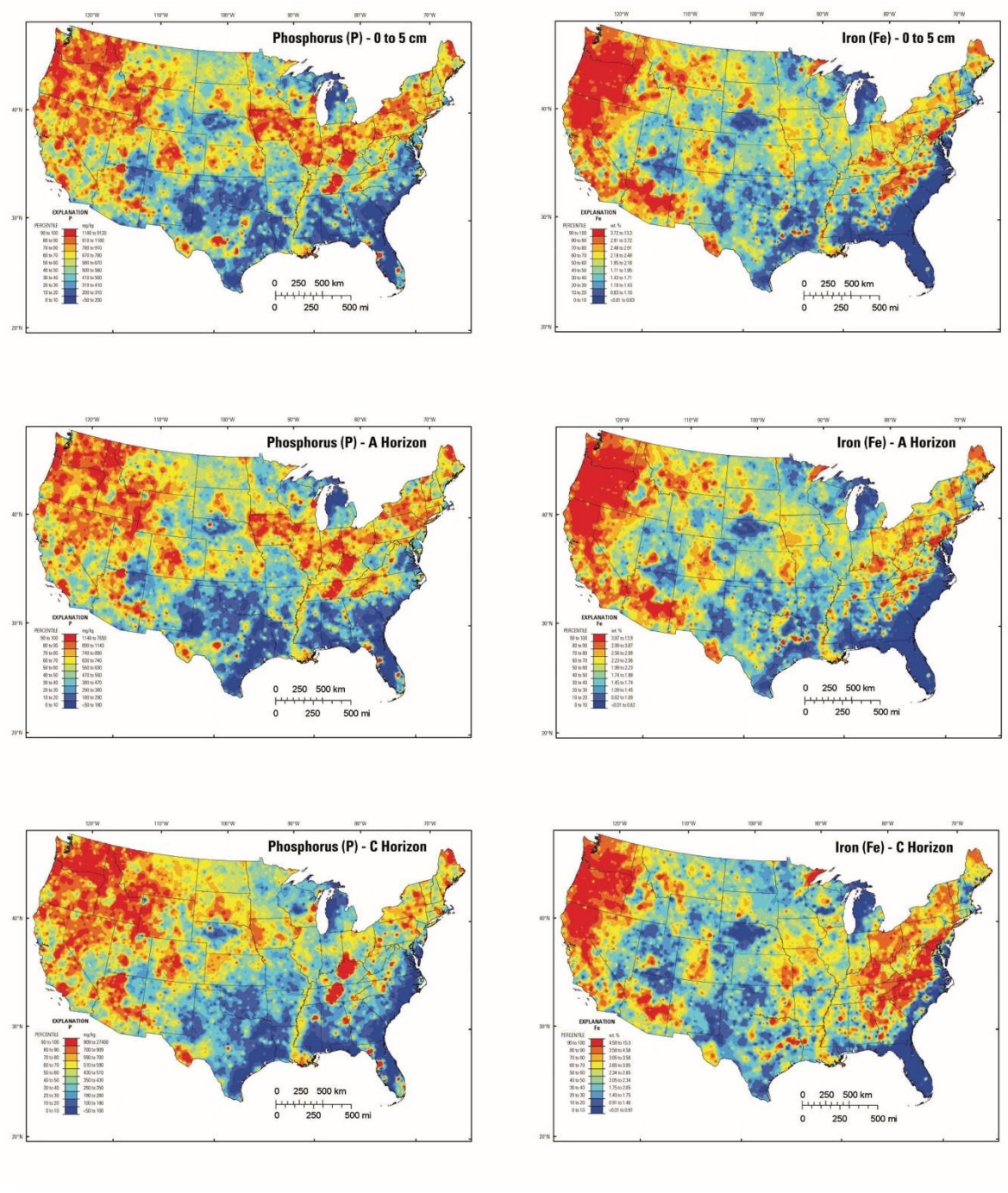

Figure A 2. P and Fe in US modern soils.

Modified from USGS database access. Maps of total P (left column) and total Fe (right column) in the conterminous United States, for Top 5 cm (top row), A horizon (middle row), and C horizon (bottom row) soils.

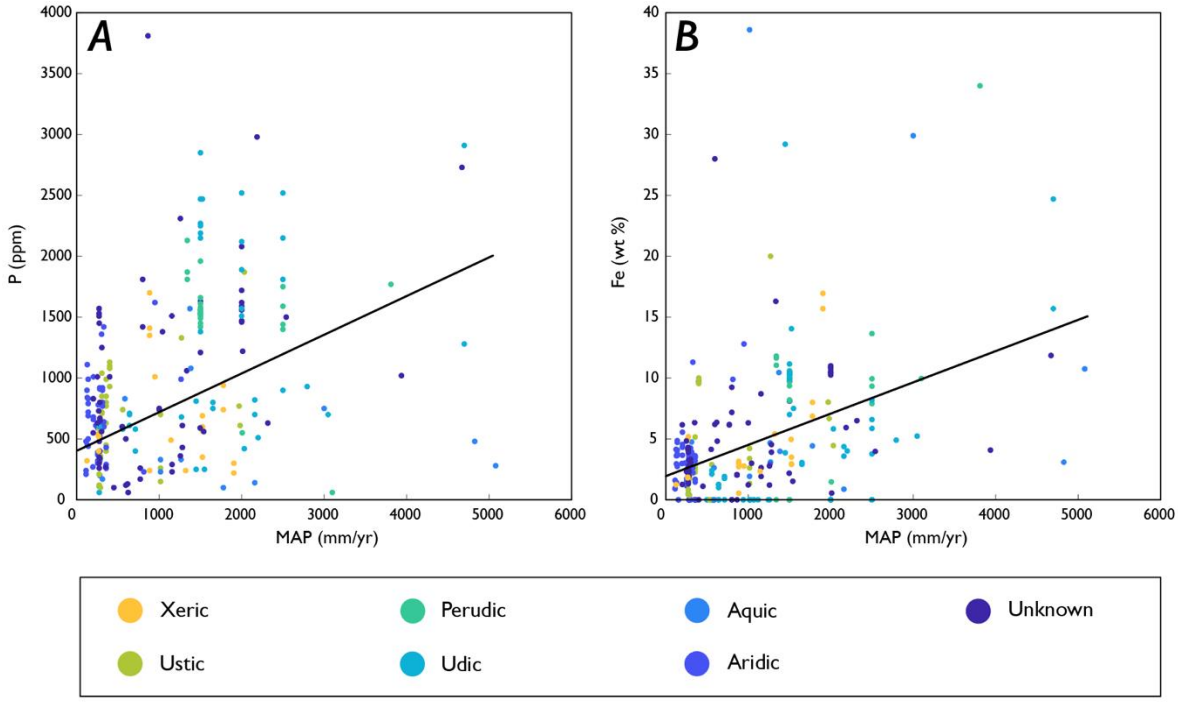

Figure A 3. MAP~Fe, MAP~P in modern soils.

New soils (all horizons) from this study, colored by soil moisture regime, plotted as mean annual precipitation (MAP) versus P and Fe. Solid lines are linear least-squares regressions. (A) No strong correlation between MAP and P (n = 250; R^2 = 0.13, p =10^{-14}), or within moisture regimes. (B) No strong correlation between MAP and total Fe (n = 251; R^2 = 0.18, p =<10^{-16}), or within soil moisture regimes.

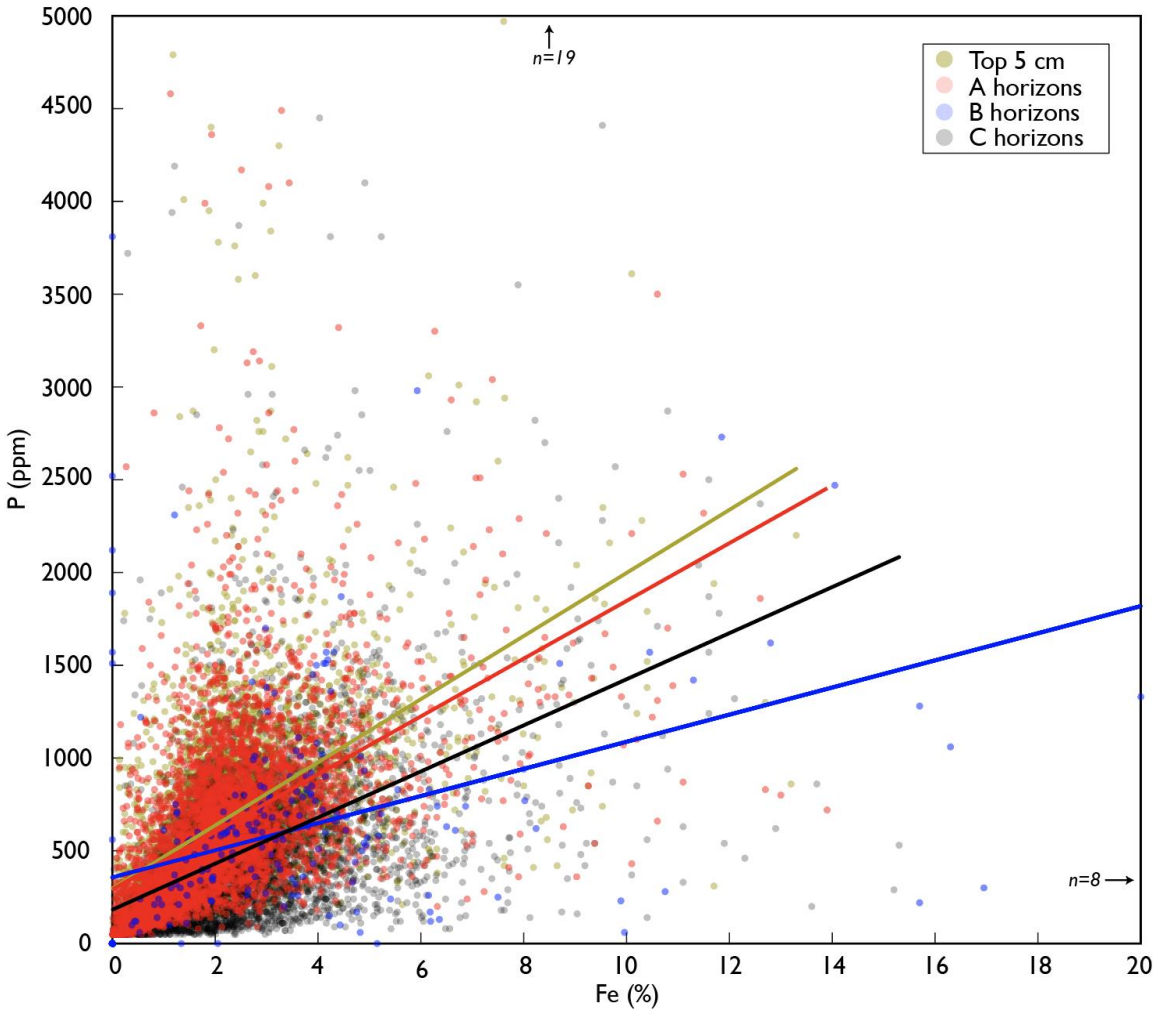

Figure A 4. Fe~P in modern soils.

There exists a general weak positive correlation between total Fe and P in soils, with variation between horizons. Solid lines are linear least-square regressions for Top 5 cm (yellow), A horizons (red), B horizons (blue), and C horizons, (black). R^2 values for Top 5, A, B, and C horizons are 0.24, 0.24, 0.27, and 0.11; for all, $p < 10^{-16}$.

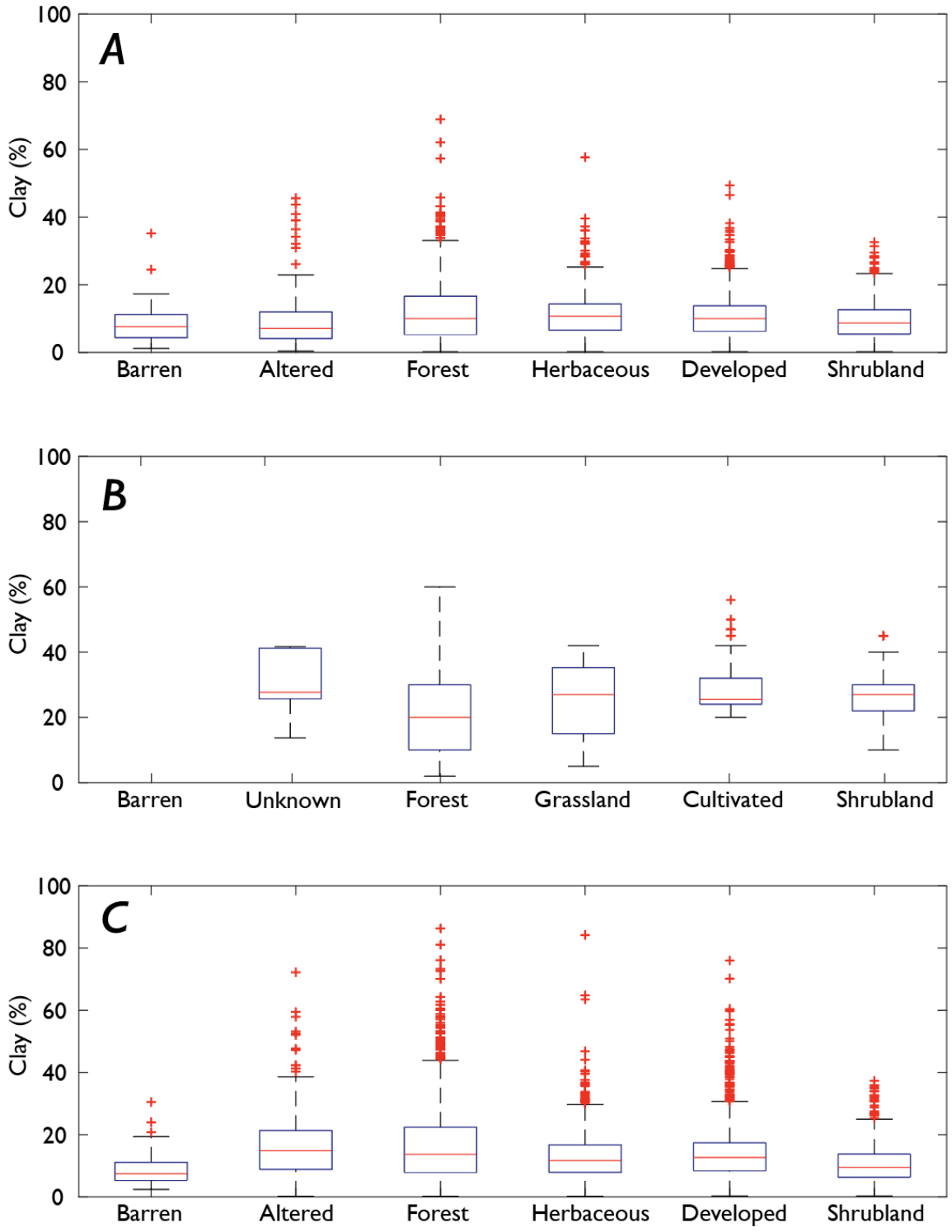

Figure A 5. Boxplots of clay content by vegetation type.

(A) Clay content, binned by vegetation type, in A horizons. (B) Clay content, binned by vegetation type, in B horizons. (C) Clay content, binned by vegetation type, in C horizons.

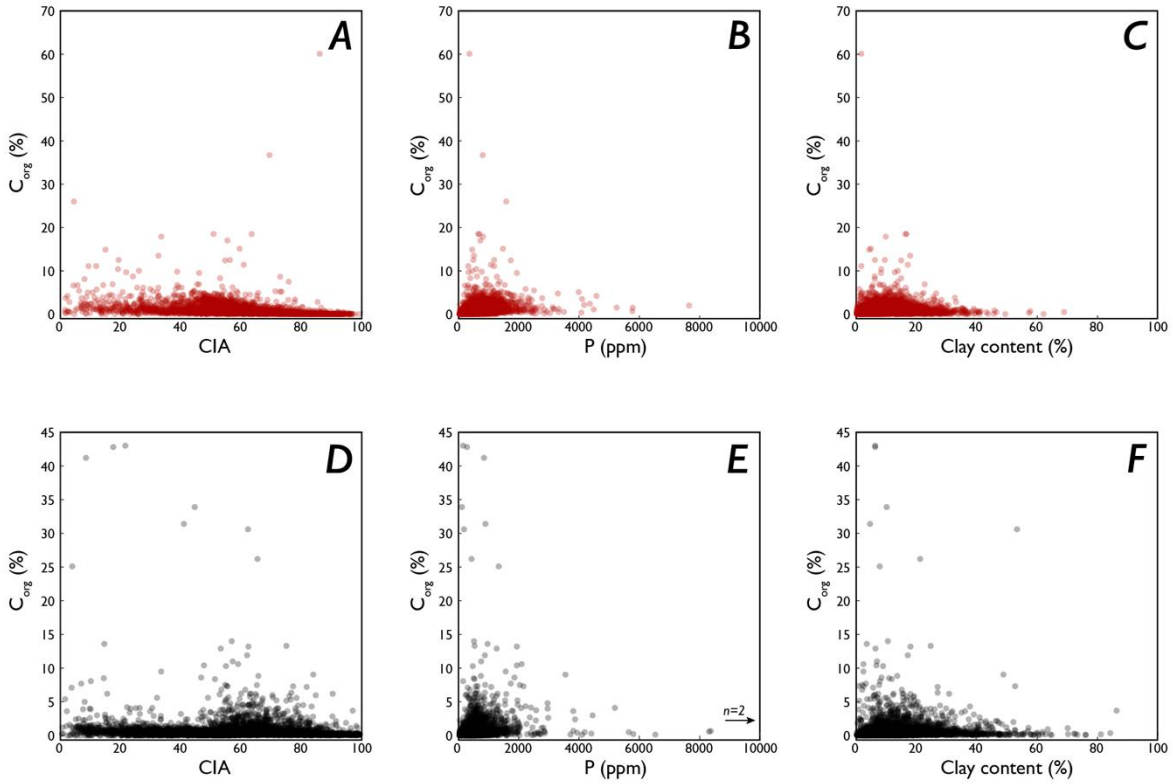

Figure A 6. CIA, P, and clay content ~ organic C in soils.

(A) CIA and organic carbon, in A horizons (R^2 0.09). (B) Total P and organic carbon, in A horizons (R^2 = 0.05). (C) Clay content and organic carbon, in A horizons (R^2 <0.01). (D) CIA and organic carbon, in C horizons. (R^2 <0.01). (E) Total P and organic carbon, in C horizons. (R^2 = 0.02). (F) Clay content and organic carbon, in C horizons (R^2 <0.01).

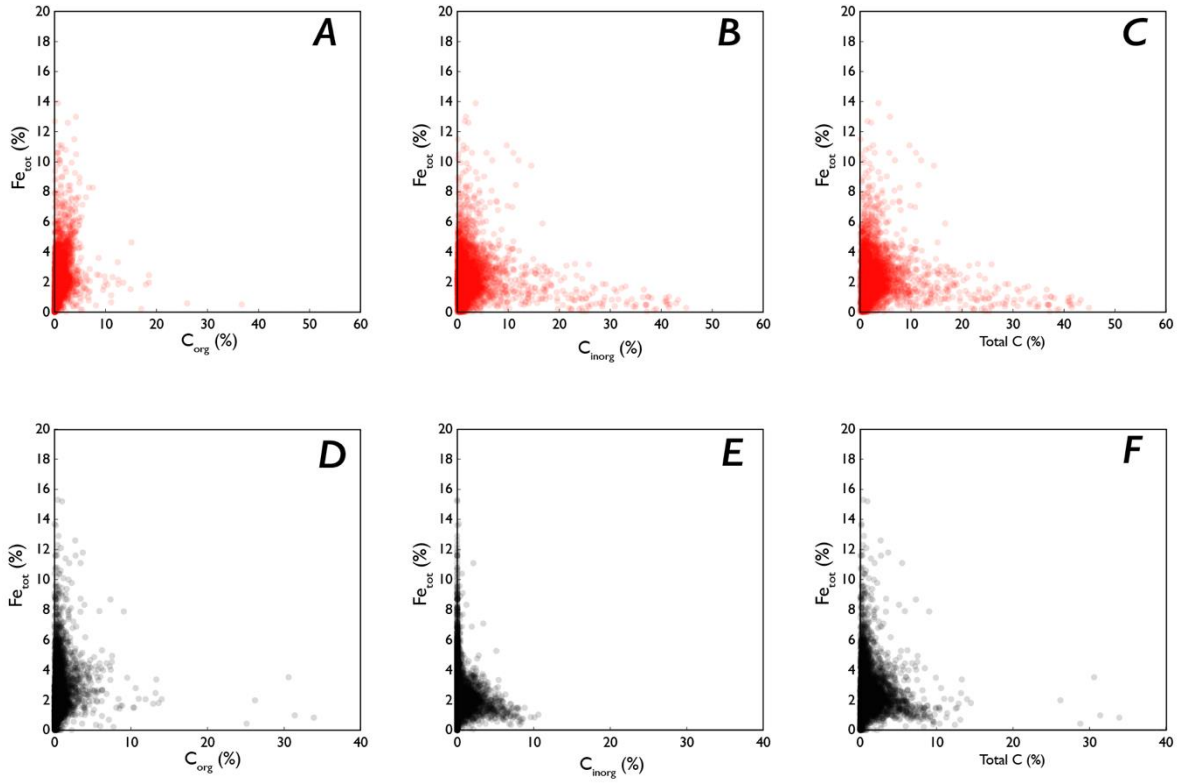

Figure A 7. Fe species~(in)organic and total C.

(A) C_{org} and Fe_{tot}, A horizons ($R^2 = 0.04$). (B) C_{inorg} and Fe_{tot}, A horizons ($R^2 < 0.01$). (C) Fe_{tot} and C_{tot}, A horizons. ($R^2 < 0.01$). (D) C_{org} and Fe_{tot}, C horizons. ($R^2 < 0.01$). (E) C_{inorg} and Fe_{tot}, C horizons. ($R^2 = 0.04$). (F) C_{tot} and Fe_{tot}, C horizons. ($R^2 < 0.01$).

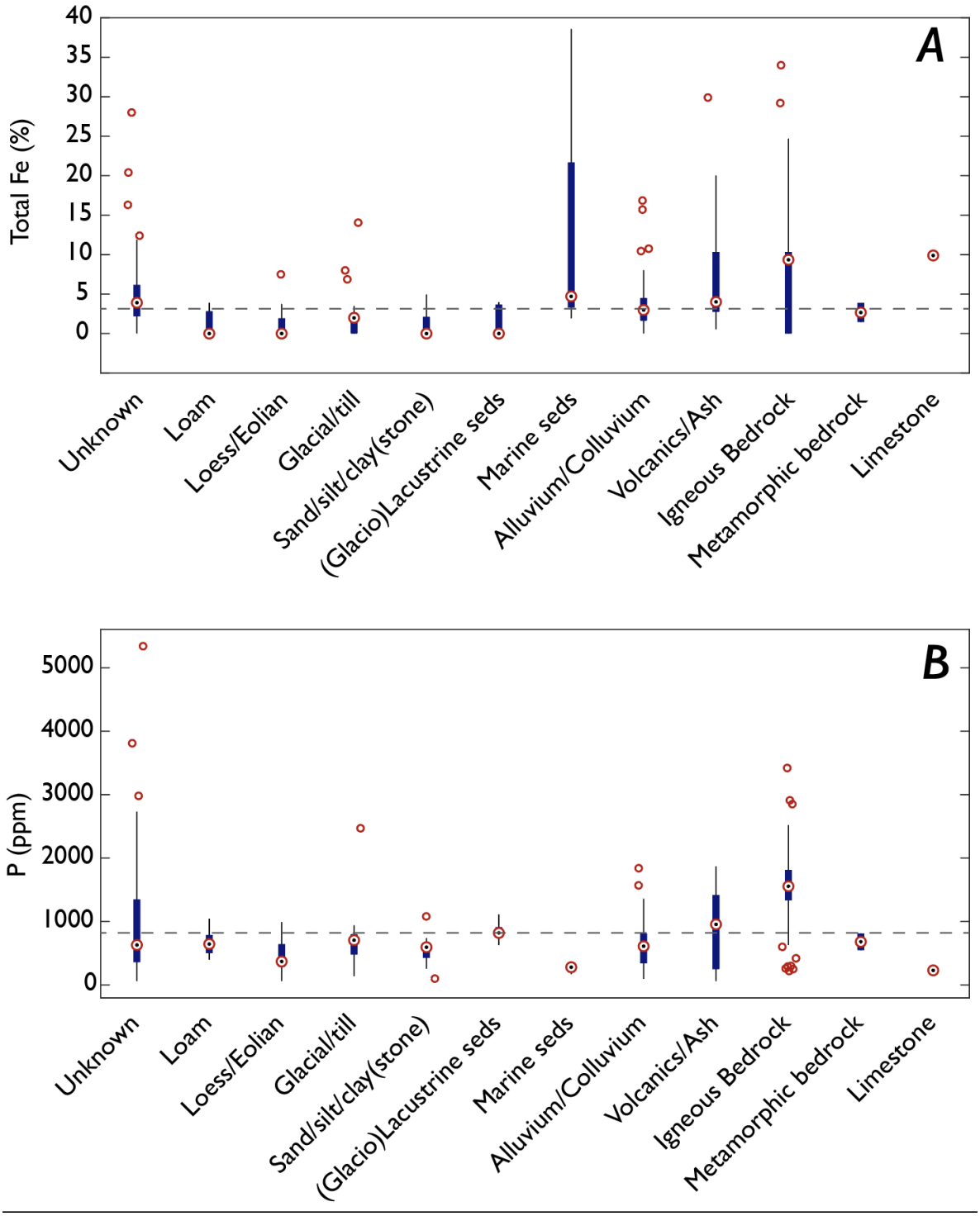

Figure A 8. Boxplots of Fe and P,by parent material.

(A) Total Fe in soils, binned by parent material. (B) Total P in soils, binned by parent material. Dashed grey lines are crustal averages.

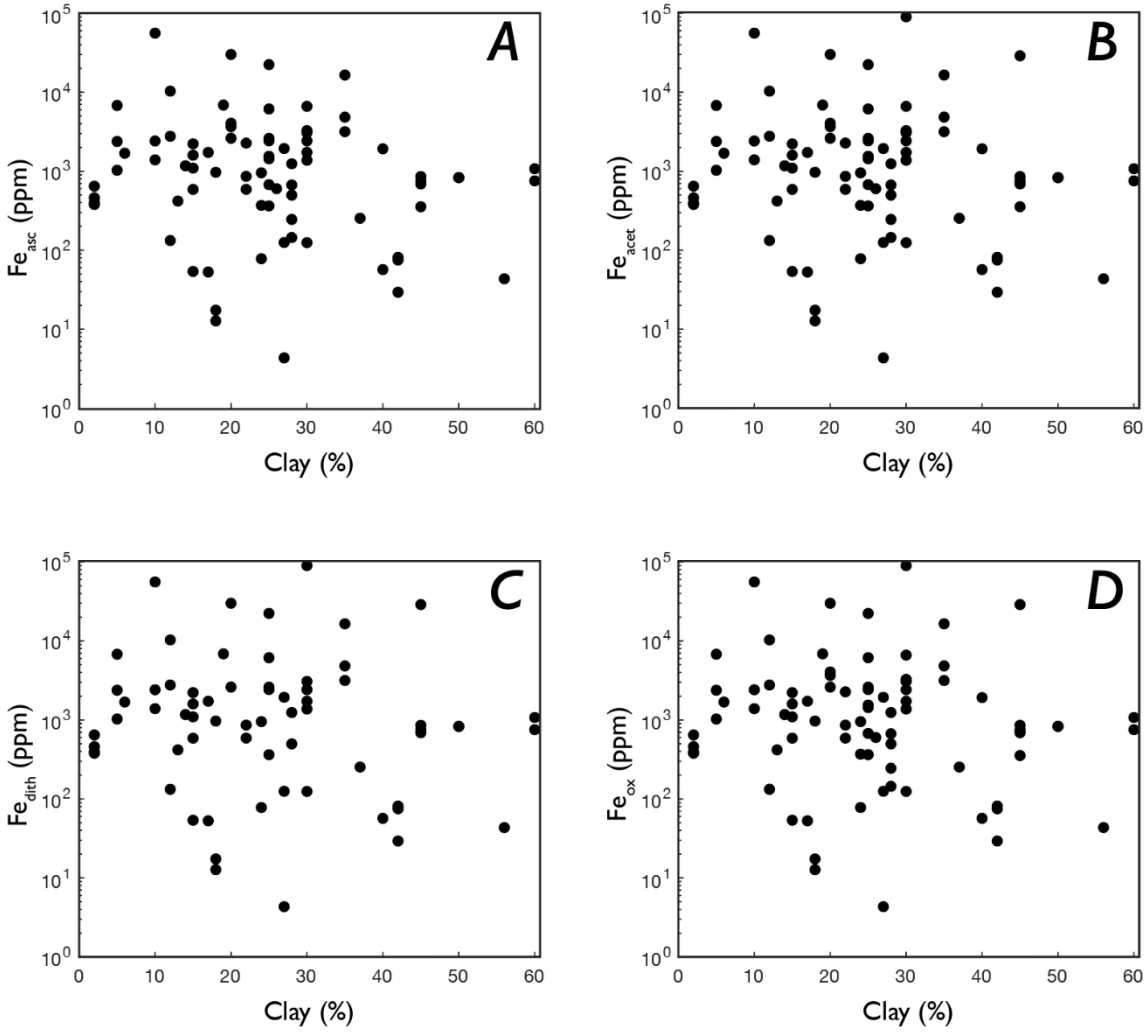

Figure A 9. Clay content and Fe species.

Clay content and Fe species in B horizons; note log scale on y-axis. (A) No correlation (R^2 = 0.07) between clay and Fe_{asc}. (B) No correlation (R^2 = 0.02) between clay and Fe_{acet}. (C) No correlation (R^2 = 0.12) between clay content and Fe_{dith}. (D) No correlation (R^2 <0.01) between clay content and Fe_{ox}.

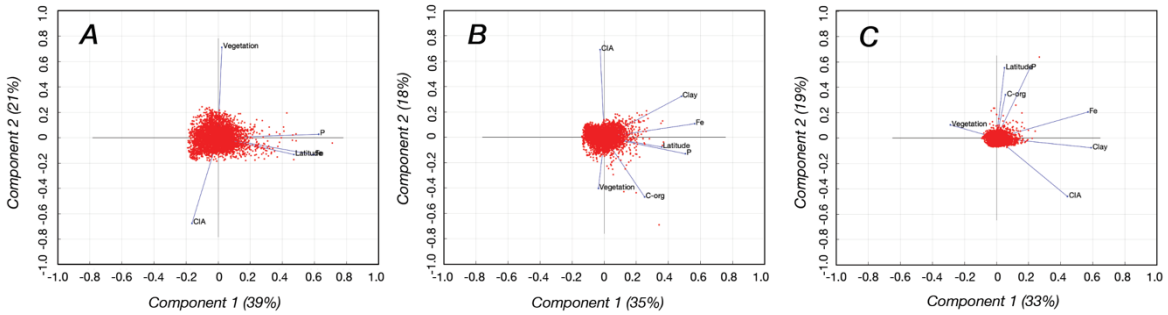

Figure A 10. PCA plots for USGS soils.

Principle Components Analysis (PCA) for USGS soils. (A) PCA for Top 5 cm (with 60% of variance explained by components 1 and 2). No clay or organic carbon data were available for this horizon. (B) PCA for A horizon (with 53% of variance explained by components 1 and 2). (C) PCA for C horizon (with 52% of variance explained by components 1 and 2).

Appendix B

Supplemental Methods and Figures for Chapter III

Paleosol compilation and screening

A range of parent materials (bedrock and alluvial) was included to capture all possible variability in the weathering products. To be included as bedrock-parented profile, paleosols/weathering profiles had to adhere the criteria outlined by Rye and Holland (1998). These are:

1. Homogenous parent material and preserved in-place;
2. Up-profile changes in mineralogy,
3. in texture, and
4. in chemical composition that follow soil weathering profiles;
5. Soft-sediment deformation between the top of the paleosol and overlying rocks (typically, corestones or rip-up clasts)

However, it should be noted that preserving the true tops of paleosols, particularly compound/composite paleosols that become more common in the Phanerozoic, is rare. While most of the profiles used in this work feature corestones or rip-up clasts at their base, fewer have the full profile preserved; while there may be soft sediment deformation at the tops, the 'tops' that are preserved are often not the top of the original soil (O,A). So although by the definitions outlined by Rye & Holland (1998) they can be classified as a paleosol, they may not necessarily be complete paleosol profiles – an important distinction to make when interpreting their chemical trends. Paleosols and weathering profiles included in this compilation were judged on these criteria; not all sedimentary beds called paleosols in the literature were included, particularly during the Precambrian. Alluvium-parented paleosols were judged on as many of these criteria as applicable and were only included if mineralogy, textures, and chemical compositions suggestive of pedogenesis, along with pedogenic features (e.g., root traces, reduction mottles, slickensides, ped structures) were present. For profile averaging, horizons

above BC were included, and for Precambrian weathering profiles where modern horizonation does not apply, the profile was considered weathered up to corestones and/or weathered bedrock (reporting style and quality varies through time). For certain Precambrian weathering profiles, mineral zones by depth were used to differentiate weathering profile from bedrock (e.g., sericite zones over bedrock). When possible, those designations were checked against geochemical down-profile trends (e.g., CIA, Al, or Ti). As a methods note, we strongly encourage anyone working with paleosols to clearly report depths, horizons, and weathering trends.

To represent larger catchments of terrestrial weathering during periods when paleosols were scarce (*e.g.*, Jacobsville Sandstone, Schrieber Beach), we included select massive, fluvial Precambrian sandstones (blue dots on Figure 1b). We believe that these are appropriate to include because while paleosols represent *in situ* weathering and P mobilization, these large-scale fluvial sandstones represent the mixed weathered product that was being eroded and ultimately transported to the oceans. Examining their P content is critical for understanding terrestrial P cycling, weathering, and transport.

For both paleosols and sandstones, nothing above greenschist-grade metamorphism was included; metamorphic grade was noted during data collection, and no systemic bias (*e.g.*, higher grade = more P) was found. Metamorphism stronger than greenschist facies was excluded because of the potential for hydrothermal alteration to P, as well as other elements. Additionally, we checked for post-pedogenesis addition of material using down-profile Ti/Al and excluded any profiles with apparent material addition (i.e., variability in Ti/Al between bedrock and overlying weathering profile/paleosol).

The complete list of sources for this compilation are found in Tables B1–3.

P enrichment/depletion

To test for changes in paleosol/weathering profile P enrichment or depletion relative to parent material (retention or loss), we took the ratio of P normalized to Ti as an immobile element (P/Ti) in soils compared to underlying bedrock. We limited this analysis to bedrock-parented paleosols/weathering profiles because of variable alluvium composition and the risk for P and/or Ti inheritance. The bedrock and appropriate paleosol horizons were averaged (reported in Supplemental Tables 1, 2). For Phanerozoic paleosols with similar horizonation to modern

soils, we averaged P/Ti in A/B horizons when available; if upper horizons were not available, B horizons were used. That value was then compared to the bedrock P/Ti value. For Precambrian weathering profiles which typically lack horizonation due to markedly different soil formation processes (i.e., long exposure times, lack of vegetation/roots, different atmospheric composition), the uppermost and least-altered 'horizon' was averaged and compared to bedrock. Any upper horizon with corestones/rip-up clasts of bedrock was not included in the 'upper' average. For the ratio of $P/Ti_{paleosol}$ / P/Ti_{parent}, we estimated the error using a fractional uncertainty approach.

$$uncertainty = \left(\frac{PTi_{paleosol}}{PTi_{parent}}\right) \times \sqrt{\left(\frac{\sigma \times PTi_{paleosol}}{PTi_{paleosol}}\right)^2 + \left(\frac{\sigma \times PTi_{parent}}{PTi_{parent}}\right)^2}$$

We note the importance of horizon choice in making paleosol enrichment/depletion calculations; including all samples from a multiple-meter-thick Precambrian weathering profile (e.g., Hao et al., 2020) will result in a larger range of enrichment/depletion values that, unless horizons/weathering zones are marked, are difficult to interpret in a meaningful way.

Data distributions and bootstrap analyses

Geochemical data were resampled using a Monte Carlo bootstrapping method to compare between time periods and sample types (Figures B3, B5, B6), following Reinhard et al. (2017). Resampling (n=10,000, with replacement) showed that while shale means increase slightly, the expansion in range increases, as found in the original work (Reinhard et al., 2017).

To explore data distributions, we generated quantile-quantile plots (Figure B4) comparing the log of P/Ti data from shales and paleosols, demonstrating that both datasets are closer to log-normally distributed than Gaussian. In each plot, low values typically do not behave following a distribution; this is likely due to values at or below detection limit (instrument limitations). Because of the large size of the datasets used here, as well as their log-normal and skewed distributions, we opt not to include further commonly-applied statistical tests (e.g., Student's t-test, ANOVA) as they would not be appropriate. Violin plots of distributions in modern soils and paleosols were generated in Matlab based on Bechtold (2016).

Supplemental Figures for Chapter III

(Supplemental tables for Chapter III at DOI: 10.17632/63vr5tpmxj.1)

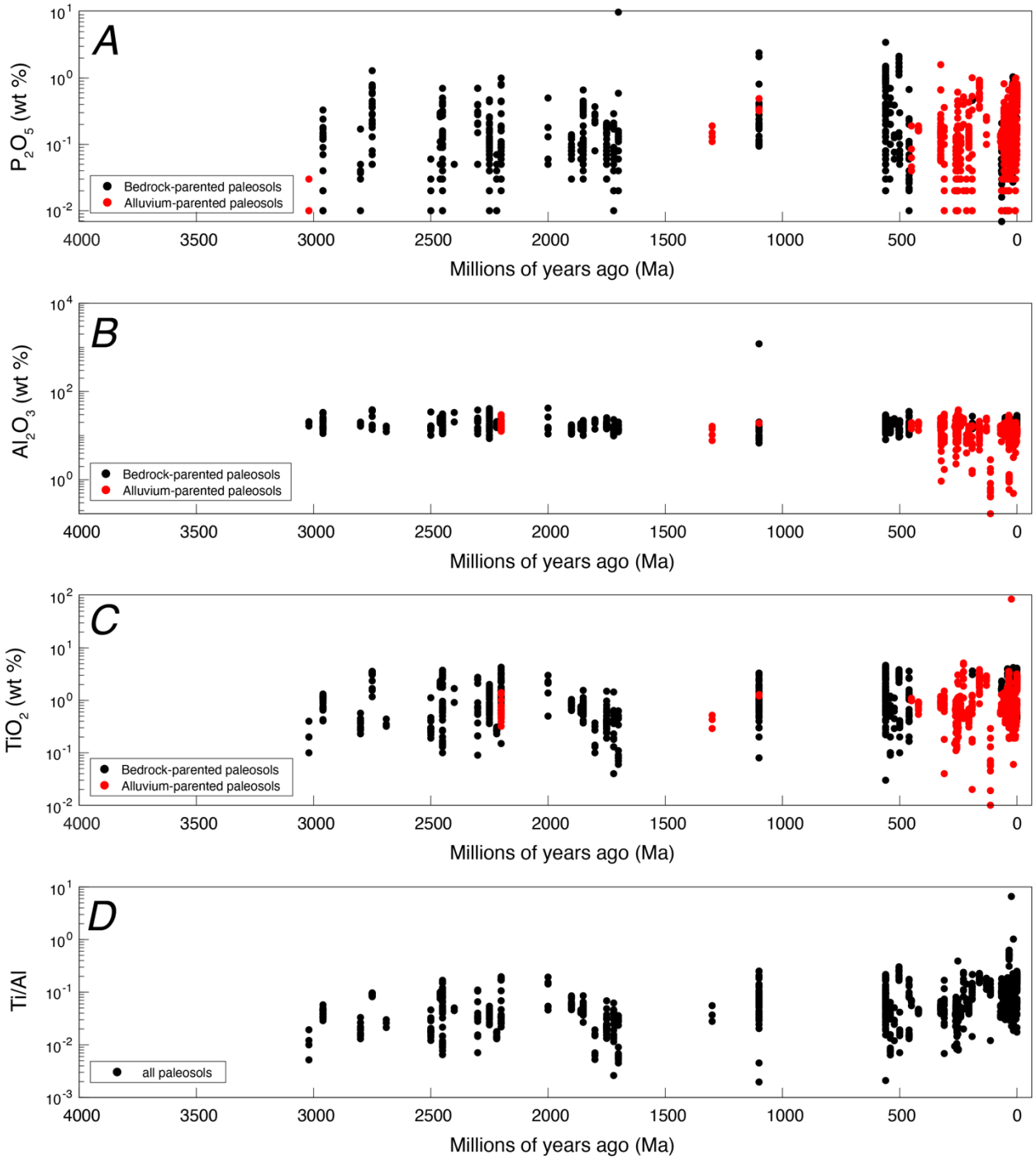

Figure B 1. P, Al, Ti, and Ti/Al through time in paleosols.

(A) Paleosol P_2O_5 through time, all data from weathering profiles and paleosols (not averaged per profile, as in Figure 3.1b). Black dots are samples from bedrock-parented paleosols; red dots

are samples from alluvium-parented paleosols. For this purpose, a sample was included if it were in the upper horizons (above BC) or, for Precambrian weathering profiles, to corestone/bedrock depth. (B) Al_2O_3 through time. (C) TiO_2 through time. (D) Ti/Al through time (all paleosols).

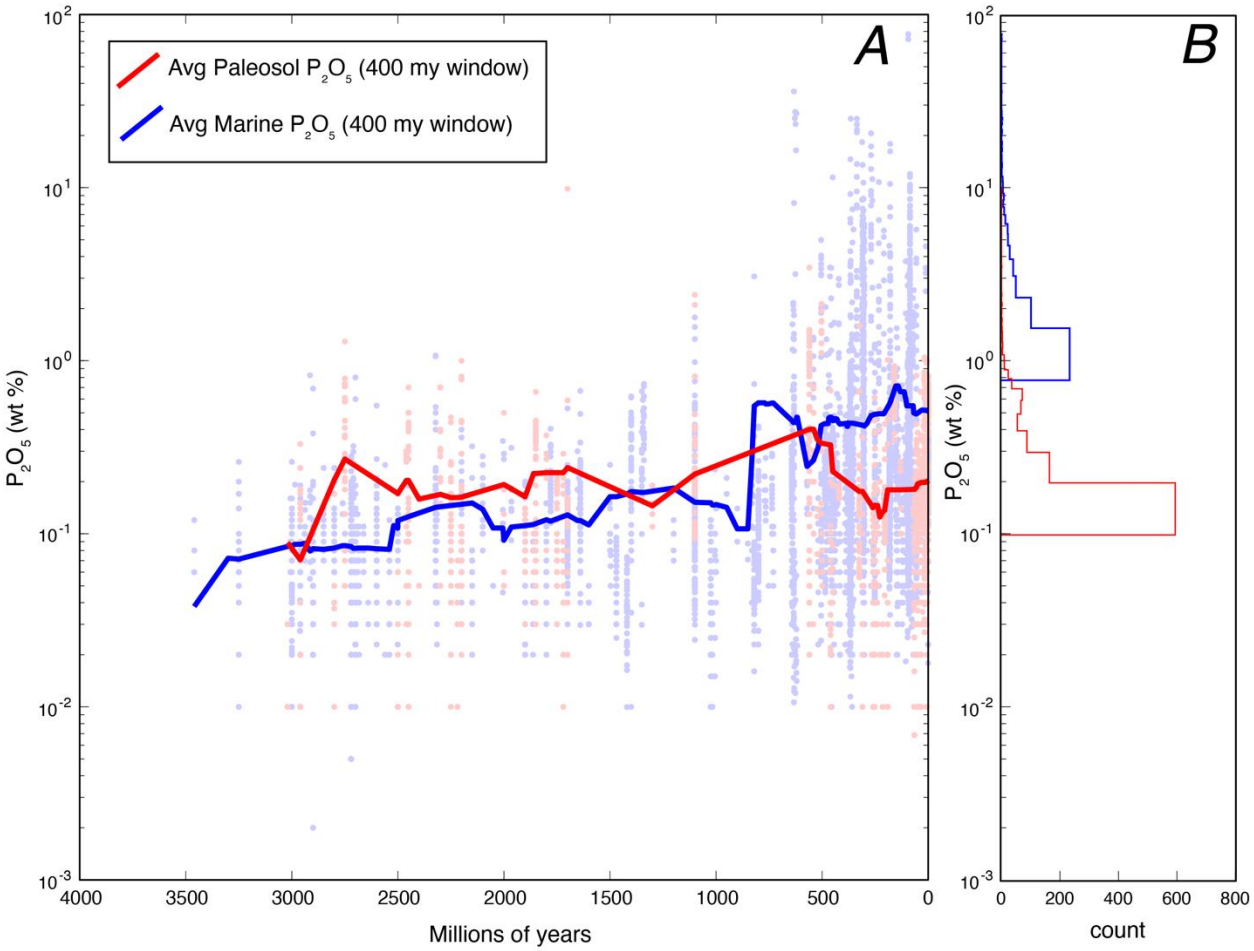

Figure B 2. Running average of P in paleosols and shales through time.

(A) Running average (400 my window) for paleosol P_2O_5 (red line) and marine shale P_2O_5 (blue line). Dots in background are individual paleosol (red) and shale (blue) samples. A large window was necessary to smooth noise due to gaps in the paleosol record. (B) Histogram of distributions for paleosols (red line) and shales (blue line).

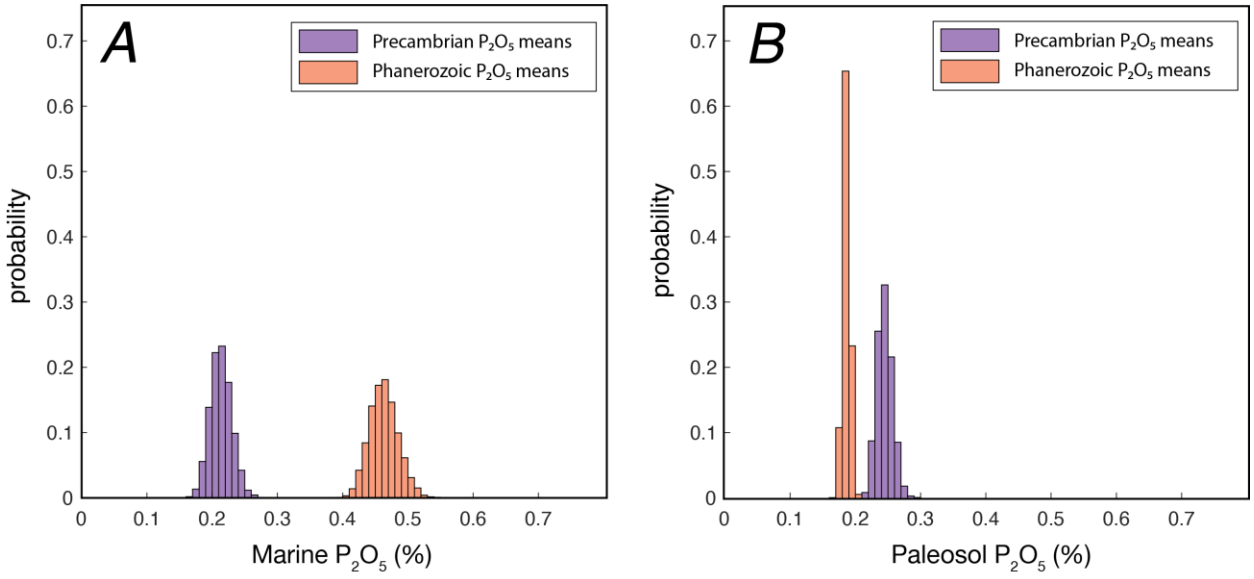

Figure B 3 Bootstrapped P in shales and paleosols, binned in PreC./Phan.

Bootstrapped P_2O_5 means (n iterations=10,000) for (A) marine shales and (B) paleosols/weathering profiles, binned into the Precambrian (purple) and Phanerozoic (orange), following Reinhard et al. (2017). Y-axis is normalized to probability.

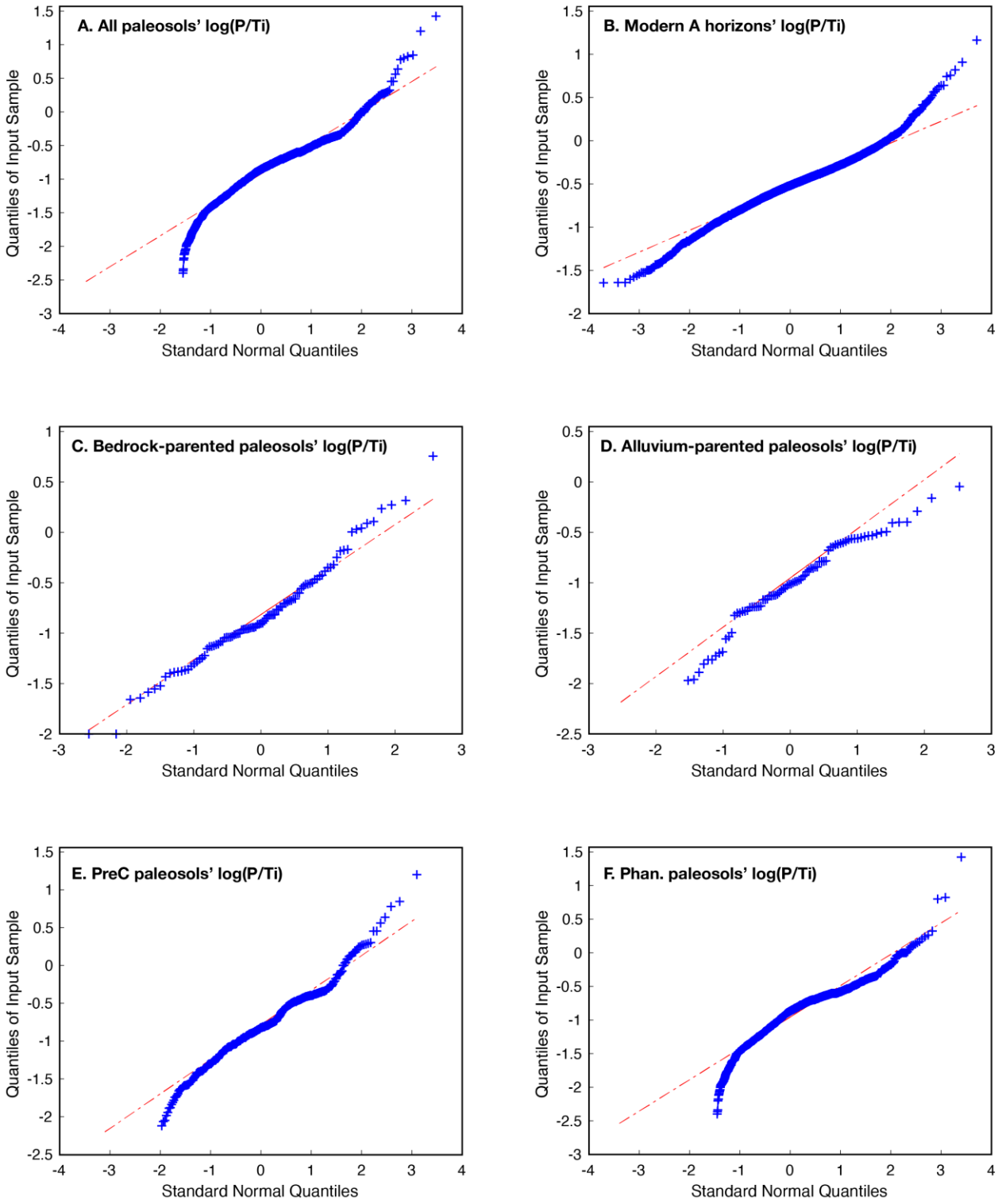

Figure B 4. Quantile-quantile plots of P/Ti in paleosols.

Quantile-quantile plots to demonstrate the near log-normal distribution of most natural systems' P populations, and to compare distributions between time bins and parent types. (A) All paleosols log(P/Ti). (B) Modern A horizons' log(P/Ti). (C) Bedrock-parented and (D) alluvium-

parented paleosols' log(P/Ti). (E) Precambrian and (F) Phanerozoic paleosols' log(P/Ti), both parent material types. Sandstones are excluded from these plots.

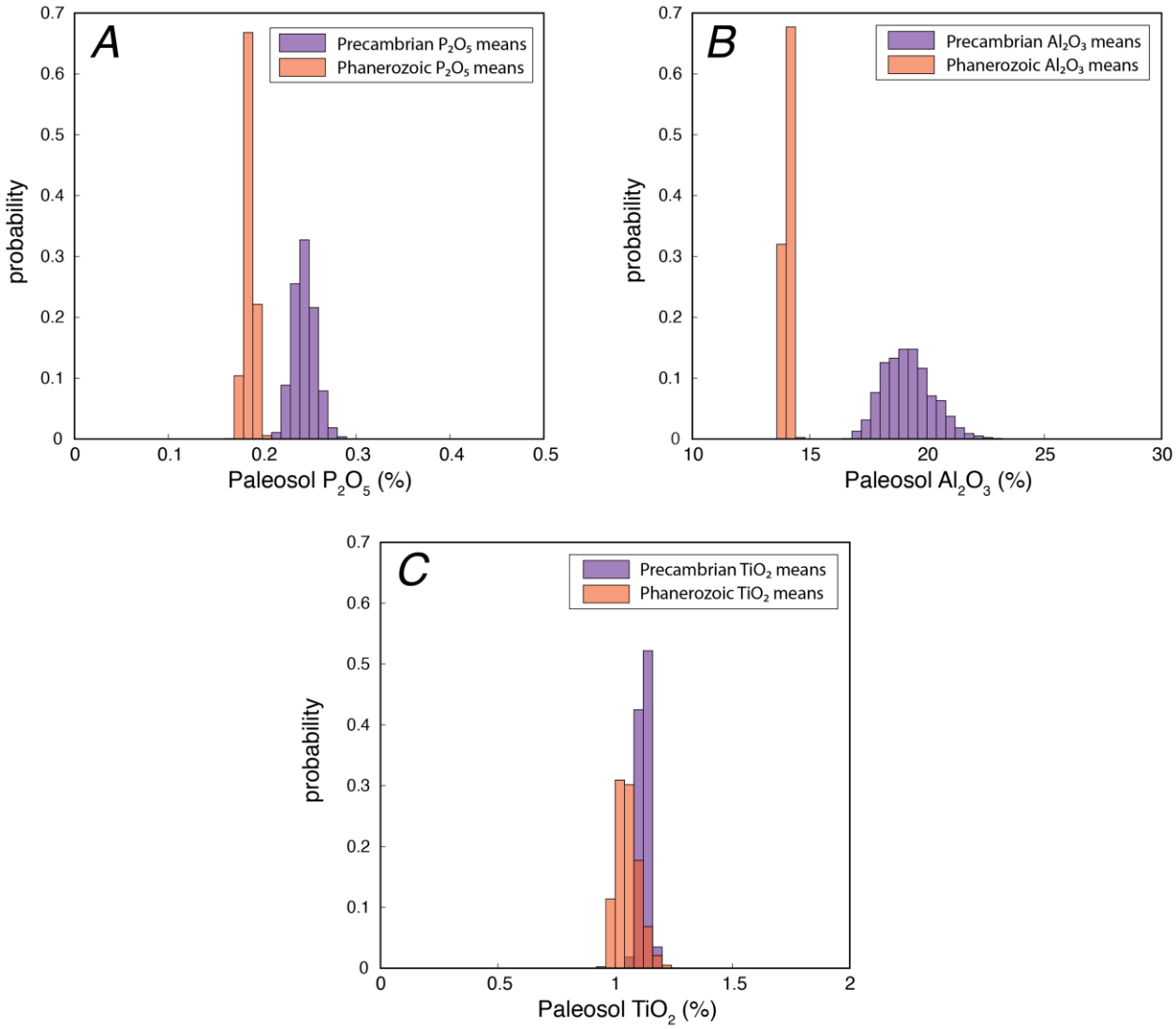

Figure B 5. Bootstrapped P, Al, and Ti in paleosols.

Bootstrapped means (n iterations=10,000) for paleosol (A) P_2O_5, (B) Al_2O_3, and (C) TiO_2, in Precambrian (purple) and Phanerozoic (orange) time bins. Only Al_2O_3 shows a significant shift between the two time bins; P_2O_5 may show a slight decrease from Precambrian to Phanerozoic, but not large enough to meaningfully interpret.

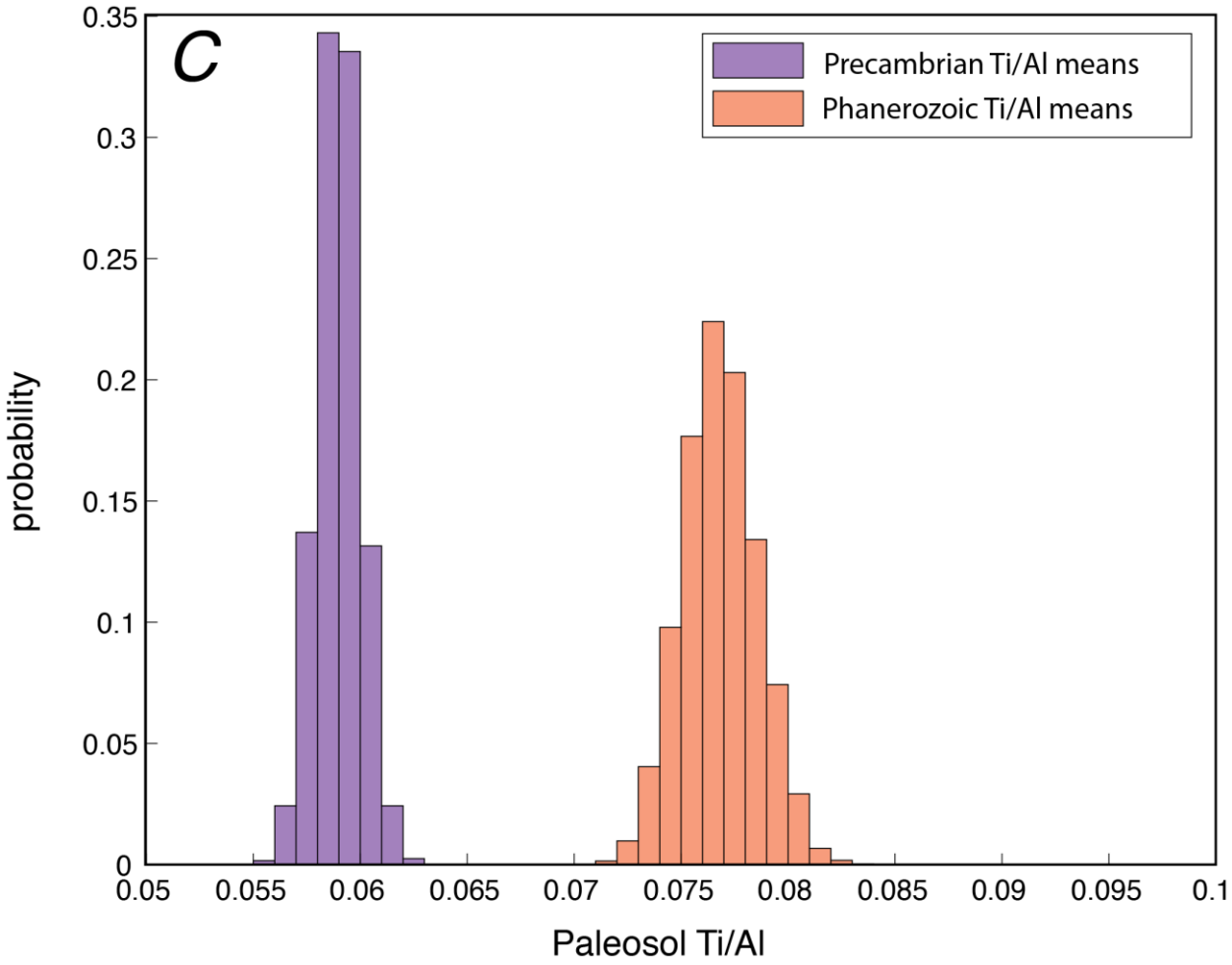

Figure B 6. Bootstrapped means for paleosol Ti/Al.

Bootstrapped means (n iterations=10,000) for paleosol Ti/Al, binned into Precambrian (purple) and Phanerozoic (orange) time bins. Ti/Al shows a statistically significant shift from Precambrian to Phanerozoic, but within the true range of Ti/Al in both paleosols and modern soils, the shift is not meaningful to interpret.

References for Appendix B

1. Rye, R. & Holland, H. D. Paleosols and the evolution of atmospheric oxygen: a critical review. *Am J Sci* **298**, 621–672 (1998).

2. Reinhard, C. T. *et al.* Evolution of the global phosphorus cycle. *Nature* **541**, 386-389 (2017).

3. Gaschnig, R. M. *et al.* Onset of oxidative weathering of continents recorded in the geochemistry of ancient glacial diamictites. *Earth Planet. Sci. Lett.* **408**, 87–99 (2014).

4. Hao, J., Knoll, A.H., Huang, F., Hazen, R.M., Daniel, I. Cycling phosphorus in the Archean Earth: Part I. Continental weathering and riverine transport of phosphorus. *Geochim. Cosmochim. Acta* **273**, 70-84 (2020).

5. Bechtold, Bastian, 2016. Violin Plots for Matlab, Github Project https://github.com/bastibe/Violinplot-Matlab, DOI: 10.5281/zenodo.4559847

Appendix C
Supplemental Figures for Chapter IV

(Supplemental tables for Chapter III are available online at DOI: 10.17632/n5yjzkpmkz.1)

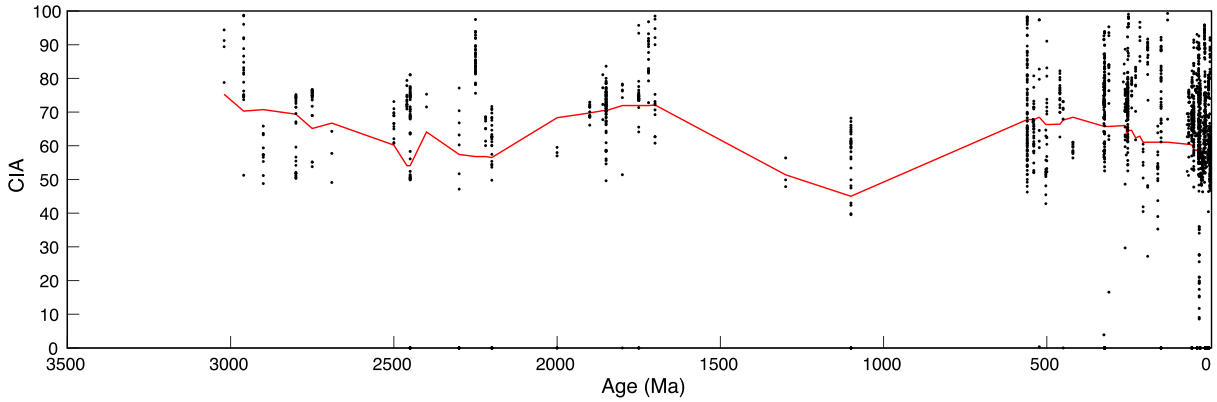

Figure C 1. Running avg. of paleosol CIA thru time.

Running average (window=400 m.y.) of CIA values in paleosols through time. Black dots are individual paleosol/upper weathering profile samples (i.e., A/B horizon). Samples with CaO >5% are excluded.

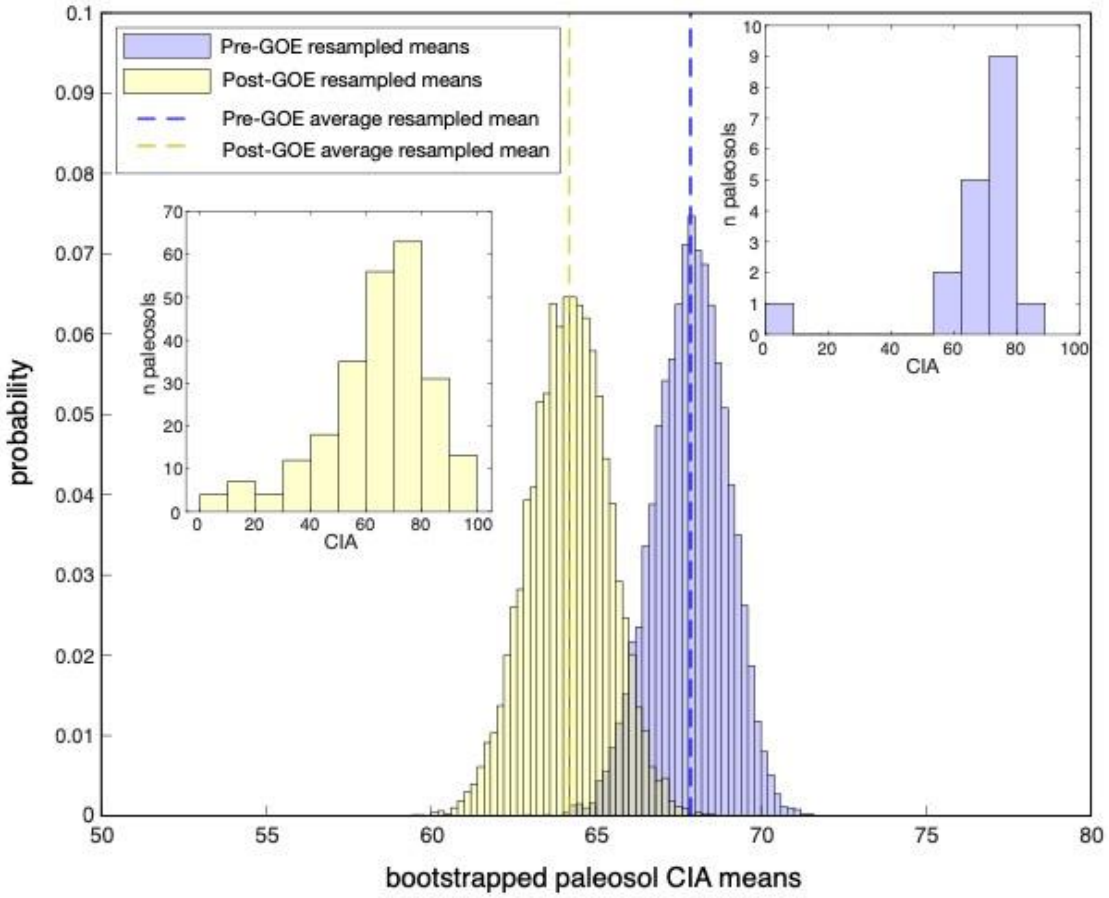

Figure C 2. Bootstrapped paleosol CIA values, divided at GOE.

Histograms (inset) and bootstrapped means for paleosol CIA values pre- (blue) and post-GOE (yellow). Dashed lines are means of the resampled data.

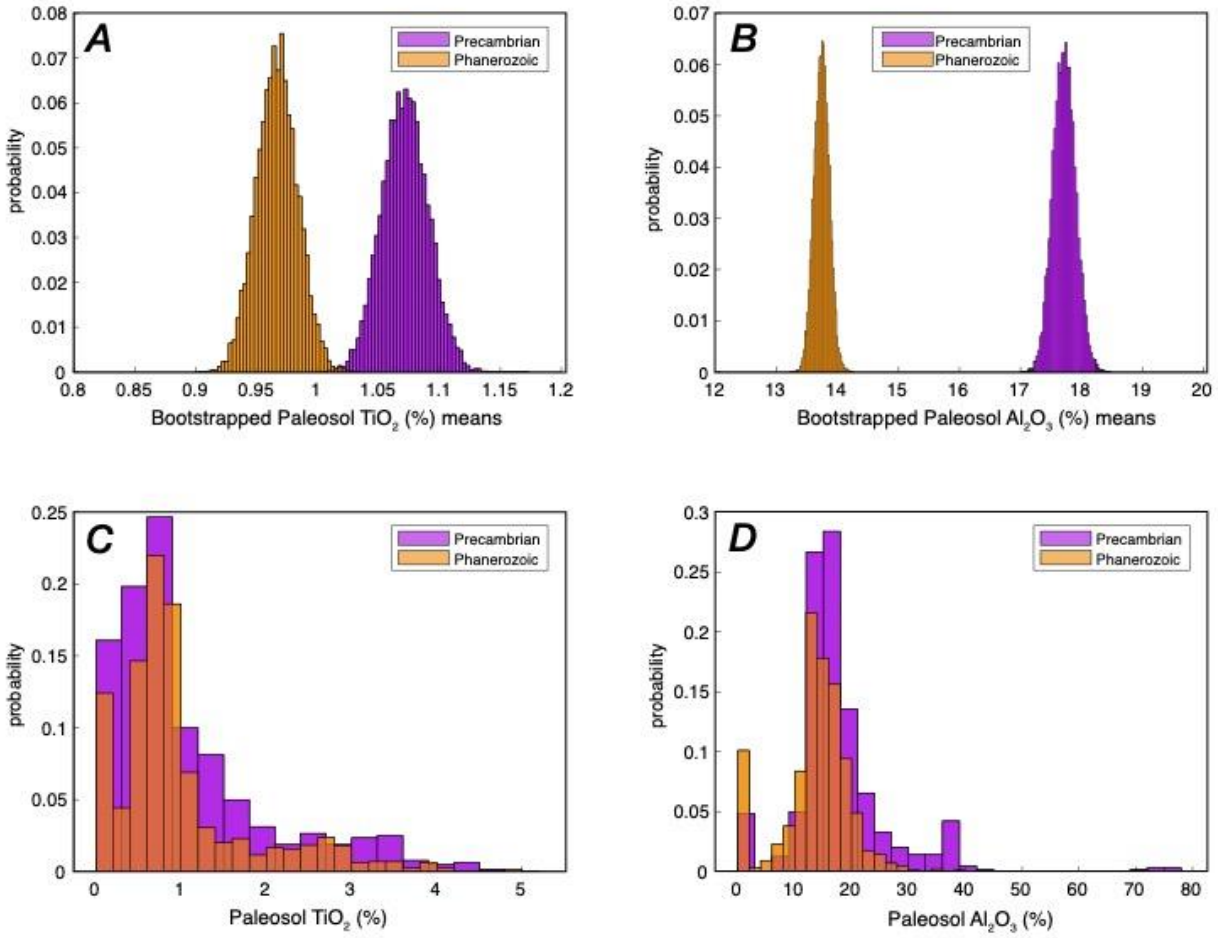

Figure C 3. Resampled TiO_2, Al_2O_3, time binned.

Bootstrap resampled means for (A) paleosol TiO_2 and (B) Al_2O_3, binned into Precambrian (purple) and Phanerozoic (orange) times. (C) Probability-normalized histogram for paleosol TiO_2 binned into Precambrian (purple) and Phanerozoic (orange) times. (D) (C) Probability-normalized histogram for paleosol Al_2O_3 binned into Precambrian (purple) and Phanerozoic (orange) times.

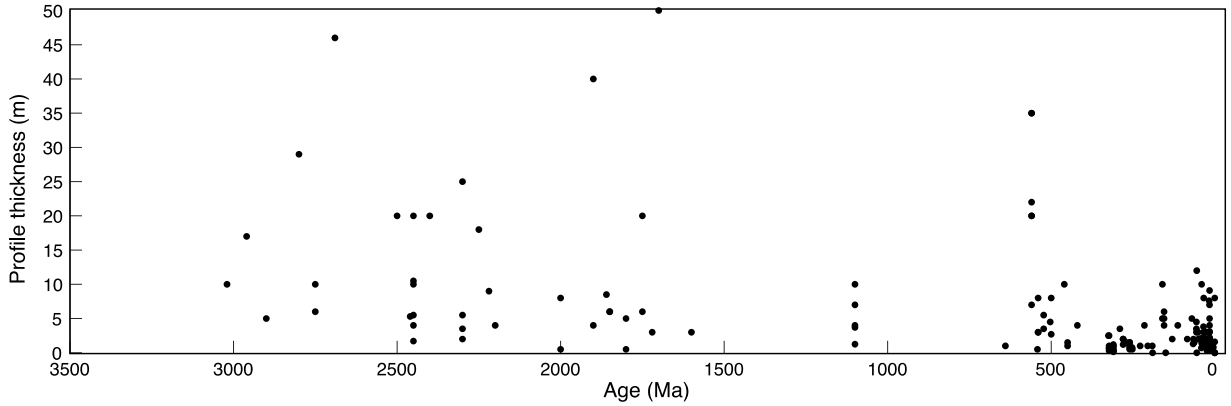

Figure C 4. Profile thickness thru time.

Profile thickness (m) through time, where each dot is a paleosol/weathering profile. Profile depths were counted until reaching BC horizon, corestones, or only moderately-weathered parent material.

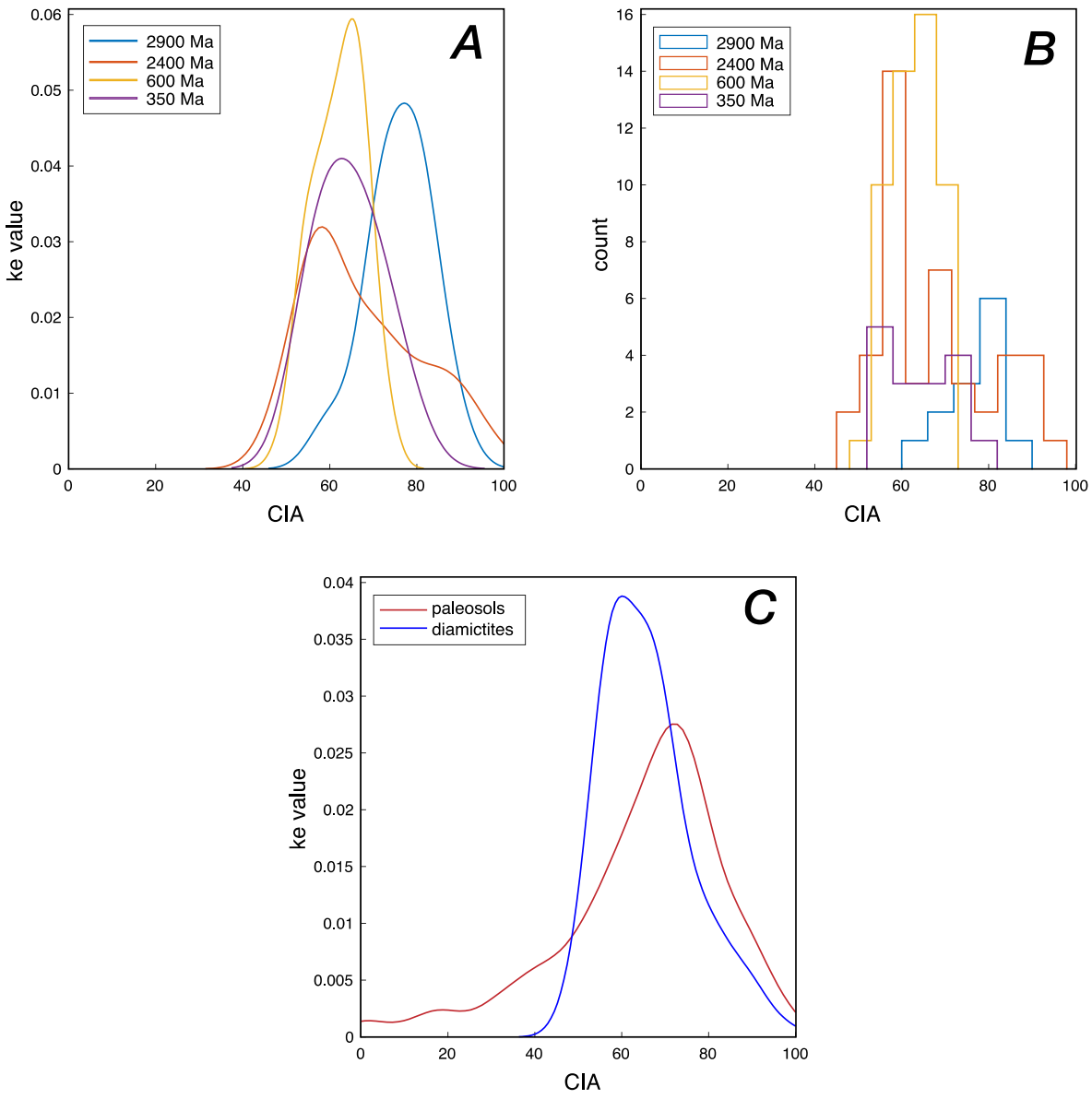

Figure C 5. CIA in glacial tillites.

(A) Kernel density estimates for CIA values in glacial tillites from Gaschnig et al. (2014). (B) Histograms of CIA values in glacial tillites. (C) Kernel density estimates for CIA values in paleosols (red line) and tillites (blue line). Tillites have a tighter distribution and generally represent lower weathering intensity than paleosols, but notably lack values <40 whereas paleosols preserve those.

Supplemental Text for Chapter IV

Soil order through time

Although this record is incomplete, we can use it to improve upon previous purely qualitative efforts at constraining the appearance of various soil orders through time (Retallack 2001). In this record (Figure 4.2d), the earliest modern soil orders identified are Entisols and Oxisols, both occurring by the Neoproterozoic (Table C3). Bandopadhyay et al. (2010) interpreted the 3.02 Ga Keonjhar paleosol as Vertic. Driese et al. (1992) interpreted the 2.2 Ga Hekpoort paleosol as Vertic; Buick et al. 1995 interpreted it as an Oxisol. Gay and Grandstaff (1980) described the 2.3 Ga Pronto paleosol as spodic/"like modern Spodosols." For the most part, the literature refrains from describing Precambrian weathering profiles with modern soil taxonomy; most would likely classify as Entisols, and many (particularly prior to ca. 2000) are described as laterites/lateritic weathering profiles. The Neoproterozoic 'Baltic paleosol' profiles (Liivamagi et al., 2015) have been designated as Oxisols. In the Phanerozoic, Vertisols make an appearance at 450 Ma (Beans Gap, TN; Driese and Foreman, 1991). Histosols are sparse in this compilation, with the earliest at 323 Ma (Pennington Fm., KY; Kahmann et al., 2008), but the earliest coals date to the early Devonian (Kidston and Lang, 1921; Krassilov, 1981; see Retallack et al., 1996 for a history of coals). Inceptisols, Alfisols, Ultisols, and Aridisols all occur following ca. 320 Ma in this compilation, but they existed prior to then and are not captured by this compilation (e.g., Morris et al., 2015). Mollisols first appear in this compilation at 33 Ma. No Gelisols are present in this record.

Some orders tend to be over-represented in the compilation, likely due to a combination of preservation/formation bias and sampling bias (e.g., Vertisols being associated with mountain-building events and of particular interest to parts of the paleosol community). For the record of soil order through time, though, it is essential to consider soil formation and preservation biases: where would a gelisol form? Would it be preserved? What about a Spodosol? Considering modern depositional environments and soil formation, it is apparent that, like the small percentage of marine particles that are eventually preserved in the seafloor, it is likely that a small subset of soils that ever exist are actually preserved in the rock record.

Soil thickness through time

Because this record is limited to paleosols and weathering profiles with bulk geochemical data available, we hesitate to draw conclusions about changes in soil profile thickness through time (Figure C3). One potential trend is an increase in the range of soil profile thicknesses preserved in the Phanerozoic as compared to the Precambrian, with thinner (often stacked/composite) paleosols more likely to be preserved. This could be due to the Sadler effect, the evolution of terrestrial geomorphology, sampling bias, or a combination of those factors. While the record needs to be improved before drawing conclusions about profile thicknesses, we note its importance for understanding the evolution of pedogenesis through time—a critical step for interpreting the paleosol record—and for points of comparison to modern soils and pedogenesis. The thickness of certain Precambrian weathering profiles has been noted with interest, perhaps being reflective of prolonged periods of exposure; however, deep weathering profiles (>10 m) exist in a range of environments today as well (e.g., Nott, 1994; Modenesi-Gautterti et al., 2011; Hewawasam et al., 2013; Olesen et al., 2013; Regmi et al., 2014; Medwedeff et al., in prep.; Biondino et al., 2020). Therefore, we should be conservative in interpreting profile thickness before we constrain the true range of both modern soil and paleosol profile thicknesses.

The complex relationships between soil production rates, soil thickness, and erosion rates observed in modern soils could also be considered in interpreting paleosols and understanding the evolution of pedogenesis through geologic time. When a soil mantle is present, it tends to decrease the degree of weathering intensity in the bedrock, a relationship that could affect the paleosol weathering record (e.g., Burke et al., 2007; Goddéris et al., 2008; West, 2012; Stockmann et al., 2014; see also section 10 in Goudie and Viles, 2012). Additionally, high erosion rates beyond a certain threshold tend to correlate with lower weathering intensity on average (see Dixon and von Blanckenburg, 2012). Because soil thickness, weathering intensity, and erosion can all be impacted by conflated factors such as climate and tectonics that would also vary with the supercontinent cycle (and indeed the complexity and distribution of terrestrial landscapes), these soil thickness-weathering-erosion relationships and controls likely varied through time (as an additional ‘changing weathering mechanism’ to covary). This point becomes increasingly important because paleosols may be preserved preferentially during one part of the supercontinent cycle, when one part of the weathering/erosion relationship may be true (see section 4.5.2). The relative relationships may have been different during stable cratonic periods

(e.g., Millot et al., 2002) and varied as alluvium- or regolith-parented soils (rather than bedrock-parented) became more common (e.g., Phillips, 2010; Norton et al., 2014). Therefore, as our understanding of those factors evolves, preservation biases in the paleosol record should be reconsidered. An in-depth analysis and discussion of these complex interactions is beyond the scope of this work, but is an interesting point for future study.

References for Appendix C

1. Bandopadhyay, P. C., Eriksson, P. G. & Roberts, R. J. A vertic paleosol at the Archean-Proterozoic contact from the Singhbhum-Orissa craton, eastern India. *Precambrian Res.* **177**, 277–290 (1981).

2. Biondino, D. *et al.* A multidisciplinary approach to investigate weathering processes affecting gneissic rocks (Calabria, southern Italy). *Catena* **187**, 104372 (2020).

3. Buick, R. *et al.* Record of emergent continental crust ~3.5 billion years ago in the Pilbara craton of Australia. *Lett. to Nat.* **375**, 574–577 (1995).

4. Burke, B. C., Heimsath, A. M. & White, A. F. Coupling chemical weathering with soil production across soil-mantled landscapes. *Earth Surf. Process. Landforms* **873**, 853–873 (2007).

5. Dixon, J. L. & von Blanckenburg, F. Soils as pacemakers and limiters of global silicate weathering. *Comptes Rendus - Geosci.* **344**, 597–609 (2012).

6. Driese, S. G. & Foreman, J. L. Traces and related chemical changes in a Late Ordovician paleosol, *Glossifungites* ichnofacies, southern Appalachians, USA. *Ichnos* **1**, 207–219 (1991).

7. Driese, S. G., Mora, C. I., Cotter, E. & Foreman, J. L. Paleopedology and stable isotope chemistry of Late Silurian vertic paleosols, Bloomsburg Formation, central Pennsylvania. *J. Sediment. Petrol.* **62**, 825–841 (1992).

8. Gay, A. L. & Grandstaff, D. E. Chemistry and mineralogy of Precambrian paleosols at Elliot Lake, Ontario, Canada. *Precambrian Res.* **12**, 349–373 (1980).

9. Goddéris, Y., Donnadieu, Y., Tombozafy, M. & Dessert, C. Shield effect on continental weathering: Implication for climatic evolution of the Earth at the geological timescale. *Geoderma* **145**, 439–448 (2008).

10. Goudie, A. S. & Viles, H. A. Weathering and the global carbon cycle: Geomorphological perspectives. *Earth-Science Rev.* **113**, 59–71 (2012).

11. Hewawasam, T. *et al.* Slow advance of the weathering front during deep, supply-limited saprolite formation in the tropical Highlands of Sri Lanka. *Geochim. Cosmochim. Acta* **118**, 202–230 (2013).

12. Kahmann, J. A., Seaman III, J. & Driese, S. G. Evaluating Trace Elements as Paleoclimate Indicators: Multivariate Statistical Analysis of Late Mississippian Pennington Formation Paleosols, Kentucky, U.S.A. *J. Geol.* **116**, 254–268 (2008).

13. Kidston, R. & Lang, W.H. On Old Red Sandstone plants showing structure from the Rhynie Chert bed, Aberdeenshire. Part V. The Thallophyta occurring in the peat bed, the succession of plants through a vertical section of the bed and the conditions of accumulation. *Royal Society of Edinburgh Transactions* **52**, 855-902 (1921).

14. Krassilov, V.A. Orestovia and the origin of vascular plants: Lethaia v. 14, p. 235-250 (1981).

15. Liivamägi, S. *et al.* Petrology, mineralogy and geochemical climofunctions of the Neoproterozoic Baltic paleosol. *Precambrian Res.* **256**, 170–188 (2015).

16. Medwedeff, W., Clark, M.K., Zekkos, D. West, A.J., Chamlagain, D. Geotechnical observations of weathered rock across a tectonic and climatic gradient in Central Nepal. In prep.

17. Modenesi-Gauttieri, M. C., de Toledo, M. C. M., Hiruma, S. T., Taioli, F. & Shimada, H. Deep weathering and landscape evolution in a tropical plateau. *Catena* **85**, 221–230 (2011).

18. Morris, J.L., Leake, J.R., Stein, W.E., Berry, C.M., Marshall, J.e., Wellman, C.H., Milton, J.A., Hillier, S., Mannolini, F., Quick, J., Beerling, D.J. Investigating Devonian trees as geo-engineers of past climates: Linking palaeosols to palaeobotany and experimental geobiology. *Palaeontology* **58**, 787-801.

19. Norton, K. P., Molnar, P. & Schlunegger, F. The role of climate-driven chemical weathering on soil production. *Geomorphology* **204**, 510–517 (2014).

20. Nott, J. The Influence of Deep Weathering on Coastal Landscape and Landform Development in the Monsoonal Tropics of Northern Australia. *J. Geol.* **102**, 509–522 (1994).

21. Olesen, O. *et al.* Deep weathering, neotectonics and strandflat formation in Nordland, northern Norway. *Nor. Geol. Tidsskr.* **93**, 189–213 (2013).

22. Phillips, J. D. The convenient fiction of steady-state soil thickness. *Geoderma* **156**, 389–398 (2010).

23. Retallack, G.J. Soils of the past: An introduction to paleopedology. 2001, Oxford, United Kingdom.

24. Retallack GJ, Veevers JJ, Morante R. Global coal gap between Permian-Triassic extinction and Middle Triassic recovery of peat-forming plants. *GSA Bulletin* **108**, 195-207 (1996).

25. Regmi, A. D., Yoshida, K., Dhital, M. R. & Pradhan, B. Weathering and mineralogical variation in gneissic rocks and their effect in Sangrumba Landslide, East Nepal. *Environ. Earth Sci.* **71**, 2711–2727 (2014).

26. Stockmann, U., Minasny, B. & Mcbratney, A. B. How fast does soil grow? *Geoderma* **216**, 48–61 (2014).

27. West, A. J. Thickness of the chemical weathering zone and implications for erosional and climatic drivers of weathering and for carbon-cycle feedbacks. *Geology* **40**, 811–814 (2012).

Appendix D

Supplemental Figures for Chapter V

(Supplemental tables for Chapter V are available online at DOI: 10.17632/m4rt8rtbr5.1)

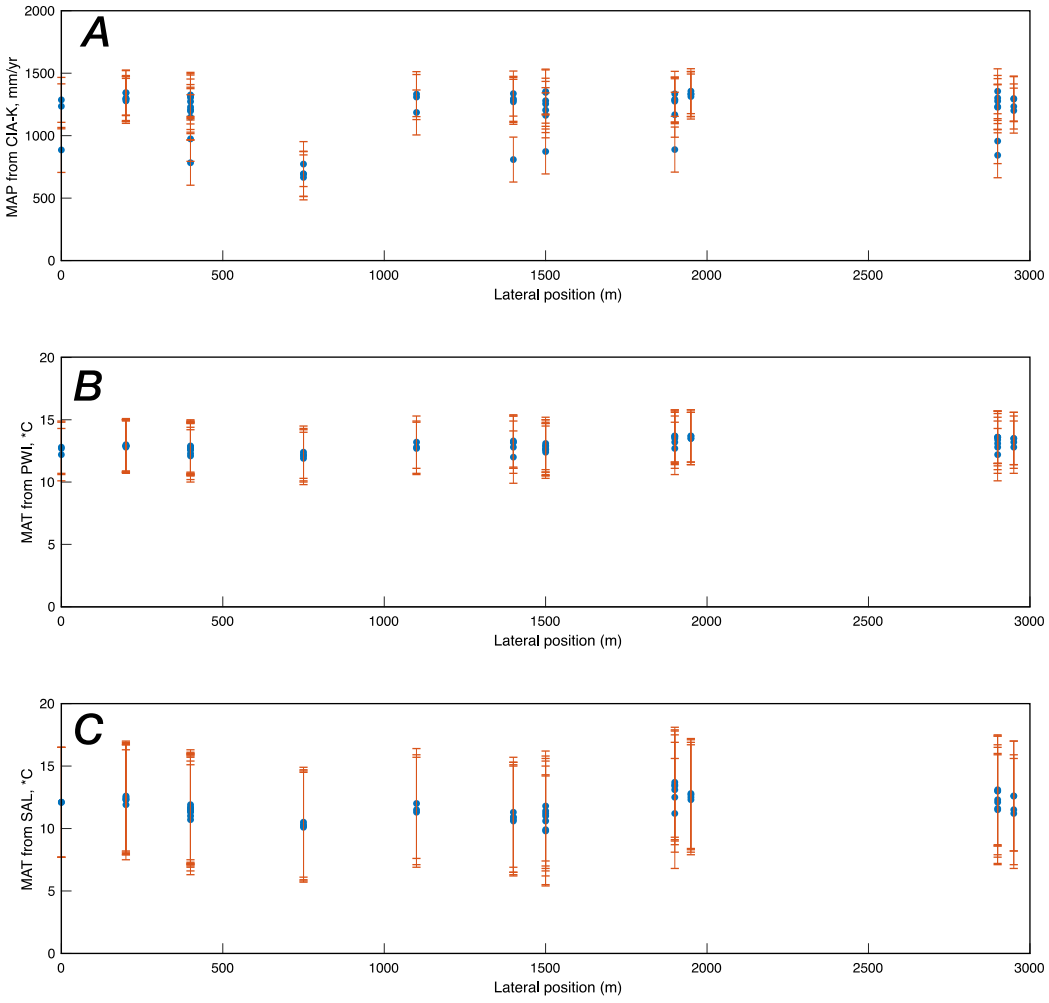

Figure D 1. Lateral MAP, MAT trends at JMH

Lateral trends in (A) MAP from CIA-K, (B) MAT from PWI, and (C) MAT from SAL at JMH. Error bars in all are respective standard errors.

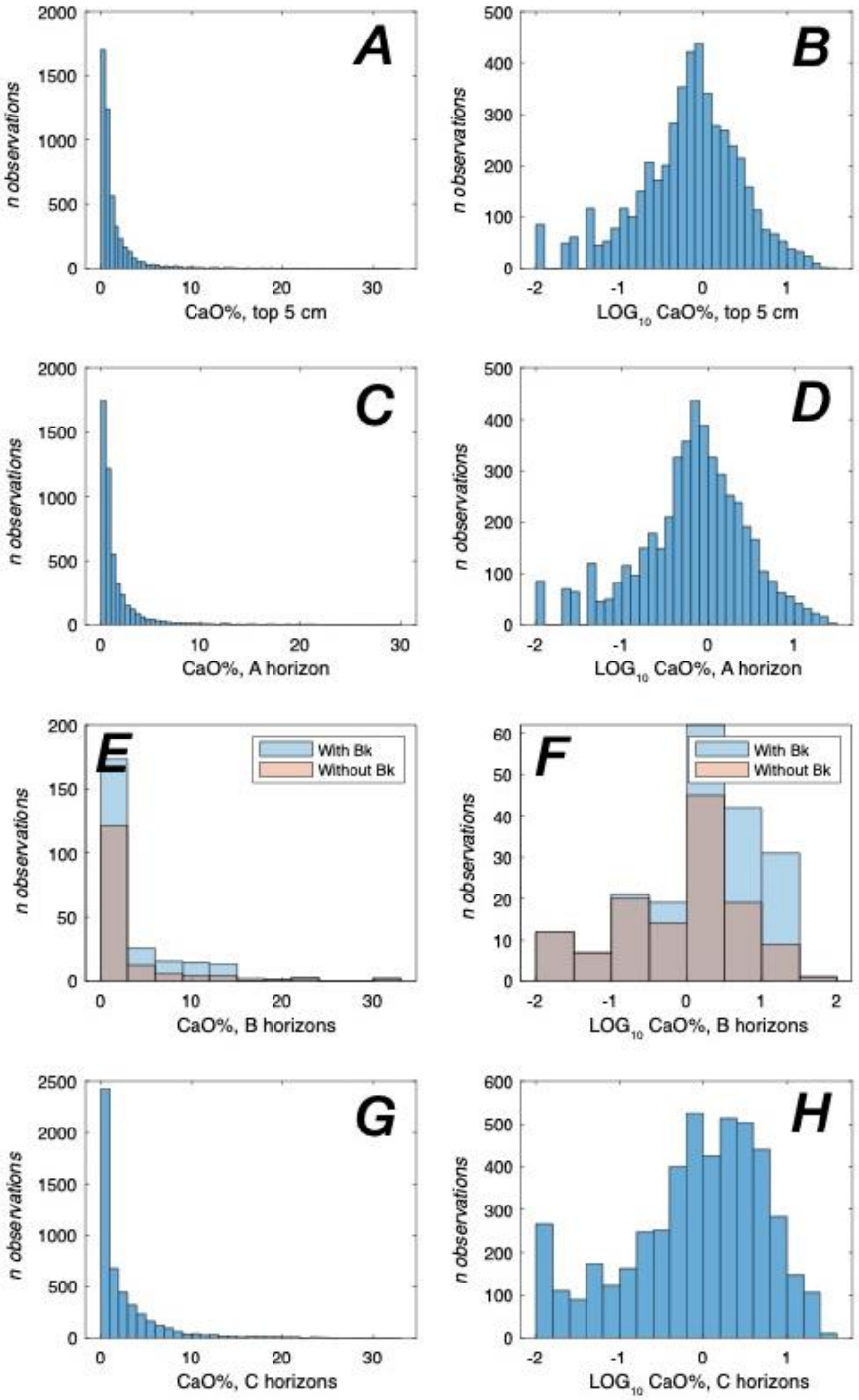

Figure D 2. CaO in modern soils.

Distribution of CaO in Top 5 cm horizons (A,B), A horizons (C,D), and C horizons (G,H) (Smith et al. (2014); distribution of CaO in B horizons (C, D) from Marbut (1935) and Dzombak and Sheldon (2020). Left column is linear scale, right column is $\log_{10}$ scale. Overall, CaO in soils tends to be log-normally distributed, with long right tails.

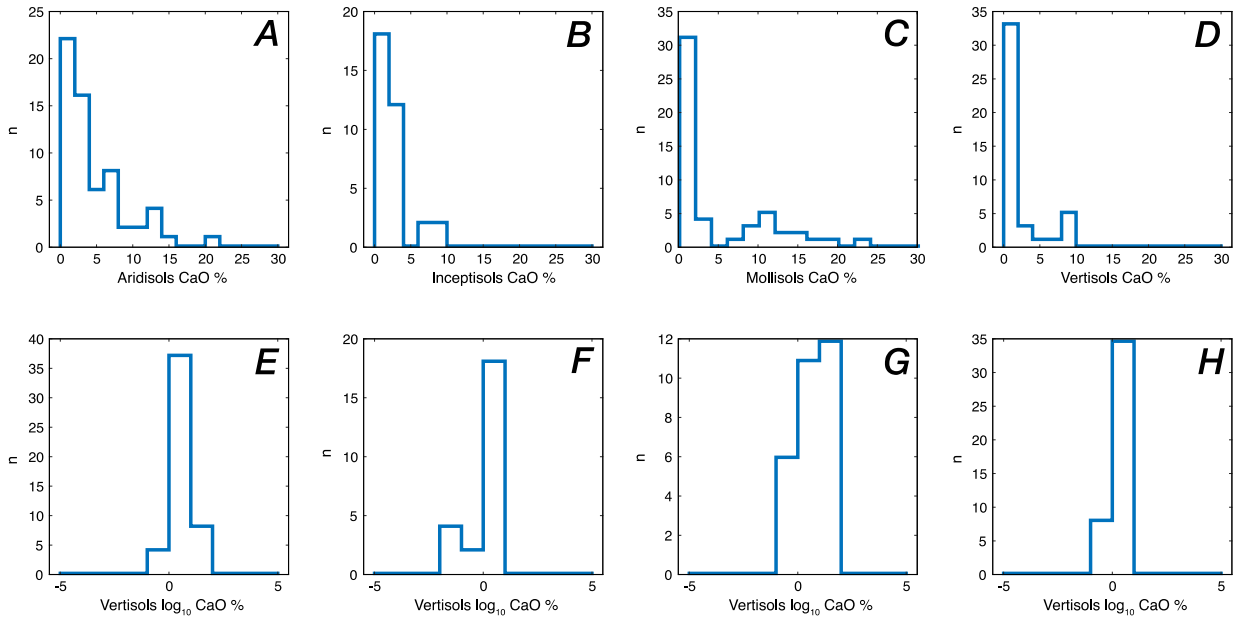

Figure D 3. CaO in modern B horizons, by soil order.

Distribution of CaO in B horizons by soil order; top row is linear scale, bottom row is $\log_{10}$ scale. (A,E) Aridisols, (B,F) Inceptisols, (C,G) Mollisols, (D,H) Vertisols. As with soil horizon bins, CaO is approximately log-normally distributed, with long right tails.

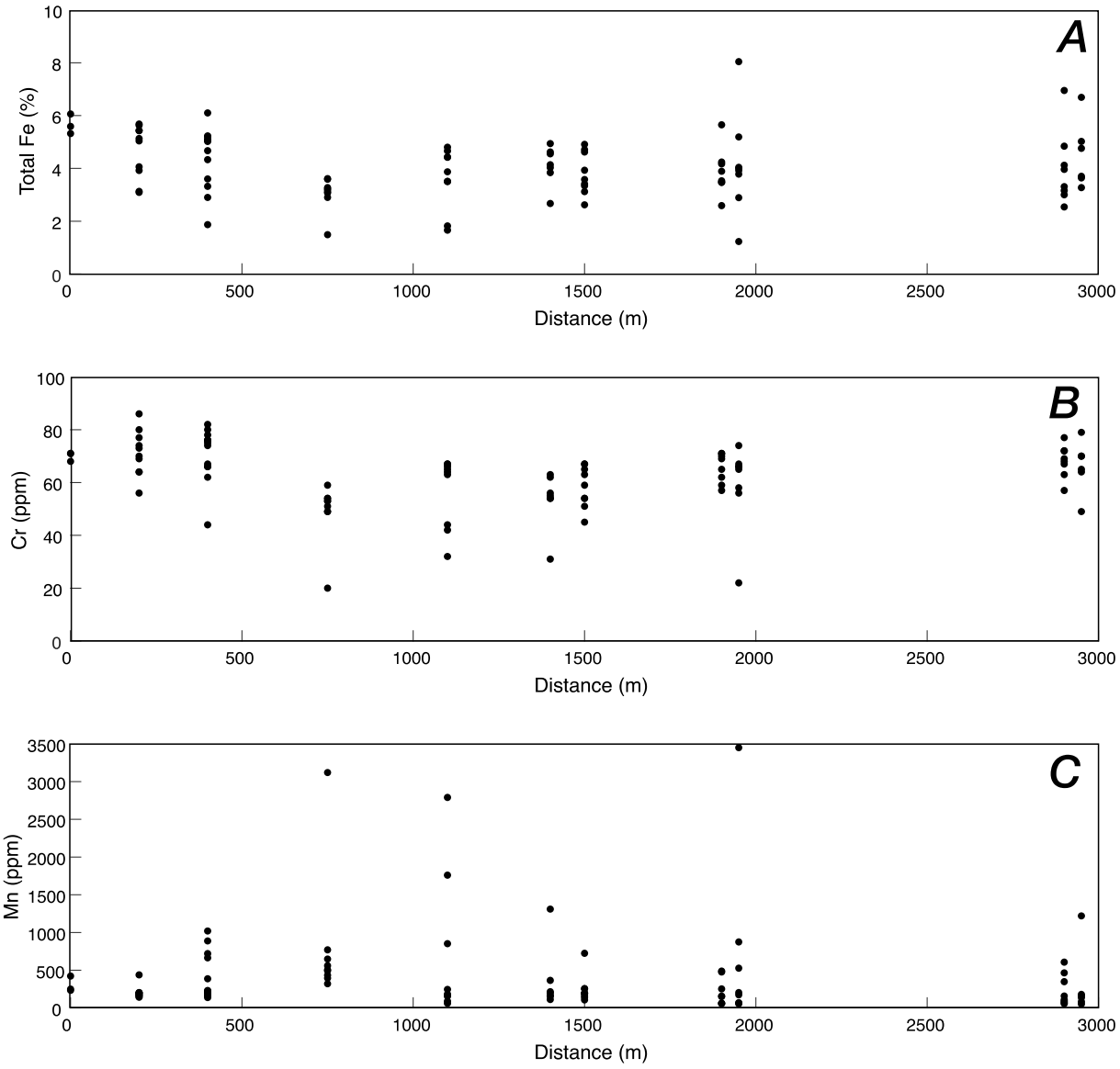

Figure D 4. Lateral redox chemistry at JMH.

(A) Variation in total Fe (%). (B) Variation in Cr (ppm). (C) Variation in Mn (ppm), which is more variable than Fe or Cr.

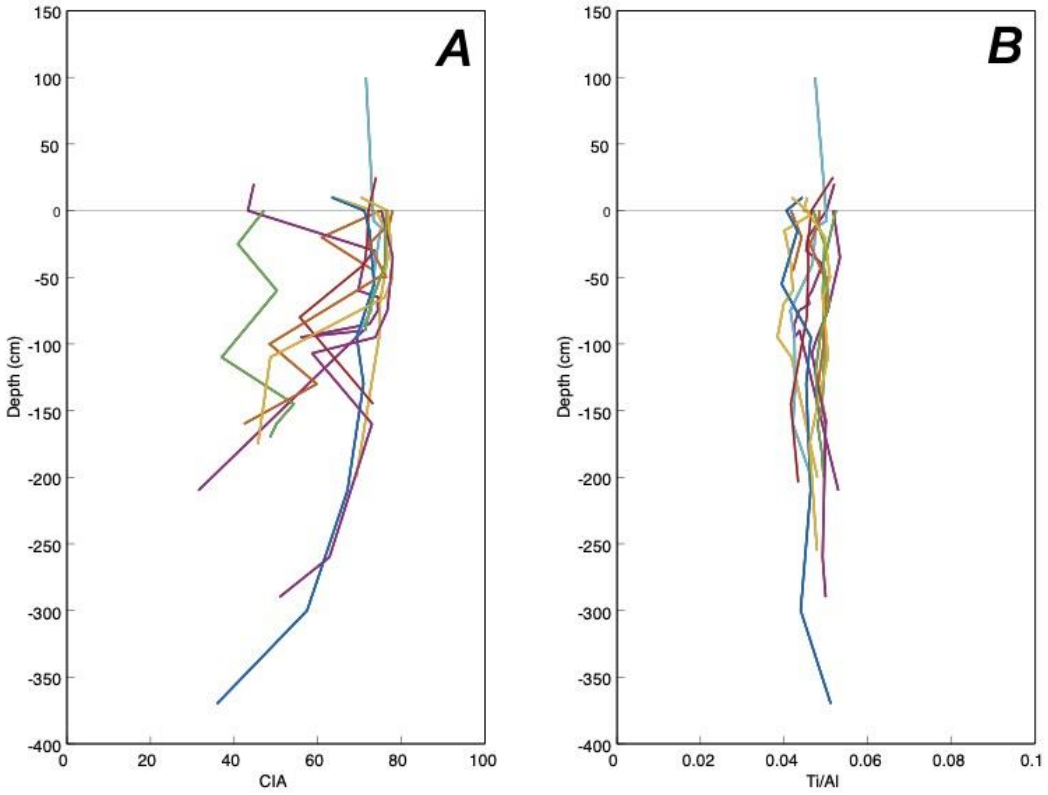

Figure D 5. CIA, Ti/Al depth profiles at JMH.

(A) Down-profile trends in CIA show expected decrease in weathering from the profile surface, although as most profile as missing A horizons, the trend is muted. (B) Down-profile trends in Ti/Al are consistent, reflecting a lack of detrital input and making the paleosols appropriate for use in paleoclimate proxies.

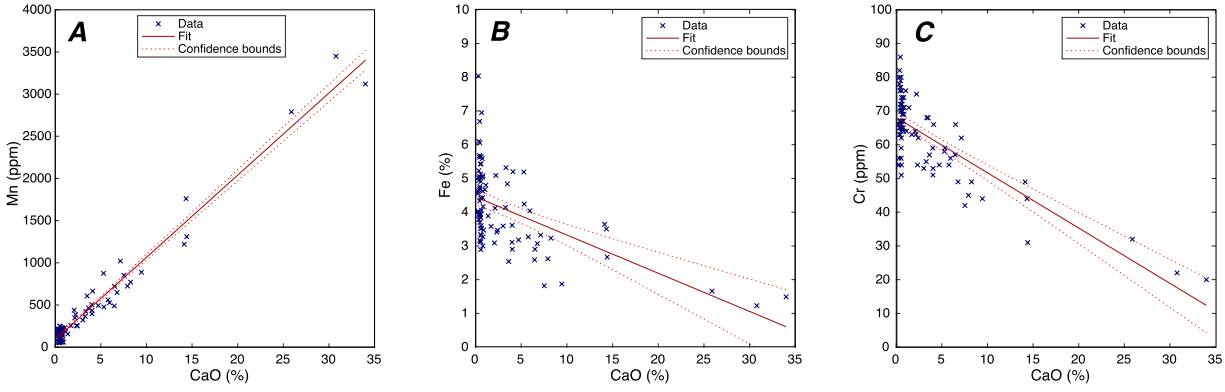

Figure D 6. Redox element correlations at JMH.

Correlations between redox-indicator elements at JMH. (A) Significant linear correlation between CaO and Mn ($r^2 = 0.95$, $p < 0.001$, n = 90). (B) The correlation between CaO and Fe is weaker and less linear than CaO~Mn ($r^2 = 0.21$, $p < 0.001$, n = 90). (C) The correlation between CaO and Cr ($r^2 = 0.48$, $p < 0.001$, n = 90).

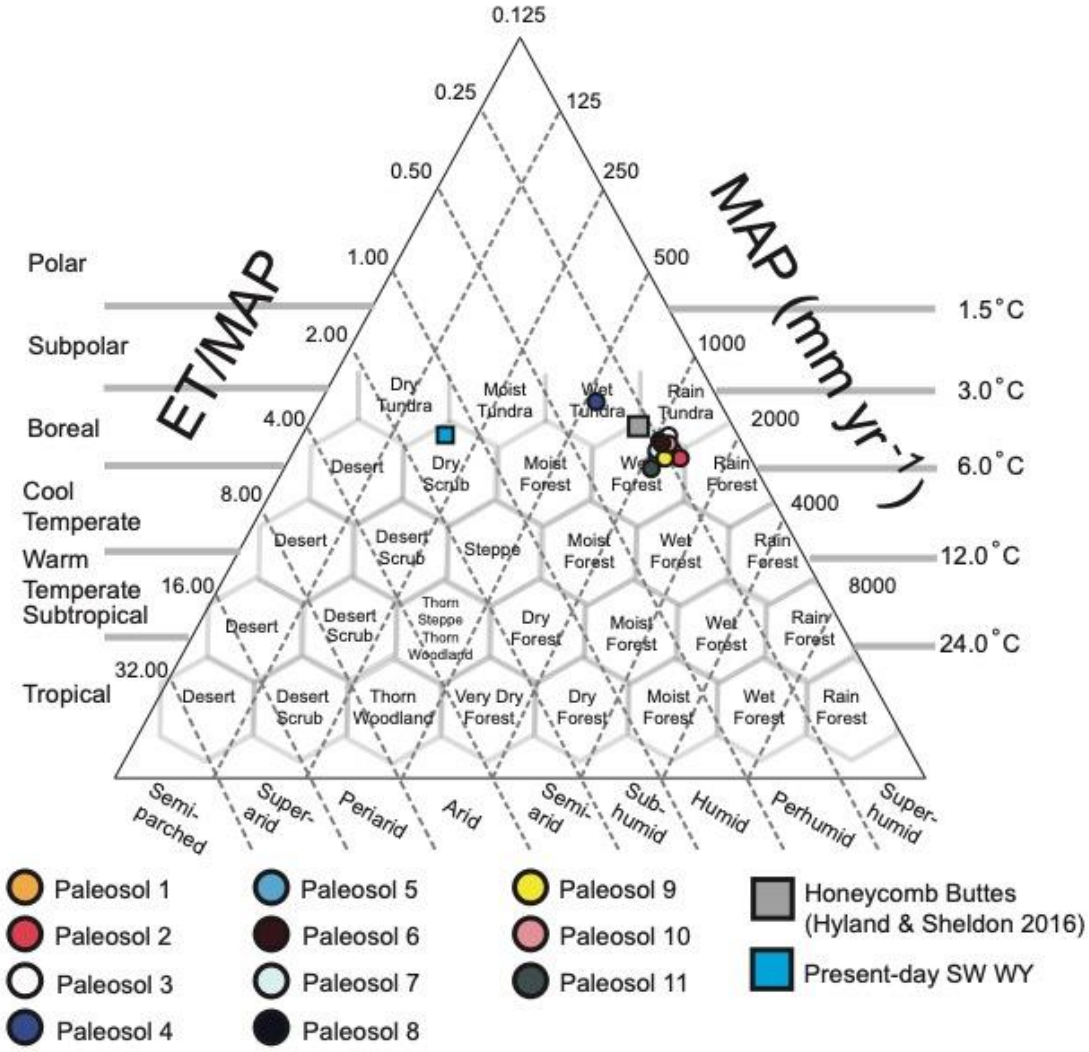

Figure D 7. Holdridge life zones at JMH.

Holdridge life zone plot showing JMH paleosols (circles), as compared with HB (gray square) and modern-day southwestern Wyoming (blue square). Note that while most JMH paleosols plot in the wet forest biome, Paleosol 4 plots in wet tundra–an inaccurate biome designation for Wyoming in the Eocene. This discrepancy is driven by that profile's high CaO samples.

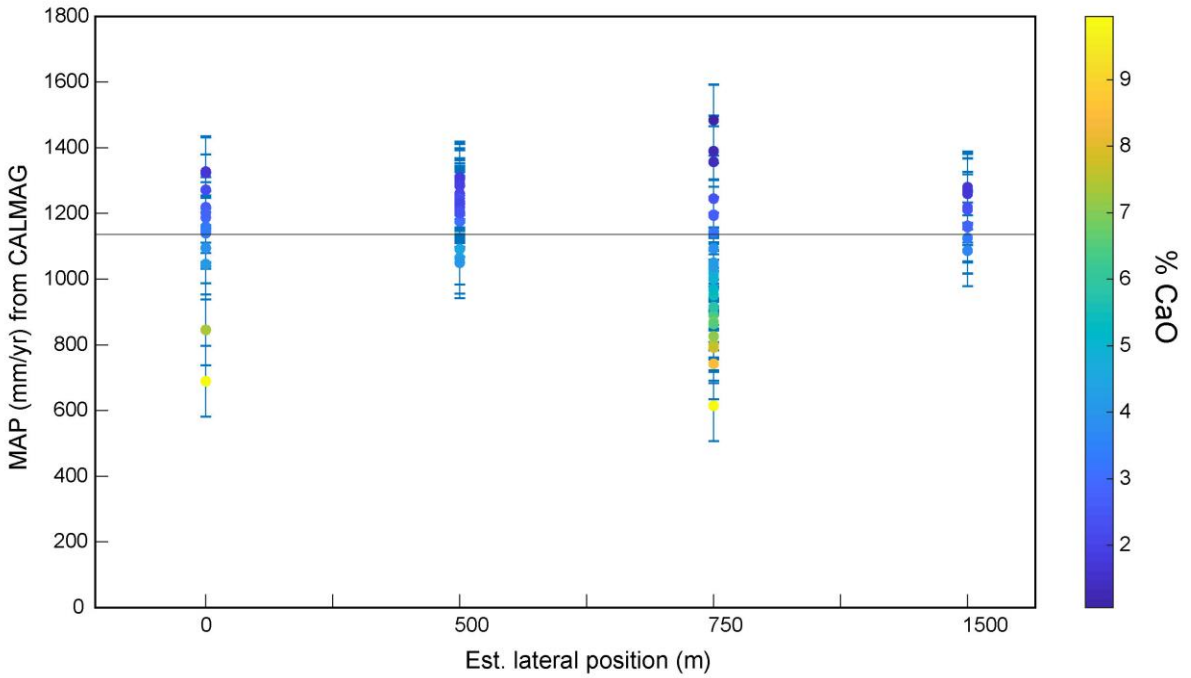

Figure D 8. Lateral variability of Kisaaka paleosol MAP.

Lateral variability in the Kisaaka paleosol's MAP values from CALMAG, with samples colored by CaO content (see color bar at right). Error bars are RMSE of CALMAG proxy. Solid black line is overall mean MAP. As with JMH, CaO content is a primary driver of geochemical variability and therefore of variability in MAP reconstructions. From left to right, profile 1σ values = 183, 68, 206, and 67, with the largest standard deviations in profiles with high-CaO samples.

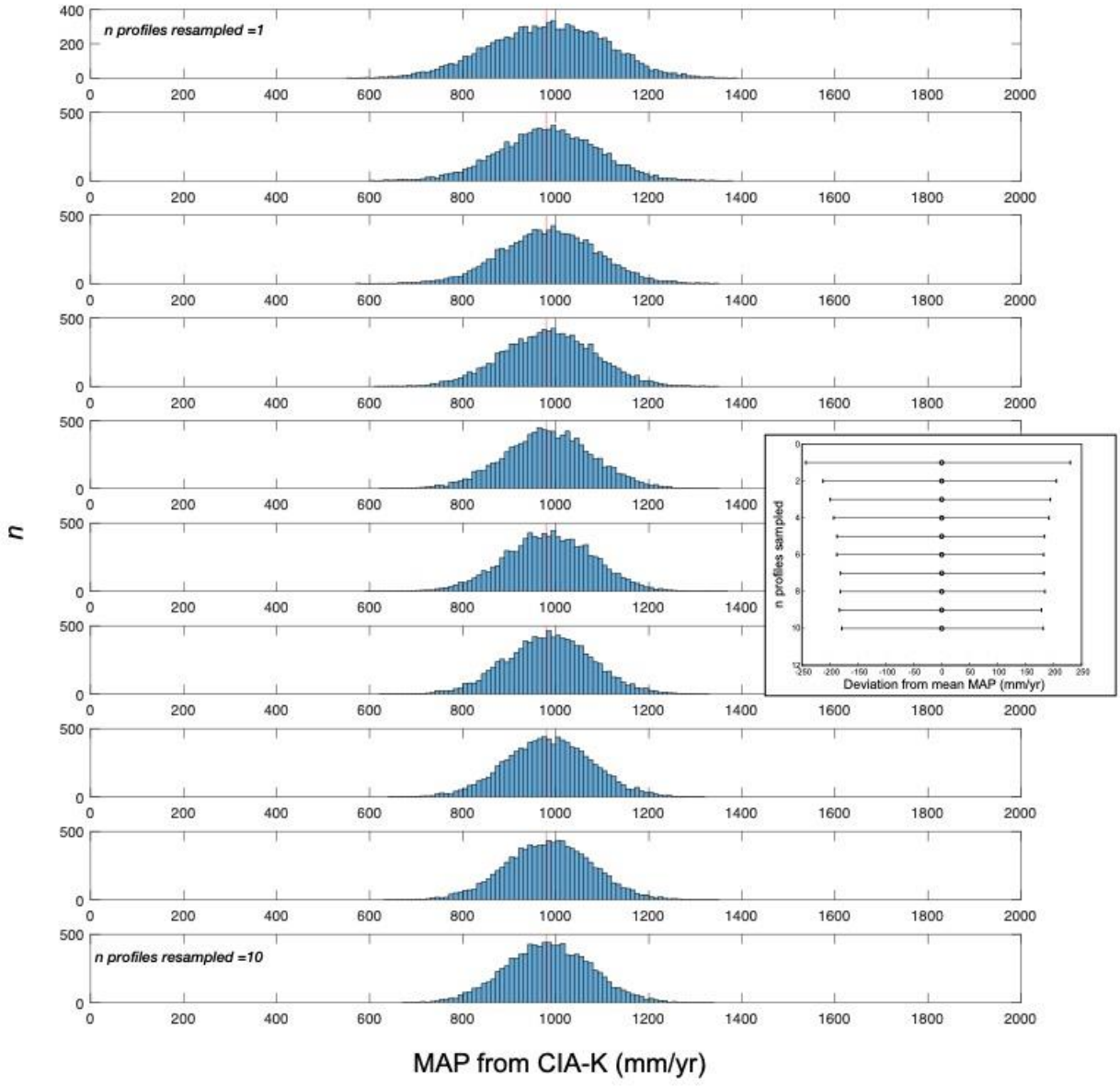

Figure D 9. Resampling MAP at HB site.

Resampling results for HB transect of Hyland et al. (2016) (B horizons). From top to bottom, the number of profiles included in the resample increases by one (i.e., top panel resamples one profile, bottom panel resamples all 10 profiles). The vertical red line is the average MAP from the HB dataset. All panels are 10,000 iterations. The bottom panel effectively represents the mean ± standard error of the regression. (Inset panel) From top to bottom, the deviation from the average MAP value for 1 to 10 profiles resampled is plotted. Because HB had less geochemical variability, the convergence pattern is muted but present.

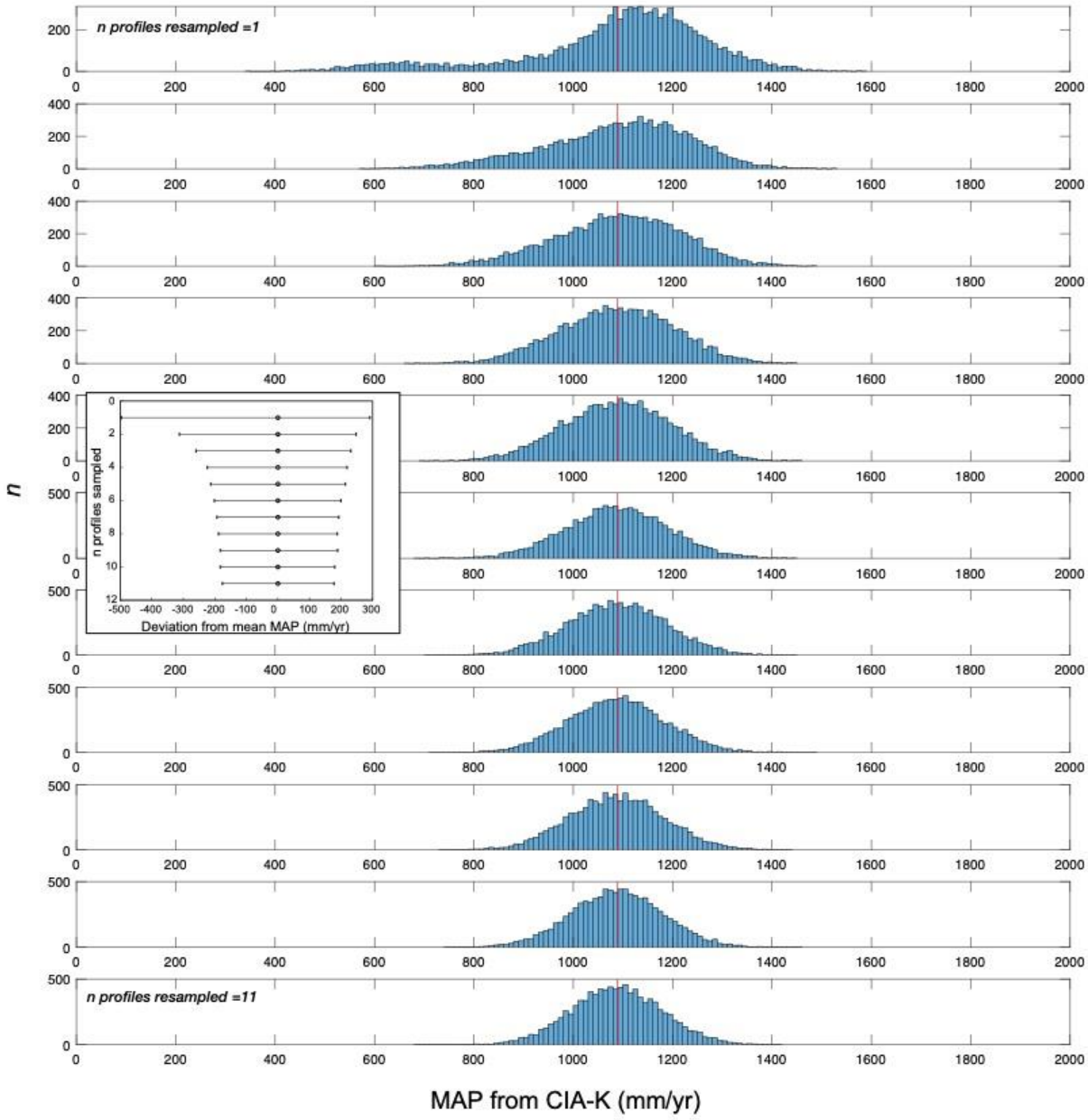

Figure D 10. Resampling MAP for JMH site, no CaO filter.

Resampling results for JMH transect (B horizons, regardless of CaO content). From top to bottom, the number of profiles included in the resample increases by one (i.e., top panel resamples one profile, bottom panel resamples all 11 profiles). The vertical red line is the average MAP from the dataset. All panels are 10,000 iterations. Including the high-CaO samples shifts the distribution slightly but does not affect the overall convergence trend. (Inset panel) From top to bottom, the deviation from the average MAP value for 1 to 11 profiles resampled.

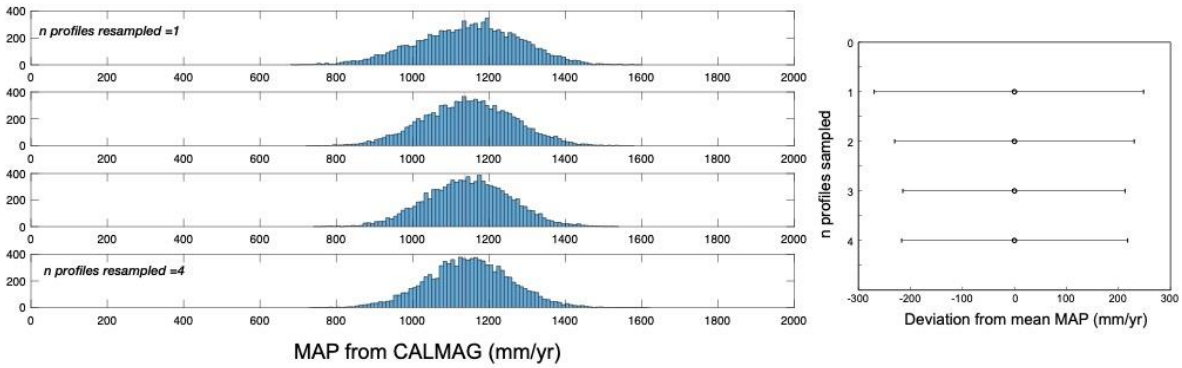

Figure D 11. Resampling MAP for Kisaaka paleosol.

(Left panel) Resampling results for Kisaaka transect (B horizons, <10% CaO). From top to bottom, the number of profiles included in the resample increases by one (i.e., top panel resamples one profile, bottom panel resamples 4 profiles). The vertical red line is the average MAP from the Kisaaka dataset. All panels are 10,000 iterations. With fewer profiles, a decrease in uncertainty is muted but present; this is a useful test of the same method on Vertisols (rather than Inceptisols/Alfisols). (Right panel) From top to bottom, the deviation from the average MAP value for 1 to 4 profiles resampled. The decrease in deviation is smaller with only 4 profiles samples.

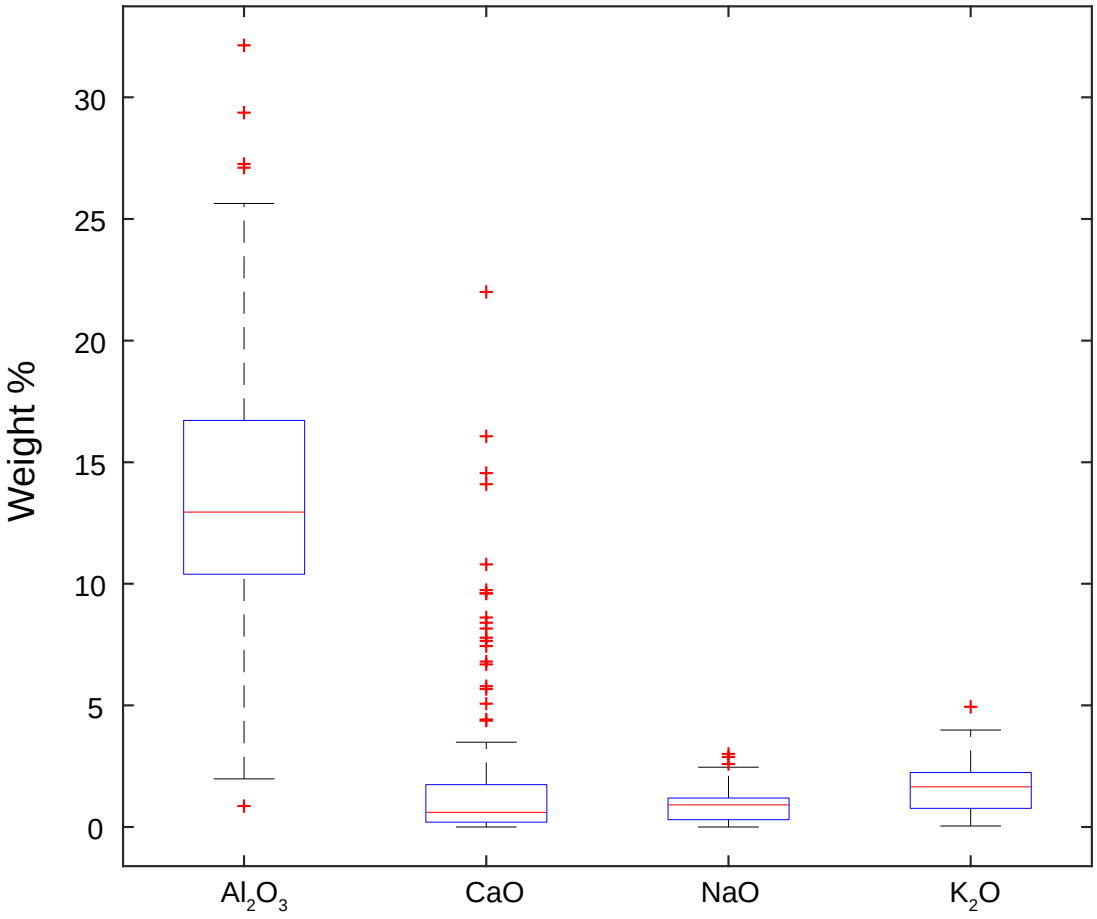

Figure D 12. Elemental distributions for B horizons from Marbut (1935).

Boxplot showing elemental distributions for (from left to right) Al_2O_3, CaO, NaO, K_2O, from Marbut (1935) dataset of B horizons in North America.

Appendix E

Descriptions and Links for Online Supplemental Tables

Data tables for Chapters II, III, IV, and IV are available as publicly-viewable, downloadable Excel files in Mendeley data. DOIs for these tables are provided below.

Chapter II DOI: 10.17632/znfgfhpp5b.3

Table A1. Description of datasets used in Chapter II
Table A2. Sample locations and details for soils compiled in Chapter II
Table A3. Soil geochemistry for soils sampled in Chapter II
Table A4. Fe species and analyses for Chapter II
Table A5. Pyrite in soils, density-normalized, for Chapter II

Chapter III DOI: 10.17632/63vr5tpmxj.1

Table B1. Bedrock-parented paleosol data in Chapter III
Table B2. Alluvium-parented paleosol data in Chapter III
Table B3. Sandstone data in Chapter III
Table B4. Continental emergence summary for Chapter III

Chapter IV DOI: 10.17632/n5yjzkpmkz.1

Table C1. Bedrock-parented paleosol data in Chapter IV
Table C2. Alluvium-parented paleosol data in Chapter IV
Table C3. Profile thickness and soil order in Chapter IV

Chapter V DOI: 10.17632/m4rt8rtbr5.1

Table D1: Paleosol sample locations and descriptions
Table D2: Paleosol geochemistry
Table D3: Modern soil Ca data
Table D4: Holdridge life zone data